The Role of Flavodoxin in The Food-Borne Pathogen *Campylobacter jejuni*

Abdulmajeed Alqurashi

BSc, Umm Al Qura University

A thesis submitted in part fulfilment for the degree of

Doctor of Philosophy

Department of Molecular Biology & Biotechnology

The University of Sheffield

December 2020

Abstract

Campylobacter jejuni is the most frequent cause of food-borne gastroenteritis worldwide but remains a poorly understood pathogen. Unusually for an aerobe, it uses pyruvate and 2-oxoglutarate oxidoreductases (POR/OOR) that reduce a flavodoxin (FldA), which acts as the electron donor to Complex I in the respiratory chain, rather than NADH. This study has focussed on additional ways in which FldA is reduced and its physiological roles in the cell, as it is unclear at present why this protein is essential for viability.

We purified and characterised FldA and identified an additional reductase, in addition to POR/OOR. This is called FqrB (Cj0559). The FqrB protein was first characterized in *H. pylori* and is a member of the NADPH oxidase protein family that contains flavin adenine dinucleotide (FAD) as a cofactor. We were able to delete the *fqrB* gene in *C. jejuni*. An *fqrB* deletion mutant was viable but displayed a significant growth defect, indicating a key role in normal cell growth. FqrB is related to flavoprotein reductases from Gram-positive bacteria that can reduce NrdI, a specialised flavodoxin that is needed for tyrosyl radical formation in NrdF, the beta subunit of Class 1b-type (Mn) ribonucleotide reductase (RNR). However, *C. jejuni* possesses a single Class 1a-type (Fe) RNR (NrdAB) that would be expected to be ferredoxin dependent. We show that CjFldA is an unusually high potential flavodoxin unrelated to NrdI, yet growth of the *fqrB* mutant, but not the wild-type or a complemented strain, was stimulated by low deoxyribonucleoside (dRNS) concentrations, suggesting FldA links FqrB and RNR activity. Using purified proteins, we confirmed the NrdB tyrosyl radical could be regenerated in a FldA, FqrB and NADPH dependent manner, as evidenced by both optical and electron paramagnetic (EPR) spectroscopy. Thus, FldA activates ribonucleotide reductase in *C. jejuni*, explaining its essentiality, which might provide a target for inhibition by anti-microbial agents. Finally, we examined the genomes of sequenced *Arcobacter* spp, close relatives of *Campylobacter* which have multiple flavodoxins, FqrB homologues and two types

of Complex I and performed some preliminary functional studies on some of these proteins from *A. butzleri*.

Acknowledgements

I would like to express my sincere thanks and gratitude to my supervisor Professor David J. Kelly for his guidance and support throughout the 4 years of my PhD. Without the help and support of him; I would not be able to complete my PhD.

Also, I would like to thank the past and present members of the Kelly lab, especially Dr. Aidan Taylor.

My warm thanks go to all my family and friends. Also, a thank you to my wife for her unfailing and unlimited support.

Publication

Abdulmajeed Alqurashi, Laura Alfs, Jordan Swann, Julea Butt and David J. Kelly (2020). Essential physiological role for the flavodoxin FldA in activation of the class 1a ribonucleotide reductase of *Campylobacter jejuni*" Submitted to Molecular Microbiology

Presentations

Alqurashi, Abdulmajeed and Kelly, David J. (2019). The Role of Flavodoxin in the food-borne pathogen *Campylobacter jejuni*. University of Sheffield 3rd year PhD symposium. Sheffield, UK. (Oral presentation)

Alqurashi, Abdulmajeed and Kelly, David J. (2018). The Role of Flavodoxin in the food-borne pathogen *Campylobacter jejuni*. University of Sheffield 2nd year PhD symposium. Sheffield, UK. (Oral presentation)

Abbreviations list

Absx	Absorbance at x nm
Acn	Aconitase
Amp	Ampicillin
APS	Ammonium persulfate
ATP	Adenine triphosphate
BHI	Brain Heart Infusion broth (Oxoid)
bp	Nucleotide basepairs
°C	Degrees Celsius
Cam	Chloramphenicol
Carb	Carbenicillin
cat	Chloramphenicol acetyltransferase
CFE	Cell free extract
CO_2	Carbon dioxide
Da	Dalton
dH_2O	Distilled water
dNTP	Deoxyribonucleotide triphosphate
EDTA	Ethylenediamine tetra-acetic acid
ETC	Electron transport chain
Fe-S	Iron sulphur
Fum	Fumarase
g	Gram
H_2O_2	Hydrogen peroxide
HCl	Hydrochloric acid
HIC	Hydrophobic Interaction Chromatography
HO·	Hydroxyl radical
hr	Hour
Icdh	Isocitrate dehydrogenase
ICP-MS	Inductively-coupled plasma mass spectrometry
IPTG	Isopropyl *β*-D-1-thiogalactopyranoside

ISA	Isothermal assembly
Kan	Kanamycin
kb	Kilobase
kDa	KiloDalton
LB	Luria-Bertani
LF	left flank
M	Molar
MCS	Multiple cloning site
mg	Milligram
MH	Mueller-Hinton
MHS	Muller-Hinton with 20 mM serine
min	Minutes
ml	Millilitre
mM	Millimolar
MW	Molecular weight
ng	Nanogram
NO	Nitric oxide
O_2^-	Superoxide
OD	an optical density
Oor	2-oxoglutarate: acceptor oxidoreductase
ORF	Open reading frame
PAGE	Polyacrylamide gel electrophoresis
PCR	Polymerase chain reaction
PEG-8000	Polyethylene glycol
pH	Hydrogen potential
PLP	Pyrixodal 5’-phosphate
Por	Pyruvate: acceptor oxidoreductase
psi	Pound force per square inch
r.p.m	Revolutions per minute
RF	right flank
RNS	Reactive nitrogen species

ROS	Reactive oxygen species
s	Second
SdaA	Serine dehydratase
SDS	Sodium dodecyl sulphate
TCA	Tricarboxylic acid cycle
TEMED	N,N,N',N'-tetramethyl- ethane-1,2-diamine
Tm	Melting temperature
TPP	Thiamine pyrophosphate
Tris	Tris(hydroxymethyl)aminomethane
UV	Ultraviolet
v/v	Concentration, volume/volume
w/v	Concentration, weight/volume
WT	Wild-type
µg	Microgram
µl	Microlitre
µM	Micromoles
µg	Microgram
ORF	Open reading frame
PAGE	Polyacrylamide gel electrophoresis
PCR	Polymerase chain reaction
PEG-8000	Polyethylene glycol
pH	Hydrogen potential
PLP	Pyrixodal 5’-phosphate
Por	Pyruvate: acceptor oxidoreductase
psi	Pound force per square inch
r.p.m	Revolutions per minute
RF	right flank
RNS	Reactive nitrogen species
ROS	Reactive oxygen species
s	Second
SdaA	Serine dehydratase

SDS	Sodium dodecyl sulphate
TCA	Tricarboxylic acid cycle
TEMED	N,N,N',N'-tetramethyl- ethane-1,2-diamine
Tm	Melting temperature
TPP	Thiamine pyrophosphate
Tris	Tris(hydroxymethyl)aminomethane
UV	Ultraviolet
v/v	Concentration, volume/volume
w/v	Concentration, weight/volume
WT	Wild-type
µg	Microgram
µl	Microlitre

Table of Contents

Chapter 1: General introduction

1.1 Introduction to *Epsilonproteobacteria*

Epsilonproteobacteria are a distinct class of Gram-negative bacteria that includes both chemolithotrophs that can be found at hydrothermal vents in the deep-sea as well as commensals and pathogens of birds and mammals. Due to their metabolic versatility, some *Epsilonproteobacteria* play vital roles in chemical homeostasis of the deep-sea environment, especially sulphur, nitrogen and other chemical element cycles. By oxidizing reduced sulfur, formate, and hydrogen coupled to nitrate or oxygen as terminal electrons acceptors, they fulfil their energy requirements (Takai *et al*., 2005). The fixation of carbon dioxide to biomass using the reversed Krebs cycle by these *Epsilonproteobacteria* is very important for deep-sea life. The reduced oxygen content of these environments and oxygen sensitivity of this pathway are correlated with their evolution in the sulfidic Mesoproterozoic oceans with low oxygen availability from photosynthesis by cyanobacteria (Anbar and Knoll, 2002). However, some species from *Epsilonproteobacteria*, which are mostly curved to spirilloid (Figure 1.1), are pathogens such as *Helicobacter spp.* found in the mammalian stomach and *Campylobacter spp.* in the intestines. The class *Epsilonproteobacteria* is represented by the families Helicobacteraceae and Campylobacteraceae. *Campylobacter*, *Sulfurospirillum*, and *Arcobacter* are the three main genera of Campylobacteraceae, which contains about forty-three species. *Campylobacter* is the most well-characterized genus and *Campylobacter jejuni* is the most well-characterized species. This is due to the major role of this genus, especially *Campylobacter jejuni* in foodborne bacterial gastroenteritis. It is mostly found living in the bodies of warm-blooded hosts. Species of the genus have been isolated from many raw foods such as pork, beef, shellfish, lamb, and milk. However, poultry is considered the largest source of the disease caused by these bacteria.

Unlike *Campylobacter spp, Arcobacter spp*. are found as free-living organisms in a wide range of environments including sea hydrothermal vents, marine sediments, groundwater, sewage sludge, and dairy (De Boer *et al*., 2013). *Arcobacter* are typically S shaped bacteria and non-fermentative. They are highly motile by means of single unsheathed polar flagella at either one or both ends of the cell (Ho *et al*., 2006). They are heterotrophs or chemolithoautotrophs and use a common method of obtaining energy used by many taxa of *Epsilonproteobacteria* subdivision, i.e. utilization of multiple alternate electron acceptors in respiration and reduction of sulfur compounds. *Arcobacter spp.* especially *A. butzleri* and *A. cryaerophilus* are classified as human pathogens (Table 1.1) (Ho *et al*., 2006).

Table 1.1: The major differences between *Campylobacter spp.* and *Arcobacter spp.* (Lau *et al*., 2002) are as follows:

Characteristic	***Campylobacter spp.***	***Arcobacter spp.***
Grow at (°C)	Grow at or above 37 °C.	Grow at room temperature (18 °C to 22 °C).
Halotolerance	Not halotolerant.	Halotolerant (up to 2 % in some species).
Oxygen tolerance	Cannot grow in a wide range of environments. Microaerobic or anaerobic environments.	Can grow in a wide range of environments. Aerobic, anaerobic and microaerobic environments.

1.2 Introduction to *Campylobacter jejuni*

1.2.1 Discovery and taxonomy

The German bacteriologist, Theodor Escherich found campylobacter like organisms in children's diarrhea stool samples in 1886, which is how

Campylobacter was first discovered (Kist, 1985; Vandamme, 2000; King and Adams, 2008; Vandamme *et al*., 2010). In 1906 in the UK, Mcfadyean and Stockman were able to reveal that the reason behind the abortions in Devon longwoolled ewes was due to the vibrio-like bacteria (Skirrow, 2006; Zilbauer *et al*., 2008). In 1918 in USA, Smith and Taylor observed that a vibrio-like bacterium was responsible for abortions in cattle as well (Kist, 1985). It was named *Vibrio fetus* by Smith and Taylor because of being morphologically similar to another *Vibrio* species (Smith, 1918). Smith and Orcutt noticed a similar spiral shaped bacterium in 1927 in the stool of cattle with diarrhea and named it *Vibrio jejuni*. In 1947, the first evidence of *Campylobacter* infection in humans was reported by Vinzent, which was found to be the reason of fetus loss in two women who had fever (Vinzent *et al.,* 1947). Elizabeth King, after 10 years, isolated two *Vibrio*-like bacteria from the blood of patients with diarrhea. However, she was unable to isolate them from the faeces of those patients due to lack of optimized protocols and techniques (Zautner and Masanta, 2016). In 1963, after studying the DNA and metabolism of *Vibrio*-like bacteria and comparing it to other *Vibrio* organisms, the genus *Campylobacter* was first proposed by Sebald and Véron. The name *Campylobacter* comes from two Greek words: kampylos, which means curved and baktron which means rod due to the twisted rod like shape (Sebald and Veron, 1963). *C. jejuni* was initially isolated from a sample of human faeces by Dekeyser and Butzler in 1968 via a filtration technique from a 20-year-old female's sample who had symptoms of severe diarrhea and fever (Altekruse *et al*., 1999). *C. jejuni* was soon realized to be an endemic pathogen (Butzler *et al*., 1973). With the development of better isolation and identification techniques, microbiologists worldwide were keen to study and understand these bacteria better.

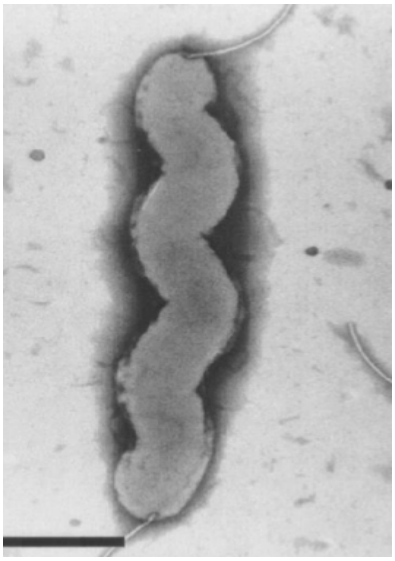

Figure 1.1: showing the cell morphology of *Campylobacter jejuni* NCTC 11168. The bar represents 1 μM (Gaynor *et al*., 2004).

Campylobacter jejuni is a Gram-negative, microaerophilic bacterium, regarded globally as a key leading cause of bacterial gastroenteritis (Gao *et al*. 2017). It is considered to be a significant economic and public health burden. The global burden of *Campylobacter jejuni* in 2010 was 7.5 million disability-adjusted life years, more than enterotoxigenic *E. coli*, which was 6.9 million and *Shigella* with 7.1 million (Platts-Mills & Kosek 2014). *C. jejuni* is commonly found as a commensal microbial flora in the gastrointestinal tracts of poultry, wild birds and animals, with infections regularly occurring in humans after the consumption of unpasteurized milk, undercooked meat or untreated water (Rahman *et al*. 2014). Upon entering the human gut, the bacteria are subject to harsh conditions e.g. from stomach acid and intestinal bile, and nutritional competition with other commensals and host organisms. The ability of *Campylobacter spp.* to compete for nutrients, such as nitrogen, organic acids, and carbon sources, is a part of pathogen physiology that has been given much consideration in recent times. *C. jejuni* is asaccharolytic, meaning that it uses carbon sources other than sugars for its growth in the host. According to Velayudhan *et al*. (2004), *Campylobacter jejuni* grows *in vitro* in the presence of amino acids by using only serine, proline, aspartate, and glutamate as sole carbon sources (Figure 1.2).

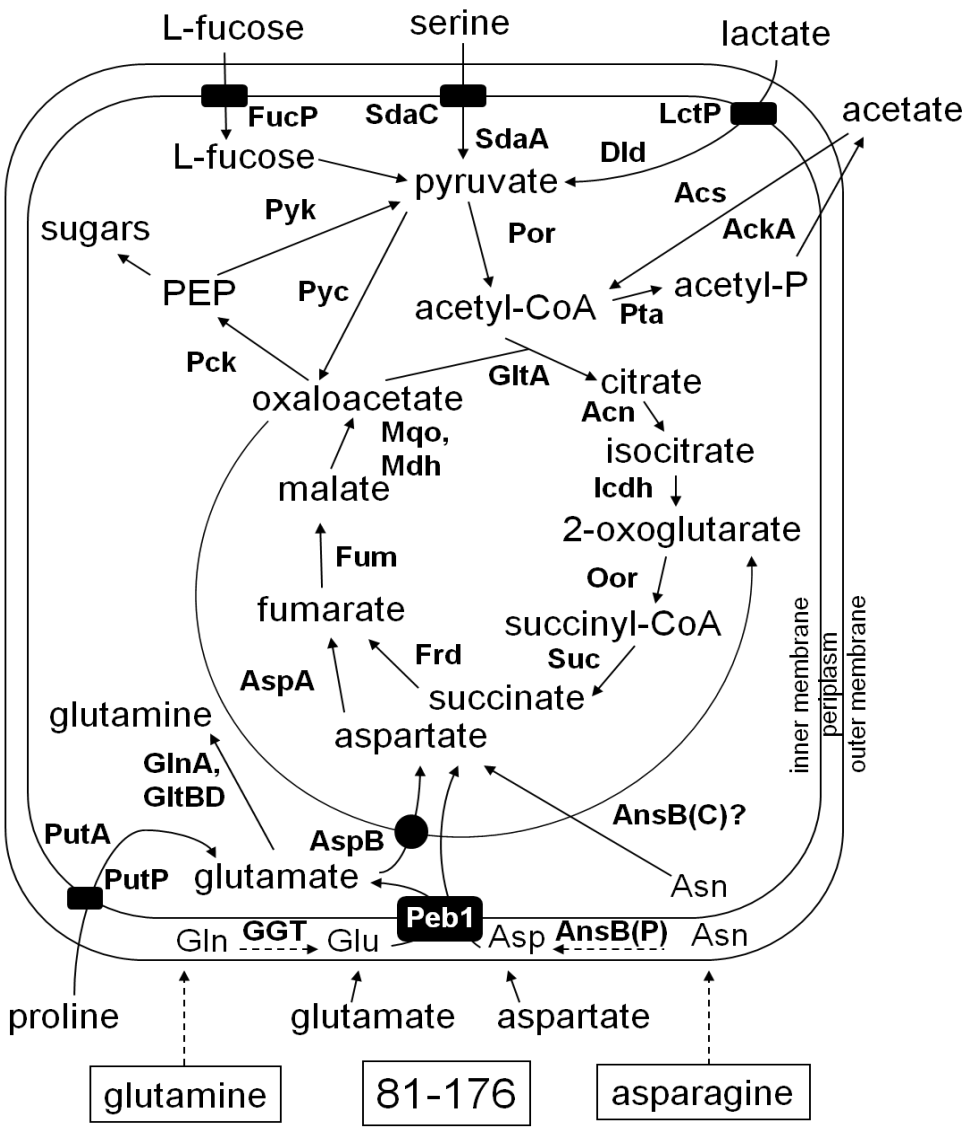

Figure 1.2: Major pathways of central carbon metabolism *C. jejuni*. OM; outer membrane, IM; inner membrane. Amino acid transporters are represented as black rectangles. PEP is phosphoenolpyruvic acid. The major enzymes are shown next to the reaction. Por is pyruvate:acceptor oxidoreductase. Oor is 2-oxoglutarate acceptor oxidoreductase, OAA is oxaloacetate. FucP is L-fucose transporter. SdaC is serine transporter. LctP is lactose transporter. SdaA is serine dehydratase. Dld is lactate dehydrogenase; Pyk, pyruvate kinase; Por, pyruvate: acceptor oxidoreductase. Acs is acetate-CoA synthase. AckA is acetate kinase. Pyc is pyruvate carboxylase. Pta is phosphotransacetylase. Pck is PEP carboxykinase. GltA is citrate synthase. Can is aconitase. Icdh is isocitrate dehydrogenase. Suc is succinyl-CoA synthetase. Fum is fumarase. Mqo is malate:quinine oxidoreductase. Frd is fumarate reductase. AspA is aspartate deaminase. AspB is glutamate transaminase. GlnA is glutamine synthase. GltBD is glutamate synthase. PutP is proline transporter. PutA is proline dehydrogenase. AnsB (C/P) is asparaginase (cytoplasmic/periplasmic) (Kelly, 2008).

1.2.2 General microbiology of *Campylobacter jejuni* and its properties

Campylobacter jejuni infection is primarily caused by ingesting contaminated food products, especially meat and milk, but also water (Kelly 2001). *Campylobacter jejuni*, being a commensal occupant of the alimentary canal of poultry animals, makes poultry the commonest origin of infection. Symptoms associated with *C. jejuni* infection comprise abdominal pains, diarrhea which contains leukocytes and blood, and fever (Rahman *et al*. 2014). The factors linked to pathogenicity and infectious ability of *C. jejuni* includes environmental adaptability to the human gut, adherence, iron acquisition, ability of invading host cells, lipooligosaccharides (LOS), and chemotaxis (Rahman *et al*. 2014). The microaerophilic nature of *C. jejuni* indicates that most strains require growth in an atmosphere of 5-10 % (v/v) carbon dioxide, and 5-10 % (v/v) oxygen (Kelly 2001). *C. jejuni* is cultured with additional growth supplements in complex media, and with blood derivatives added. These supplements are included to help inactivate noxious long-chain fatty acids or to reduce oxidative damage (Kelly 2001). *C. jejuni* in batch culture after growing *in vitro* for some days undergoes a morphological transformation typically from spiral-bacillary to coccoid forms. The static stage of coccoid forms is typified by a total loss of culturability. The function of coccoid cells in transmitting disease is still controversial. Moreover, in an experiment to examine the importance of chemotaxis in *C. jejuni*, it was found that energy taxis, the fundamental drive in environmental movement by *C. jejuni*, moves the organism in the direction of maximal chemical conditions for colonization and energy generation (Rahman *et al*. 2014). According to Vegge *et al*. (2009), substances observed in this study that promoted attraction of *C. jejuni* were also found to support the growth of *C. jejuni*. These substances were grouped as: (i) electron donors, comprising succinate, D-lactate, L-malate and formate; (ii) metabolic substrates, comprising L-glutamate, 2-oxoglutarate, L-aspargine, pyruvate, L-serine, L-cysteine, and L-aspartate; and (iii) electron acceptors, comprising hydrogen peroxide, nitrate, DMSO, fumarate, and nitrite. It was also concluded that pyruvate and L-serine, being the most preferred growth

substrates, were the most robust attractants under microaerophilic conditions (Vegge *et al*. 2009; Rahman *et al*. 2014).

1.2.3 Overall carbon metabolism of *C. jejuni*

Amino acids and organic acids are the key carbon sources that *C. jejuni* could use *in vivo* for growth. It is well-known that *Campylobacter jejuni* is incapable of metabolizing supplied sugars externally since phosphofructokinase, a critical glycolytic enzyme is absent (Kelly 2001). The pathway is believed to operate in reverse for gluconeogenesis, though genes for other glycolytic enzymes are present. Evidence has been provided for L-fucose utilisation by *C. jejuni* through the construction of a mutation in the gene encoding a putative fucose permease (FucP), and it was found that the locus (*fucP* operon) is needed for fucose utilisation (Wayne *et al*. 2011). Also, the transcription of the genes in the locus in agreement with their role in fucose utilization and is highly inducible by fucose (Muraoka & Zhang 2011). The anaerobic utilization of fucose by *C. jejuni* is similar to that of *Bacteroides thetaiotaomicron* since both lead to pyruvate production (Stahl, Butcher & Stintzi 2012). According to Stahl *et al*. (2011), the exact mechanism of the degradation pathway of L-fucose in *C. jejuni* remains elusive, since only a fucose permease and *E. coli* aldolase homologue, responsible for converting lactaldehyde to lactate under aerobic conditions, were implicated in fucose degradation by *C. jejuni*. In anaplerotic pathways in *C. jejuni*, there are homologues of both phosphoenolpyruvate (PEP) carboxylase and pyruvate carboxylase, which may play a vital role in PEP and oxaloacetate synthesis respectively (Velayudhan and Kelly, 2002). *C. jejuni* is asaccharolytic due to lacking phosphoenolpyruvate synthase and phosphofructokinase, but through PEP (phosphoenolpyruvate) carboxykinase (oxaloacetate ↔ PEP), organic acids go into the gluconeogenic pathway (Velayudhan and Kelly, 2002). Through the oxaloacetate intermediate, and via PEP carboxykinase and pyruvate carboxylase, PEP synthesis from pyruvate is made possible. Interestingly, in a study aimed to determine the variations in carbon source utilization by *C. coli* and *C. jejuni* strains, it was found that *C. jejuni* demonstrated the absence of genes

required for metabolism of the short-chain fatty acid propanoate (abundant in the intestine), while the multi-genome analysis of *C. coli* showed the presence of genes needed for metabolism of propanoate (Wagley *et al*. 2014). The results of this study reveal the genotypic and phenotypic methods of distinguishing between *C. coli* and *C. jejuni* strains based on propionic acid utilisation. The current understanding of the metabolism of *C. jejuni in vivo* is based on amino acid utilisation in aiding the proliferation and establishment of colonization in the host gut.

1.2.4 Amino acid catabolism and nitrogen assimilation

The crucial energy and carbon sources of asaccharolytic food-borne human pathogen *C. jejuni* are amino acids. In a study to examine the importance of L-serine in the colonization of the avian gut by *C. jejuni*, it was shown that L-serine catabolism through an oxygen-labile L-serine dehydratase is vital for the *in vivo* growth of *C. jejuni*, and also crucial for the colonization of the avian gut by *C. jejuni* (Velayudhan *et al*. 2004). Studies have shown that *C. jejuni* only significantly used serine, proline, glutamate, and aspartate during its microaerobic growth in amino acid-rich complex media (Guccione *et al.* 2008). Guccione *et al*. (2008) examined the catabolism of glutamate and aspartate, and it was found that a *C. jejuni* mutant in *aspB*, lacking aspartate: glutamate aminotransferase and an aspartase (*aspA*) mutant both exhibited severely impaired growth in complex media. A *C. jejuni* mutant lacking serine dehydratase could not grow in complex media unless it was supplemented with fumarate, and pyruvate (Guccione *et al*. 2008).

1.2.5 Electron transport chains in *C. jejuni*

An electron transport chain has three critical components. They include a membrane soluble quinone to enable an electron transfer, a primary dehydrogenase which accepts electrons from an initial electron donor substrate and a terminal reductase that reduces an electron acceptor. Electron transport generates a proton electrochemical gradient due to the energy released between the less negative terminal electron acceptor and the

highly negative electron donor. The role of the electron transport chain is thus to pump H+ ions through the bacterial membrane thus giving the energy required for ATP production, motility and solute transport. Studies on the respiration physiology of *Campylobacter jejuni* revealed the presence of a vibrant complement of cytochromes and the fact that some non-jejuni species could undergo anaerobic growth by fumarate and formate respiration in the same manner as the related obligate anaerobe *Wolinella succinogenes* (Kelly 2001; Taylor and Kelly, 2019). *C. jejuni* is an obligately microaerophilic organism with a respiratory metabolism. However, recent studies are indicating some interesting anaerobic electron transport pathways. *C. jejuni* is characterized by a branched electron transport chain that enables respiration with various electron acceptors and donors. A *cb*-type cytochrome c oxidase is present for oxygen-dependent electron transport which primarily receives electrons from a cytochrome bc_1 complex through a periplasmic c-type cytochrome (Kelly 2001; Taylor and Kelly, 2019). A highly coupled proton-translocating respiration chain is then terminated by this reaction. Moreover, *C. jejuni* also possesses two separate genes encoding cytochrome c peroxidases, which may be responsible for detoxification of hydrogen peroxide in the periplasm and an alternative quinol oxidase (CydAB homologue). The quinone pool gets its electron input through a hydrogenase, a complex I-type membrane-bound quinone reductase and other various crucial substrate dehydrogenases. The actual source of electrons for *C. jejuni* complex I is not reduced nicotinamide adenine dinucleotide (NADH) since *C. jejuni* complex I does not possess the two subunits with which other bacteria bind NADH (Kelly 2001; Taylor and Kelly, 2019). The likelihood of anaerobic growth with fumarate as the terminal electron acceptor is made possible by the presence of genes for fumarate reductase. For the fact that the mammalian or avian gut is practically anaerobic, the anaerobic growth of *C. jejuni* is very pertinent, and it appears probable that, *in vivo*, electron acceptors apart from oxygen will play a crucial role. However, outside of a host there are widespread electron acceptors such as dimethylsulphoxide, trimethylamine-N-oxide or nitrate, and *C. jejuni* may be able to survive using these (Kelly 2001). With all of the vital enzymes present, *C.*

jejuni has a complete oxidative citric acid cycle, including a nicotinamide adenine dinucleotide-linked malate dehydrogenase and the homologues of a and b subunits of succinyl-CoA synthetase (Kelly 2001). Fumarate reductase Frd present in *C. jejuni* may permit anaerobic electron transport but is reversible (succinate dehydrogenase activity) and thus also involved in the oxidative citric acid cycle (Kelly 2001; Taylor and Kelly, 2019).

1.2.5.1 Electron donors and oxygen as a terminal electron acceptor

A variety of electron donors can be used for anaerobic and oxidative respiration. According to Weerakoon & Olson (2008), the action of the 2-oxoglutarate:flavodoxin oxidoreductase (Oor) and pyruvate:flavodoxin oxidoteductase (Por) enzymes will generate two electrons per molecule that are used to reduce flavodoxin before transfer to Complex 1. *C. jejuni* also utilizes other key donors like hydrogen through using a membrane-bound periplasm-facing Ni-Fe-type hydrogenase and formate (Weerakoon *et al*., 2009). According to Weerakoon & Olson (2008) *C. jejuni* uses the proton pump Complex 1 under optimal microaerobic growth environments to move electrons from donors to the quinone pool. This quinone pool consists of methylmenaquinone or menaquinone (Guccione *et al*., 2010). Complex 1 shares some homology with NADH:ubiquinone oxidoreductases which are present in many other eukaryotic and prokaryotic organisms. However, it uses flavodoxin as an electron donor instead of NADH (Weerakoon & Olson, 2008). These electrons are passed to the CioAB quinol oxidase from Complex 1 or to the *cb*-oxidase through the cytochrome *c* or cytochrome bc_1 complex (Jackson *et al*, 2007).

According to van der stel *et al*. (2017), *C. jejuni* depends on hydrogen or formate to survive in the anaerobic lumen of the gut, and near the epithelial cell layer oxygen is preferred in the generation of a pmf to maintain efficient motility and growth. Invariably, only in the presence of hydrogen, formate as an electron donor or oxygen as an electron acceptor is proton motive force (pmf) is generated. The study also revealed that ATP generation is driven either by substrate-level phosphorylation or the proton motive force, and in response to

low oxygen tension, *C. jejuni* increases the transcription of alternative respiration acceptor complexes, and also increases the activity and transcription of the donor complexes hydrogenase (HydABCD) and formate dehydrogenase (FdhABC) (van der Stel *et al*. 2017).

1.2.5.2 Alternative electron acceptors

C. jejuni has the ability to utilize a number of alternative electron acceptors under oxygen-limited conditions. The electron transport pathways for these have been recently reviewed in detail by Taylor and Kelly (2019). In summary, the electron acceptors include;

a) Nitrate via the periplasmic nitrate reductase (NapA).

b) Fumarate via a reversible cytoplasmic facing fumarate reductase (Frd)

c) Fumarate, mesaconate and crotonate via an unusual periplasmic facing methylmenaquinol: fumarate reductase (Mfr), which is unidirectional and cannot oxidise succinate (Guccione *et al.,* 2010).

d) Nitrite via a periplasmic cytochrome *c* nitrite reductase (NrfA) (Pittman *et al*, 2007).

e) Tetrathionate ($S_4O_6^{2-}$) via the periplasmic diheme TsdA (Liu *et al*., 2013).

f) Trimethylamine-N-oxide (TMAO) via the molybdoenzyme TorAB.

This diversity allows *C. jejuni* growth and continued energy conservation under conditions where oxygen may be limiting.

1.2.5.3 2-oxoacids and the TCA cycle

2-oxoacids are organic molecules containing a keto group adjacent to a carboxyl group. These 2-oxoacids are essential for TCA cycle metabolism. Pyruvate is synthesized from carbohydrates via the glycolysis pathway, amino acids via the deamination of serine and fatty acids via lactate dehydrogenation. Also, 2-oxoglutarate can be formed by isocitrate dehydrogenation and deamination of glutamate in the presence of oxaloacetate by AspA (Guccione *et al*., 2008). The oxidative decarboxylation of pyruvate and 2-oxoglutarate lead to the production of acetyl-CoA and succinyl-CoA respectively and to release electrons that are transferred to the electron carrier FldA.

1.2.5.4 2-oxoacid dehydrogenases

In most aerobes and eukaryotes, the oxidative decarboxylation of pyruvate and 2-oxoglutarate to acetyl-CoA and succinyl-CoA respectively are catalyzed by NADH-dependent dehydrogenase complexes. 2-oxoacid dehydrogenase complexes are multimeric structures that have 3 distinct domains, which are:

a) (E1) the thiamine pyrophosphate-dependent dehydrogenase (TPP)
b) (E2) dihydrolipoamide acetyltransferase which is specific to either pyruvate or 2-oxoglutarate.
c) (E3) the dihydrolipoamide dehydrogenase is a domain common to both (Guest *et al*., 1989).

These enzymes do not contain Fe-S clusters and they use NAD^+ as the electron carrier.

1.2.5.5 2-oxoacid: acceptor oxidoreductases

A lot of anaerobic and some microaerobic organisms like *C. jejuni* depend on 2-oxoacid acceptor oxidoreductases to convert pyruvate to acetyl-CoA and 2-oxoglutarate to succinyl-CoA rather than using 2-oxoacid dehydrogenases. Such enzymes have certain characteristics that are distinct. One is that they evolved earlier than multi-enzyme complex dehydrogenases (Weerakoon & Olson, 2008). Secondly, they use ferrodoxin or flavodoxin for electron acceptors instead of NAD^+ (midpoint redox potential = -320 mV). Thirdly, according to Imlay, (2006), since they depend on Fe-S clusters for internal electron transfer, it makes them susceptible to damage by oxygen radicals. POR and OOR contain TPP that is responsible for converting pyruvate and 2-oxoglutarate to acetyl-CoA and succinyl-CoA in the presence of CoA in a multi-step reaction. This process releases electrons (Kerscher & Oesterhelt, 1982). These enzymes are very important in *C. jejuni* metabolism and their oxygen/ROS sensitivity has been proposed as contributing to the microaerophilic growth phenotype (Kendall *et al.,* 2014). This is discussed below.

1.2.6 The genome sequences of *C. jejuni*

The *C. jejuni* genome is unique because it is typified by an extremely small number of repeated sequences with nearly no phage-related or insertion

sequences. A study that examined the genome sequence of *Campylobacter jejuni* NCTC11168 reports that the bacterium has 1,641,481 base pairs of circular chromosome (Marchant, Wren & Ketley 2002). Its chromosome with G+C of 30.5 percent is believed to encode 1,654 proteins and 54 stable RNA (Cooper *et al*. 2011). A minimum of 20 forecasted coding sequences (CDS) out of the 1,654 CDS are likely to be pseudogenes. The mean gene length is put at 948 base pairs and proteins constitutes 94.3 percent of the genome codes indicating that *C. jejuni* genome sequences are the most densely packed bacterial sequences identified so far. Hypervariable sequences have been discovered in the *C. jejuni* genome (Parkhill *et al* 2000). Many of these hypervariable sequences coexist with the gene bundles implicated in flagellar adaptation, lipooligosaccharide and extracellular polysaccharide biosynthesis. Likewise, *C. jejuni* strain S3 genome has 28 forecasted pseudogenes and 3 rRNA operons. It also has 44 tRNA enveloping the entire amino acids. The strain S3 of *C. jejuni* comprises a single plasmid (Cooper *et al*. 2011). This plasmid of S3 comprises 43, 222 base pairs, 49 putative protein-coding genes and a G+C of 30.0 percent. According to Cooper *et al*. (2011), comprehensive *C. jejuni* S3 genome aids as a significant means of the characterization of genes represented in the newly detected *Campylobacter jejuni*-integrated element 1(CJIE1) and CJIE4.

1.2.7 The major virulence factors of *C. jejuni*

The key factors that give *C. jejuni* its virulence are considered to be its motility and chemotaxis, its several surface polysaccharide structures and protein glycosylation, its adhesion and invasion, its toxins and its two-component regulatory systems. Enterocolitis is induced when cytolethal distending toxin (CDT) is generated and when epithelial cells are invaded (González-Hein *et al*. 2013). One of the major consequences of cell invasion is cellular injury. The reduction in the absorptive ability of the intestine is caused by this cellular injury. The role of CDT production in the bacterial virulence mechanisms is based on the release of interleukin-8 (IL-8). IL-8 is implicated in mucosal inflammatory response (González-Hein *et al*. 2013). CDT comprises three smaller units

denoted as CdtA, CdtB and CdtC. Induction of genotoxic effects occurs through translocating of CdtB to the host nucleus which eventually triggers DNA repair cascades responsible for cell arrest and cell death (Marchant, Wren & Ketley 2002). Elevated transcription of a carbon starvation regulator (CsrA) gene in *Campylobacter jejuni* signifies that the gene plays a prominent function in the continued existence of *C. jejuni* in its host milieu (González-Hein *et al*. 2013). Furthermore, the capacity of *C. jejuni* to react to particular chemicals through chemotaxis, and its ability to change their motility is a vital determining factor for the bacterial pathogenesis. A study shows that *C. jejuni* harbors different chemotaxis genes that are responsible for its survival and host pathogenesis (Marchant, Wren & Ketley 2002) (Figure1.3).

Figure 1.3: *C. jejuni* can colonise and cause disease in the intestines of humans. (https://www.alamy.com/campylobacteriosis. Image ID: MYDR34)

1.2.8 The molecular basis for microaerophily and capnophily of *C. jejuni*

Microbes are considered to be microaerophilic when they cannot grow at normal atmospheric oxygen tension; though they need oxygen for their growth, they

have developed adaptation for specific environments which are characterized by low oxygen concentrations (Kendall *et al*. 2014). *C. jejuni* is part of this category of microbes because it needs low oxygen concentrations for its growth. Perhaps, for its DNA synthesis it depends on a single NrdAB-type ribonucleotide reductase. The unsophisticated molecular hypothesis for oxygen sensitivity of these microaerophilic microbes could be an insufficiency of oxidative stress defense enzymes (Kim *et al*. 2015). All aerobic bacteria are subject to oxidative damage by molecular oxygen by producing reactive oxygen species (ROS), which must be removed by defence enzymes like catalase, thiol peroxidases and superoxide dismutase. *C. jejuni* possesses all of these defences. There are two significant iron-sulphur (FeS) cluster enzymes present in anaerobic bacteria. These Fe-S cluster enzymes could make the citric acid cycle (CAC) weakened by oxygen impairment. In most aerobic bacteria, the conversion of pyruvate by oxidative decaboxylation to acetyl-coenzyme A (acetyl-CoA) occurs by utilizing the oxygen stable pyruvate dehydrogenase multi-enzyme complex, with the electron acceptor being NAD^+ (Kendall *et al*., 2014). The entrance of carbon from pyruvate into the CAC depends on this reaction. Nonetheless, this essential reaction is catalyzed by flavodoxin:pyruvate oxidoreductase or Por in many anaerobes. This Por comprises three [4Fe-4S] clusters (Kendall *et al*. 2014). Por could be inactivated by molecular oxygen because of its high sensitivity to it (Kim *et al*. 2015). Interestingly, *C. jejuni* has this enzyme. Moreover, *C. jejuni* also has 2-oxoglutarate: acceptor oxidoreductase (Oor), which is responsible for oxidative decarboxylation of 2-oxoglutarate to succinyl-CoA. The study conducted by Kendall *et al*. (2014) to investigate the mechanisms possibly protecting enzyme activity and to detect the function of hemerythrin HerA (Cj0241) in the citric acid cycle for *C. jejuni* showed that hemerythrins aid in preventing enzyme damage during oxygen transients or microaerobically, and poor repair of 2-oxoglutarate: acceptor oxidoreductases (Oor & Por) and oxygen lability are the key contributors to microaerophily in *C. jejuni*. Oor is considered to act in place of the oxygen-stable 2-oxoglutarate dehydrogenase multienzyme complex found in

aerobes. As will be shown in my results described below, both Por and Oor are involved in the donation of electrons to the flavodoxin FldA in *C. jejuni*.

Along with being microaerophilic*, C. jejuni* requires CO_2 i.e. it is capnophilic. 5-10 % (v/v) is the required level of CO_2 for optimal growth, which is greater than the average environmental level (average ~0.04 %) (Bolton and Coates, 1983). The explanation for this is not clear, however, one possible reason is the presence of acetyl-CoA carboxylase (Burns *et al*., 1995), phosphoenolpyruvate carboxykinase, and carbonic anhydrase (Kelly, 2001). Such enzymes may be inefficient in utilizing carbon dioxide. Acetyl-CoA carboxylase, which is necessary for synthesis of fatty acids, displayed low affinity for CO_2 in *Helicobacter pylori* suggesting one reason for the high CO_2 requirement of *H. pylori* (Burns *et al*., 1995). CanB (Cj0237) which is one of the two carbonic anhydrase enzymes encoded by the C. *jejuni* 11168 genome to convert gaseous CO_2 to bicarbonate, has low CO_2 affinity yet is important for bacterial growth in low CO_2 concentrations which leads to poor conversion of CO_2 to bicarbonate (Al-Haideri *et al*., 2016). CanB (Cj0237) is thought to be responsible for the capnophilic phenotype.

1.2.9 Defences against oxidative (ROS) and nitrosative (RNS) stress

Oxidative stress and iron are inseparable when exploring defences against oxidative stress. This is due to the reaction of iron and oxygen which produces reactive oxygen species (ROS) (Birben *et al*. 2012). The surge of free radical production can also lead to generation of toxic oxygen species which are responsible for damaging cell proteins, DNA and lipids through oxidation (Birben *et al*. 2012). Superoxide dismutase (SOD) can be found in almost all aerobic organisms (Pesci *et al*., 1994). SOD has a metal as cofactor that is used to catalyze superoxide into oxygen and hydrogen peroxide. This metal varies between species (copper, zinc, iron and manganese). *C. jejuni* expresses a single superoxide dismutase, which uses iron as cofactor. The reaction by which the (SOD) converts superoxide into oxygen and hydrogen peroxide:

i) Fe^{3+}-SOD + O_2^- → Fe^{2+}-SOD + O_2

ii) Fe^{2+}-SOD + O_2^- + $2H^+$→ Fe^{3+}-SOD + H_2O_2

After that the hydrogen peroxide generated is removed either by peroxidase or catalase. *katA* is the sole catalase gene in *C. jejuni* which is induced by hydrogen peroxide and superoxide (Grant & Park, 1995). *C. jejuni* has monofunctional catalase that contains a heme group. With the assistance of the heme cofactor *C. jejuni* changes hydrogen peroxide to oxygen and water. Through the action of catalase *C. jejuni* is able to adapt to the presence of hydrogen peroxide. *C. jejuni* unlike most other organisms has two cytochrome *c* peroxidase genes (Cj0358 and Cj0020c) (Atack & Kelly, 2009) which detoxify hydrogen peroxide in a similar way to catalase. Also, *C. jejuni* possesses a number of other defences against oxidative stress for instance thiol peroxidase, alkyl hydroperoxide reductase and desulforuberythrins.

In regards of nitrosative stress defences, *C. jejuni* has two haemoglobins that are regulated by the NO-mediated transcriptional regulatior NssR (Elvers *et al*., 2005). At least one of these haemoglobins (Cgb) is involved in the nitrosative stress response by acting to convert NO to nitrate.

1.3 Ribonucleotide Reductase (RNR)

In the 1950s, ribonucleotides were shown to be precursors of deoxyribonucleotides through *in vivo* experiments (Reichard & Estborn, 1951). The difference between different ribonucleotide precursors and their turnovers had also been observed. Moreover, these *in vivo* experiments clarified that deoxyribonucleotides were formed by direct reduction i.e. oxygen removal from the compound (Thelander & Reichard, 1979) (Reichard *et al*, 1961). This is an early catalytic step to supply the cells with the “building blocks” dATP, dGTP, dCTP, and dTTP. Providing the cell with a sufficient and balanced source of

dATP, dGTP, dCTP, and dTTP is a vital procedure for all living organisms. In the cell, unbalanced dNTPs lead to mutations and this could be fatal. In *E. coli,* a very important observation was made that the ribonucleotide reductase subunits α-subunit and *β*-subunit were inactive on their own. However, the enzyme only can be active as a complex (α-subunit and *β*-subunit) with iron as a cofactor. Until today, the entire picture of how the enzyme ribonucleotide reductase (RNR) functions is still unclear even though some aspects of the regulation, structure and function were understood early on (Reichard, 1987). Since then, ribonucleotide reductase (ribonucleotide diphosphate reductase) has been studied in many organisms like viruses, bacteria, yeasts, mouse, and mammalian cells (Hofer *et al*, 2012).

1.3.1 RNR classification and radical formation

The nature of the thiyl radical, their metal cofactors, and their interaction with oxygen are the basis for dividing RNRs into three classes (Cotruvo & Stubbe, 2011):

1: Class I: these are heterocomplexes that need oxygen i.e. aerobic. It has three subclasses:

Ia: This subclass called NrdA (B1) and NrdB (B2) contains a diferric centre and tyrosyl radical (Fe^{III}-O-Fe^{III}-$Y^{\bullet}$). By apo-*β*2, Fe^{II}, O_2, and a reducing equivalent, the $Fe^{III}{}_2$-$Y^{\bullet}$ cofactor can be self-assembled. After reducing the diferric to the diferrous, the *β*-subunit of RNR reacts directly with O_2 to generate a *μ*-peroxodiferric intermediate. A neighboring tryptophan residue reduces a *μ*-peroxodiferric intermediate to produce a Fe^{III} Fe^{IV} intermediate, intermediate X and a tryptophan cation radical ($W^{+\bullet}$). Intermediate X is responsible for generating tyrosyl radical $Y^{\bullet}$ (Figure 1.4).

Ib: This subclass is called NrdE (B1) and NrdF (B2). For providing and stabilization of the tyrosyl radical $Y^{\bullet}$, this enzyme uses manganese instead of iron

(Mn^{III}-O-Mn^{III}). Mn^{III}_2-$Y^{\bullet}$ cofactor can be assembled by Mn^{II}, O_2, and the reduced (hydroquinone, hq) form of a flavodoxin (NrdI). In order to oxidize the Mn^{II}_2 cluster, reduced NrdI reacts with O_2 to generate an oxidant component. It is still unclear whether reduced NrdI generates hydrogen peroxide or superoxide as oxidant as reduced NrdI has the ability to produce both (Figure 1.5).

Ic: this enzyme type uses a mixed manganese and iron centre (Mn^{IV}-O-Fe^{III}).

2: Class II: these are homocomplexes that do not require oxygen. Their radical is formed by adenosylcobalamin (AdoCbl).

3: Class III: these are homocomplexes whose cofactor is a glycyl radical. These can only function under anaerobic conditions.

Class I RNRs can be found in eukaryotes, bacteria, archaea, and viruses (Nordlund & Reichard, 2006). On the contrary, the class II and III RNRs are mainly found in bacteria, archaea, and viruses and only in a small number of eukaryotes. The different classes can sometimes be found in the same species, giving them an evolutionary benefit. The structures of the three classes are different, class I containing a heterocomplex of α and *β* subunits that are required for enzyme activity. Classes II and III contain homocomplexes of only α subunit. The substrates used for synthesizing dNTPs are also different among the classes; classes II and III use NTPs in contrast to class I using NDPs (Cotruvo & Stubbe, 2011). The α-subunit 10-stranded α/β barrel has a tertiary structure that is similar in all the classes of RNR enzymes despite the changes in aerobic properties, free radical chemistry, subunit structures, substrates used, and allosteric regulation (Hofer *et al*, 2011).

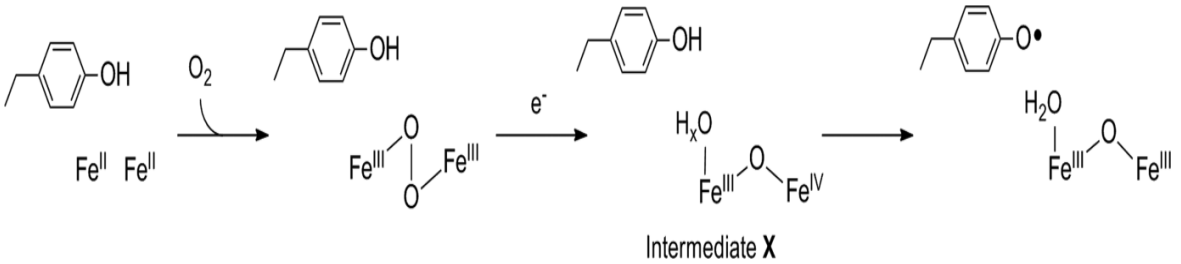

Figure 1.4: Diagram shows the mechanism by which class Ia RNRs diferric-Y• cofactor is assembled (Cotruvo *et al*, 2013).

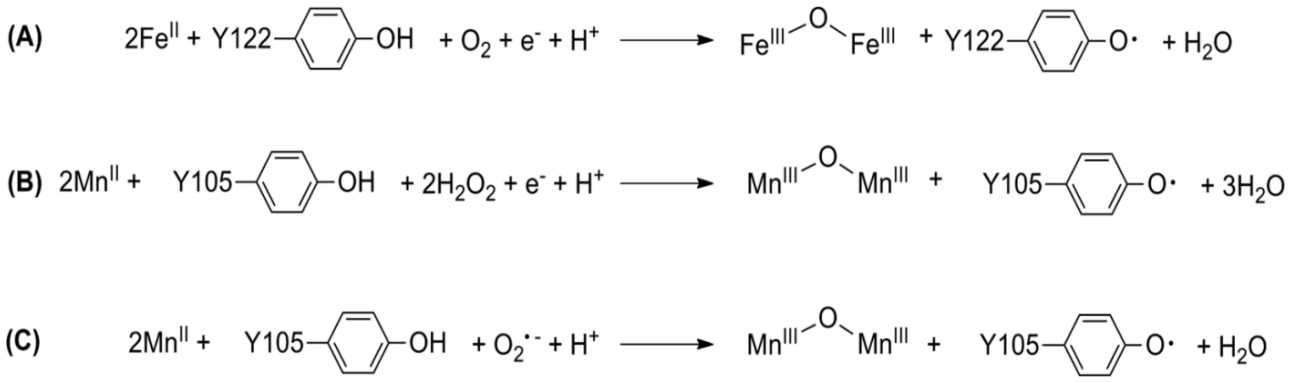

Figure 1.5: Diagrams show the stoichiometries of diferric-Y• cofactor assembly **(A)** and dimanganese-Y• cofactor assembly **(B, C)** (Cotruvo *et al*, 2013).

1.3.2 Ribonucleotide Reduction mechanism

The 5-carbon sugar ribose is converted to deoxyribose through a direct substitution reaction. The RNR enzyme along with its metallocofactor has the ability to catalyze the reduction of a hydroxyl group (–OH) in position 2' of ribose to a hydrogen (–H), converting ribonucleotide diphosphates (NDP) into their deoxy forms (dNDP) (Nordlund & Reichard, 2006) (Figure 1.6).

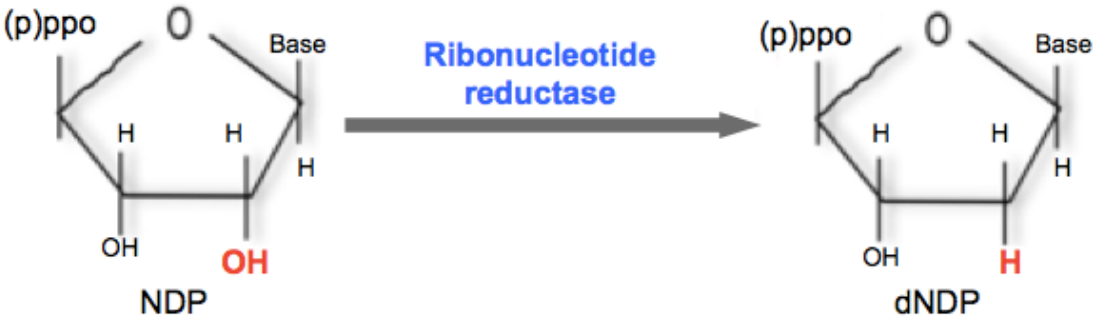

Figure 1.6: In a highly regulated step ribonucleotide reductase (RNR) catalyses the synthesis of dNDPs. Ribonucleotide diphosphates (NDP) will be reduced into their deoxy form: deoxyribonucleotide diphosphates.

1.3.3 General structure of Class Ia ribonucleotide reductase

Class Ia RNRs were first described as heterotetramers that are composed of a large subunit (B1), a catalytic subunit that requires the radical, and a small subunit (B2) that generates the radical. The enzyme is active in a α2β2 conformation (Cotruvo & Stubbe, 2011). The crystal structures of RNR subunits have been resolved. However, each subunit is modified depending on the state of the enzyme and there are still some uncertainties about the configuration of the quaternary structure, in particular *in vivo.* It has been suggested that the B1 dimer will be on top of the B2 dimer. The mechanisms behind activation/inactivation of the RNR complex are not fully understood. RNR is known as an allosteric enzyme that uses allosteric feedback through binding dNTPs to control further production of dNTPs. Enzyme activity can be regulated by binding of activating-ATP or inhibitory-dATP on the activity site on the large subunit B1 (Figure 1.7).

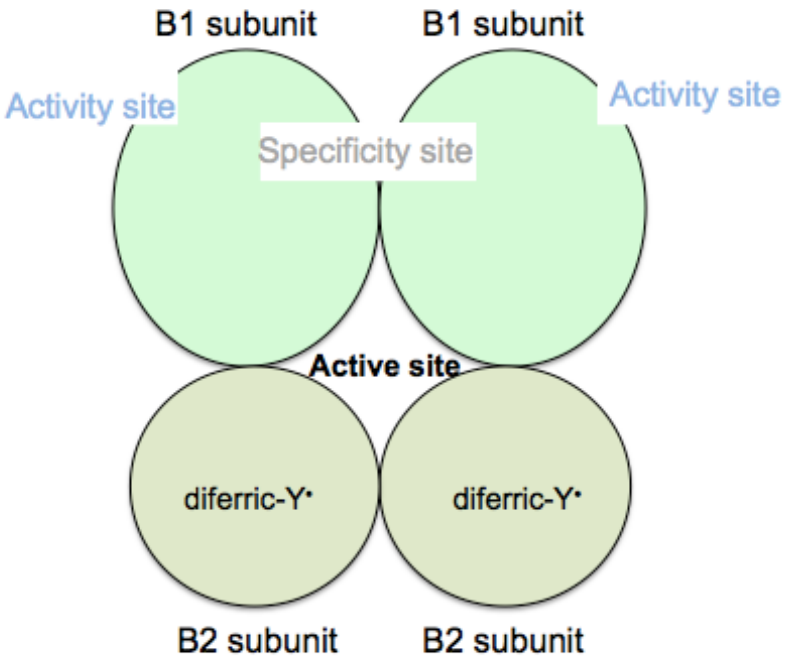

Figure 1.7: Model showing that the active form of Class Ia RNR is α2β2. B1 that is the large subunit has the activity site for (ATP and dATP) and the specificity site for (ATP, dATP, dTTP and dGTP). B2 that is the small subunit has the diferric centre to generate the tyrosyl radical (Sengupta & Holmgren, 2014).

1.3.4 The large subunit (B1 α-subunit) of Class Ia RNR

Each B1 subunit is inactive on its own. In order to be activated, B1 subunits are first dimerized. In *in vivo* experiments, it was observed that the binding between these two subunits is weak and requires Mg^{2+} ions otherwise they will be easily dissociated. There are two allosteric binding sites on each B1 subunit (Cotruvo & Stubbe, 2011):

- H-site: the overall activity control site, is also known as the cone domain. This site is for binding of dATP. Adenosine Triphosphate (ATP) acts as activator while the role of inhibitor is played by deoxyadenosine triphosphate dATP. The general level of dNTP pools tends to inhibit the activity level of RNR.

- I-site: the specificity site is also known as a low affinity-binding site of dATP molecules. This specific site allows binding for several molecules ATP, dATP, dTTP and dGTP. This is based on a multifaceted feedback regulation system, which will allow further balance of the 4 different dNTPs in the cell through this mechanism. When ATP binds to the RNR, CDP and UDP will be reduced. When dTTP binds to the RNR, GDP will be reduced. Finally, when dGDP binds to the RNR, ADP will be reduced.

α-subunit also has a catalytic site with the activation of dithiols (-SH). This is essential for the process of reduction. B1 can regulate the appropriate balance of dNTPs through the specificity site with the aid of complex allosteric regulations. In the reduction process of the NDP-ribose 2'-OH, the catalytic site plays a vital role. It was suggested that the C-terminal of B2 can 'swing out' due to its flexibility to act as a reduction shuttle (Hofer *et al*, 2011)

1.3.5 The small subunit (B2 *β*-subunit) of Class Ia RNR

The small subunit B2 is also inactive on its own and becomes active as a dimer. The B2 subunit has a binuclear ferric (Fe^{III}) iron center, which is essential for generating the tyrosyl radical and enzyme activity. In other words, apoprotein B2 (lacking the iron center) is not functional. In order to generate and maintain the tyrosyl radical ($Y^{\bullet}$), a process of oxidation/reduction occurs with the iron center and specific amino acids (Asp84, Glu115, His118, Glu204, Glu238 His241) (Hofer *et al*, 2011). The B2 subunit is one of the first proteins discovered that has an amino acid working as a free radical (Reichard, 1987). Tyr122 in B2 is an organic radical buried inside a hydrophobic pocket (10 Å 1 nm from nearest surface) (Larsson *et al*, 1988) so that the radical in B2 cannot come into contact with B1 directly, but must be transferred over a long distance to the active site cysteines in B1 to form a thiyl radical that is directly responsible for ribonucleotide reduction. The stability of the tyrosyl radical differs from species to species (four days in *E. coli* vs. 25 minutes in humans) (Hofer *et al*, 2011). The protein without free radical is called metB2 but it still possesses the iron centre, whilst apoB2

refers to the loss of both the iron centre and free radical. MetB2 and apoB2 proteins can be obtained by treating the protein with radical scavengers such as hydroxyurea (HU) and iron-chelating agents, respectively. Studying B2 structure reveals that the iron centers of B2 are 2.5 nm apart. However, in a metB2 it seems to have shifted further apart although how the metB2 is modified not fully understood (Eklund *et al*, 2001). The C-terminal of B2 is highly mobile, enabling the C-terminal of B2 to interact with the C-terminal of B1 which is also mobile as motioned above. The N-terminal portion of of B2 is not important for enzyme activity with a random coil structure (Eklund *et al*, 2001) (Figure1.8).

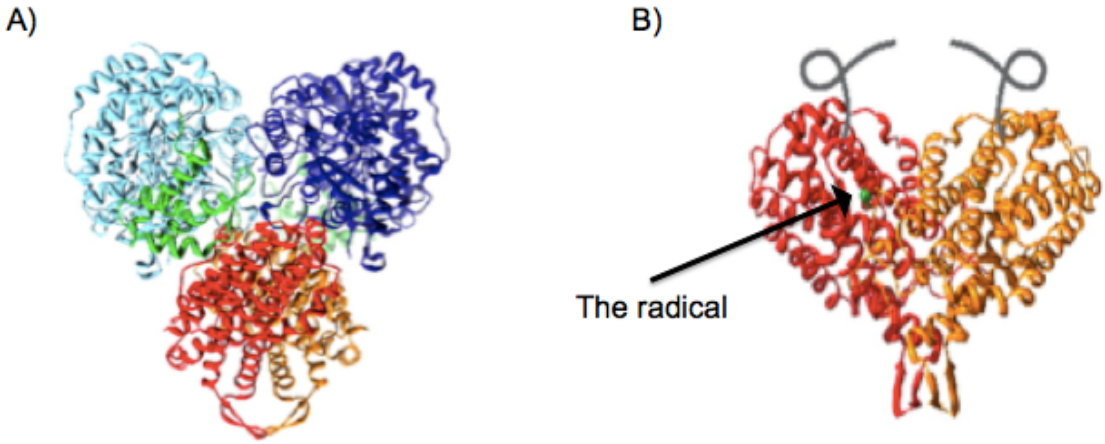

Figure 1.8: Picture **(A)** represents the model for the docking between the 2 homodimers of B1 and B2, to form the complex α2β2. Picture **(B)** is the homodimer of B2 in order to represent the structure of the small subunit, with a disorder C-terminal necessary for binding with B1. The free radical on Tyr122 is embedded inside the protein (Ando *et al*, 2011).

1.3.6 Regulation of RNR

The function of RNR is not only providing the cell with sufficient quantities of dNTPs. It has another vital role that is maintaining the balance between dATP, dGTP, dCTP, and dTTP (Chabes & Thelander, 2003). This important requirement can be accomplished by allosteric regulation of the RNR activity. The overall enzyme's activity can be controlled by the activity site of the enzyme. Providing the cell with the right balance of dNTPs is regulated by allosteric binding to activity and specificity sites. The activity site can bind to either ATP or

dATP, resulting in “switching on” of RNR or switching off the entire activity, respectively. The affinity of ATP for both the activity site and the specificity site is the same, but the affinity of dATP for the activity site is much lower than the specificity site, meaning that only at very high concentrations will dATP bind to the activity site and inhibit overall activity. The specificity site is able to bind ATP, dATP, dTTP and dGTP but is unable to bind dCTP. ATP and dATP will trigger the reduction of CDP and UDP. While, dTTP will trigger GDP reduction and dGTP will in turn start ATP reduction (Hofer *et al*, 2012).

Finally, it has been proposed that the large distance between the tyrosyl radical (Y•) site of B2 and the thiyl radical site of B1 which is approximately 35 Å is used as an activity control mechanism. The distance between the proton coupled electrontransfer (PCET) sites implies some relatively large conformational rearrangements. If the distances are too large, the PCET can be disrupted, meaning that the PCET control is important to regulate the enzyme’s activity (Cotruvo & Stubbe, 2011).

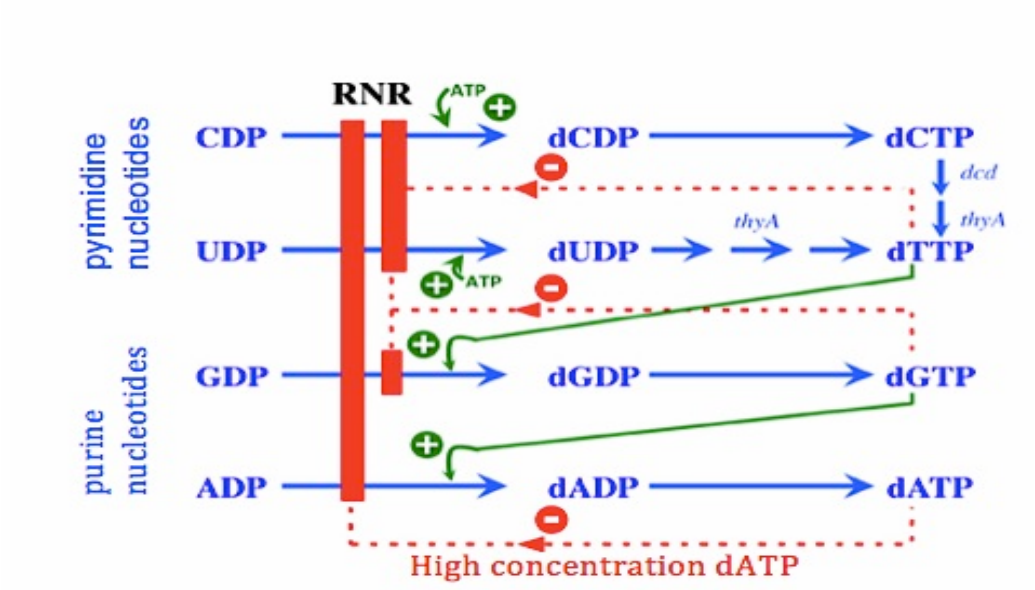

Figure 1.9: model showing the allosteric regulation of class 1a for dNTPs production through the specificity site. ATP plus low concentration of dATP will trigger synthesizing dCDP and dUDP. Whilst, dTTP will trigger producing dGDP and dGTP in turn will activate dADP production. High concentration of dATP will inhibit overall activity of the enzyme (Torrents 2014).

1.4 Aim of the project

There are unanswered questions about how the TCA cycle works in *C. jejuni* and the role of some key enzymes. In particular, the way in which flavodoxin is reduced and its physiological roles in the cell, as it is unclear at present why flavodoxin (FldA) is essential for viability. We hypothesise that FldA might be involved in other crucial systems in the cell that need electrons, such as isoprenoid synthesis and ribonucleotide reduction as the source of these have not yet been identified (Figure 1.10 A, B). We therefore aim to answer these specific questions:

1. What are the redox properties of FldA?
2. Is FldA the electron acceptor for POR in cell free extracts (CFE)?
3. How does FldA interact with NuoX and NuoY?
4. What is the role of “FqrB” (Cj0559) in FldA reduction and do FqrB/FldA have other roles in the cell?
5. How does *C. jejuni* compare with other *Epsilonproteobacteria* with regard to the use of flavodoxin, fqrB and Complex I? We will use *Arcobacter spp.* as a model system.

A)

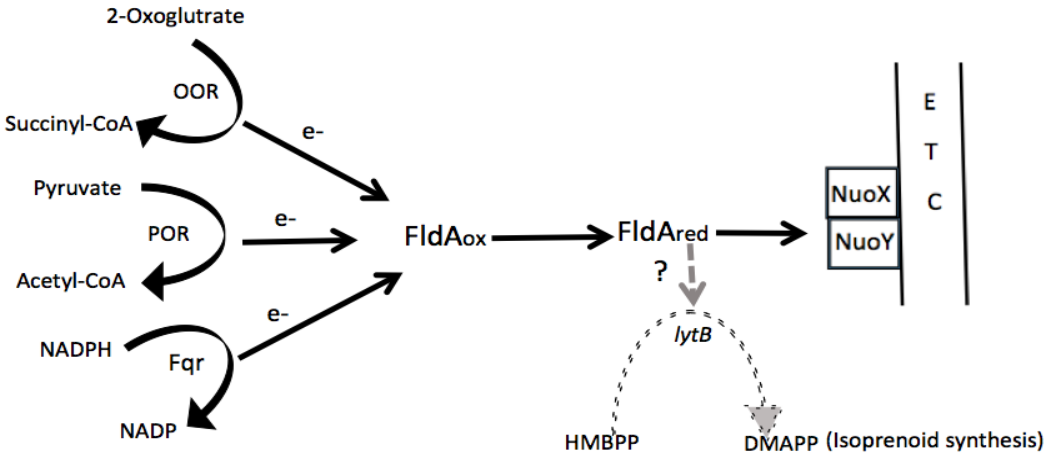

B)

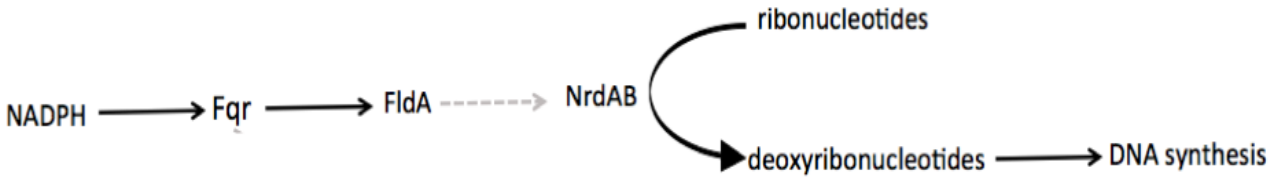

Figure 1.10: Different possible functions of Fqr and FldA. **(A)** contributing to FldA reduction. **(B)** contributing to DNA synthesis pathways along with FldA.

Chapter 2: Materials & Methods

2.1 Organisms and growth media:

2.1.1 Organisms used in this study:

C. jejuni, *E. coli and Arcobacter spp.* strains that used in this study are described in Table1. *C. jejuni*, *E. coli* and *Arcobacter spp* stocks were stored at -80 °C in Brain Heart Infusion (BHI) broth containing 15 % (v/v) glycerol.

Table 2.1: *C. jejuni* strains used in this study:

Strain	Description/genotype	Source / Reference
C. jejuni		
Wild type NCTC11168	Laboratory wild type strain	Parkhill *et al*., 2000
Δ*cj0559* (*fqrB*)	*C. jejuni* NCTC 11168 *cj0559*:: *kan*	This study
⌀*cj0559* (*fqrB*)	*C. jejuni* NCTC 11168 *cj0559*:: *kan* complementation	This study
Δ*cj0537* (*oorB*)	*C. jejuni* NCTC 11168 *cj0537*:: *kan*	This study
E. coli		
DH5a	F– Φ80 *lac*ZΔM15 Δ(*lac* ZYA- *arg* F) U169 *rec* A1 *end* A1 *hsd* R17 (rK– , mK+) *pho* A *sup*E44 λ– thi -1 *gyr* A96 *rel* A1	Invitrogen
BL21 (DE3)	F– *omp* T *hsd*SB(rB–, mB–) *gal dcm* (DE3)	Invitrogen
BTH101	F-, *cya-99 , araD139, galE15, galK16, rpsL1 (Str r) , hsdR2, mcrA1, mcrB1*.	Euromedex (Cat N°: EUK001)
Arcobacter spp.		
Arcobacter butzleri RM4018	Laboratory wild type strain	Dr. William G. Miller U.S. Department of Agriculture Western Regional Research Center, USA

Arcobacter cibarius RM15232	Laboratory wild type strain	Dr. William G. Miller U.S. Department of Agriculture Western Regional Research Center, USA
Arcobacter nitrofigilis DSM7299	Laboratory wild type strain	Dr. William G. Miller U.S. Department of Agriculture Western Regional Research Center, USA

2.1.2 Media preparation for *C. jejuni* growth

Columbia Blood Agar CM0331 (Oxoid, Basingstoke, UK) was dissolved in dH_2O, following manufacturers instructions to make agar plates for *C. jejuni.* The agar was autoclaved for 30 - 60 minutes at 121 °C and 15 psi. 5 % (v/v) lysed horse blood (SR0050C, Thermo Scientific) was added after cooling, mixed and heated in a microwave until the colour of the media became brown (3 x 20 s). 10 μg ml^{-1} vancomycin, 10 μg ml^{-1} amphotericin B, and appropriate selective antibiotics were added after the media had cooled before the media was poured into plates. 21 g L^{-1} Mueller-Hinton broth (Oxoid) was added in dH_2O with 20 mM L-Serine (MHS) and autoclaved for 30-60 minutes at 121 °C and 15 psi for sterilization.

2.1.3 Media preparation for *E. coli* growth

LB agar plates and LB broth were used to grow *E. coli*. LB broth was made by dissolving 20 g L^{-1} broth granules (Oxoid) in dH_2O. LB agar was made by dissolving 20 g L^{-1} broth granules (Oxoid) and 10 g L^{-1} agar (Melford) in dH_2O. Both media were autoclaved for 20 minutes at 121 °C and 15 psi for sterilization. Appropriate antibiotics were added to the agar at optimum temperature before it was poured into plates.

2.1.4 Antibiotic Solutions

Amphotericin B 10 μg ml^{-1}, kanamycin 50 μg ml^{-1}, ampicillin/carbenicillin 50 μg ml^{-1}, chloramphenicol 20 μg ml^{-1} and vancomycin 10 μg ml^{-1} as final concentration were used in this study. All antibiotic solutions were made in sterile dH_2O. Chloramphenicol was dissolved in ethanol. Amphotericin B needs a basic

solvent; therefore, a few drops of concentrated NaOH (10 M) were added in dH_2O. 0.2 µm filters were used to filter sterilize stock solutions of antibiotics before keeping it at 4 °C.

2.2 DNA preparation and manipulation

2.2.1 Genomic DNA (gDNA) isolation

In order to isolate the genomic DNA used for amplifying targeted genes, *C. jejuni* NCTC11168 or *Arcobacter butzleri* RM4018 cells were streaked on Columbia Blood Agar plates and incubated overnight microaerobiclly for *C. jejuni* and aerobically for *Arcobacter*. 5 Prime ArchivePure DNA Cell/Tissue Kit was used to extract DNA following the manufacturer's instructions. Cells grown on plates were harvested and resuspended in 1 ml BHI broth, before pelleting by centrifuging at 9,000 x g for 1 mintue at 4 °C. The pellet was resuspended by gentle pipetting in 600 µl of Cell Lysis Solution (ArchivePure) after the supernatant was discarded. The sample was then incubated at 80 °C for 5 minutes. 3 µl of RNAse A solution (4 mg ml^{-1}) (ArchivePure) was added to the sample. The sample was mixed by vortexing 30 seconds after which it was incubated for 30 minutes at 37 °C. 200 µl of protein precipitation solution (ArchivePure) was added to the sample after it was cooled to room temperature. Sample was then vortexed for 20 seconds and was centrifuged at 12,550 x g for 3 minutes at 4 °C. Supernatant containing genomic DNA was then transferred to 600 µl of 100 % Isopropanol containing clean microfuge tube which was then mixed by inverting and incubated at room temperature for 5 minutes. The sample was then centrifuged at 15,550 x g for 1 minute at 4 °C. The tube was drained on a clean absorbent paper after the supernatant was discarded. The pellet containing DNA was washed with 600 µl 70 % ethanol by inverting several times and then centrifuged at 15,550 x g for 1 minute at 4 °C. The pellet was air dried for 15 - 20 minutes after the supernatant was discarded. The pellet was then resuspended in 100 µl Nuclease-Free Water (Promega) and stored at -20 °C.

2.2.2 Nucleotide concentration measurement

gDNA and plasmid concentration was measured by Nanodrop (Genova Nano-Jenway) spectrophotometer against dH_2O as blank. Concentration was determined according to manufacturer's instructions.

2.2.3 Polymerase chain reaction (PCR)

Red MyTaq was utilized for primer Tm optimisation and colony screens. In a 12.5 µl reaction; 0.5 µl forward primer, 6.25 µl x 2 Red MyTaq, 5.25 µl dH_2O and 0.5 µl reverse primer. Not less than 10 µg of template DNA was utilized per reaction. Initial denaturation was done at 98 °C for 3 minutes, 30 cycles of denaturation were observed for 15 seconds at 94 °C, annealing 15 seconds at Tm, extension 10 sec/kb at 72 °C and then final extension for 5 minutes at 72 °C. Reactions were performed with respect to guidelines from the manufacturer and run using a Techgene Thermal Cycler (Techne). Basic cycling requirements comprised an annealing temperature about 5 degrees less than the primer Tm with an extension time of around 30 seconds for every thousand base pairs of final product.

Phusion Polymerase was used for genomic amplifications. In a 20 µl reaction; 10 µl x 2 Flash Phusion, 1 µl forward primer (10 µM), 1 µl reverse primer (10 µM), 10 ng template DNA, and 28 µl dH2O. Initial denaturation was done at 98 °C for 3 minutes, 30 cycles of denaturation were observed for 15 seconds at 94 °C, annealing 15 seconds at 55 °C, extension 1min/kb at 72 °C and then final extension of 5 minutes at 72 °C. The purification of all PCR products was performed through the use of QIAquick (PCR Purification Kit Qiagen).

2.2.4 PCR primers used in this study

Primers were designed by using the xBase or Kegg pathway database websites for sequences of genes we are interested in for screening and cloning aims. Targeted gene sequences were checked for internal digestion sites for restriction enzymes. Restriction site sequences were added to the primers. Ideal primers

were designed to have a Tm of 55 °C with moderate to mild secondary structure and low to zero chance of forming dimers. Upon receipt, the primers utilized in this study were re-suspended to 100 µM in dH_2O. This was followed by dilution of primer stocks to a concentration of 10 µM before adding to a final reaction concentration of 200 nM. All primers used in this study were ordered from Sigma-Aldrich.

Table 2.2: Primers used in this study.

Primers (5`-3`) used in protein overexpression studies	
T7 forward	TAATACGACTCACTATAGGG
T7 reverse	GCTAGTTATTGCTCAGCGG
cj1382 NdeI F	*TATATT*CATATGTCAGTAGCAGTAATCTATGGTAGT
cj1382 XhoI R	*ATTTAT*CTCGAGAGCAAAATAAGGTTTGATTT
cj1382 XhoI R	*ATTTAT*CTCGAGTTAAGCAAAATAAGGTTTGA
cj1575c NdeI F	*TATATT*CATATGAGAAGGGTAGATTTAAGAAAAA
cj1575c XhoI R	*ATTTAT*CTCGAGTACCCTCTCCTTTTTTATAACA
cj1574c NdeI F	*TATATT*CATATGATTTATGATAATGCTCTTTGTTT
cj1574c XhoI R	*ATTTAT*CTCGAGTCATTTTGCTTCCTTTATG
cj1573c NdeI F	*TATATT*CATATGATGACAGTTAAGATTAATGGTATA
cj1573c XhoI R	*ATTTAT*CTCGAGCTCATGGTTTGCTCCTAA
cj0559 NdeI F	*TATATT*CATATGAAAAAAATAGATTTAATTGTAGTAGG
cj0559 XhoI R	*ATTTAT*CTCGAGAAGCACAGAAAGAATTTTCA
cj0231 NdeI F	*TATATT*CATATGCAAAGAAAAAGAATTTACAATC
cj0231 XhoI R	*ATTTAT*CTCGAGGAAGTCATCAAAGCTTATACTACC
cj0231 NdeI F	*TATATT*CATATGCAAAGAAAAAGAATTTACAATC
cj0231 XhoI R	*TATATT*CATATGTTAGAAGTCATCAAAGCTTATACT
cj0024 NdeI F	*TATATT*CATATGAAAGTTATTAAAAGAAATGGTCG
cj0024 XhoI R	*ATTTAT*CTCGAGTTGGCAACCTTCACATT
Primers (5`-3`) used in protein-protein interaction studies	
cj1382 XbaI F	*TATATT*TCTAGACATGTCAGTAGCAGTAATCTATGG
cj1382 KpnI R	*ATTTAT*GGTACCTTAAGCAAAATAAGGTTTGAT
cj1574c XbaI F	*TATATT*TCTAGACATGATTTATGATAATGCTCTTTG
cj1574c KpnI R	*ATTTAT*GGTACCCGTTTTGCTTCCTTTATGCGAATTGG
cj1575c XbaI F	*TATATT*TCTAGAGATGAGAAGGGTAGATTTAAGAA
cj1575c KpnI R	*ATTTAT*GGTACCCGTACCCTCTCCTTTTTTATAAC
C. jejuni NCTC 11168 knock out primers 5`-3`	
cj0559 F1 F	GAGCTCGGTACCCGGGGATCCTCTAGAGTCCATTTGTAAATTTTGCTTCA
cj0559 F1 R	AAGCTGTCAAACATGAGAACCAAGGAGAATGACCTGCACCTACTACAATT
cj0559 F2 F	GAATTGTTTTAGTACCTAGCCAAGGTGTGCAGCAAGTATAGTTACAGGGTTA

cj0559 F2 R	AGAATACTCAAGCTTGCATGCCTGCAGGTCAATACTCCAAAATTCCGAT
cj0537 F1 F	GAGCTCGGTACCCGGGGATCCTCTAGAGTCAAATCCTTTCTTTACAGGTTAT
cj0537 F1 R	AAGCTGTCAAACATGAGAACCAAGGAGAATCATTGAGTAGGCATTTTATCTA
cj0537 F2 F	GAATTGTTTTAGTACCTAGCCAAGGTGTGC TTATGAAGAAGTACGTCGTG
cj0537 F2 R	AGAATACTCAAGCTTGCATGCCTGCAGGTCGAACCATATGAAGCATAGTT
cj1382 F1 F	GAGCTCGGTACCCGGGGATCCTCTAGAGTCTAATGCATGTTTCATTTGG
cj1382 F1 R	AAGCTGTCAAACATGAGAACCAAGGAGAAT GCACTACCTAGATTACTGTA
cj1382 F2 F	GAATTGTTTTAGTACCTAGCCAAGGTGTGC AGAATTGATGCTTGGGTAG
cj1382 F2 R	AGAATACTCAAGCTTGCATGCCTGCAGGTCTTTCACACAAAGCTTTATTC
cj1476c F1 F	GAGCTCGGTACCCGGGGATCCTCTAGAGTCTTATCGTGAAATTTATGCAC
cj1476c F1 R	AAGCTGTCAAACATGAGAACCAAGGAGAATATCAGCCATAGGAGAACTAG
cj1476c F2 F	GAATTGTTTTAGTACCTAGCCAAGGTGTGC TCAACGTCGCTATAGACAG
cj1476c F2 R	AGAATACTCAAGCTTGCATGCCTGCAGGTCCATTTGATGATATTGACAGA
cj1575c F1 F	GAGCTCGGTACCCGGGGATCCTCTAGAGTCGCATAAAATACGATTACGC
cj1575c F1 R	AAGCTGTCAAACATGAGAACCAAGGAGAATCTTCAAAAAGCTCTTTGCT
cj1575c F2 F	GAATTGTTTTAGTACCTAGCCAAGGTGTGCATCAAGTCGATTGGACTATT
cj1575c F2 R	AGAATACTCAAGCTTGCATGCCTGCAGGTCATCTTGCAAATTTGCTCTA
cj1574c F1 F	GAGCTCGGTACCCGGGGATCCTCTAGAGTCATCCTGTATGTAAGTGCTT
cj1574c F1 R	AAGCTGTCAAACATGAGAACCAAGGAGAATTCTAAAAAACAAAGCATTAT
cj1574c F2 F	GAATTGTTTTAGTACCTAGCCAAGGTGTGCATTTTACTCCAATTCGCAT
cj1574c F2 R	AGAATACTCAAGCTTGCATGCCTGCAGGTCCCATGCTCTCTTTAAAGCT
oorABCD F1 F	GAGCTCGGTACCCGGGGATCCTCTAGAGTCCTTCTGAAGAATGTAAGTTAGG
oorABCD F1 R	AAGCTGTCAAACATGAGAACCAAGGAGAATTTTACATCTATGCTCATCTACC
oorABCD F2 F	GAATTGTTTTAGTACCTAGCCAAGGTGTGCGAGAAATTTTAGCAGAAGCA
oorABCD F2 R	AGAATACTCAAGCTTGCATGCCTGCAGGTCATCAAAAGTTGGTTCAGATG
C. jejuni NCTC 11168 knock out mutant complementation primers 5`-3`	
pA(1)cj0559 F	*ACACCAATTGCATCTAACAAAAGCCTATCTTT*
pA(1)cj0559 R	*ACACTCTAGA*TTATTTTGCATATGAATTTTCTAG
pA(2)cj0559 F	*ACACTCTAGA*GAAAGGTAAATATAAATGAAAAAAA
pA(2)cj0559 R	*ACACCAATTG*TTATTTTGCATATGAATTTTCTAG
Primers used to amplify kanamycin cassette	
Kan F	ATTCTCCTTGGTTCTCATGTTTGACAGCTTAT
Kan R	GCACACCTTGGCTAGGTACTAAAACAATTC

Colored sequences in overexpression and protein-protein interaction sections are restriction sites (green is NdeI restriction site, blue is XhoI restriction site, purple is XbaI restriction site, grey is KpnI restriction site and pink is KpnI restriction site). Colored sequences in knock out section are adaptors corresponding to pGRM3zf vector (red) and corresponding to kanamycin antibiotic resistant cassette (yellow).

2.2.5 Agarose gel electrophoresis

Agarose gel used to run PCR products was made by dissolving 1 g agarose in 100 ml TAE (1 mM EDTA, 40 mM Tris-acetate pH 8.0) buffer. To dissolve the agarose, the mixture was heated by microwave. To check the size of PCR

product, 1 kb DNA hyperladder-1 (Bioline) was used. Ethidium bromide (0.1 µg ml^{-1}) was added to the gel so that the DNA can be visualized in ultraviolet light. 12-20 µl from samples were loaded into the gel wells to separate them by electrophoresis (Bio-Rad Powerpac 300) using a constant voltage of 100 V for 35-45 minutes.

2.2.6 Agarose gel extraction

PCR products in some cases after purification may not be adequately pure to progress with more cloning steps. The total volume of the sample of 1 % agarose gel was prepared, loaded and run as describe above. The visualization of The DNA was carried out under UV light and the specific bands were excised by using a scalpel. Then, the gel slice that contains the gene that we are interested in was purified by using a Gel Extraction Kit (Qiagen).

2.2.7 Digestion of DNA with restriction enzymes

PCR products and the plasmid were digested with enzyme according to the manufacturer's instructions. For overexpression cloning, 1000 ng of pET-21a /pET-28a plasmid and 500 ng of the target gene were double digested with 0.5 µl NdeI and 0. 5 µl XbaI in 2 µl CutSmart buffer and the mixture incubated at 37 °C for 1 hr. 1 µl rSAP (alkaline phosphatase) was added to the plasmid. After 1 hr restriction enzymes were heat inactivated at 60 °C for 20 minutes. For mutations, 1000 ng of pGEM3Sf(-) plasmid was single digested with 1 µl HincII in 2 µl CutSmart buffer (NEB). 1 µl rSAP was added to the plasmid to prevent religation. After 1 hr HincII enzyme heat inactivated at 80 °C for 20 minutes. For complementation, 1000 ng of pRRA plasmid and 500 ng of targeted gene was double digested with 0.5 µl MfeI and 0.5 µl XbaI in 2 µl CutSmart. The mixture was incubated at 37 °C for 1 hr. 1 µl rSAP was added to the plasmid. After 1 hr restriction enzymes were heat inactivated at 80 °C for 20 minutes. All reactions were made with a final volume of 20 µl with dH_2O. Digested products were cleaned from enzymes and buffers by QIAquick PCR Purification Kit (Qiagen). Concentration of the products was measured and stored at -20 °C.

2.2.8 PCR product clean up

By using Qiagen QAIquick PCR purification kit, digested plasmids and PCR products were purified by as follows:

1- 750 µl of Buffer PB was added to PCR products and vortexed for 10 seconds.
2- The mixture was transferred to a QIAquick column (Qiagen) and centrifuged at 12,000 x g for 1 minute.
3- After emptying the collection basket, QIAprep spin column was washed with 750 µl Buffer PE (Qaiagen) by centrifuging at 12,000 x g for 1 minute.
4- Again collection basket was emptied and column was centrifuged for 1 minute.
5- The QIAprep spin column was placed in a new 1.5 ml eppendorf tube, and digested plasmid eluted with 50 µl of Nuclease-Free Water.

2.2.9 Alkaline Phosphatase Treatment

In order to prevent self-ligation of blunt sticky ends, Shrimp Alkaline Phosphatase rSAP (NEB) was added to digested plasmid to remove the 5` phosphate group.

2.2.10 DNA Ligation

In order to add the insert and vector in molar ratio of insert to vector: 1: 1, 3: 1, 5: 1, and 10: 1, DNA concentration was measured by Nanodrop. In a 10 µl reaction the right amount of digested plasmid and insert were added along with 0.5 µl of T4 DNA ligase (NEB) and 1 µl 10 x T4 DNA ligase buffer (NEB). The mixture was incubated at room temperature for 1 hour or overnight at 37 °C.

2.2.11 Isothermal assembly (ISA) cloning

Through the use of an adapted ISA cloning method, one-step synthesis of *C. jejuni* gene-knockout vectors with kanamycin resistance cassettes was carried out (Gibson *et al*. 2009). Primers were used to amplify surrounding regions of a gene with specific 'linker' regions attached (that were homologous to either HincII

digested pGEM3Zf or an antibiotic resistance cassette). The preparation of the 5x isothermal assembly [ISA] buffer (500 mM Tris-HCl pH 7.5, 100 mM dGTP, 100 mM dCTP, 50 mM $MgCl_2$, 100 mM dATP, 25 % (w/v) polyethylene glycol 8000 [PEG-8000], 100 mM NAD, 100 mM dTTP, 50 mM dithiothreitol [DTT]) was done before dividing it into 40 aliquots and storing at -20 °C. For the preparation of ISA reaction master mix, 0.125 µl T5 Exonuclease, 20 µl Taq ligase (NEB), and 2.5 µl Phusion polymerase (NEB) were added to a 40 µl aliquot of ISA buffer before making it up to 150 µl with dH_2O. After amplification the antibiotic resistance cassette and the two-gene fragments (designated left flank (LF) and right flank (RF) were PCR purified. This was followed by the digestion of the cloning vector pGEM3ZF with HincII. Then, digested vector was treated with rSAP. Each fragment (LF, RF, resistance cassette, pGE3ZF/HincII) of between 10 ng and 100 ng was used to prepare an equimolar mixture. 5 µl of this mixture was added to 15 µl of ISA reaction buffer and then incubated at 50 °C for 1hr. Then, *E. coli* DH5α was directly transformed with the mutagenesis vector mixture. The transformation of competent *C. jejuni* was done after confirmation using different combinations of KanR, LF and RF primers.

2.3 Plasmids

2.3.1 Plasmid isolation

E. coli DH5α was used to propagate the plasmid before isolating them by Qiaprep® Spin Miniprep Kit (Qiagen).

2.3.2 Plasmids used in this study

Table 2.3: Plasmids used in this study

Plasmid	Description	Resistance markers	Source
pGEM®3Zf(−)	Standard cloning vector used for mutagenesis. MCS I frame with *lac* operon to allow blue/white selection.	Amp^R	Promega

pET-21a(+)	Over-expression plasmid containing the IPTG inducible T7 promoter. Used to over-produce and purify proteins with a C-terminal His tag.	Car^R	Novagen
pET-28a	Over-expression plasmid containing the IPTG inducible T7 promoter. Used to over-produce and purify proteins with a N-terminal His tag.	Car^R	Novagen
pJMK30	Cloning vector containing the *aph*AIII gene encoding kanamycin resistance	Amp^R, Kan^R	(van Vliet *et al*., 1998)
pGEMcj0559	pGEM-3Zf(−) containing *cj0559* gene fragment interrupted with kanamycin resistance cassette	Amp^R, Kan^R	This study
pGEMcj0537	pGEM-3Zf(−) containing *cj0537* gene fragment interrupted with kanamycin resistance cassette	Amp^R, Kan^R	This study
pRRA	Group of vectors for complementation of *C. jejuni* mutants by insertion at the cj0046 pseudogene locus	Apr^R	Cameron *et al*., 2014
pETcj1382	pET-21a containing the *cj1382* gene with no stop codon inserted at NdeI/XhoI restriction sites	Car^R	This study
pETcj1382	pET-21a containing the *cj1382* gene with stop codon inserted at NdeI/XhoI restriction sites	Car^R	This study
pETcj1575c	pET-21a containing the *cj1575c* gene with no stop codon inserted at NdeI/XhoI restriction sites	Car^R	This study
pETcj1574c	pET-21a containing the *cj1574c* gene with no stop codon inserted at NdeI/XhoI restriction sites	Car^R	This study
pETcj0559	pET-21a containing the *cj0559* gene with no stop codon inserted at NdeI/XhoI restriction sites	Car^R	This study
pETcj1573c	pET-21a containing the *cj1573c* gene with no stop codon inserted at NdeI/XhoI restriction sites	Car^R	This study
pETcj0231	pET-21a containing the *cj0231* gene with no stop codon inserted at NdeI/XhoI restriction sites	Car^R	This study
pETcj0024	pET-21a containing the *cj0024* gene with no stop codon inserted at NdeI/XhoI restriction sites	Car^R	This study

pETcj0231	pET-28a containing the *cj0231* gene with no stop codon inserted at NdeI/XhoI restriction sites	Car^R	This study
pKT25cj1382	pKT25 containing the *cj1382* gene cloned into XbaI/KpnI sites	Kan^R	This study
pUT18cj1574c	pKT25 containing the *cj1382* gene cloned into HindII/KpnI sites	Amp^R	This study
pUT18cj1575c	pKT25 containing the *cj1382* gene cloned into HindII/KpnI sites	Amp^R	This study

2.4 Manipulation of *E. coli*

2.4.1 Growth of *E. coli*

E. coli strains were obtained from frozen stocks and grown on LB plates and in LB broth containing appropriate antibiotics. The media was incubated overnight at 37 °C under aerobic conditions with liquid cultures incubated on shaker at 250 rpm.

2.4.2 Growth measurement by spectrophotometer

Optical density (OD) was used for measuring culture growth in liquid media with a Jenway 6705 UV spectrophotometer at 600 nm wavelength (OD_{600}) against control media. 1 ml plastic cuvettes were used for measurement.

2.4.3 Preparation of competent *E. coli*

In order to make competent *E. coli,* two chemical solutions, RF1 and RF2 were prepared (Hanahan, 1983).

The recipes of RF1 and RF2 are:

Table 2.4: The recipes of RF1 and RF2. The solutions used to make competent cells.

Component	Final concentration	Mass in g in 50 ml dH_2O
RF1 pH 5.8		
Potassium chloride KCl	100 mM	0.373
Manganese (II) chloride tetrahydrate $MnCl_2\,4H_2O$	50 mM	0.495
Potassium acetate CH_3COOK	30 mM	0.147
Calcium chloride $CaCl_2\,2H_2O$	10 mM	0.0735
Glycerol	15 %	7.5 ml
RF2 pH 6.8		
MOPS	10 mM	0.105
Potassium chloride KCl	10 mM	0.0375
Calcium chloride $CaCl_2\,2H_2O$	75 mM	0.55
Glycerol	15 %	7.5 ml

In 100 ml, LB *E. coli* was grown to OD_{600} 0.5. These cells harvested by centrifugation at 6000 x g for 20 minutes at 4 °C. Pellet was resuspended by pipetting in ice-cold 50 ml RF1.The cells incubated on ice for 15 minutes before harvesting the cells by centrifugation at 6000 x g for 20 minutes at 4 °C. Pellet was resuspended by pipetting in ice-cold 8 ml RF2. The Cells were incubated on ice for 20 minutes before dividing them into 20 x 400 µl aliquots and stored at – 80 °C.

2.4.4 Transformation of competent *E. coli*

Before the addition of either 10 ng (pure plasmid) or 5 ng (ligations and ISA products) of DNA, a 50 µl aliquot of competent *E. coli* cells was thawed gently on ice. The mixture was incubated on ice for 20 minutes, followed by exposing the mixture to heat shock at 42 °C for 1.5 minute, and then ice for 2 minutes. Cells were recovered by adding 800 ul of LB prior to incubation at 37 °C with shaking for 60 minutes. Cells were plated on LB agar supplemented with selective antibiotics. The incubation of the plates was carried out at 37 °C overnight or until

sufficient colony growth was seen. Alongside experimental ligations reactions, positive control undigested vector and negative no insert controls were also conducted.

2.5 Manipulation of *C. jejuni*

2.5.1 Preparation of competent *C. jejuni*

The preparation of competent *C. jejuni* started by re-suspending 1 day-old plate into 1 ml of wash buffer which was then pelleted by centrifugation (11000 rpm, 5 min, 4 °C). Again, it was re-suspended in 1 ml ice-cold *Campylobacter* wash buffer (15 % (v/v) glycerol, 9 % (w/v) sucrose) before pelleting by centrifugation (11 000 rpm, 5 minutes, 4 °C). This washing step was done again thrice. On the final repeat, the cells were re-suspended in 300 µl wash buffer. Competent cells were used instantly or stored at -80 °C**.**

2.5.2 Transformation of competent cells by electroporation

An *E. coli* gene *pulser* (Bio-Rad) was used for cotransformation in two hybrid system experiments. 2000-1000 ng of each plasmid (pKT25, pUT18) was added to 100-200 µl of competent *E. coli* BTH101. The mixture was transferred into an electroporation cuvette that had been stored at -20 °C (Bio-Rad). This electroporation cuvette was kept on ice before being electroporated at 2.5 kV. Cells were recovered by adding 100 µl of fresh LB broth to the cuvette, and after that plated on either MacConkey + maltose or LB + X-gal and incubated 30 °C or 37 °C for 36-40 hr. The same procedure was used to transform competent *C. jejuni* with mutagenesis plasmids. 100-1000 ng of mutagenesis plasmid was added to freshly made or thawed on ice competent wild type *C. jejuni* and transferred to electroporation cuvettes. After electroporation, cells were plated on non-selective Columbia blood agar. This was followed by microaerobic incubation of the plates overnight at 42 °C before harvesting the cells. The cells were pelleted by centrifugation and then re-suspended in 300 µl MH broth. This was plated on three columbia blood agar plates supplemented with selective

antibiotics. The selective plates were incubated microaerobically at 42 °C for 2-4 days until distinct colonies formed. Colonies were harvested, screened by colony PCR with different combination primers and subcultured onto new selective blood agar plates. Successful mutants were marked on to individual selective plates and glycerol stocks stored at -80 °C.

2.5.3 Growth of *C. jejuni*

A MACS growth cabinet (Don Whitley Scientific, Shipley, UK) was set to microaerobic conditions [10 % (v/v) O_2, 5 % (v/v) CO_2, and 85 % N_2] for growing *C. jejuni* strains at 42 °C. Bacterial cells were obtained from frozen stocks (-80 °C) and streaked on Columbia plates containing the appropriate antibiotics. The plates were incubated overnight in the MACS growth cabinet. 50-100 ml MHS broth was inoculated using these plates. MHS broth cultures were incubated on a shaker at 150 rpm in the MACS cabinet for 6-12 hr depending on the growth stage required for each particular assay. Culture growth was monitored on 1-3 hourly basis by measuring OD_{600} and comparing it against relevant control (blank) media. The starting OD_{600} was usually adjusted to 0.1 depending on the requirement of the particular assay. MHS was routinely added with 10 μg ml^{-1} of vancomycin and amphotericin B each.

2.6 Protein manipulation

2.6.1 Overexpression Optimization of Soluble Proteins using pET21a

To optimize overexpression, 4 x 100 ml LB broth batches containing carbenicillin 50 μg ml^{-1} in four 250 ml flasks were inoculcated by a starter culture that was incubated at 37 °C overnight. Cells were grown in all 4 flasks at 250 rpm up to OD_{600} 0.5. Different overexpression conditions were tested; two concentrations of IPTG (0.1 mM and 0.4 mM) and two temperatures (25 °C and 37 °C). 1 ml and 10 ml samples were taken at times 0, 1, 3, 5, and 24 hr. 1 ml samples were centrifuged at 12000 x g for 5 minutes and then resuspended in 20 μl dH_2O (insoluble protein). 9 ml samples were centrifuged at 12000 x g for 5 minutes and

resuspended in 300 µl 10 mM Tris HCl pH 7.4 (soluble protein). The samples were stored at -20 °C. In order to check protein solubility, the soluble samples were prepared as cell free extraction (CFE) by sonication 4 x 20 seconds (Soniprep 150) with 16 µM amplitude sound waves. To avoid overheating the sample, they were kept on ice. In 0.5 ml tube, all samples were prepared as 1:1 (20 µl protein + 20 µl loading dye) and boil them for 3 minutes. Before loading samples were spun at 15000 x g for 5 minutes.

2.6.2 Purification of Recombinant Proteins by Nickel Affinity Chromatography

E. coli BL-21 (pET XXX) cells were cultured in LB with carbenicillin (50 µg ml^{-1}) followed by induction with 1 mM IPTG at OD_{600} as described above. The requirements needed to accomplish maximum yield of soluble protein were dependent on time, temperature and total volume. Through centrifugation (10000 x g, 10 minutes, 4 °C), the harvesting of cells was carried out and cells were re-suspended in binding buffer (20 mM phosphate buffer pH 7.4, 0.5 M NaCl, 20 mM imidazole [Sigma]) before cell disruption by sonication (MSE Soniprep, 16 rpm, 6 x 1 seconds bursts). The soluble and insoluble proteins were separated by centrifugation (20000 x g, 20 minutes, 4 °C). The CFE, consisting of the soluble fraction, was filter-sterilised (0.2 µm pore size) to separate any cell fragments from it. After that the filter-sterilised CFE was kept on ice for further purification steps. For every litre harvested, the total volume of cells re-suspended in binding buffer was less than 20 ml.

The filter-sterilised CFE comprising soluble His-tagged recombinant protein was pumped onto a 5 ml-HisTrap HP column fixed to an AKTA Prime Protein Purification System. The elution of the recombinant protein was followed by washing of the column with elution buffer (20 mM phosphate buffer, pH 7.4, 0.5 mM NaCl, and 0.5 M imidazole). There was a variation between each recombinant protein studied in the concentration of imidazole required to fully inhibit the binding of the His-tag to the HisTrap column. The purity of the

recombinant protein was verified by using SDS-PAGE. By centrifugation through the use of Vivaspin (Sartorius Stedim) spin columns and a molecular weight cut off (MWCO) of at least 50 % smaller than the protein, the purified recombinant proteins were concentrated.

2.6.3 Protein concentration determination

UV absorbance measurement was used to determine the concentration of the purified protein with a UV-Vis spectrophotometer UV2401 (SHIMADZU). The following formula was applied to calculate the concentration, where A is the light absorbance at a specific wavelength and ε is the molar extinction coefficient of the protein. The extinction coefficient of the protein was determined from the amino-acid sequence using the ProtParam tool at the ExPASy website.

$$\text{Protein concentration (M)} = \frac{A_{280} - A_{320}}{\varepsilon\ (M^{-1}\ cm^{-1})}$$

2.6.4 Protein concentration measurement by Lowry assay

For protein concentration of whole cells or crude extracts, the Lowry assay was performed in 96-well plates with Bovine serum albumin or BSA as standard protein. Stock solutions of solution A and solution B were stored until needed for the test, while solution C and Folin–Ciocalteu Phenol or FCP reagent was freshly prepared for the test. Recipes for the reagents are as follows:

Solution A (in dH_2O)	
Sodium carbonate	2 %
Sodium hydroxide	0.4 %
Sodium tartrate	0.16 %
SDS	1 %

Solution B (in dH_2O)	
Cupric Sulfate ($CuSO_4$)	4 %

Solution C and Folin- Ciocalteau Phenol (FCP) reagent was made fresh on the day. By mixing 100 parts of A and 1 part of B Solution C was made and by diluting 2N reagent with equal volume of dH_2O FCP was made. BSA was prepared by dissolving it in 10 ml distilled water. The solution was then diluted 100 times and filtered using a 0.2 µm filter. The final concentration obtained was 100 µg ml^{-1}. 6 different concentrations of BSA were prepared to obtain a standard curve (100, 80, 60, 40, 20 and 0 µg ml^{-1}). Each protein sample was diluted 100 times with distilled water in eppendorfs to a minimum of 200 µl. The reaction was carried out in triplicate using 96-well flat-bottom plates. First, 50 µl of all concentrations of BSA (standard protein) and diluted samples were added to plates. 150 µl of solution C was added to all wells containing protein standards and samples. The mixture was incubated for 1 hr at room temperature. Then, 15 µl 1 x FCP reagent was added to each well and incubated for 45 minutes at room temperature. The absorbance of wells was noted at 600 nm with a 96-well plate reader. Protein concentration in samples was calculated with their absorbance using BSA standard curve.

2.6.5 Protein visualization by Sodium dodecyl sulphate polyacrylamide gel electrophoresis (SDS-PAGE)

SDS-PAGE was utilized to visualize protein samples. SDS-PAGE was carried out through the use of BioRad MiniProtean system; assembled gels were made by diluting 30 % (w/v) acrylamide 0.8 % (w/v) bisacrylamide solution (Sigma) to 12 % acrylamide and adding 1 M Tris-HC1 pH 8.8 and 0.1 % (w/v) SDS. This was followed by initiation of polymerisation by gently mixing this solution and by addition of 0.1 % (w/v) ammonium persulphate and 0.01 % (w/v), 1 % (TEMED) (Sigma). Stacking gels (6 % acrylamide (w/v), 1 M Tris-HC1 pH 6.8, 0.1 % (w/v)

SDS, 0.1 % (w/v) ammonium persulphate, 0.01 % (w/v) TEMED) were made. Then, they were transferred by pipette on top of the resolving gel. This was followed by insertion of a comb without leaving air bubbles, and the gel was allowed to set before immediate use. The gels that were not used were wrapped in dH_20-soaked paper towel and covered in cling film before storing them at 4 °C.

To prepare loading dye (60 mM Tris-HCl pH 6.8, 2 % (w/v) SDS, 0.5 ml of 0.1 (w/v) bromophenol blue, 5 % (w/v) 10 % (v/v) glycerol), *β*-mercaptoethanol [Sigma] adding just before using the loading buffer so the loading buffer can be used for long time. In 10ml universal tube, 8.5 ml of 60 mM Tris HCl pH 6.8 + 200 mg SDS + 0.5 ml of 0.1 % (w/v) bromophemol blue + 1 ml of 100 % glycerol were mixed to prepare 10 ml of loading buffer. By mixing the same volume of protein with loading buffer (20 µl + 20 µl) and boiling for 5 minutes, the protein samples were prepared, and then loaded. The concentration of the sample determined the volume of each sample to be loaded on the gel. Loading volumes used for insoluble samples from protein overexpression trials was (0 hr: 10 µl, 1 hr: 9 µl, 3 hr: 7.5 µl, 5 hr: 6 µl, 24 hr: 4 µl) and for soluble samples (0 hr: 20 µl, 1 hr: 18 µl, 3 hr: 15 µl, 5 hr: 12 µl, 24 hr: 8 µl). The loading of samples was carried out alongside a molecular weight standard, Unstained Protein Molecular Weight Marker (Thermo Scientific). Protein gels were subjected to electrophoresis at 50 V 50 minutes and 180 V till the trailing dye got to the base of the gel. Visualization of protein bands was performed by first submerging and incubating the gel in stain with gentle rocking for at least an hour, before transferring it to the destain and incubating with mild swinging until protein bands were fully clear. Running buffer 10x prepared as follows: Tris base 30 g L^{-1} + glycine 144g L^{-1} + SDS 10 g L^{-1}.

2.6.6 Protein dialysis

For salt removal from proteins, dialysis was performed using an 8 kDa mw cut off dialysis bag. The protein solution was added to the bag and 1.5 L of cold dialysis

buffer (50 mM Tris-HCl buffer, pH 7.5; 100 mM NaCl) was used for dialysis. The dialysis bag was placed in dialysis buffer for 2 hr, and then again for 16 hr.

2.6.7 Protein unfolding and refolding with urea

For attempts to remove the extremely stable NrdB tyrosyl radical, unfolding the protein was done using an 8 kDa molecular-weight cut-off dialysis bag. The dialysis was carried out against 1 L of cold unfolding buffer, consisting of 50 mM Tris-HCl buffer pH 7.5, 100 mM NaCl, and Urea 5 M, for 15 hr. Also, unfolding-refolding using the AKTA prime system with a HisTrap column was used, here the 5 M Urea was added to elution buffer without adding EDTA that would chelate the metal in the column. In both cases, the protein precipitated.

2.6.8 Tyrosyl radical removal

For tyrosyl radical removal from NrdB, there were unsuccessful attempts including; high concentration of urea, urea + EDTA, hydroxyurea, hyroxyurea + EDTA. The tyrosyl radical was succesfully quenched by using 1 mM hydroxylamine with incubation for 30 minutes at room temperature, followed by dialysis or buffer exchange. Any residual hydroxylamine was detected by adding a mixture of 8-hydroxyquinoline and sodium carbonate that was made just before use. 10 μl of the mixture was added to treated NrdB and heated for 90 °C for 1 minute. Green color indicates the presence of hydroxylamine.

2.6.9 Sitting drop crystallization trials

Purified and dialyzed protein (NrdB) was concentrated to at least 10 mg ml^{-1}, and tested against screen buffers PACT, JCSG, and Proplex (Qiagen). 96 well 2-Drops Sitting Drop crystallization plates were used. 50 µl of buffer was added to the side well. Using a Matrix_Hydra II Plus One crystallization robot, 100 nl of protein (134 µM NrdB) were added to the same volume of mother liquor in sitting drop vapor diffusion experiments. The plate was covered and kept in a 4 °C room. A Matrix_Hydra II Plus One crystallization robot was used because the amount is too small to withdraw with micropipettes.

2.6.10 Hanging drop vapor diffusion protein crystallization

96 well plates from the crystallization trial were checked to determine favorable conditions. Then, 24 well plates (VDX plate) were used for growing protein (macromolecular) crystals. 3 µl of protein was added to 3 µl of precipitant solution on siliconized cover slip hanging against 100 µl of precipitant solution. Grease was placed around the well to seal it.

2.6.11 Mass-Spectrometry of NrdB

When NrdB was purified, two bands were consistently seen. To determine whether this was due to contamination, degradation of the protein or a Post-translational modification (PTM), the two bands from the gel were cut and chopped into small pieces to increase the surface area. The gel was initially de-stained in 500 µl acetonitrile1:1 $(NH_4)_2 CO_3$ buffer (ammonium bicarbonate 100 mM, pH 8.0). After the supernatant was pipetted off carefully, the gel pieces were washed thrice with 500 µl of acetonitrile1: 1 $(NH_4)_2 CO_3$ buffer for 5 minutes each time. In the final dehydration, the gel pieces were incubated with 500 µl acetonitrile for 10 minutes. 200 µl of 50 mM TCEP in $(NH_4)_2 CO_3$ buffer was added to reduce cysteines and incubated for 20 minutes at a temperature of 70 °C. After discarding the supernatant and cooling down the gel pieces, cysteines were acetylated by adding 200 µl of 50 mM Iodoacetamide in $(NH_4)_2CO_3$ buffer, incubating with shaking in the dark. Gel pieces were washed and dehydrated as before.

Then, the protein was digested by trypsin. To do so, the gel pieces were incubated in 200 µl of 1 ng μl^{-1} trypsin in $(NH_4)_2CO_3$ buffer overnight at a temperature of 37 °C. 100 µl of acetonitrile was added the next day and gel pieces were incubated for 15 minutes at a temperature of 37 °C. The digested peptides were released in the supernatant and collected in a separate tube. 50 µl of 0.5 % formic acid was added to the gel pieces and incubated on a shaker for 15 minutes. Then 100 µl of acetonitrile was added to the gel and incubated for an additional 15 minutes. The supernatant was transferred to the collection tube and

the extraction with formic acid and acetonitrile was repeated. Finally, the supernatant was incubated with 100 µl of acetonitrile shaking for 15 minutes resulting a final volume of 700 µl of digested peptides in the collection tube. A SpeedVac concentrator was used to dry the peptides. To analyse the peptides via HPLC-MS, the pellet was resuspended in 40 µl 0.5 % formic acid. 20 µl of peptide solution transferred to a vial and analysed as below by the “Biological Mass Spectrometry Facility” Sheffield University.

By using a Dionex Ultimate 3000 system (ThermoFisher Scientific) equipped with an Acclaim™ PepMap™ 100 C18, 20 mm x 75 µm trap column (3 µm, 100 Å,) and an EASY-Spray™ C18, 150 mm x 50 um (2 µm, 100 Å) analytical nano-column, HPLC was done at 45 °C. Mobile phase A consisted of 0.1 % formic acid in water and mobile phase B consisted of 0.1 % formic acid in 80 % acetonitrile as gradient that separated the peptides for 45 minutes. The gradient was done at a flow rate of 250 ml min^{-1} as follows: 0-5 minutes at 4 % B, then two steps of linear increase first 40 % B for 40 minutes, second 90 % B for 50 minutes. A LTQ Orbitrap Elite (Thermo Scientific) hybrid ion trap-orbitrap mass spectrometer, an EASY-Spray source (Thermo Scientific) and an EASY-Spray source (Thermo Scientific) with an ion transfer capillary at 250 °C and a voltage of 1.8 kV were equipped together. MS survey scans in positive ion mode were acquired in the FT-orbitrap analyzer using a m/z window from 375 to 1600, a resolution of 60´000, and an automatic gain control target setting of 1 x 106. Using collision induced dissociation (CID), 20 most intense precursor ions were selected for the acquisition of tandem mass spectra in the dual cell linear ion trap at normal scan rate. Charge states 1+ were not including for precursor selection. Normalized collision energy was set to 35 %, activation time to 10 ms, isolation width to 2 m/z, and automatic gain control value was set to 1 x 104. Identification of peptides/proteins was performed by MaxQuant search with default parameters. Protein sequences were downloaded from Uniport Proteomes and from a database including the theoretical sequences of the expressed proteins. For further studies, identification findings were saved in an excel file.

2.6.12 Bacterial Two-Hybrid system

Using Bacterial Adenylate Cyclase-based two-hybrid system (BATCH), the interaction between NuoX/NuoY proteins against Flavodoxin (FldA) was investigated. NuoX, NuoY and Flavodoxin genes were amplified using primers listed in Table 2.2. *nuoX* or *nuoY* genes were inserted into pKT25 plasmid digested with XbaI and KpnI. *fldA* was inserted into pUT18 plasmid digested with HindIII and KpnI. As a result, each *nuoX/nuoY* gene was cloned as an in-frame fusion at the *C*-terminal end of T25 in pKT25 plasmid and *fldA* was cloned as an in-frame fusion at the N-terminus end of T18 in pUT18. After plasmids were propagated in *E. coli* DH5α, they were purified using Qiagen miniprep kit. These plasmids were used to cotransform competent *E. coli* BTH101. *E. coli* BTH101 is a reporter strain that is used as host for detection of protein-protein interactions. Transformed cells were then plated on LB agar medium containing appropriate antibiotics and incubated at 37 °C overnight. After successful electroporation, one colony was picked and inoculated into 5 ml LB broth containing appropriate antibiotics and incubated at 37 °C for 18 hr. 10 µl of culture sample was poured onto indicator media plates (LB + X-gal and MacConkey + maltose) with appropriate antibiotics and IPTG for induction. The plates were then incubated at 30 °C for 36 to 40 hr. Noteworthy, the indicator plates should be inoculated with an overnight grown culture not directly from glycerol stock.

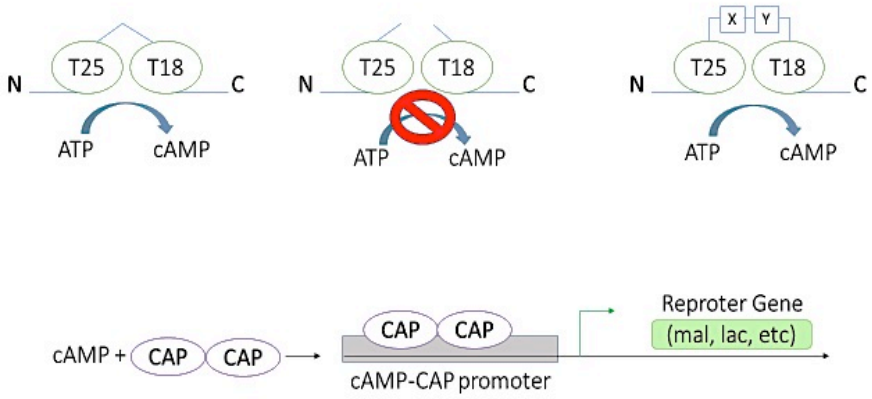

Figure 2.1: A scheme of the two-hybrid BACTH system. In order to generate Cyclic AMP (cAMP) that binds to CAP to allow binding at specific promoter, the catalytic domain fragments of adenylate cyclase from *Bordetella pertussis* should be expressed in *E. coli* BTH101 as a full-length protein and come close enough. This occurs when two genetically fused proteins (X and Y) bind together, leading to a transcription of the reporter gene (Karimova *et al.*, 1998).

2.6.13 *β*-Galactosidase assay

For quantitative measurement of protein-protein interaction, *β*-Galactosidase assay was done. 25 ml of cotransformed *E. coli* BTH101 were grown at 37 °C overnight. For the assay, the OD_{600} for a starter culture was measured and 10 ml LB was inoculated. The 10 ml culture was incubated at 37 °C on a shaker until an optical density of 0.6 to 1.0 OD_{600} was reached. Then, *E. coli* BTH101 were kept on ice and 1 ml was taken and incubated for 10 minutes at 28 °C in a water bath.

	Volume
Transformed cell culture	100 µl
Z-buffer	700 µl
β-Mercaptoethanol	1.89 µl
0.1 % SDS	10 µl
Chloroform	20 µl

These components were added to a new eppendorf tube. After vortexing the mixture for 10 seconds, it was incubated for 5 minutes at 29 °C. Then, the reaction was started by adding 200 µl of Ortho-Nitrophenyl-*β*-galactoside

(ONPG) prepared as follows 4 mg of ONPG dissolved in 1 ml Z-buffer. The reaction was timed, using a stopwatch, and stopped with 500 µl of 1 M Na_2CO_3 when yellow color was observed. After centrifugation of mixture for 3 minutes, the absorbance of supernatant was measured at 420 nm to calculate *β*-Galactosidase activity. This is the formula to work out the activity

$$\frac{\text{A420 nm}}{\text{time(min)} * \text{culture volume(ml)} * \text{OD600}} * 1000$$

To prepare Z-buffer components below dissolved in 1 L dH_2O. pH was calibrated to 7.

	Volume
$Na_2HPO_4.7H_2O$ (0.06 M)	16 g
$NaH_2PO_4.H_2O$ (0.04 M)	5.5 g
KCl (0.01 M)	0.75 g
$MgSO_4.7H_2O$ (0.001 M)	0.246 g
	1 L

2.7 Enzyme Assays

All enzyme assays were conducted by using *C. jejuni* cell-free extract, with pure recombinant protein, or with *C. jejuni* membranes where needed. Reactions were conducted in 1 ml total volume at 37 °C in a UV-240 recording spectrophotometer (Shimadzu). Cell-free extract protein concentrations were evaluated using the Lowry assay.

2.7.1 Preparation of *C. jejuni* cell-free extract

20 ml of MHS flask were inoculated with one-day old plate *C. jejuni* and incubated on a shaker at 150 rpm in the MACS growth cabinet for 12-16 hr. Next day, cells were harvested by centrifugation (10000 g, 4 °C. 5 minutes). Then the pellet was re-suspended in 1 ml N_2 sparged 100 mM Tris-HCl pH 8 + 1 ml O_2 scavenging system. The sonication of the cells was carried out in a MSE Soniprep 150 (3 x 20 seconds bursts, 12 pm amplitude) the 2 ml eppendorf stayed on ice while the cell disrupted. This was followed by the centrifugation for (15000 g, 4 °C, 5 minutes) to remove cell debris and any unbroken cells. The supernatant (CFE) was poured into a sparged tube. The head-space of the tube was sparged as well. Cell-free extracts were kept on ice till they were needed. They were only utilized on the day of production.

All spectrophotometric assays were conducted at 37 °C in a Shimadzu UV-2401 spectrophotometer. The ability of pyruvate and 2-oxoglutarate to act as electron donors to FldA via the action of the POR and OOR enzymes was assayed using cell-free extracts (CFE) of *C. jejuni* prepared under anaerobic conditions as described previously, in the presence an oxygen-scavenging system consisting of glucose oxidase, glucose and catalase (Kendall *et al*., 2014).

In the cuvette:
Coenzyme A 0.2 mM (100 µl of stock)
Thiamine pyrophosphate 0.1 mM (100 µl of stock)
$MgCl_2$ 2 mM (100 µl of stock)
TrisHcl 100 mM pH 8 (530 µl)
FldA 50 µM (100 µl)

The mixture was sparged for 10 minutes, then 50 µl of anaerobic CFE was added and mixed by inversion and the control rate measured for 20 seconds. Then paused, 20 µl substrate added (Pyruvate 5 mM or 2-oxoglutarate 5 mM), mixed by inversion and the rate measured for 180 seconds.

To prepare stock solutions

Table 2.8: Stock solutions used in experments of FldA reductases by pyruvate 5 mM or 2-oxoglutarate.

x10 stock	In 10 ml 100 mM pH 8 Tris HCl
20 mM $MgCl2.6H_2O$	40.7 mg
1 mM TPP	4.6 mg
x10 stock	In 5 ml 100 mM pH 8 Tris HCl
2 mM CoA	7.7 mg
x5 stock	In 5 ml 100 mM pH 8 Tris HCl
250 mM Pyruvate	138 mg
250 mM 2-oxoglutrate	283 mg
x1000 Enzyme stock	in 1 ml of 10 % glycerol
Glucose Oxidase	50 mg
Catalase	10 mg
O_2 scavenging system	in 5 ml 100 mM pH 8 Tris HCl
10 % w/v glucose	500 mg
50 µg ml^{-1} glucose	5 µl of 1000x stock
10 µg ml^{-1} catalase	5 µl of 1000x stock

2.7.2 Total membrane protein extraction from *C. jejuni*

500 ml of MHS were inoculated from a one-day old plate. Next day, the cells were harvested by centrifugation (5000 g, 4 °C, 30 minutes). The pellet was gently resuspended in 20 ml of ice cold 20 mM Na Phosphate buffer. Then, the cells disrupted by French press x 3. After centrifugation at 15000 g, 4 °C, 30 minutes the supernatant contains cell free extract including membranes. The CFE was then transferred to ultracentrifuge tubes filled completely and the tubes were then balanced precisely within 0.01 g. Samples were then centrifuged at 100,000 x g, 4 °C for 1 hr in a benchtop ultracentrifuge (Beckman). After the supernatant was discarded carefully, the pellet was resuspended in 1 ml 25 mM phosphate buffer (pH 7.4) with gentle pipetting. The suspension was then transferred to a glass homogeniser and homogenized gently. The homogenised

total membrane protein solution was stored at -80 °C and protein concentration was measured by Lowry assay.

2.7.3 Measurement of respiratory enzyme activity by Clark-type oxygen electrode

By centrifuging (10000 x g, 4 °C, and 10 minutes), *C. jejuni* cells were washed thrice and re-suspended in 3 ml of 25 mM pH 7.5 phosphate buffers after the final washing and kept on ice. Through the use of the Lowry assay, protein concentration was evaluated (Martell *et al*. 1978)**.** Then, the oxygen consumed by the cell suspension or membranes reduced by NADPH + FqrB was measured in a Clark-type oxygen electrode (Rank Brothers). The electrode was calibrated through the use of sodium dithionite for the zero reading and air-saturated 25 mM pH 7.5 phosphate buffer for the maximum reading. The electrode chamber was kept at a temperature of 37 °C and mixed at a constant rate. Before adding substrate (5 mM pyruvate, 5 mM 2-oxoglutarate or 10 mM sodium formate), cell suspension (between 10 and 100 µl) was added to 2 ml air-saturated buffer in the electrode chamber. The electrode was washed with saturated KCl and excess KCl was absorbed using cigarette paper. A square shaped semipermeable membrane, which was only permeable to gases, was placed on the electrodes. The apparatus was assembled to make it air-tight using rubber rings. The water circulating the assembly was kept at a constant temperature throughout the oxygen consumption process. Hamilton syringes were used to inject in 50 µl of cell suspension.

2.8 Phylogenetic analysis

Protein sequences were obtained from Uniprot. Multiple sequence alignments were made with CLUSTAL Omega and phylogenetic trees were generated and analysed in JALVIEW, using publicly available software at www.expasy.org.

2.9 EPR spectroscopy

EPR measurements were made with an X-band Bruker EMX EPR spectrometer equipped with a helium flow cryostat (Oxford Instruments). EPR spectra were measured at 10 K at the following instrumental settings: microwave frequency, 9.471 GHz; microwave power, 3.18 mW; modulation frequency, 100 kHz; modulation amplitude, 5 G; time constant, 82 ms; scan rate, 22.6 G/s; single scan per spectrum. The spectra were aquired by Dr Dima Svistunenko at the Biomedical EPR Facility, University of Essex, UK.

2.10 Protein film electrochemistry

Cyclic voltammetry was performed using a three-electrode cell configuration inside a Faraday Cage within a N2-filled chamber (atmospheric oxygen < 5 ppm). The reference electrode was Ag/AgCl (saturated KCl) and the counter electrode a platinum wire. The working electrode was pyrolytic graphite with the edge plane exposed to sample. Preparation of the working electrode was essentially as described by Seagel *et al* (2017). Firstly, the surface was polished with 0.3 μm Al_2O_3 as an aqueous slurry, sonicated, rinsed with Milli-Q water and dried with a tissue. Secondly, 5 μL of 10 mM didodecyldimethylammonium bromide (DDAB) in Milli-Q water was placed on the electrode surface, the electrode covered with a beaker and left to dry overnight at ambient temperature. Finally, the DDAB coated working electrode was taken into the N2-filled chamber and 5 μL of 200 μM flavodoxin (in 50 mM phosphate, 150 mM NaCl, pH 7.5) deposited on the surface. After 20 minutes the working electrode was introduced to the electrochemical cell, which contained an aqueous solution of 50 mM potassium phosphate, pH 7. Cyclic voltammetry was performed with a PGSTAT30 potentiostat (Metrohm Autolab) under the control of NOVA 1.11 software. Measured potentials were converted to values versus SHE by addition of 197 mV.

2.11 ICP-MS

Purifed NrdB samples were added to 1 ml concentrated HNO_3 (65 % v/v), left in acid overnight and then analysed at the University of Sheffield ICP-MS facility.

2.12 Optical spectroscopy

Mediated potentiometric titration monitored by electronic absorbance spectroscopy was performed by the method of Dutton *et al.* (1970) with minor modification. The reductant was sodium dithionite and the oxidant was potassium ferricyanide. The sample contained 50 mM CjFldA in 10 mM potassium phosphate buffer, pH 7.0 with the following mediators each at 10 mM; diaminodurene (E_m +240 mV), phenazine methosulphate (E_m +80 mV), phenazine ethosulphate (E_m +55 mV), juglone (E_m +30 mV), duroquinone (E_m +5 mV), menadione (E_m -70 mV), anthraquinone 2,6-disulphonate (E_m -184 mV), anthraquinone-2-sulphonate (E_m -225 mV). Flavodoxin semiquinone was quantified from the absorbance at 610 nm using an extinction coefficient of 3900 $M^{-1}cm^{-1}$ (Mayhew *et al*., 1969). The plot of semiquinone concentration versus sample potential was fitted to the equation describing two sequential one-electron transfers to a single site:

semiquinone population= $1/(1+ \theta_1+ \theta_2^{-1})$ where $\theta_i = exp\ (39(E- E_i))$,

E is the sample potential and E_1 and E_2 are the reduction potentials for addition of the first and second electron respectively. Equivalent experiments without flavodoxin showed there was negligible spectral change from the mediators at 610 nm for potentials where the semiquinone was observed.

I would like to thank Dr Dima Svistunenko (Director, Biomedical EPR Facility, University of Essex, UK), Prof Nick Le Brun and Dr Justin Bradley (School of Chemistry, University of East Anglia, UK) for obtaining the EPR spectra and advice on sample preparation and EPR interpretation (section 2.9 EPR spectroscopy). Also, I would like to thank Dr Julea Butt of the University of East Anglia for examining the redox properties of FldA (sections 2.10 Protein film electrochemistry and 2.12 Optical spectroscopy).

Chapter 3: The properties and role of Flavodoxin in the food-borne pathogen *C. jejuni* NCTC 11168

3.1. Introduction

C. jejuni is a microaerophile, adapted for growth at low oxygen niches in the host, with most strains unable to grow at atmospheric oxygen levels. Compared to conventional aerobes, *C. jejuni* is unique in utilizing oxidant-labile enzymes in central metabolic pathways, which are critical for growth. In particular, it employs pyruvate and 2-oxoglutarate: acceptor oxidoreductases (POR and OOR), rather than oxygen-stable NAD-linked 2-oxoacid dehydrogenases, to transfer substrate-derived electrons to the respiratory chain (Weerakoon and Olson, 2008; Kendall *et al*., 2014). These enzymes contain Fe-S clusters vulnerable to oxidative damage. The electron acceptor for OOR has been shown to be the flavodoxin FldA (Cj1382), which is the sole flavodoxin encoded in the genome of *C. jejuni* NCTC 11168. Reduced FldA is then thought to be re-oxidised by donation of electrons to the membrane bound Complex I of the respiratory chain (Weerakoon and Olson, 2008).

The complex I (a proton pump) is encoded by a set of 14 genes called *nuo* genes (*N*ADH: *u*biquinone *o*xidoreductase). Twelve out of these 14 genes in *C. jejuni* are conserved as in other bacteria and archaea. However, two of the *nuo* genes, NuoE and NuoF that encode for the NADH dehydrogenase module, are replaced by two novel genes, Cj1575c (*nuoX*) and Cj1574c (*nuoY*), in the genome of *C. jejuni*. NuoX and NuoY are thought to form a docking site for reduced FldA to deliver electrons to the Fe-S clusters of NuoG. While *nuoX* and *nuoY* seem essential as they were reported to be unable to be deleted (Weerakoon and Olson, 2008), it has been possible to make deletions in all the other *nuo* genes (Weerakoon and Olson, 2008), as several other primary dehydrogenases can donate electrons to the menaquinone pool (Taylor and Kelly, 2019). However, it has not been possible to delete the *fldA* gene, suggesting that flavodoxin must have other essential functions in *C. jejuni*.

One essential function that can be suggested for FldA is in isoprenoid biosynthesis via the methyl erythritol phosphate (MEP) pathway. Here, IspG and IspH are Fe-S enzymes that catalyse the last two steps in the formation of the isoprenoid precursors isopentyl pyrophosphate (IPP) and dimethylallyl pyrophosphate (DMAPP); in other bacteria both reactions require reduced flavodoxin as the electron donor (Rhodich *et al*., 2003; Puan *et al*., 2005).

The aim of this chapter is to investigate the biochemical properties of the *C. jejuni* flavodoxin FldA and its possible interaction with Complex I proteins. The redox potentials of purified FldA will be measured using different approaches. Evidence to show that FldA is the electron acceptor for POR will be sought. How FldA interacts with the Nuo complex in the membrane through NuoX/NuoY will be investigated, using both direct protein-protein interaction experiments with purified proteins and the bacterial 2-hybrid system.

3.2. Results

3.2.1 FldA overexpression and purification

The *C. jejuni* FldA is encoded by the *cj1382c* gene. This was cloned into the expression vector pET21a as shown in (Figure. 3.1). The primers used are detailed in Chapter 2 Table 2.2. The cloning results in the formation of a C-terminal 6 x his affinity tag that can be used for purification. FldA was overproduced in *E. coli* BL21 (DE3) after IPTG induction (Figure. 3.2). Solubility trials were carried out at 25 and 37 °C to determine if the overproduced protein was soluble in the cell cytoplasm and folded correctly. A strong band on Coomassie stained gels of ~ 17 kDa corresponding to the size of FldA was observed. Some insoluble protein was observed at both induction temperatures, but there was also a large amount of soluble protein at both 25 °C and 37 °C (Figure. 3.2). It was decided to use induction with 0.4 mM IPTG and induction at 37 °C for 4 hr as the standard induction protocol.

The purification of FldA was achieved by a combination of nickel affinity and hydrophobic interaction chromatography (see Materials and Methods chapter 2 for details). Initial purification on a nickel chelate column resulted in considerable enrichment of the 17 kDa FldA but this was still impure (Figure 3.3.). Further purification on a HIC column resulted in a pure protein as judged by Coomassie blue staining on SDS-PAGE gels (Figure 3.3.).

A) B)

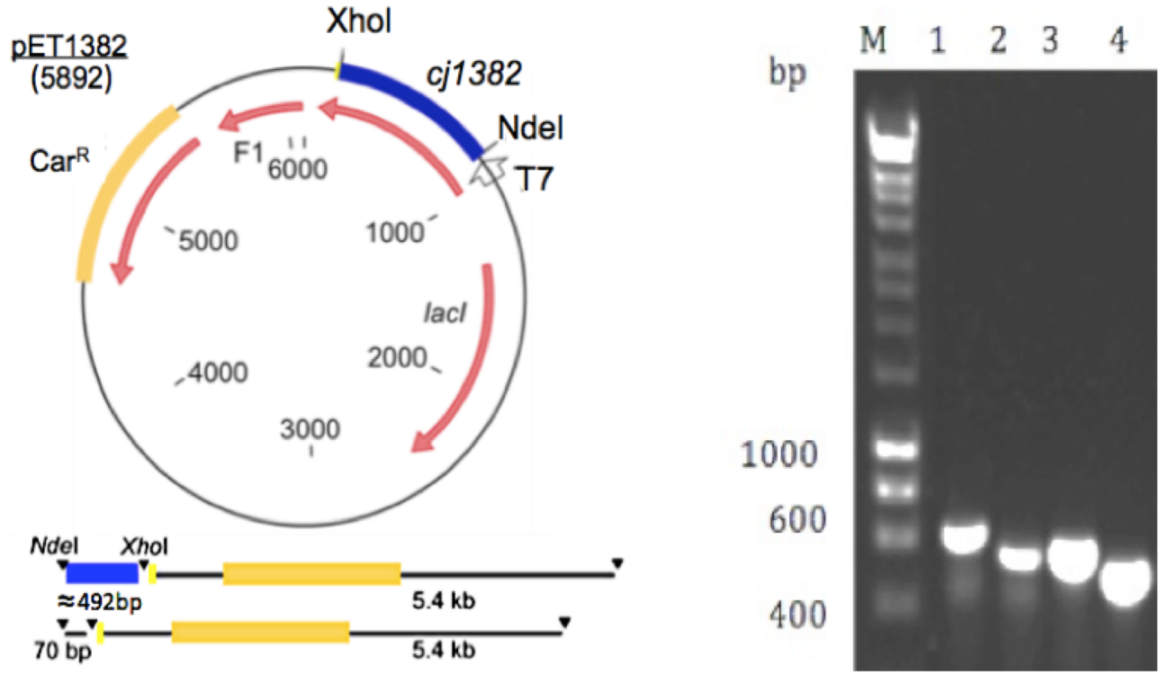

Figure 3.1: Generation of overexpression plasmid pETFldA. **(A)** pETFldA plasmid was made by inserting PCR amplified *cj1382c* between the NdeI and XhoI restriction sites in pET21a. **(B)** The cloning was confirmed by using PCR with different combination of T7 primers and *fldA* primers and the pETFldA as template. Lane1 T7F + T7R. Lane 2 FldAF + T7R**.** Lane 3 T7F + FldAR. Lane 4 FldAF + FldA.

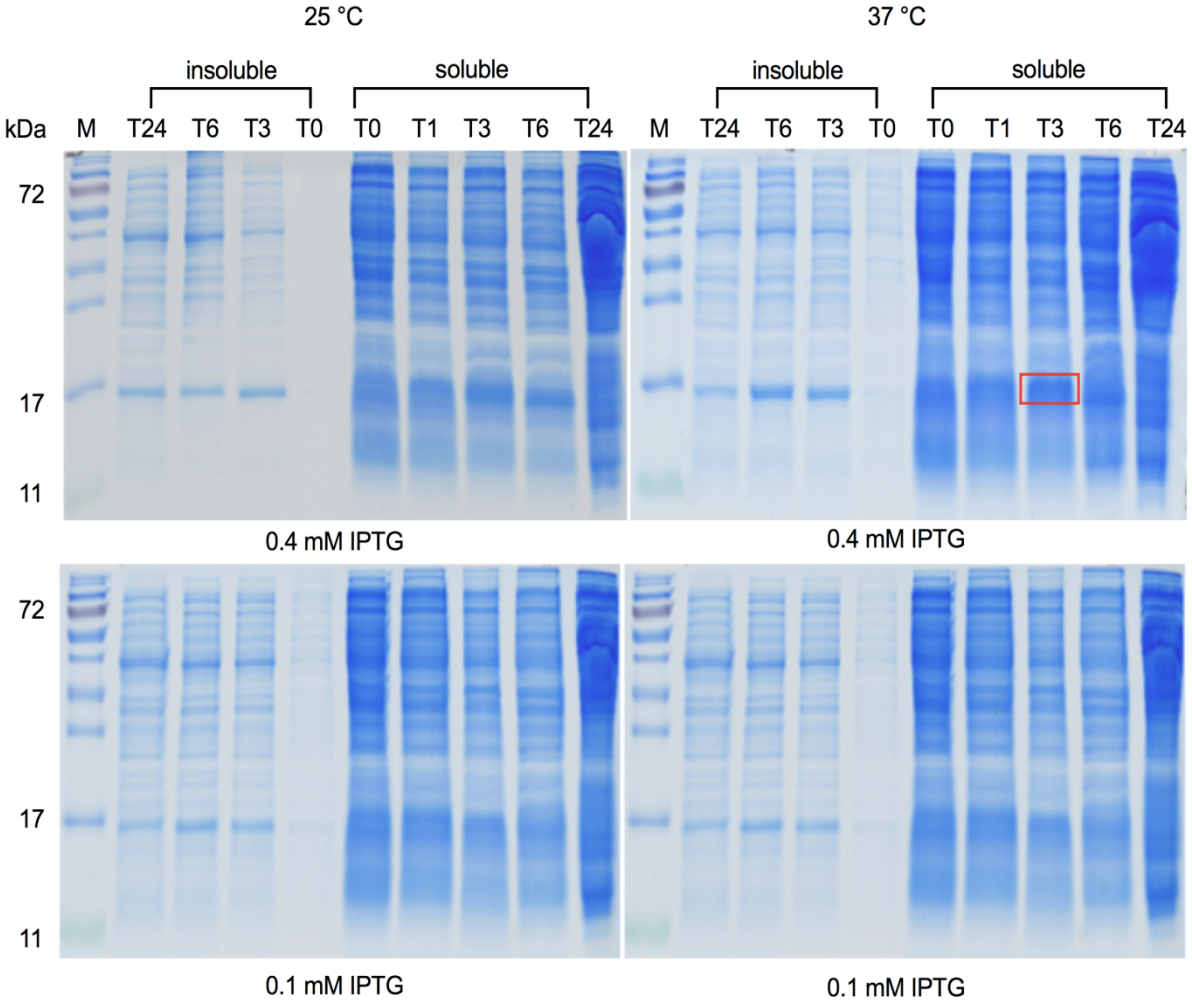

Figure 3.2: Solubility trials of FldA were conducted by culturing the transformed *E. coli* BL-21 in LB with carbenicillin (50 µg ml^{-1}) to an OD_{600} 0.6 before inducing over-expression by the adding 0.1 mM IPTG or 0.4 mM IPTG. At both 25 °C and 37 °C cells were cultured and sampled periodically (T0, T1, T3, T5, T7, T24 hr) to ascertain the optimum temperature and time post-induction for adequate production of protein. These cells were resuspended in binding buffer, sonicated and centrifuged to produce soluble fraction and insoluble fractions resuspended in dH_2O. M = Protein Molecular Weight marker. Protein band in the red box is flavodoxin protein after growing transformed *E. coli* BL-21 in LB with 0.4 mM IPTG at 37 °C for 3 hr (the condition used to overexpress flavodoxin).

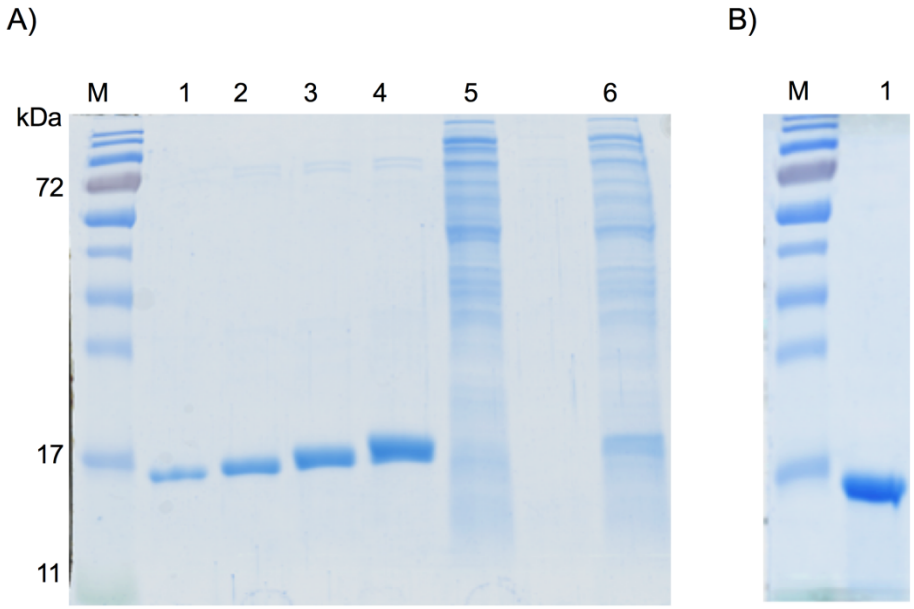

Figure 3.3: Purification of FldA. **(A)** Lane 6 is CFE that was loaded onto the His-trap column. The purification was done in two steps firstly by nickel-affinity chromatography then HIC. Lanes 1, 2, 3 and 4 show the protein peak obtained after elution with imidazole from the his-trap column. Lane 5 is flow through. **(B)** Lane 1 shows protein peak after HIC with elution by a decreasing salt gradient. M = Protein Molecular Weight marker

3.2.2. Optical absorbance and redox properties of the *C. jejuni* flavodoxin FldA

The optical and redox properties of FldA were rexamined in collaboration with Dr Julea Butt of the University of East Anglia. The as-purified, oxidized FldA protein has a typical flavodoxin absorption spectrum (Figure 3.4) with maxima at ~380 and ~460 nm that matched those of a previous study reporting the purification of this protein (Weerakoon and Olson, 2008). The semi-reduced protein was obtained by adding a less than stoichiometric amount of the reductant sodium dithionite; it displays absorbance maxima at ~ 460 nm and ~600 nm that are characteristic of neutral semiquinone (Figure. 3.4). The fully reduced FldA was obtained by addition of excess dithionite (McIver *et al.,* 1998).

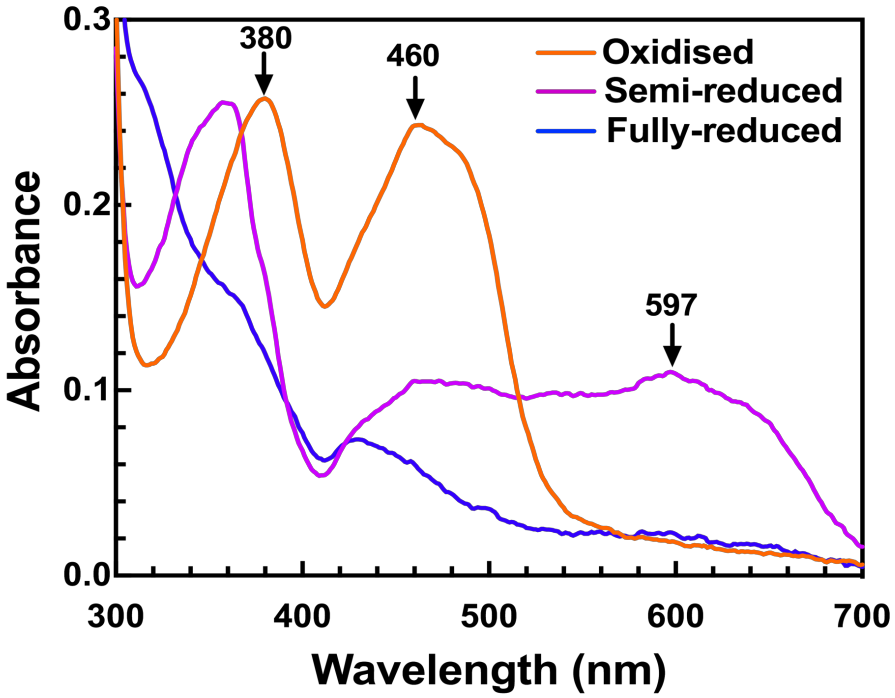

Figure 3.4: Redox properties of the *C. jejuni* flavodoxin FldA. In (A) the electronic absorption spectra of the fully oxidized (orange), semi-reduced (purple) and fully reduced (blue) states of FldA are shown. The spectra were recorded for 50 μM protein in an anaerobic buffer (50 mM potassium phosphate buffer, pH 7.0. Path length = 1 cm). The semi-reduced state was produced by stoichiometric addition of sodium dithionite. Excess dithionite was added to obtain the fully-reduced state. Spectra obtained by Dr Julea Butt, University of East Anglia.

The large changes in the FldA spectra upon reduction were exploited in optically monitored potentiometric titrations (Figure. 3.5), to define the flavodoxin reduction potentials at pH 7. These were determined to be -170 mV vs Standard Hydrogen Electrode (SHE) for the oxidized-semiquinone transition (E_2) and -190 mV vs SHE for the semiquinone-hydroquinone transition (E_1).

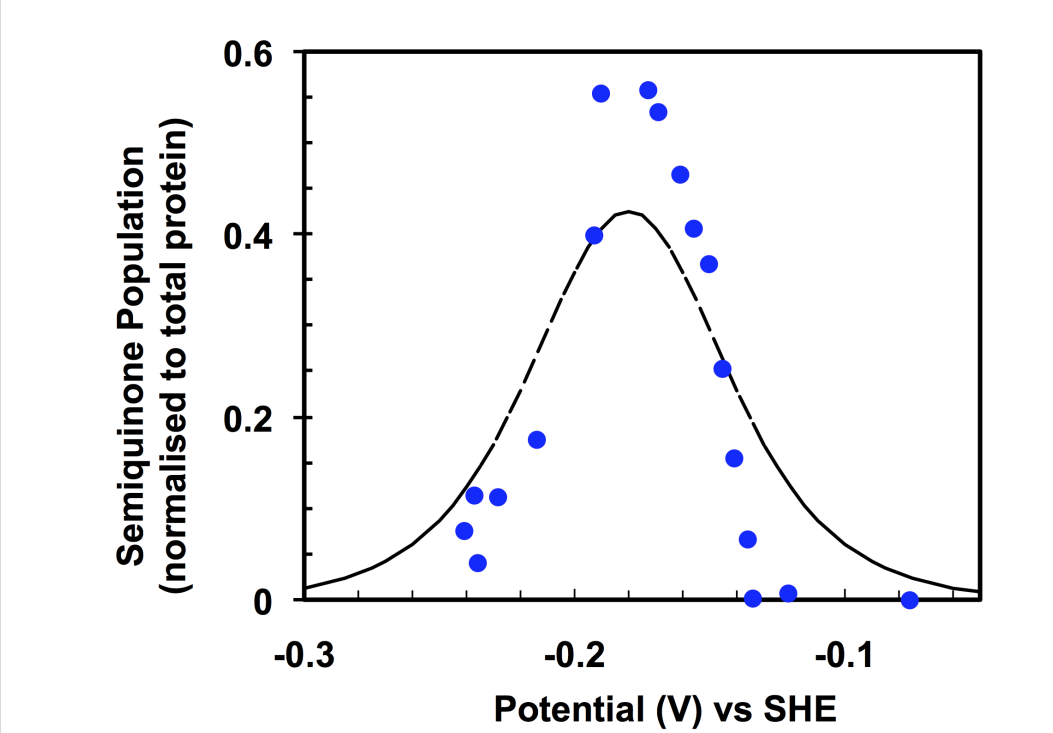

Figure 3.5: Optically monitored potentiometric titration of FldA at 610 nm. The data (blue circles) and fit (dashed line) to the equation describing sequential one electron additions to a centre with E2 = -170 mV and E1 = -190 mV. Sample contained 50 µM protein in an anaerobic buffer (10 mM potassium phosphate buffer, pH 7.0.) Path length = 1 cm. Experiment carried by Dr Julea Butt, University of East Anglia.

Independent assessment of the redox properties of CjFldA was afforded by cyclic voltammetry (Figure. 3.6). For these experiments the flavodoxin was deposited onto the surface of a pyrolytic graphite edge electrode coated with the surfactant didodecyldimethylammonium bromide (DDAB) (Rusling, 1998; Seagel *et al*., 2017). Cyclic voltammetry revealed two redox processes. The lower potential process had a mid-point potential of approx. -250 mV. The higher potential process had a mid-point potential of approx. -150 mV. Neither process was present in voltammetry of DDAB-coated electrodes that had not been exposed to flavodoxin. Thus, we assign the processes observed with the CjFldA sample to FMN either within FldA or that had dissociated from the protein. Direct electrochemistry of bacterial flavodoxins using solid electrodes, has been reported by several groups (Barker, 1988; Heering and Hagen, 1996; Seagel *et al*., 2017). From those findings there are two points of particular significance for interpretation of the voltammetry of CjFldA. Firstly, peaks for the SQ/HQ

transformation are well-defined while those of the Q/SQ transformation are typically absent. Secondly, free FMN typically contributes peaks with a mid-point potential of approx. - 200 mV at pH 7. The voltammetry of CjFldA is consistent with Q/SQ *and* SQ/HQ mid-point potentials above - 300 mV vs SHE. This conclusion is in agreement with the results from potentiometric titration. Based on voltammetry of CjFldA measured at several independently prepared electrodes and inspection of the relative peak heights and widths for the two processes, it is likely that the higher potential peaks describe the contribution of free FMN. However, we cannot rule out a contribution from the Q/SQ process at these potentials as noted in the voltammetry of *Azotobacter vinelandii* flavodoxin II studied at similarly DDAB-coated graphite electrodes (Seagel *et al*., 2017).

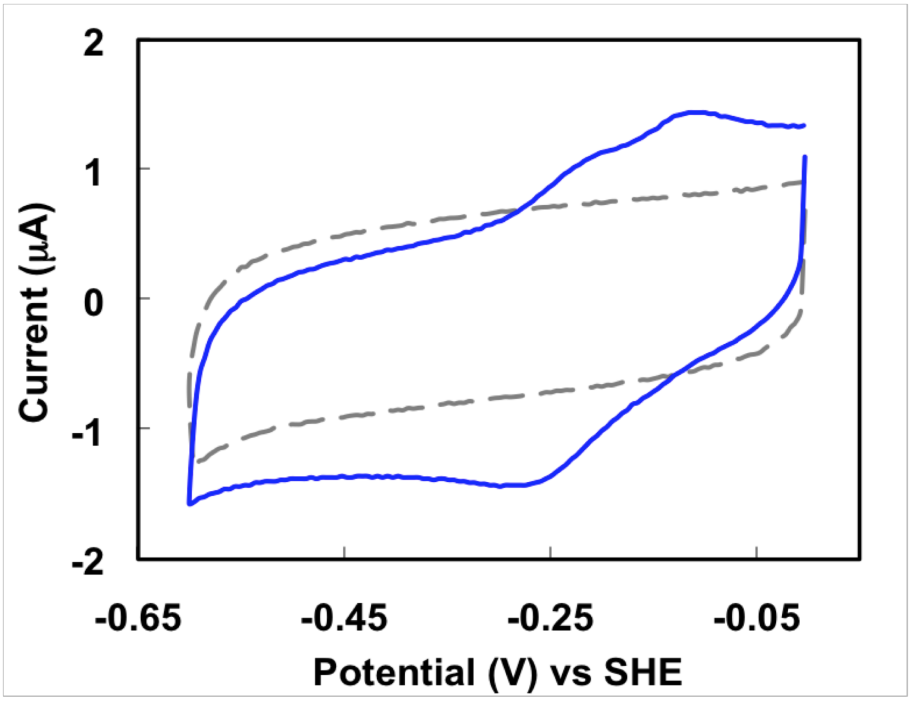

Figure 3.6: Cyclic voltammetry of CjFldA (continuous blue line) adsorbed on a DDAB-coated pyrolytic graphite edge electrode. Cyclic voltammetry of the DDAB-coated electrode is also shown (broken grey line). Measurements performed in 50 mM potassium phosphate, pH 7 at 20 °C with a scan rate of 20 mV s^{-1}. Experiment carried by Dr Julea Butt, University of East Anglia.

3.2.3 Both POR and OOR can reduce FldA

The ability of FldA to act as electron acceptor for the POR and OOR enzymes was tested by adding cell-free extract plus CoA to the purified protein under anaerobic conditions and initiating the reaction by addition of either pyruvate or 2-oxoglutarate. A rapid reduction in the FMN absorbance in the 460-470 nm region was observed with either substrate (Figure. 3.7). While FldA has previously been identified as the electron acceptor for OOR (Weerakoon *et al*., 2007) these results show POR also reduces FldA.

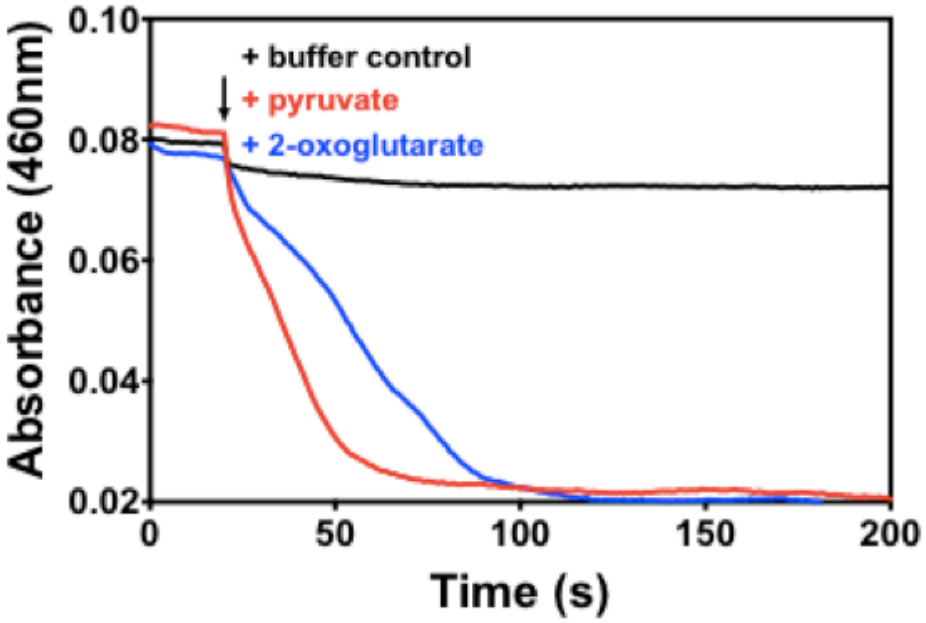

Figure 3.7: Pyruvate and 2-oxoglutrate dependent reduction of pure flavdoxin. *C. jejuni* cell-free extract was added to nitrogen-sparged 100 mM Tris-HCl buffer pH 8, 2 mM $MgCl_2$, 0.2 mM Coenzyme A, 0.1 mM thiamine pyrophosphate and 50 μM purifed FldA in stoppered anaerobic cuvettes. The reaction was started by injection of anaerobic pyruvate (red trace) or 2-oxoglutarate (blue trace) to 5 mM final concentration. The black trace was a control which was without pyruvate or 2-oxoglutrate.

3.2.4. Testing for interaction of FldA with Complex I: interactions of FldA with NuoX and NuoY

Complex I (a proton pump also known as the Nuo complex) is the first enzyme of the respiratory chain in many bacteria, archaea and *Camplybacter jejuni*, encoded by a set of 14 genes called *nuo* genes (*N*ADH: *u*biquinone *o*xidoreductase). Twelve out of these 14 genes in *C. jejuni* are conserved as in other bacteria and archaea. However, two of the *nuo* genes, *nuoE* and *nuoF* that encode for the NADH binding dehydrogenase "module", are replaced by two novel genes, *Cj1575c (nuoX)* and *Cj1574c (nuoY),* in the genome of *C. jejuni*. Since there is no NuoE and NuoF in *C. jejuni*, it is thought that the electrons are donated to complex 1 by flavodoxin, encoded by *fldA* gene, instead of NADH (Weerakoon and Olson, 2008).

It was hypothesized that NuoY and/or NuoX mediates the flow of electrons from reduced flavodoxin into the respiratory chain, but there is no experimental evidence for this. They may be a binding or docking site for FldA. Therefore, it would be expected that there are FldA-NuoX/Y interactions, as FldA is the electron donor for the Nuo complex. In order to investigate this hypothesis, we wanted to use FldA, NuoX and NuoY in interaction studies. Firstly, by overexpressing and purifying FldA, NuoX and NuoY by affinity chromatography and gel filtration, the proteins were mixed in different combinations; 'NuoY + NuoX + FldA', 'NuoX + FldA' and 'NuoY + FldA' (with FldA being un-tagged), followed by SDS-PAGE analysis for evidence of any protein-protein interaction. Secondly, we used the bacterial two-hybrid system (BACTH; Karimova *et al.*, 1998) to see if we could detect interactions *in vivo.* FldA was already available, so the first step was to clone, express and purify NuoX and NuoY.

3.2.4.1 NuoX overexpression and purification

The Cj1575c coding region was amplified by PCR using primers with NdeI and XhoI sites, as listed in Chapter 2 in Table 2.2. The gene was cloned into pET21a using the same procedures as described above for *fldA* to produce pETNuoX

(Figure. 3.8). Overexpression trials of *E. coli* BL21 (DE3) (pETNuoX) were conducted at 25 °C and 37 °C with 0.1 mM and 0.4 mM IPTG induction (Figure. 3.9).

A) B)

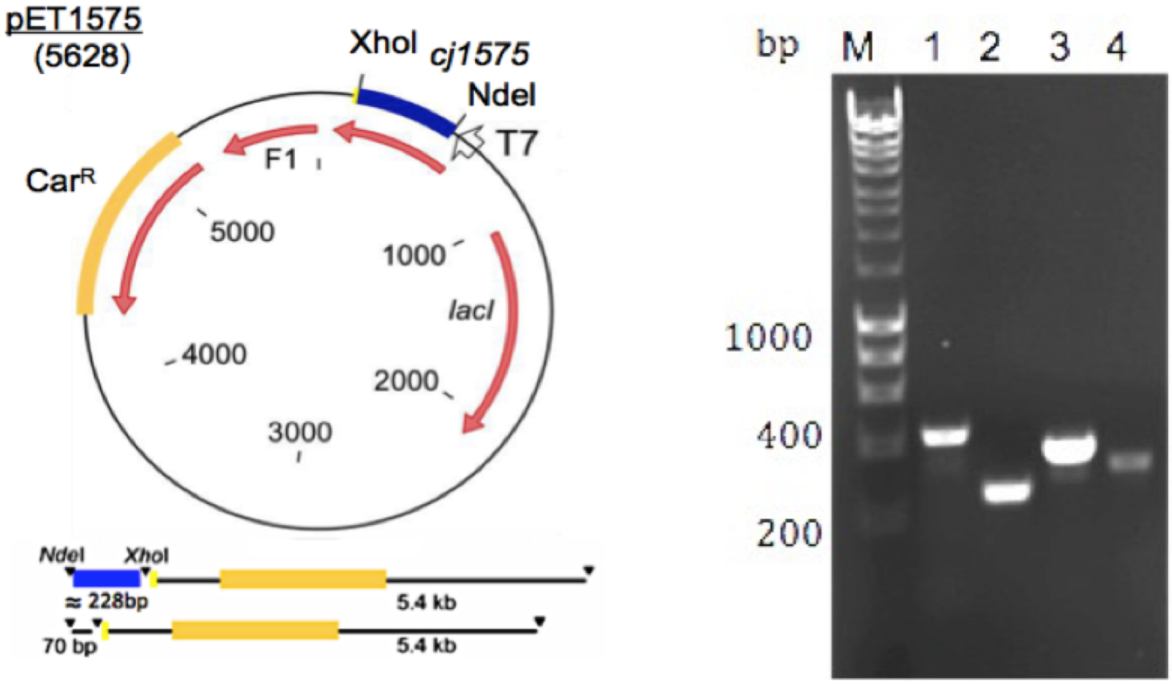

Figure 3.8: Generation of overexpression plasmid pETNuoX. (A) pETNuoX plasmid was made by inserting the gene of interest with an NdeI restriction site and a XhoI restriction site. **(B)** The cloning was confirmed by using PCR with different combination of T7 primers and *nuoX* primers and the pETNuoX as template. Lane 1 T7F + T7R. Lane 2 NuoXF + NuoXR. Lane 3 T7F + NuoXR. Lane 4 NouXF + T7R.

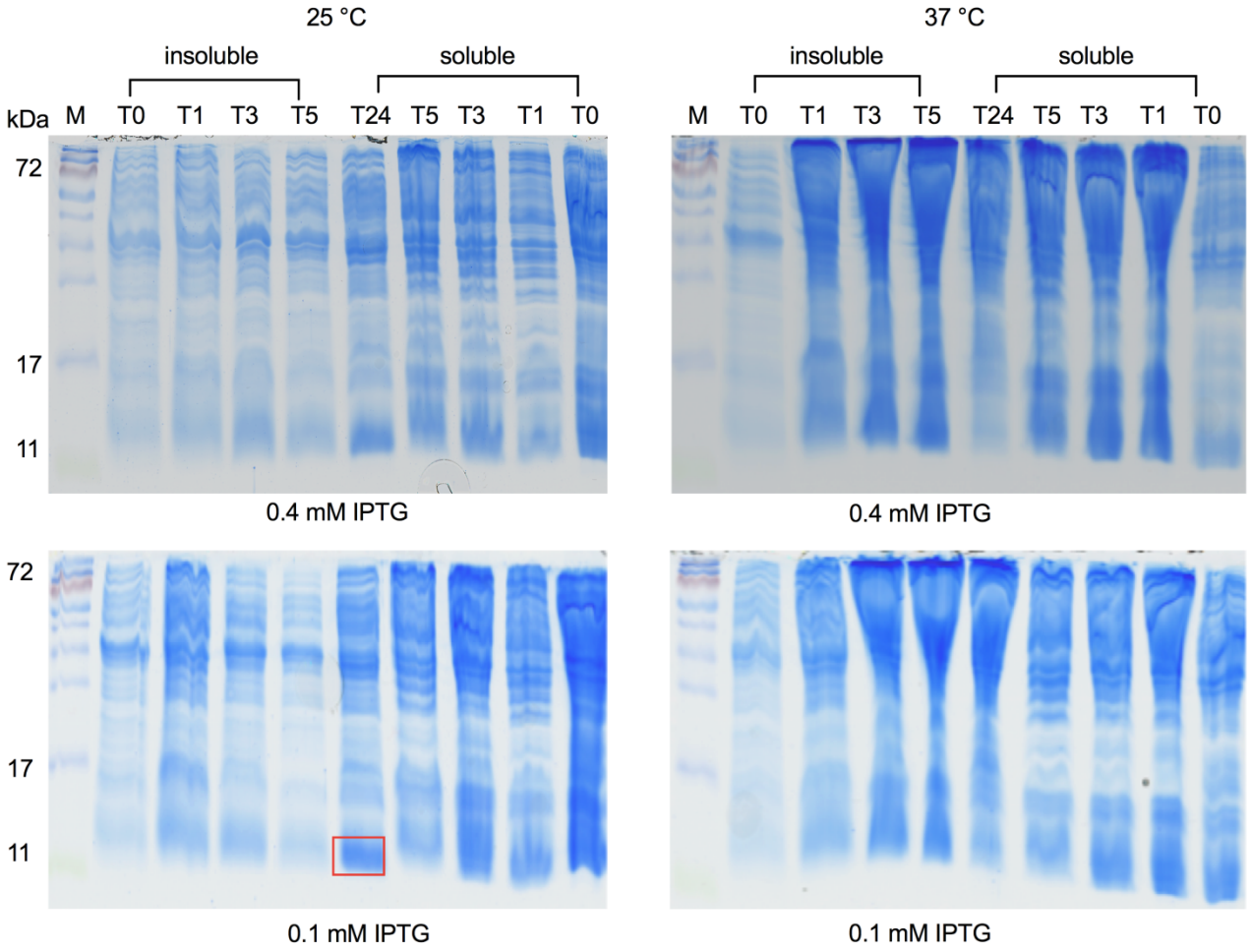

Figure 3.9: Overexpression of NuoX. Solubility trials of NuoX were conducted by culturing the transformed *E. coli* BL21 in LB with carbenicillin (50 µg ml^{-1}) to an OD_{600} 0.6 before inducing over-expression by adding 0.1 mM IPTG or 0.4 mM IPTG. At both 25 °C and 37 °C cells were cultured and sampled periodically (T0, T1, T3, T5, T7, T24 hr) to ascertain the optimum temperature and time post-induction for adequate production of protein. These cells were resuspended in binding buffer, sonicated and centrifuged to produce soluble fraction and insoluble fractions resuspended in dH_2O. M = Protein Molecular Weight marker. Protein band in the red box is NuoX protein after growing transformed *E. coli* BL-21 in LB with 0.1 mM IPTG at 25 °C for 24 hr (the condition used to overexpress NuoX).

The predicted size of NuoX is 10 kDa. A band of this size could be seen on SDS-PAGE gels up to 24 hr in the soluble fraction of cells induced at 25 °C (Figure 3.9). Cells induced under these conditions (0.1 mM IPTG, 25 °C, 24 hr) were lysed and extracts subjected to nickel affinity chromatography (Figure 3.10). This

resulted in a very significant enhancement in NuoX abundance and purity but there were still some high molecular weight contaminants present. These were successfully removed by gel filtration (Figure 3.10).

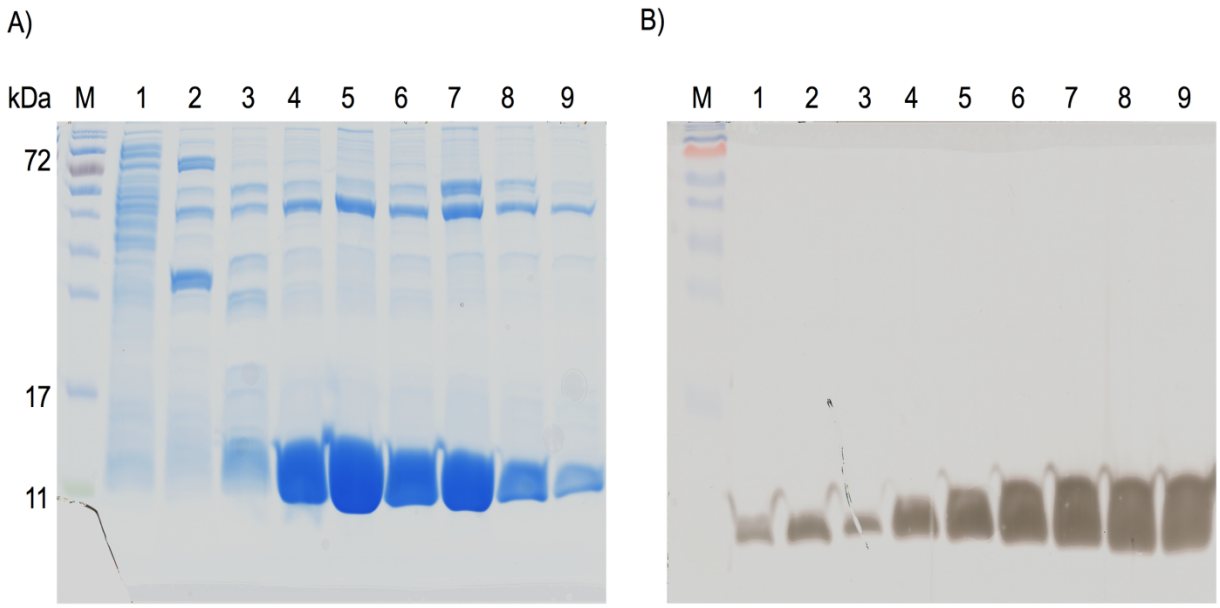

Figure 3.10: Purification of the NuoX protein. Panel **(A)** Lane 1 is CFE after induction, with faint band at ~ 12 kDa. Lane 2 is flow through. Lanes 3-9 are NuoX protein purified by nickel-affinity chromatography. Panel **(B)** Lanes 1-9 are peak fractions from gel filtration run on SDS-PAGE and silver stained to show purity. M = Protein Molecular Weight markers.

3.2.4.2 NuoY overexpression and purification

The Cj1574c coding region was amplified by PCR using primers with NdeI and XhoI sites, as listed in in Chapter 2 Table 2.2 in Chapter 2. The gene was cloned into pET21a using the same procedures as described above for *fldA* and *nuoX* to produce pETNuoY (Figure. 3.11). *E. coli* BL21 (DE3) (pETNuoY) were induced under the same conditions for NuoX (0.1 mM IPTG, 25 °C, 24 hr). The predicted size of NuoY is 25 kDa. The protein was partially purified by nickel affinity chromatography, but was still impure (Figure. 3.12 A). Pure protein was obtained after gel filtration (Figure. 3.12B).

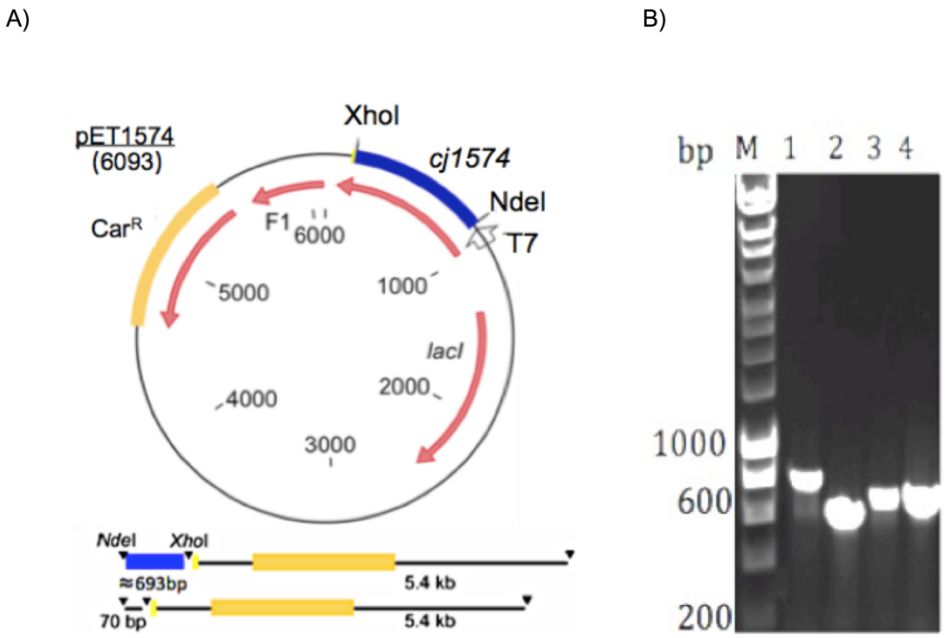

Figure. 3.11: Generation of overexpression plasmid pETNuoY. (A) pETNuoY plasmid was made by inserting the gene of interest with an NdeI restriction site and a XhoI restriction site. **(B)** The cloning was confirmed by using PCR with different combination of T7 primers and *nuoY* primers and the pETNuoY as template. Lane 1 T7F + T7R. Lane 2 NuoYF + NuoYR. Lane 3 T7F + NuoYR. Lane 4 NouYF + T7R.

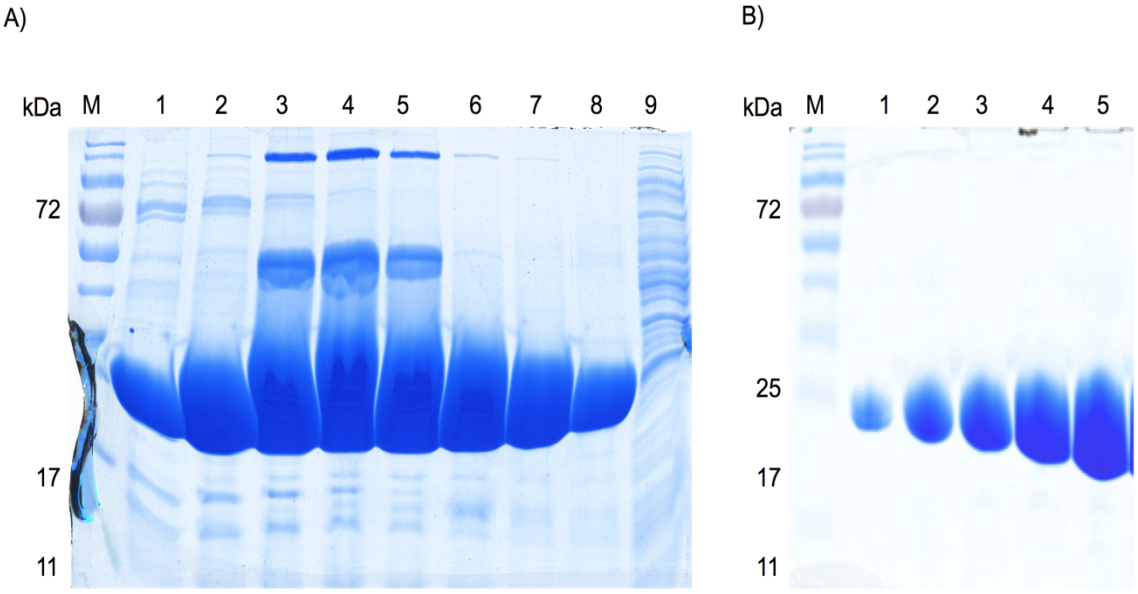

Figure 3.12: Purification of NuoY. Panel **(A)** Lane 1-8 NuoY protein purified by nickel-affinity chromatography. Lane 9, CFE after induction. Panel **(B)** Lane 1-5 NuoY protein fractions purified by gel filtration. M = Protein Molecular Weight markers.

3.2.4.3 Interaction of FldA, NuoX and NuoY

After overexpressing and purifying target proteins (his-tagged-NuoX, his-tagged-NuoY and untagged-FldA), the AKTA prime system was used to investigate the protein-protein interactions by affinity chromatography. His-tagged proteins, either his-tag-NuoX or his-tag-NuoY were first loaded onto a HisTrap column. Then, untagged-FldA was run through the column. The flow through was collected, followed by SDS-PAGE analysis. SDS-PAGE gels were loaded with pure untagged-FldA, pure his-tagged-NuoX, his-tagged-NuoY and the flow through. If there is interaction between his-tagged-protein and untagged-FldA, they should elute together. The buffers (binding buffer and elution buffer) used in these experiments were prepared without adding sodium chloride, which might prevent protein-protein interaction. Different ratios of protein were tested by mixing the protein in the binding buffer at ratios of 1:1, 1:2 and 1:3 and running them through His-Trap column (Figure 3.13 C). Also, two different temperatures were examined. First experiments were done at room temperature 25 °C. As *C. jejuni* is considered as a mildly thermotolerant bacterium, 42 °C (growth) temperature was examined, as well. It is clear that there was no interaction between NuoX or NuoY with FldA (Figure 3.13 A, B, C). This result is not expected as FldA is the electron donor to Nuo complex. To confirm this result, a different approach was used, the bacterial two-hybrid system (BACTH).

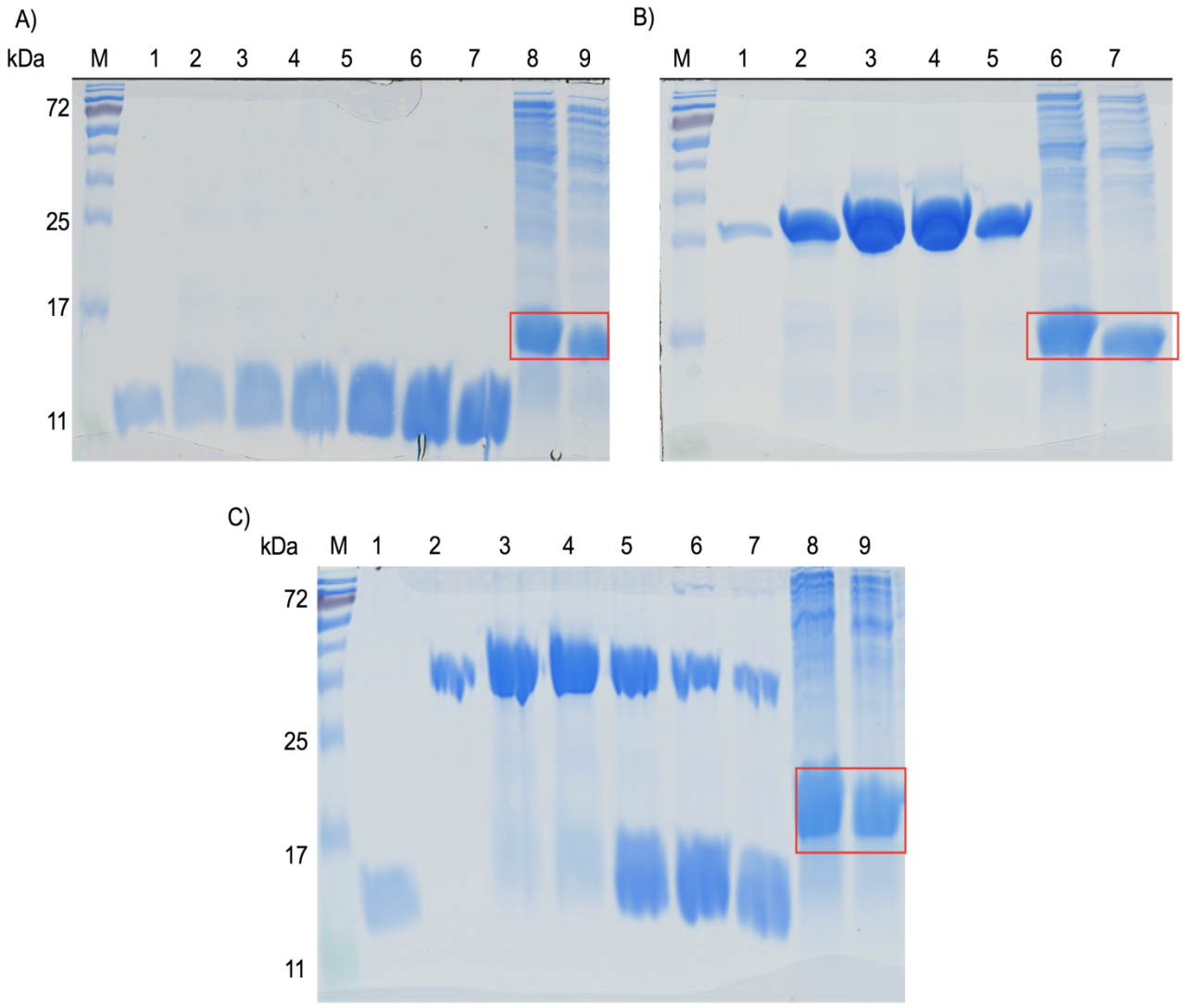

Figure 3.13: 12 %SDS-PAGE gel of potential interactions. Panel **(A)** Lane 1: pure his-tagged NuoX before mixing with un-tagged FldA. Lanes 2-7 his-tagged NuoX that eluted from his-tag column. Lane 8: Un-tagged FldA (some impurities) before mixing with his-tagged NuoX. Lane 9: Flow through that contains only un-tagged FldA. Panel **(B)** Lane 1: pure his-tagged NuoY before mixing with un-tagged FldA. Lanes 2-5 his-tagged NuoY that eluted from his-tag column. Lane 6: Un-tagged FldA (some impurities) before mixing with his-tagged NuoY. Lane 7: Flow through that contains only untagged FldA. Panel **(C)** Lane 1: pure his-tagged NuoX before mixing with un-tagged FldA. Lane 2: pure his-tagged NuoY before mixing with un-tagged FldA. Lane 3-7: his-tagged NuoX and his-tagged NuoY that eluted from his tag column. Lane 8: Un-tagged FldA before mixing with his-tagged NuoY. Lane 9: Flow through that contains only untagged FldA.

3.2.4.4 Testing interactions using the bacterial two-hybrid system (BACTH)

After detecting no Interaction between NuoX-FldA, NuoY-FldA and NuoX-NuoY-FldA using affinity chromatography (3.2.4.3), the Bacterial Adenylate Cyclase-based two-hybrid system (BACTH) (Figure 1 chapter 2) was used. *nuoX, nuoY* and *fldA* genes were amplified using primers listed in Table 2.2. *nuoX* or *nuoY* genes were inserted into pKT25 plasmid digested with XbaI and KpnI. *fldA* was inserted into pUT18 plasmid digested with HindIII and KpnI. As a result, each *nuoX/nuoY* genes was cloned as an in-frame fusion at the C-terminal end of T25 in pKT25 plasmid and *fldA* was cloned as an in-frame fusion at the *N*-terminal end of T18 in pUT18 (Figure 3.15 A). The plasmids were cotransformed by electroporation (2.5.2 chapter 2) into competent *E. coli* BTH101. *E. coli* BTH101 is a reporter strain that is used as the host for detection of protein-protein interactions. From (Figure 3.15 B and 3.16) it can be seen that no beta-galactosidase is being produced by the interaction plasmids and thus there is no evidence for interaction between FldA and Nuo complex via NuoX/NuoY. These results leave us with one possibility, that FldA donates electrons directly to NuoG. In order to test this hypothesis, NuoG was overexpressed and purified (Section 3.2.6)

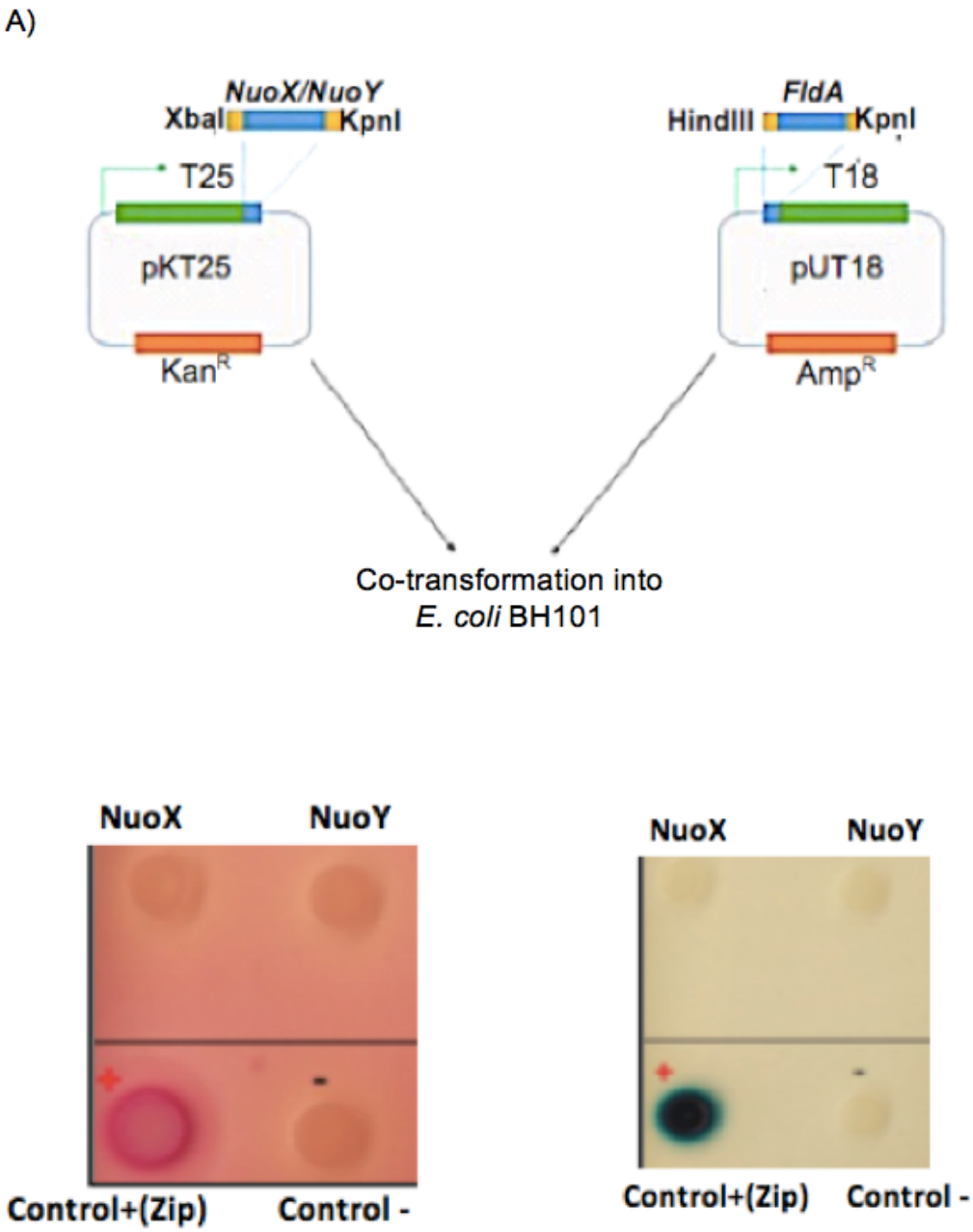

Figure 3.15: Testing protein-protein interaction between NuoX and NuoY against FldA of *C. jejuni* using BACTH system. Panel **(A)** FldA was fused in frame into pUT18 in order to detect the interaction with NuoX/NuoY-pKT25. Both plasmids were used to co-transform *E. coli* BTH101. Panel **(B)** In order to detect the interaction between proteins, *E. coli* BTH101 cotransformed with pUT18-FldA and pKT25 pated on LB+ X-gal agar and MacConkey + maltose. These plates contain appropriate antibiotics and IPTG. As positive control *E. coli* BTH101 co-transformed with pKT25-zip and pUT18-zip plasmids that are part of the Euromedex kit. As negative control *E. coli* BTH101 co-transformed with pKT25 and pUT18 that has no insert.

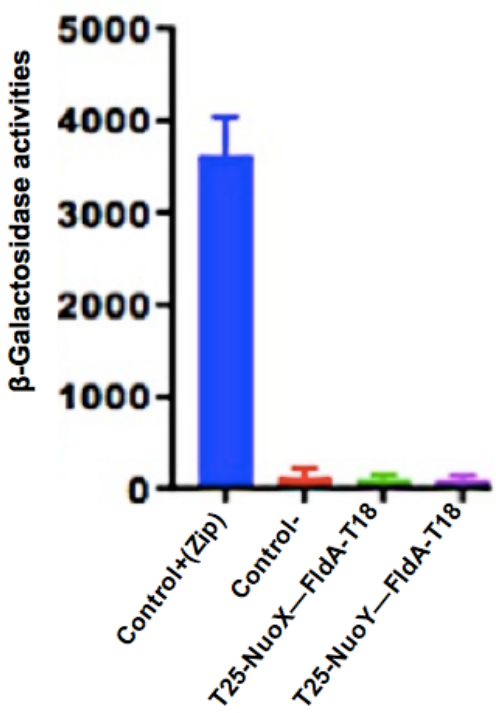

Figure 3.16: Interaction between (T25-NuoX—FldA-T18) and (T25-NuoY—FldA-T18) that should enhance the *β*-Galactosidase production were measured (green, purple columns). As positive control *E. coli* BTH101 co-transformed with pKT25-zip and pUT18-zip plasmids that come with the Euromedex kit (blue column). As negative control *E. coli* BTH101 co-transformed with pKT25 and pUT18 that has no insert (red column).

3.2.5 Attempts at construction of *nuoX* and *nuoY* mutants in *C. jejuni*

NuoX and NuoY are colorless proteins that have no redox centres. It has been reported that it is possible to delete all of the Nuo complex genes except for these two genes (Weerakoon and Olson, 2008). We have obtained evidence by two approaches there is no interaction between FldA and Nuo complex via NuoX/NuoY. These results may indicate that NuoX/NuoY has another role different than the Nuo complex, but yet to be identified. To confirm whether *nuoX/nuoY* genes are essential for viability for *C. jejuni* or not, attempts were made to delete them.

3.2.5.1 Constructing a mutagenesis plasmid for *nuoX* and *nuoY* using ISA cloning

Isothermal assembly (ISA) cloning (Gibson *et al*., 2009) was used to generate a

plasmid for transformation into *C. jejuni*, that deletes *cj1575 or cj1575* (*nuoX/nuoY*) by allelic exchange mutagenesis, replacing most of the coding region with a kanamycin resistance cassette derived from pJMK30 (van Vliet *et al*., 1998), which carries a constitutive promoter and no terminator. The ISA reaction assembled 4 PCR amplified fragments; HincII digested pGEM3Zf(-) vector, two regions of ~ 500 bp flanking *cj1575/cj1574*, such that only the first few and last few codons of the gene were retained, and the kanamycin resistance cassette was inserted between the two flanking regions. The kanamycin resistance cassette was amplified from pJMK30 using primers Kan F and Kan R (Table 2.2). The left flanking region of the gene was amplified using primers (NuoX F1 F and F1 R) (NuoY F1 F and F1 R) (Table 2) and the right flanking region was amplified by (NuoX F2 F and F2R) NuoY F2F and F2R. The ISA reactions were performed as previously described (Gibson *et al*., 2009) and used to directly transform competent *E. coli* DH5α cells, with selection on LB + kanamycin agar plates. Colonies were screened by PCR with using different combinations of KAN and insert primers. pGEMNuoX/pGEMNuoY was electroporated into *C. jejuni* NCTC 11168 and cells plated out on Columbia agar plates, incubated overnight in microaerobic conditions at 42 °C. The growth was then transferred to Columbia blood agar plates plus kanamycin. The growth was also transferred to Columbia blood agar plates plus kanamycin and 25 mM Na formate that is considered an excellent alternative electron donor for *C. jejuni* and incubated for 4 days. For both mutations in both conditions no colonies appeared on plates, indicating that these genes may indeed be essential.

A) B)

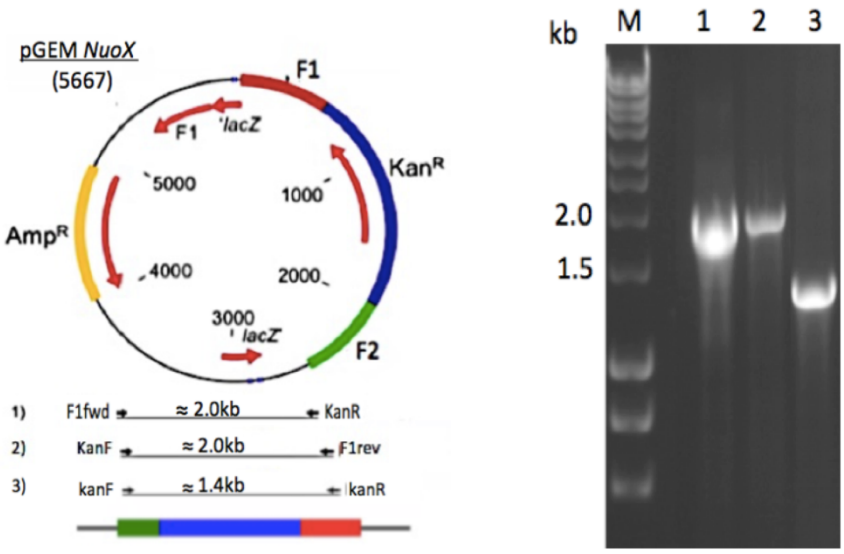

Figure 3.17: Generation of mutagenesis plasmid by ISA using pGEM-3Zf plasmid that digested at the HincII restriction site. (A) Plasmid map of pGEM *NuoX* shows that flanking regions of targeted gene. Red is Flank 1 (F1), 600 bp that is upstream *NuoX* gene. Green is Flank 2 (F2) that is downstream *NuoxX* gene. Targeted gene is interrupted by kanamycin resistant cassette (blue). The other regions in the plasmid are AmpR region (gold), F1 origin of replication and the lacZ. **(B)** Different combination of KanR, F1 and F2 primers were used to confirm cloning. M is ladder. Lane 1, PCR product is 2.0 kb. Lane 2, PCR product is 2.0 kb. Lane3 PCR product is 1.4 kb.

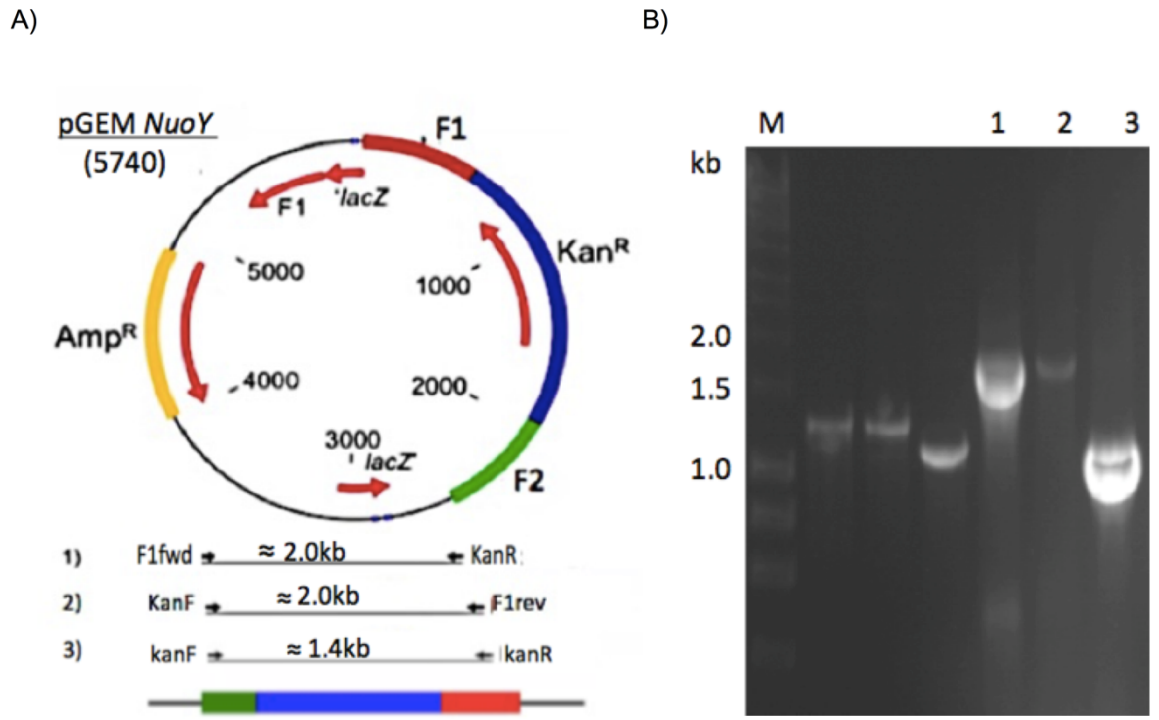

Figure 3.18: Generation of mutagenesis plasmid by ISA using pGEM-3Zf plasmid that digested at the HincII restriction site. (A) Plasmid map of pGEM *NuoY* shows that flanking regions of targeted gene. Red is Flank 1 (F1), 600 bp that is upstream *NuoY* gene. Green is Flank 2 (F2) that is downstream *NuoY* gene. Targeted gene is interrupted by kanamycin resistant cassette (blue). The other regions in the plasmid are AmpR region (gold), F1 origin of replication and the lacZ. **(B)** Different combination of KanR, F1 and F2 primers were used to confirm cloning. M is ladder. Lane 1, PCR product is 2.0 kb. Lane 2, PCR product is 2.0 kb. Lane3 PCR product is 1.4 kb.

3.2.6 NuoG overexpression and purification

The NuoG protein in *C. jejuni* is known to be modified and contains a putative extra Fe-S cluster site that may be needed to allow electron flow from FldA to NuoG directly (Friedrich *et al*. 1995). Therefore, given that there appears to be no interaction between NuoX/NuoY and FldA, we wished to investigate NuoG-FldA interactions. The full length *nuoG* gene was amplified without a stop codon using PCR with primers listed in Table 2. The gene was cloned into pET21a at NdeI and XhoI restriction sites. By using the same procedures as described above for *fldA* and *nuoX* to produce pETNuoG that has *nuoG* gene fused to a 6x His tag that was used to purify the protein (Figure 3.20). *E. coli* BL21 (DE3) (pETNuoG) was

induced using 0.4 mM IPTG at 37 °C, for 24 hr). The predicted size of NuoG is 94 kDa. Unfortunately, although a band of the correct predicted size was observed on gels (Figure 3.20), the preparation was quite impure. The protein purified was also almost colorless and it is expected to be brown because of the several iron-sulphur clusters. The UV-VIS spectrum does show a characteristic feature of iron sulfur cluster absorbance at 420 nm, but this is weak (Figure 3.20). It is therefore unlikely NuoG contains the complete complement of iron-sulphur clusters. Clearly, NuoG overexpression and purification needs more optimisation and time did not allow this to be taken further in this study.

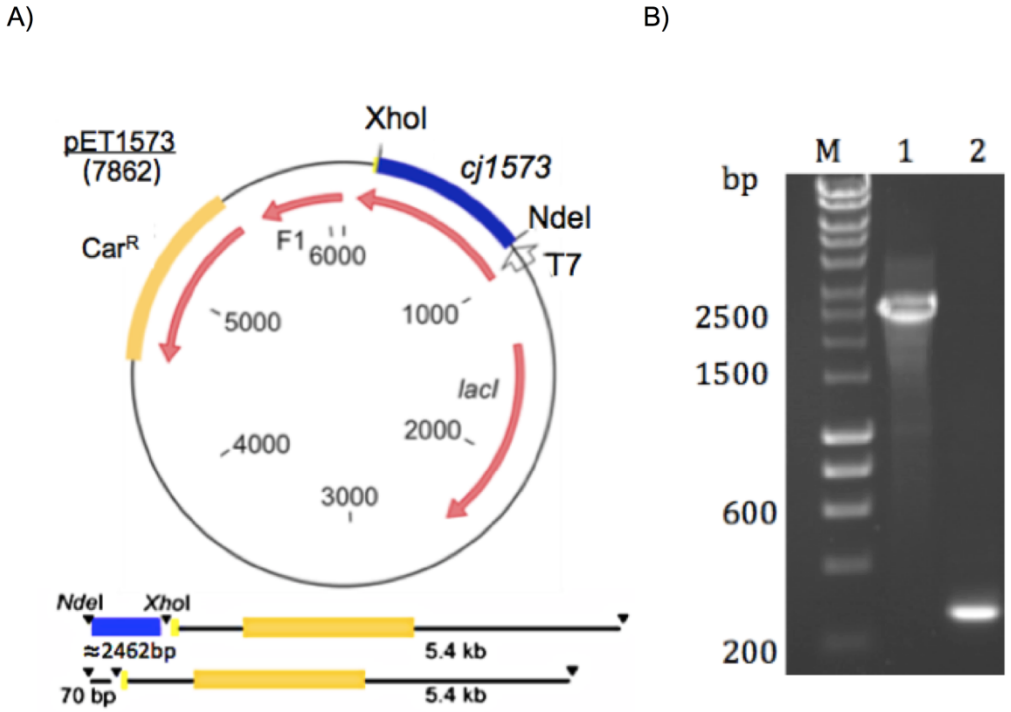

Figure 3.19: Generation of overexpression plasmid pET *NuoG*. **(A)** pET *NuoG* plasmid was made by inserting the gene of interest with an NdeI restriction site and a XhoI restriction site. **(B)** The cloning was confirmed by using PCR with T7 primers and the plasmid as template. Lane1 pET *NuoG.* Lane2 pET21.

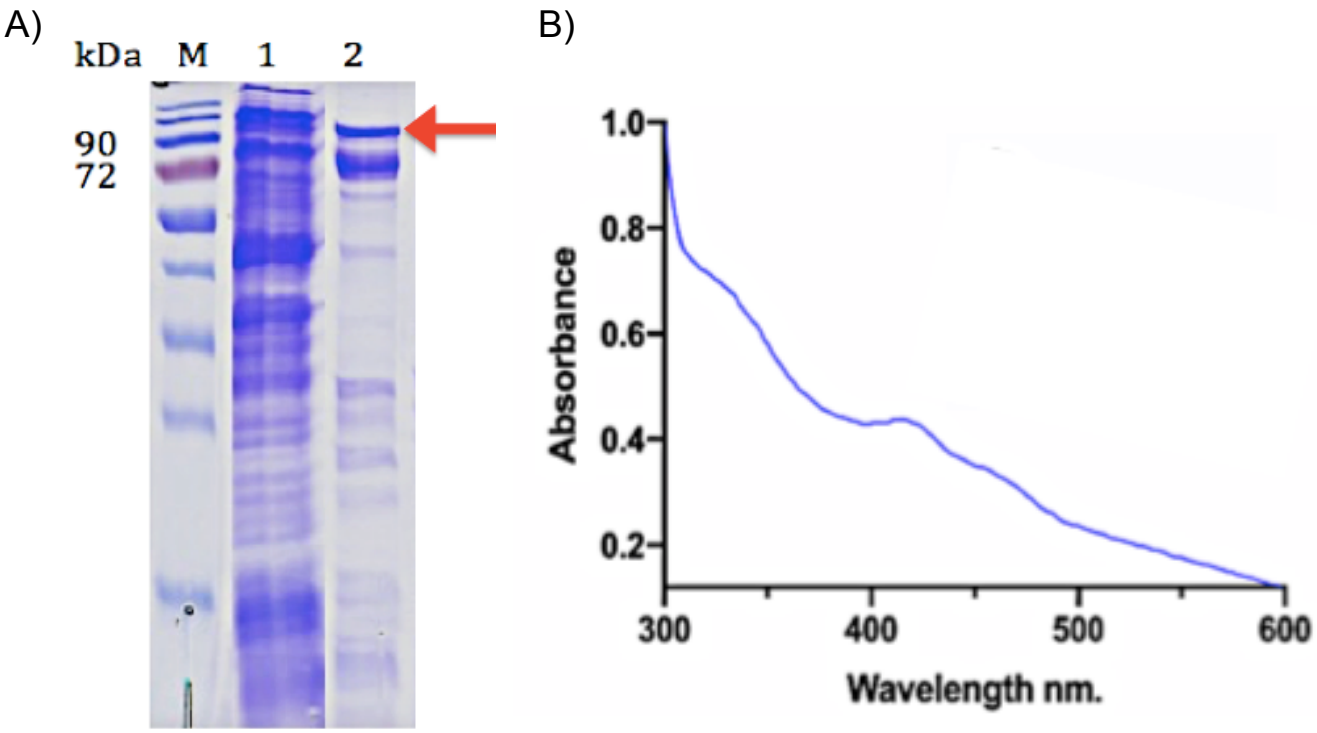

Figure 3.20: 12 % SDS PAGE gel of NuoG protein. **(A)** Lane 1 CFE. Lane 2 NuoG protein purified by nickel-affinity chromatography**. (B)** NuoG-6His spectrum shows characteristic feature of iron sulfur cluster at 420 nm.

3.3. Discussion

Redox properties of the *C. jejuni* flavodoxin FldA

C. jejuni FldA was characterized in this work and we found that, surprisingly, it is a high redox potential flavodoxin, with the $FldA_{ox}/FldA_{sq}$ and $FldA_{sq}/Fld_{hq}$ couples having E_m values of -170 mV and -190 mV respectively. Flavodoxin protein redox properties depend on flavin mononucleotide (FMN), which is the reactive component in these flavoproteins. The structure of flavodoxins is formed of five-stranded parallel β-sheets in the center of the protein and they are flanked by five α helixes (Figure 3.22). FMN consists of the isoalloxazine ring (flavin), the ribityl tail and a phosphate group. Chemical properties of the isoalloxazine ring enables flavodoxins to stabilize different redox states, each of which has distinct chemical features and redox potentials (Figure 3.21). This can be seen by comparing the structure of flavoenzymes with enzymes that use nicotinamide adenine dinucleotide (NAD) as a cofactor. All of the structures where NAD^+/NADH bind

are homologous to each other and in fact these structures don't perturb the NAD^+ redox potential. On the other hand, flavins don't maintain a single type of binding site due to the isoalloxazine ring having much more diverse redox states. This enables the active site to tune the redox potential and facilitate transfer of two electrons, one electron or the combination of the two. The picture is quite complex and several residues influence the binding of the flavin. By replacing one residue the redox potential can shift either more positive or negative. In flavodoxins, the FMN is sandwiched between two loop regions known as the 50s or W-loop and 90s or Y-loop in classical flavodoxins, or the 40s loop and 70s loop in NrdI proteins, which are a distinct group of flavodoxins (Table 3.1). These loops contain aromatic/hydrophobic residues (highlighted in orange) that stack over the isoalloxazine ring. A preponderance of anionic residues (blue) in the loops in flavodoxins is thought to contribute to lowering of the E_1 redox potential in particular, while in NrdI proteins the environment is more neutral or charge compensated (cationic residues in red) (Table 3.1). Canonical flavodoxins involved in electron transport usually have a wide separation in their E_1 and E_2 redox potentials, due to a negative electrostatic environment around the isoalloxazine ring of the FMN, causing destabilization of the hq form and shifting the E_1 potential much more negative than free FMN. For example, *Desulfovibrio vulgaris, Synechocystis* and *Azotobacter vinelandii* all have E_1 values of < -400 mV (Table 3.1). This is also reflected in the pI values of such flavodoxins, which are usually acidic. NrdI proteins, however, have a bi-modal distribution with both low pI (mainly Firmicutes) and high pI (*E. coli* and most other proteobacteria) types (Johansson *et al*., 2010). Both types tend to have a more neutral (or charge compensated) environment in the loops surrounding the bound FMN, resulting in higher and often more similar E_1 and E_2 redox potentials than canonical flavodoxins (Table 3.1). The *C. jejuni* FldA is a long-chain flavodoxin with a predicted pI of 3.9 and it possesses conserved anionic residues in the W- and Y-loop regions involved in FMN binding (Table 3.1) that might be expected to result in a much lower E_1 redox potential than the -190 mV determined here. A crystal structure will be needed to rationalize the reasons for this disparity.

Table 3.1: Comparison of redox potentials and FMN binding loop regions in selected flavodoxins and NrdI proteins

Flavodoxin	pI	E_1 (mV)	E_2 (mV)	Δ (mV)	50s (W) loop	90s (Y) loop	Ref
D. vulgaris	4.0	- 440	- 143	297	STWGDDSIE	DSS--YE	[1]
Synechocystis	3.5	- 433	- 238	195	PTWNVGELQ	DQVGYAD	[2]
A. vinlandii	4.4	- 483	- 187	296	PTLGEGELP	DQVGYPE	[3]
C. jejuni	3.9	- 190	- 170	20	STWGSGDLQ	DSESYSD	This study
NrdI	**pI**	**E_1 (mV)**	**E_2 (mV)**	**Δ (mV)**	**40s loop**	**70s loop**	**Ref**
E. coli	9.4	- 255	- 264	-9	GGGGTAG	NRNFGEA	[4]
B. cereus	5.0	- 309	- 252	57	GFGNVPER	NRNWGDM	[5]
B. anthracis	5.4	- 385	- 270	115	GFGNVPER	NRNWGDM	[6]

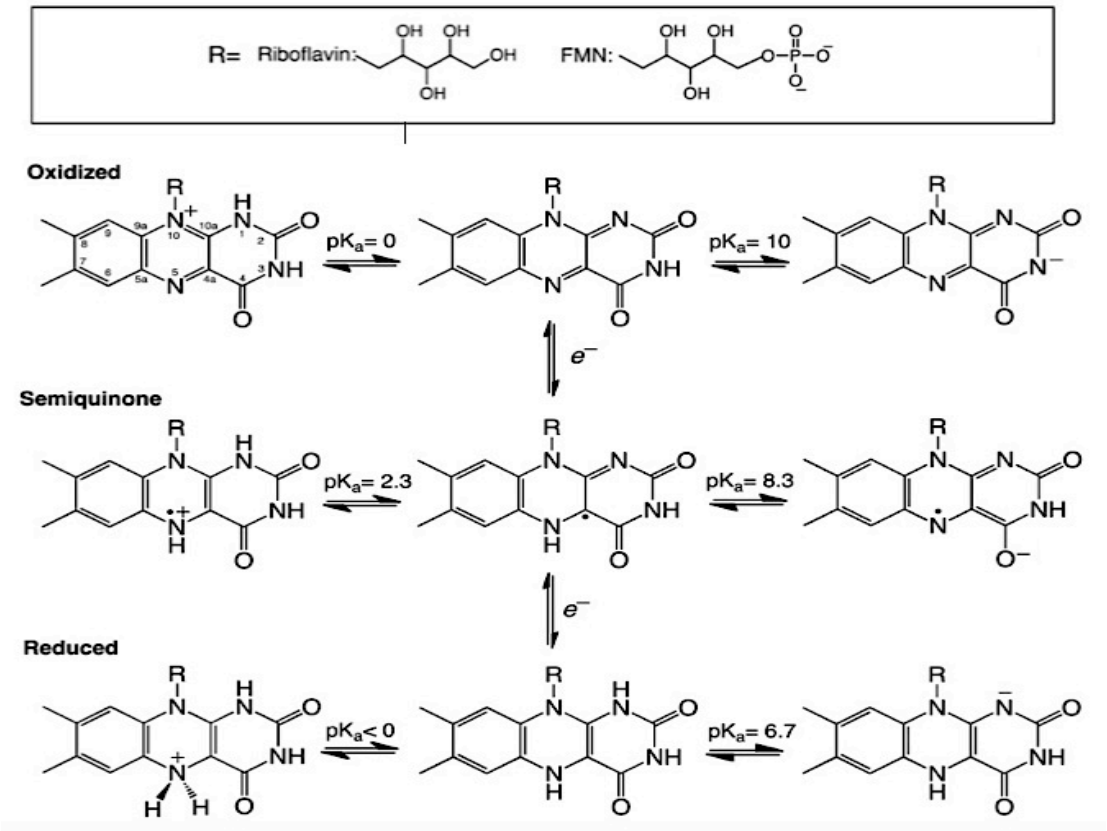

Figure 3.21: A scheme showing some of the different redox states of the isoalloxazine ring (Sobrado, 2012).

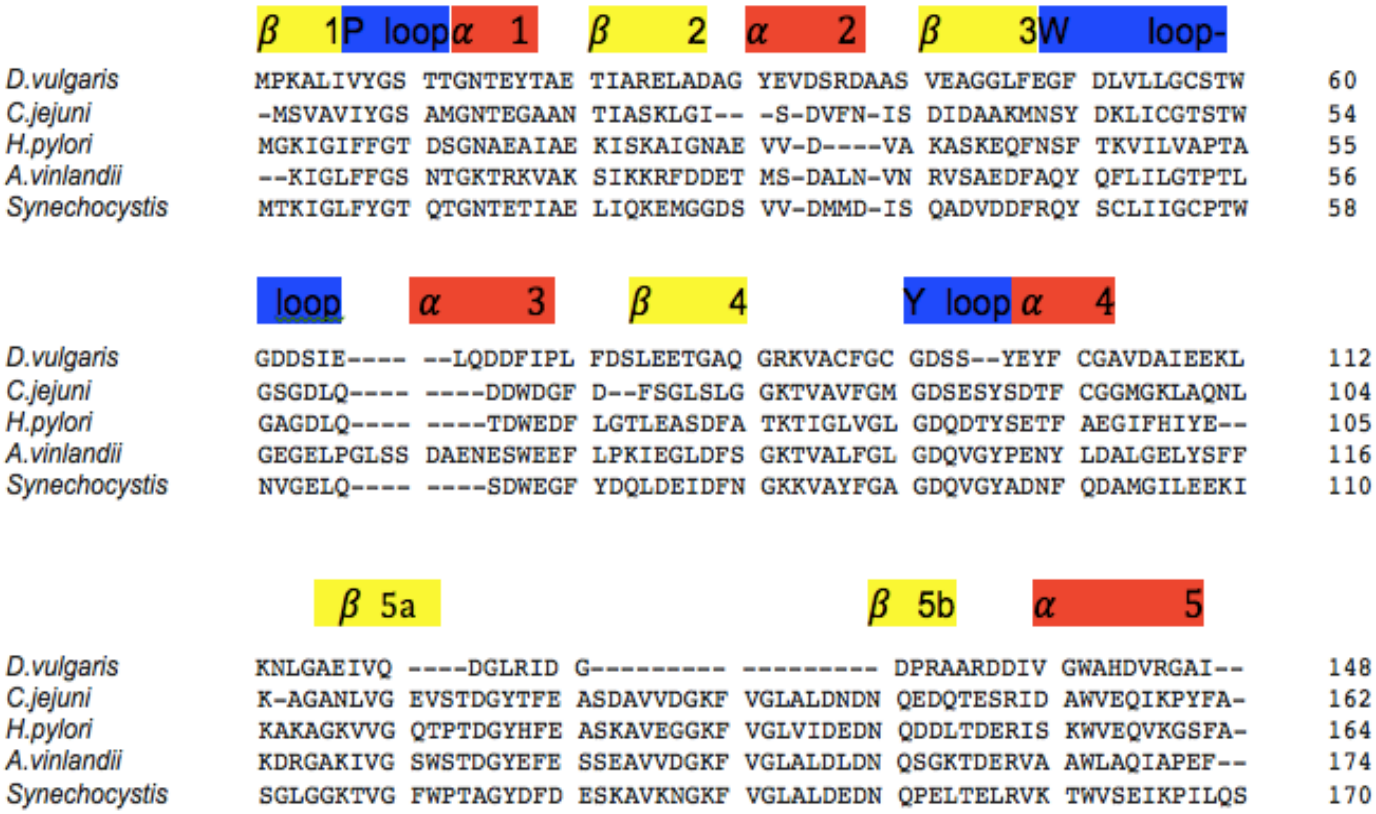

Figure 3.22: Protein sequences of a selection of flavodoxins from different species showing the functional loops of the flavodoxins. The sequences were from UniProt and aligned with ClustalOmega (Sancho *et al*, 2006, Alagaratnam *et al*, 2005).

Consequences of using a high potential flavodoxin for generating a membrane potential (Δψ) via Complex I

The proton motive force (pmf or Δp), drives bacterial motility, growth, and ATP synthesis. It is the pmf that is implicated in driving the rotation of flagella, which plays a prominent role in the colonization of the microaerophilic human pathogen *C. jejuni* in the gut of warm-blooded animals. The high redox potential of *C. jejuni* FldA has implications for the bioenergetics of Complex I in *C. jejuni*, which uses FldA as the electron donor instead of NADH. Aerobic bacteria that use NADH (E_m -320 mV) coupled with ubiquinone as the electron acceptor for Complex I (E_m +100 mV) will have an overall ΔE of ~420 mV to drive proton translocation

electrogenically, against an existing Δ*p* of ~180 mV. However, only menaquinone-8 (MK-8) and methylmenquinone-8 (mMK-8) are present in *C. jejuni* membranes (Carlone and Anet, 1983). The E_m for MK-8 is about -75 mV and for mMK-8 it is -124 mV (Junkhe *et al*., 2009) or as low as -140 mV (Hein *et al*., 2018). The ΔE for FldA reduction of MK-8 is therefore only ~ 100 mV and for mMK-8 it is ~50 mV; considerably lower than Δ*p.* Unless the *in vivo* redox potentials of the menaquinones and/or the FldA flavin are considerably different from those measured in solution, it remains an open question if electrogenic proton pumping can occur through Complex I in *C. jejuni*. Interestingly, according to van der Stel *et al*. (2017), direct measurements of Δ*p* using ion-selective electrodes showed that pyruvate produced the lowest Δ*p* compared to electron donors like formate, that do not couple with FldA. Also, *C. jejuni* depends on hydrogen or formate to survive in the anaerobic lumen of the gut, and near the epithelial cell layer oxygen is preferred in the generation of a pmf to maintain efficient motility and growth. Invariably, only in the presence of hydrogen, formate as an electron donor and oxygen as an electron acceptor is a high proton motive force (pmf) generated.

How does FldA interact with Complex I?

In *E. coli* and many other bacteria, the Nuo complex consists of fourteen subunits (NuoA-N). NuoA, H, and J-N are integral membrane proteins and the remaining subunits are peripheral components. NuoE and NuoF are the NADH binding proteins containing a flavin mononucleotide (FMN) and three iron-sulphur cluster (Fe-S) centres, through which electrons are transferred via the three Fe-S centres in NuoG to the rest of the complex (Friedrich and Schelde, 1998). Whilst *C. jejuni* possesses homologues of the nuoA-D and nuoG-N genes, nuoE and nuoF are replaced by proteins of unknown functions (Cj1575c and Cj1574c respectively) (Parkhill *et al.,* 2000). These two proteins have no homologues outside epsilonproteobacteria.

According to Schuller *et al*. (2019), the structure of the photosynthetic complex I in *Synechocystis* is lacking NuoEFG but contains a novel subunit, NdhS. Similarly to NuoX/NuoY, NdhS has no redox centers such as a Fe-S cluster. NdhS may use a “fly-casting” mechanism to “catch" Fld via electrostatic interaction using five positively charged residues at the C-termini. NuoX has RIKEAK and NuoY has KKERV at the very C-termini of the protein. It is possible that NuoX, NuoY and FldA use the same mechanism for interaction as NdhS. If this were the case it would be expected that the binding occurs too fast to be detected by the His-Trap elution methods used in this study. This may explain why we could not demonstrate any interaction between NuoX/NuoY and FldA.

However, in *C. jejuni* the Nuo complex genes can be deleted but not nuoX/nuoY. So, despite the fact that these two genes are located within the same complex I operon, it is possible that they may not be part of complex I. Supporting this hypothesis, the NuoG protein in *C. jejuni* is modified, containing an extra Fe-S cluster that may be needed to allow electron flow from electron carrier FldA to NuoG directly. The same is true for some *cyanobacteria* which lacks three genes encoding for the NADH dehydrogenase subunits of NDH-1, here, NAD(P)H: or ferrodoxin:plastoquinone oxidoreductases may be able to donate electrons to the complex (Friedrich *et al.* 1995, Friedrich *et al.* 2000). Also, according to Calderon-Gomez *et al*. (2017) both NuoX and NuoY proteins can bind free FAD and NuoY has the ability to bind to lactate and malate. If correct, this might hint at other functions for these proteins unrelated to Complex I. Thus, it is still unclear whether these proteins are really part of Complex I and interact with FldA or not. Answering this question also needs more investigation on the possible direct interaction between NuoG and FldA.

>NdhS
MATSSITIPTIRTPIHRSKFLGQTHQFSTVNRSVFPPPKQQSKLYQVKAMGKFNLWEVMGGRGLC
NGEKGIEKELQRNIEDEQETSKAENNETERESDDSNLSFKVPEDGFEKEMMGLTGGFPGGEKG
LKTFIEKNPPPPPPPPPAKQGSDASAVATDKKPKAPKLPLLMPGMIAIVKNQNSPYHMYCGIVQRI
TDGKAGVLFEGGNWDRLITFRLEELERREKGPPGKN PKSCILEPLIEQMQKEEAAP
>NuoY
MIYDNALCFLDMPSLKNKNLCEKIGVNSINISCLEDKNLKAKFYKCEIASLSFVLALLCKLSDEGQF
CDLDEGYLSAESCFGEEEAGEVLAFLKEVKYLIIDKNIHSYKDSENIKYFLNFLSVKYGLKILDSDE
EECDFKKAKLNTLKELDNYDGLVLFRANLQDKNLHCSKQFLQIAKCKDQSEVEILAKDFSFKTKLC
LDENLQGTIAFLNYENNGFDFTPIRIKEAK
>NuoX
MRRVDLRKSKELFEDLAQIIKEAKQGEVLVVLFEIGDFSPVEKSFSFVKEQGCELLNSLKFNQVD
WTIVIKKERV

Figure 3.23: Protein sequences of NdhS, NuoX and NuoY show residues that may be used for transient association with flavodoxin. The sequences were from UniProt.

Chapter 4: The role of Fqr and Flavodoxin as an electron donor system for ribonucleotide reductase (RNR)

4.1 Introduction

In *C. jejuni* the electron donor for ribonucleotide reductase (RNR) is unknown. From chapter 3, it can be seen that there is biochemical similarity between NrdI, (an atypical flavodoxin that along with an FAD-containing reductase, contributes to the DNA synthesis pathway), and *C. jejuni* FldA in that the difference between E_1 and E_2 redox potentials is small.

A study in the closely related epsilonproteobacterium *Helicobacter pyrlori* (St Maurice *et al.,* 2007) reported that an FAD-containing and NADPH oxidizing enzyme named FqrB (HP1164) could act as a flavodoxin reductase in addition to the POR of that bacterium. However, based on in vitro studies these authors proposed that the physiological function of FqrB was in the production of NADPH via the reversed reaction, i.e. the transfer of electrons from pyruvate to NADPH via POR, flavodoxin and FrqB. In *H. pylori*, FqrB is seemingly an essential enzyme as attempts to produce an fqrB deletion mutant were unsuccessful (St. Maurice *et al*., 2007). Analysis (Xbase *C. jejuni*) showed that *C. jejuni* also contains a homologue of the FAD-containing flavoenzyme FqrB and so we wished to explore if this could act as an additional reductase for FldA.

The only biochemical pathway by which organisms reduce NDPs to convert them to dNDPs needed for growth is catalyzed through RNR, the activity of which should be finely regulated. The binding of ATP, or dATP at an allosteric site controls RNR activity of class 1a. *C. jejuni* cannot grow under strictly anaerobic conditions, even in the presence of alternative electron acceptors that do allow growth under oxygen-limiting conditions (Sellars *et al*. 2002). This seems to be due to the presence of a single class 1a-type ribonucleotide redcutase (RNR) that would require catalytic amounts of oxygen to sustain DNA synthesis. This RNR is composed of an alpha subunit (NrdA; Cj0024) that is predicted to catalyse

ribonucleotide reduction using a cysteine radical, generated by long-range transfer from a tyrosine radical formed in the beta subunit (NrdB; Cj0231). In Class Ia RNRs, the tyrosine radical in NrdB is generated by oxygen and electrons from two reduced iron centres in a μ-oxo-bridged configuration, while in class 1b enzymes which have oxygen unreactive manganese ions instead of iron, superoxide generated by a reduced flavodoxin (NrdI) is used to form the radical in the beta subunit, designated NrdF (Stubbe and Cotruvo, 2011).

This chapter reports evidence that FqrB provides an additional route for flavodoxin reduction using NADPH as the ultimate electron donor and that both FqrB and FldA are involved in tyrosine radical formation in, and thus activation of, the *C. jejuni* RNR.

4.2 Results

4.2.1 Bioinformatic analysis of *C. jejuni* FqrB

The sequence of FqrB (Cj0559) protein was subjected to BLAST analysis, multiple sequence alignment and phylogenetic analysis (Figure. 4.1). The results indicated that Epsilonproteobacterial enzymes including *C. jejuni* Cj0559, cluster with a specific group of reductases from Gram-positive bacteria found in *Bacillus subtilis* (YpdA) and *B. cereus/B.anthracis* (FNR3) but are distinct from thioredoxin reductases (TrxR) and CoA disulphide reductases (Cdr). YpdA is a putative bacillithiol disulphide reductase (Gaballa *et al*., 2010; Mikheyeva *et al*., 2019) and FNR3 enzymes have been characterized as flavodoxin reductases; *B. cereus* FNR3 can reduce NrdI, a specific flavodoxin required for formation of the tyrosyl radical in the Mn-containing Class Ib RNR's in many Gram-positive bacteria (Lofstad *et al*., 2016). The FNR1 and FNR2 enzymes also reduce NrdI, with FNR2 being most efficient (Lofstad *et al*., 2016), but these are more distantly related to FqrB (Figure 4.1).

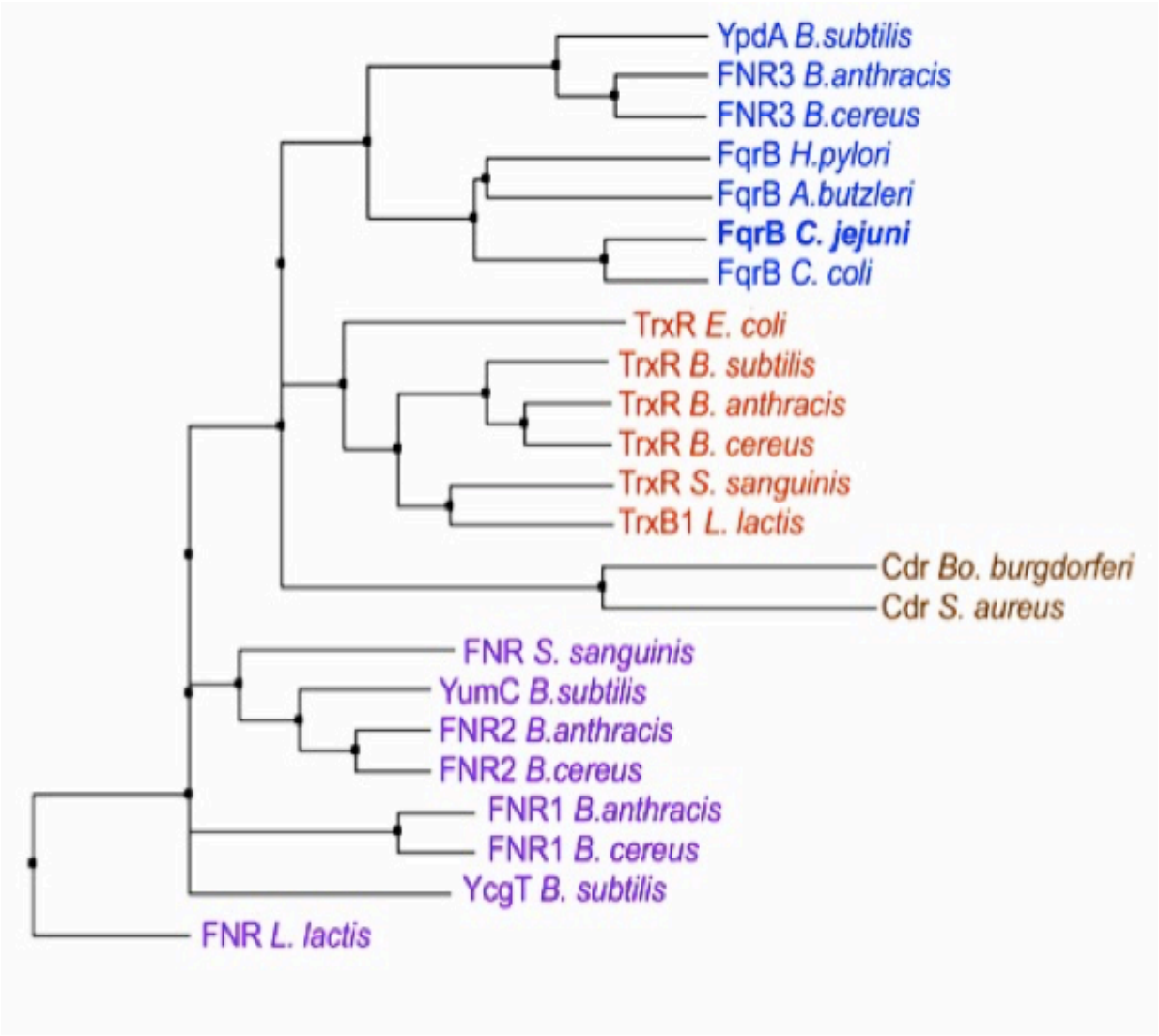

Figure 4.1: FqrB is related to flavodoxin reductases in Gram-positive bacteria. Phylogenetic tree of a selection of PNDOR enzymes from Gram-negative and Gram-positive bacteria. A multiple sequence alignment was generated in CLUSTAL omega then JALVIEW used to construct the tree shown. Sequences were obtained from UNIPROT.

After showing that FAD/FMN-containing proteins in Gram-positive bacteria and *C. jejuni* FqrB/FldA are related and have biochemical similarities, the hypothesis that *C. jejuni* FqrB/FldA may fulfil the same role in RNR activation was examined by both *in vivo* and *in vitro* experiments.

4.2.2 Construction of an *fqrB* mutant and complemented strain

In vivo experiments started with attempting to delete the *fqrB* gene and studying the phenotype by supplementing the growth media with deoxyribonucleosides. Isothermal assembly (ISA) cloning (Gibson *et al*., 2009) was used to generate a plasmid for transformation into *C. jejuni*, that deletes *cj0559* (*fqrB*) by allelic exchange mutagenesis, replacing most of the coding region with a kanamycin resistance cassette derived from pJMK30 (van Vliet *et al*., 1998), which carries a constitutive promoter and no terminator. To complement this mutant with the wild-type *fqrB* gene driven by its native promoter, the gene plus ~200 bp upstream sequence was amplified with primers FQRB_COMP_F and FQRB_COMP_R (Table 2.2) and cloned into the pRRA vector (Cameron and Gaynor, 2014) at MfeI and XbaI sites. This recombines the gene at one of the 16S rRNA loci. This plasmid was electroporated into the *fqrB* mutant and colonies selected on Columbia blood agar plates plus kanamycin and apramycin.

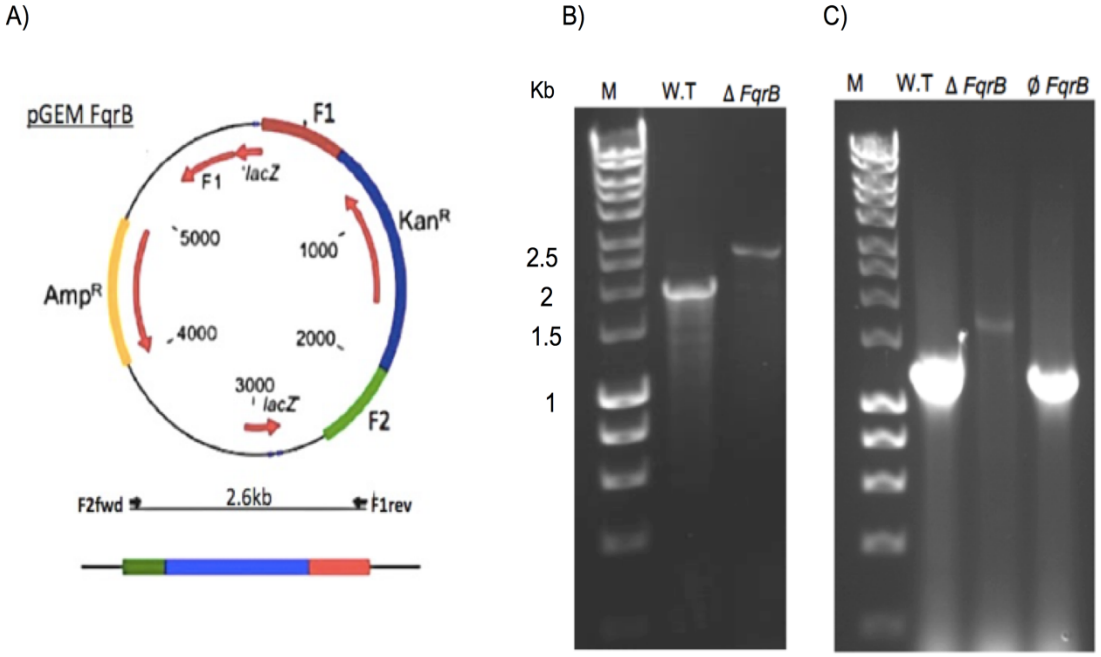

Figure 4.2: Generation of fqrB mutagenesis plasmid by ISA using pGEM-3Zf. **(A)** Plasmid map of pGEMFQR shows the flanking regions of the targeted gene. Red is Flank 1 (F1), 600 bp that is upstream of the fqrB gene. Green is Flank 2 (F2) that is downstream of the fqrB gene. Targeted gene is interrupted by kanamycin resistant cassette (blue). The other regions in the plasmid are AmpR region (gold), F1 origin of replication and the lacZ gene. **(B)** KanF plus F1R primers were used to confirm cloning. Lane W.T, the expected PCR product is 2.0 kb. Lane ∆ FqrB, the expected PCR product is 2.6 kb. **(C)** To confirm cloning, PCR was done on colonies grown on media supplemented with (Ampicillin +kanamycin for ∆ FqrB) and (ampicillin +kanamycin+ apramycin for ⌀ FqrB) as template with FQRB_COMP_F and FQRB_COMP_R primers. Lane W.T, the expected PCR product is 1.2 kb. Lane ∆ FqrB, the expected PCR product is 1.6 kb. Lane ⌀ FqrB, the expected PCR product is 1.6 kb. M is ladder.

4.2.3 Growth phenotype of an *fqrB* mutant and complemented strain

Given the phylogenetic relationship noted above between FqrB and some NrdI reducing enzymes in Gram-positive bacteria, and the identification of FqrB as a redox partner for FldA, we sought *in vivo* evidence that FqrB might be involved in ribonucleotide reduction. Although *hp1164* (*fqrB*) was reported to be essential in *H. pylori*, we were able to construct a deletion mutant in the *cj0559* gene by replacing most of the coding region with a non-polar kanamycin resistance

cassette via allelic exchange mutagenesis. The mutant was also complemented with a wild-type gene copy inserted at the *cj0046* pseudogene locus, driven by the *metK* promoter.

The mutant formed small colonies on plates and in liquid culture on complex media it exhibited a significant growth defect compared to the wild-type and complemented strain (Figure 4.3A). When grown with a mixture of all four deoxyribonucleosides (dRNS) at 0.1 mM each (final concentration), the final cell yield of the wild-type and complemented strain was not significantly different from that of the controls, whereas the mutant showed a similar growth rate but statistically significant ~25 % increase in final cell yield (Figure 4.4B). Interestingly, in the presence of a higher concentration (1 mM each) of dRNS, the growth rate and final cell yield of the wild-type and complemented strain were severely inhibited, an effect probably due to an imbalance in the intracellular concentrations of DNA precursors (Torrents 2014). However, the growth rate and final cell yield of the *fqrB* mutant was unaffected (Figure 4.4 A). The mutant was also significantly less affected by the toxic nucleotide analogues 6-thioguanine and 6-mercaptopurine compared to the wild-type and complemented strains (Figure 4.5). Taken together, these results suggest that the lack of FqrB in the mutant affects dRNS uptake and metabolism; a slower conversion of ribonucleotides to deoxyribonucleotides via ribonucleotide reductase might explain the partial growth stimulation by exogenous dRNS.

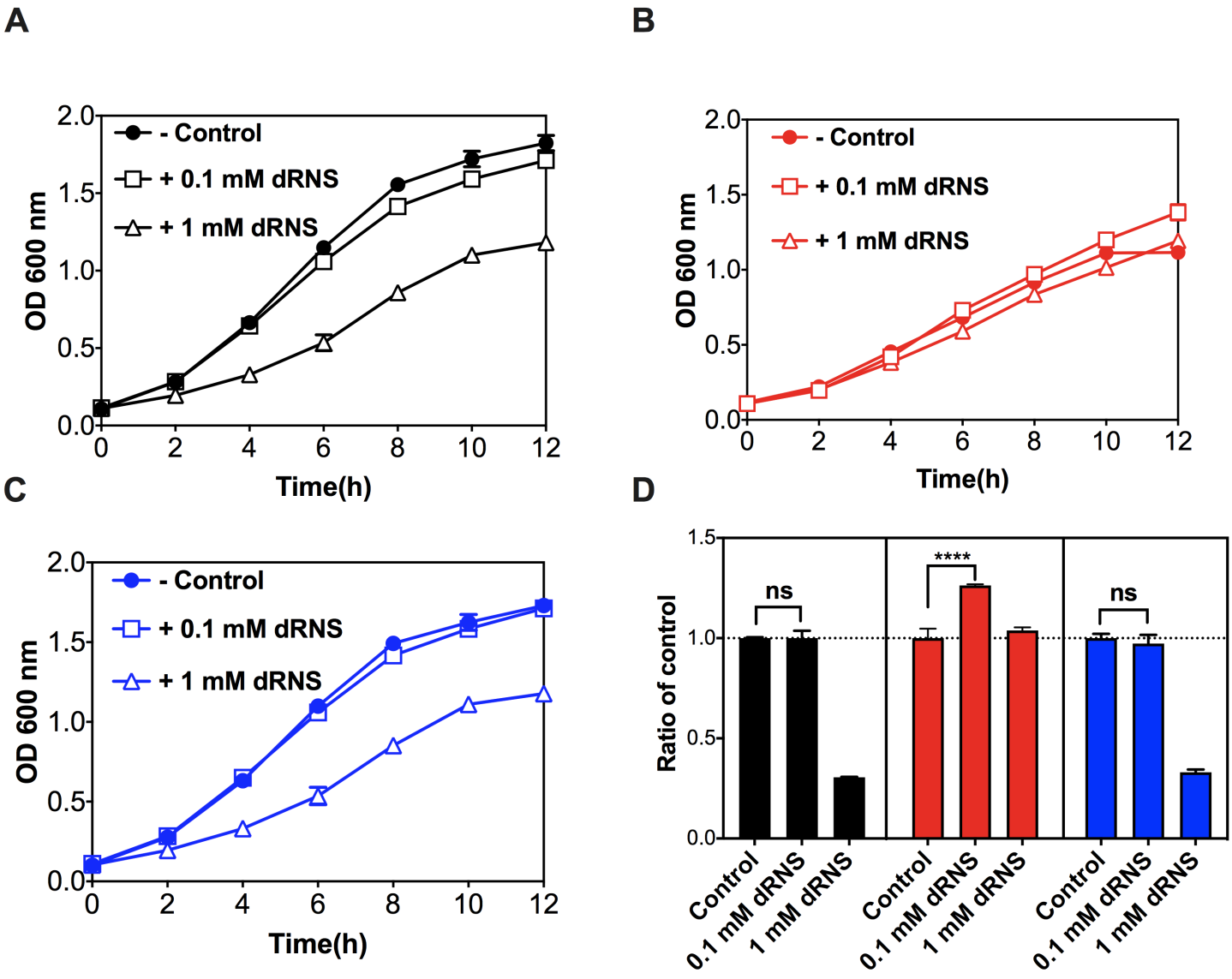

Figure 4.4: Growth phenotypes of wild-type, *fqrB* mutant and complemented strains and effect of deoxyribonucleoside addition. In **(A)**, **(B)** and **(C)** growth curves of wild-type (black symbols) **(A)**, *fqrB* mutant (red symbols) **(B)** and complemented strain (blue symbols) **(C)** under standard microaerobic conditions in complex MHS media are shown over a 12 hr period in the absence or the presence of the indicated concentrations of a mixture of the 4 deoxyribonucleosides (dRNS). The data points are means of duplicate cultures with error bars (SD), too small to be seen in many cases. In **(D)** independent cultures as in **(A, B and C)** were set up in triplicate and the OD600 nm measured after 12 hr. The data are expressed as a ratio of the controls without dRNS addition. Error bars show SD and the significance of the effect of 0.1 mM dRNs estimated by Student's t-test (ns, not significant; **** P <0.0001).

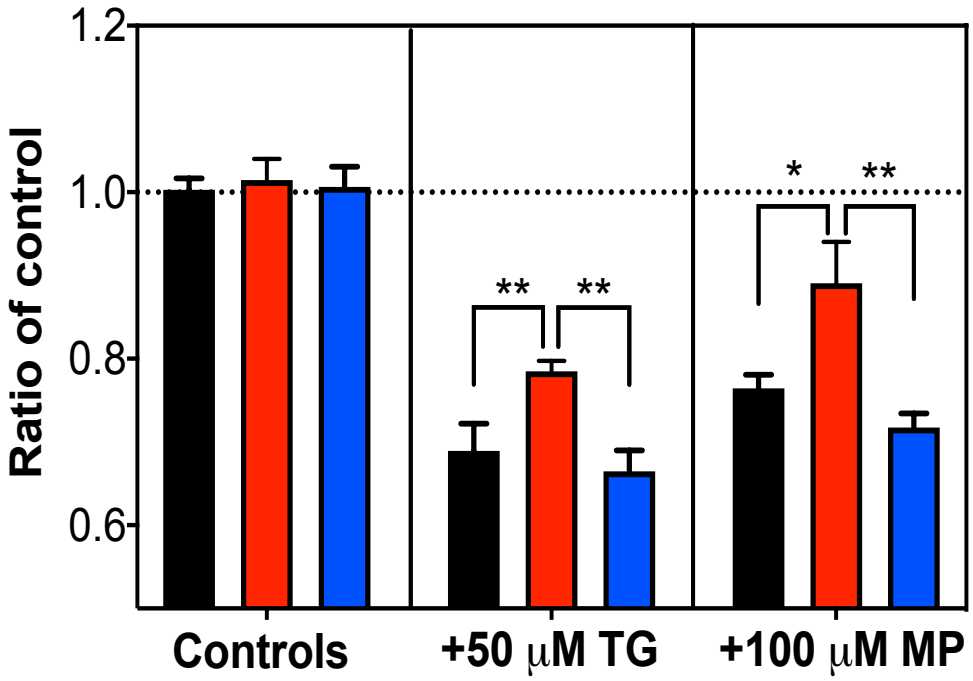

Figure 4.5: The effect of the toxic nucleotide analogues 6-thioguanine (TG) and 6-mercaptopurine (MP) on wild-type (black bars), *fqrB* (red bars) and complemented strain (blue bars) were evaluated by growth in MHS media. Cultures as in Figure. 4.4 A were set up in triplicate and the OD600 nm measured after 12 hr. The data are expressed as a ratio of the controls without TG or MP addition Error bars show SD and the significance of the effect of TG or MP estimated by Student's t-test (** P <0.01; * P <0.05).

As noted above, NrdI is itself reduced by a specific reductase of the PNDOR family. Also, the dRNS growth stimulation observed in the *C. jejuni fqrB* mutant (Figure 4.4), could be explained if radical formation in the *C. jejuni* NrdB protein required FldA, with FqrB acting as a physiologically relevant flavodoxin reductase. However, CjFldA is distinct from NrdI proteins and the alpha and beta subunits of *C. jejuni* RNR and other Epsilonproteobacteria are related to other Class Ia NrdA and NrdB proteins from Gram-negative bacteria and are not Class 1b enzymes. The *C. jejuni* NrdA subunit also has a typical N-terminal ATP-cone domain that is characteristic of a Class 1a enzyme (Hofer *et al.*, 2011). Therefore, we wished to test if radical formation in *C. jejuni* NrdB required flavodoxin, by producing purified

radical free NrdB and reconstituting with FldA, FqrB and NADPH to determine if the radical could be regenerated *in vitro*.

4.2.4 FqrB overexpression and purification

The *fqrB* was cloned between the NdeI and XhoI sites of the pET21a vector such that a 6-his tag was attached in-frame to the C-terminus of the cognate protein. The primers used are shown in Chapter 2 (Table 2.2). Then the pETFqrB (Figure 4.6) plasmid was transformed into *E. coli* BL21(DE3), grown in 1-5 L batches of LB media (plus carbenicillin 50 μg ml^{-1}) at 37 °C to an OD_{600} nm of 0.5, then protein production induced by 0.4 mM isopropyl-thiogalactoside (IPTG) for up to 5 hr. The predicted size of FqrB is 36 kDa. The protein was purified by nickel affinity chromatography and then by a HIC column. FqrB was heterologously overproduced and purified. The purity of the protein was verified by SDS-PAGE (Figure 4.7A). FqrB is a yellow-coloured protein with an absorption spectrum typical of a flavoprotein with maximum at ~375 nm and ~460 nm (Figure 4.7B).

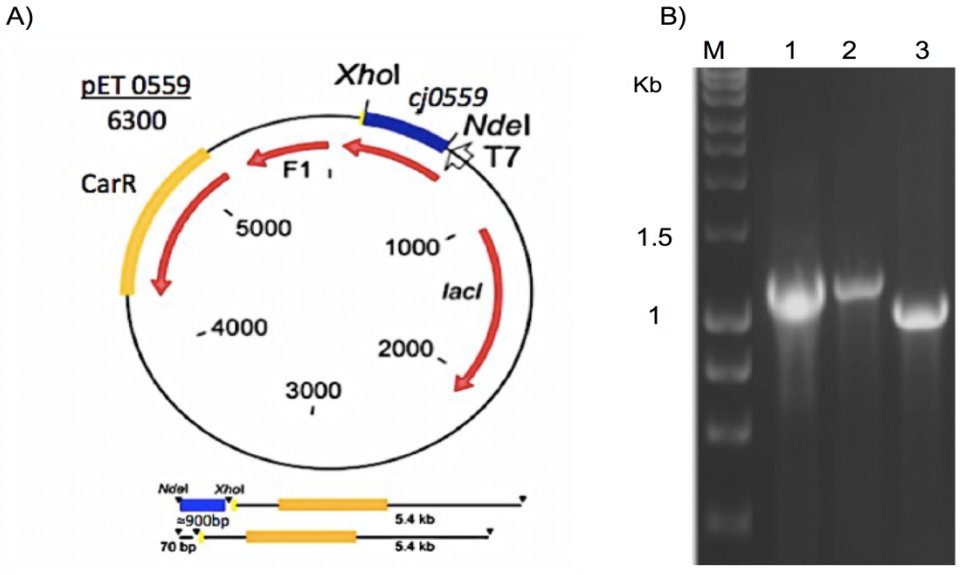

Figure 4.6: Generation of overexpression plasmid pETFqrB. **(A)** pETFqrB plasmid was made by inserting PCR amplified *cj0559c* between the NdeI and XhoI restriction sites in pET21a. **(B)** The cloning was confirmed by using PCR with different combination of T7 primers and *fqrB* primers and the pETFqrB as template. Lane 1 FqrBF + T7R**.** Lane 2 T7F + FqrBR. Lane 4 FqrBF + FqrBR.

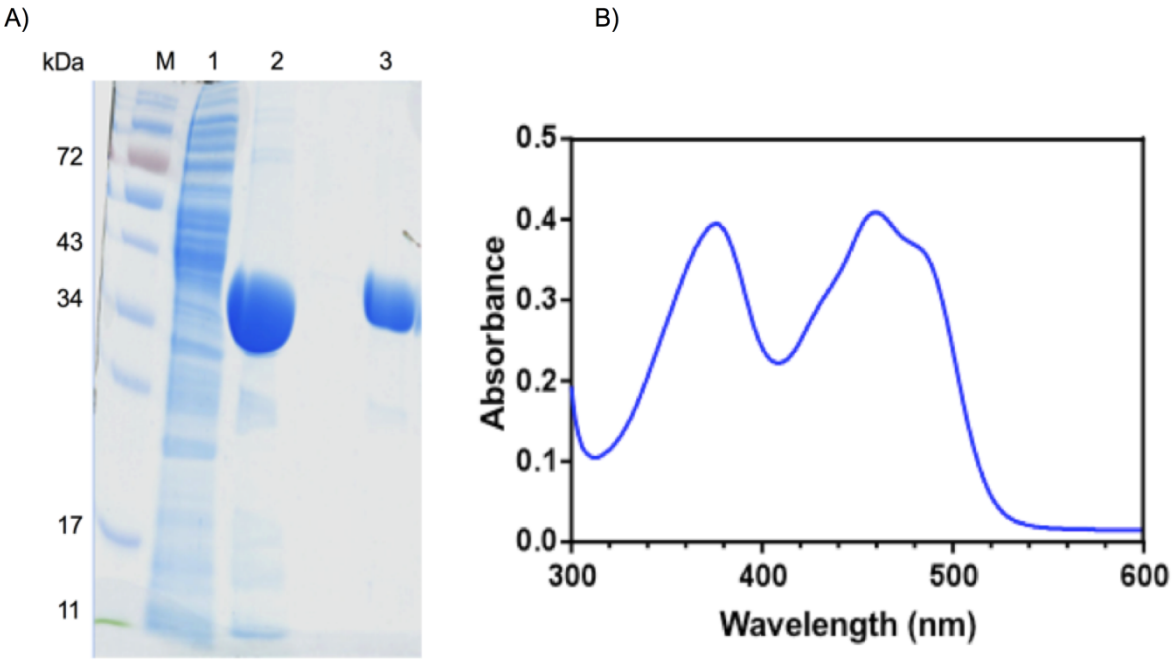

Figure 4.7: Purification of FqrB. (A) Lane 1: Flow-through after running the sample through a His-column. Lane 2: Fqr protein from His column with faint bands indicating that the protein is not pure. Lane 3: pure Fqr protein aftrer further purification on a HIC column. **(B)** UV-VIS absorption spectrum of purifed *C. jejuni* FqrB (50 μM) with FAD peaks at 375 nm and 460 nm. M = Protein Molecular Weight markers

4.2.5 FqrB redox properties and FldA reduction

FqrB initial reduction studies started with performing NADH/NADPH oxidase assays for purified FqrB using O_2 as substrate. With oxygen, the results indicated that Fqr preferentially uses NADPH rather than NADH as an electron donor (Figure 4.8). Then, the ability of the purified C-terminally his-tagged recombinant FqrB to act as an NAD(P)H-dependent reductase for the flavodoxin FldA was tested. In aerobic buffer at pH 7.5 FqrB exhibited a low rate of NADPH oxidase activity (0.79 ± 0.07 μmol min^{-1} mg $protein^{-1}$, n = 3 determinations), but activity with NADH was over 10-fold lower (0.06 ± 0.01 μmol min^{-1} mg $protein^{-1}$, n = 3). When incubated under strictly anaerobic conditions with a molar excess of FldA, FqrB readily catalyzed the reduction of FldA with NADPH (Figure 4.9 and inset) but not with NADH (Figure 4.9 and inset). Using an estimated extinction coefficient for flavodoxin FMN of 12 mM^{-1} at 460 nm (Mayhew and Tollin, 1992) we determined

a rate of 14.5 ± 0.2 μmol FMN reduced min^{-1} mg FqrB $protein^{-1}$ with NADPH as reductant (n = 3). These data show that *C. jejuni* FqrB is an efficient FldA reductase specific for NADPH. This supports a role in maintaining a reduced FldA pool using NADPH as electron donor in addition to the POR and OOR reactions.

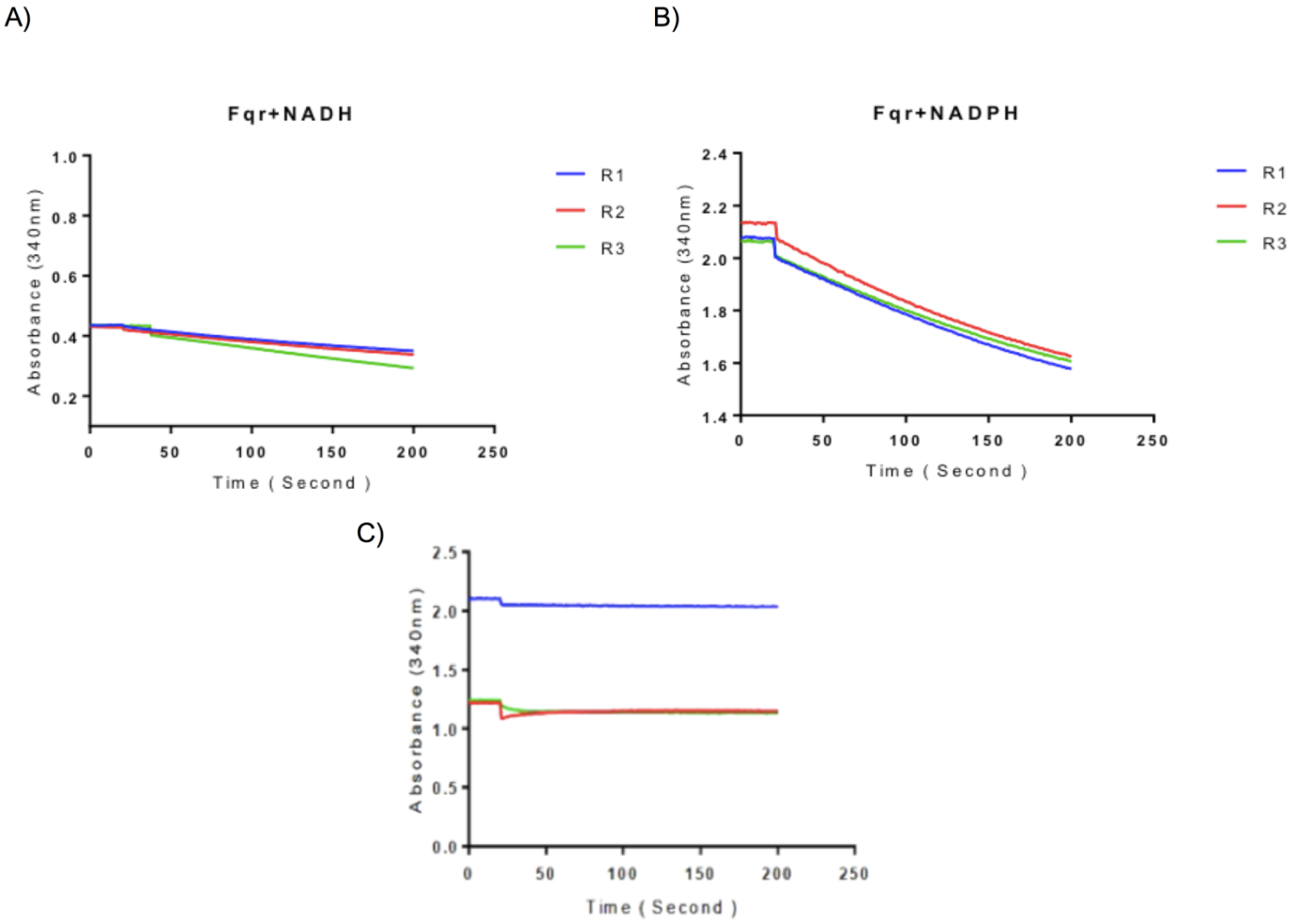

Figure 4.8: NAD(P)H oxidase activity of Fqr. The absorbance of 0.3 mM NADH/NADPH in 50 mM Tris-HCl buffer pH 7.5 was recorded alone for 30 seconds. Then, 0.1 mM FqrB was added to start the reaction and recorded for 3 minutes. **(A)** Oxidation of NADH was followed aerobically at 340 nm in the presence of pure Fqr. **(B)** oxidation of NADPH was followed aerobically at 340 nm in the presence of pure Fqr. The oxidation reaction was measured thrice for NADH and NADPH. **(C)** As a control the same reactions were measured anaerobically.

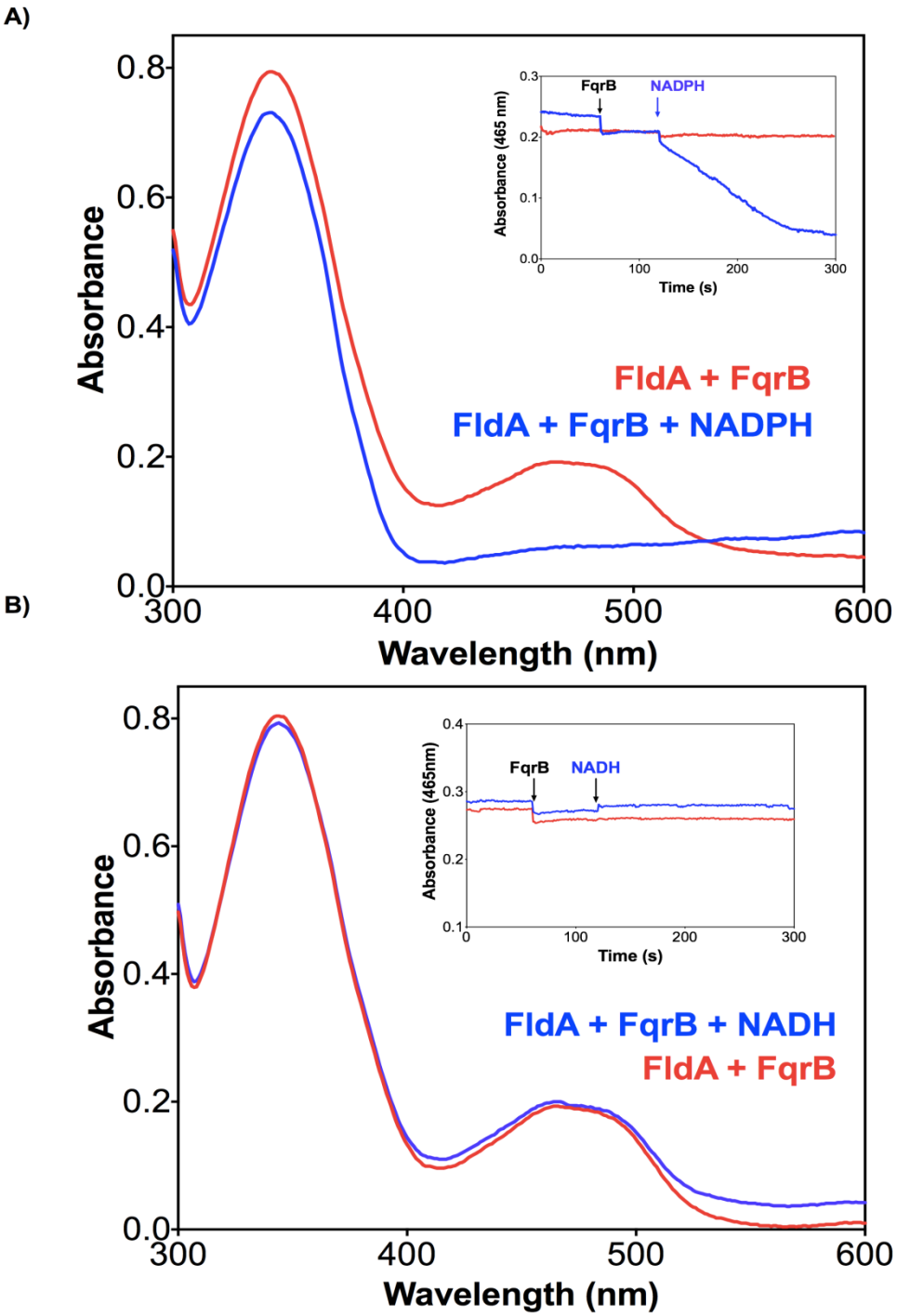

Figure 4.9: FqrB is an NADPH specific FldA reductase. (A) NADPH dependent reduction of FldA catalysed by FqrB. The absorbance spectrum of a mixture of FldA (50 μM) and FqrB (0.1 μM) in 50 mM Tris-HCl buffer pH 7.5 was recorded alone (red trace) or 5 minutes after the addition of NADPH (150 μM final concentration). The *inset* shows a kinetic trace at 465 nm, to show the FldA FMN reduction**. (B)** same as **(A)** but with NADH.

4.2.6 NrdB overexpression and purification

The Cj0231 coding region was amplified by PCR using primers with NdeI and XhoI sites, as listed in Chapter 2 in Table 2.2. The gene was cloned into pET21a using the same procedures as described above for *fqrB* to produce pETNrdB (Figure 4.10). Solubility trials were carried out at 25 and 37 °C to determine if the overproduced protein was soluble in the cell cytoplasm and folded correctly. A strong band on Coomassie stained gels of ~ 40 kDa corresponding to the size of NrdB was observed. Some insoluble protein was observed at both induction temperatures, but there was also a large amount of soluble protein at both 25 °C and 37 °C (Figure 4.11). It was decided to use induction with 0.4 mM IPTG and induction at 37 °C for 5 hr as the standard induction protocol.

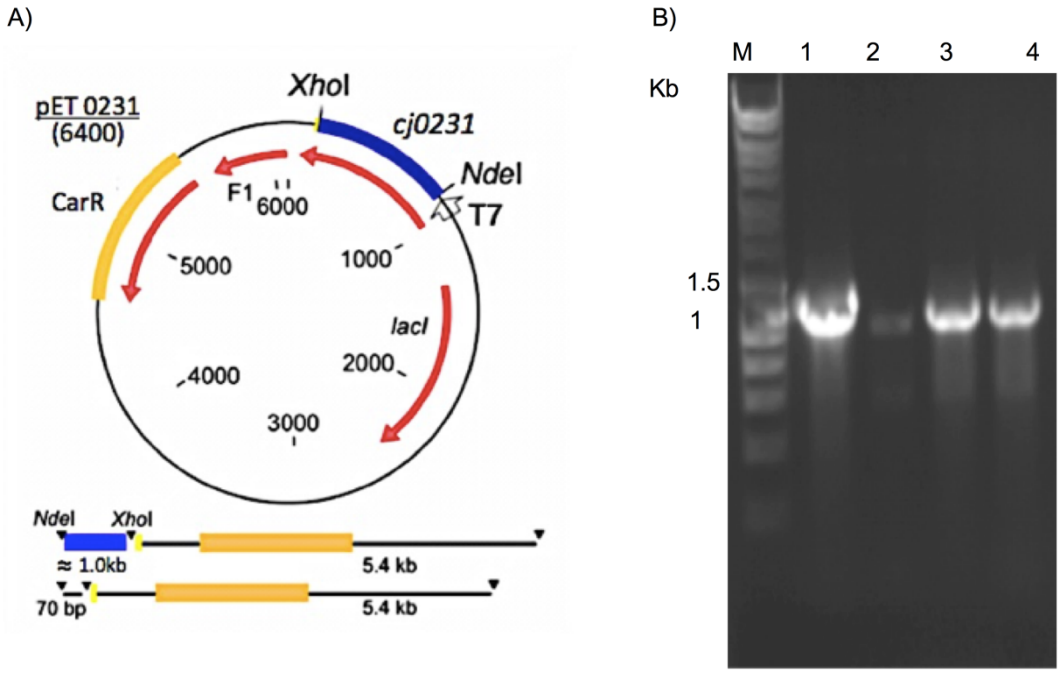

Figure 4.10. Generation of overexpression plasmid pETNrdB. **(A)** pETNrdB plasmid was made by inserting PCR amplified *cj0231c* between the NdeI and XhoI restriction sites in pET21a. **(B)** The cloning was confirmed by using PCR with different combination of T7 primers and *nrdB* primers and the pETNrdB as template. Lane1 T7F + T7R. Lane 2 NrdBF + T7R**.** Lane 3 T7F + NrdBR. Lane 4 NrdBF + NrdBR.

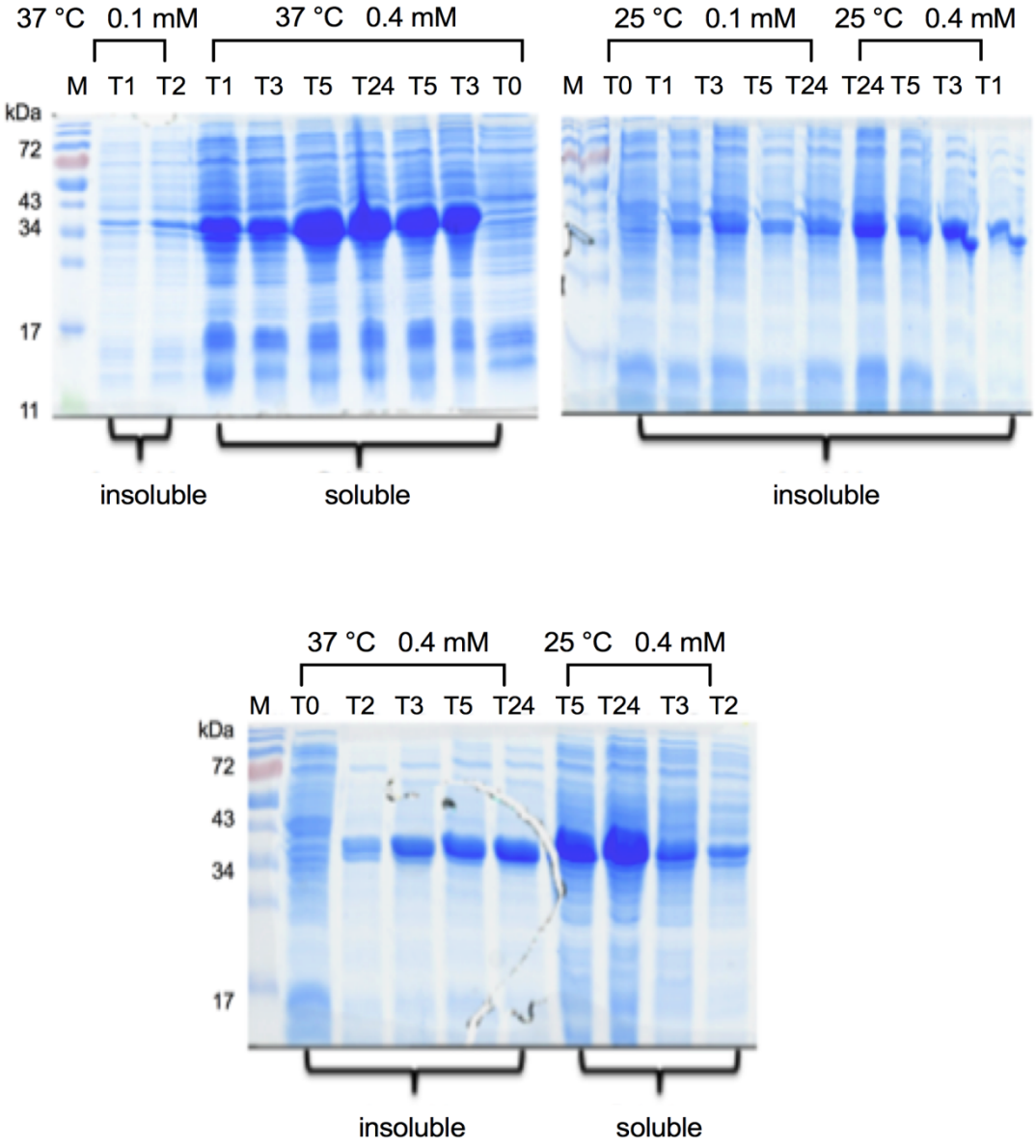

Figure 4.11: Solubility trials of NrdB were conducted by culturing the transformed *E. coli* BL-21 in LB with carbenicillin (50 μg ml^{-1}) to an OD_{600} 0.6 before inducing over-expression by the adding 0.1 mM IPTG or 0.4 mM IPTG. At both 25 °C and 37 °C cells were cultured and sampled periodically (T0, T1, T3, T5, T7, T24 hr) to ascertain the optimum temperature and time post-induction for adequate production of protein. These cells were resuspended in binding buffer, sonicated and centrifuged to produce soluble fraction and insoluble fractions resuspended in dH_2O. M = Protein Molecular Weight marker.

After determining the optimal conditions, NrdB was expressed as a C-terminally his-tagged protein and purified by nickel affinity chromatography. Two bands were consistently seen Figure 4.12. The upper band corresponds to the right size for NrdB (40339 Da). In order to separate these two bands, elution by a decreasing salt gradient on a HIC column and gel filtration were used. Both purification approaches were unsuccessful. This may indicate that the lower band is cleaved off the protein as they both behave the same against high salt concentration and the size of two bands is too close to be separated by gel filtration. The gene was also cloned and expressed as an N-terminally his-tagged protein. In both proteins (C-terminally his-tagged protein, N-terminally his-tagged protein) the lower band size is (36000 Da) which means that this is not protein degradation from the N-terminal end, otherwise the size of the lower band would be different. To determine whether this was due to contamination or Post-translational modification (PTM), the two bands from the gel were analysed via HPLC-MS in “Biological Mass Spectrometry Facility” Sheffield University. Each band was analysed separately and the tryptic peptides that were found in the bands compared in Figure 4.13. Both bands contain the same peptides, suggesting the two bands are the same protein (ie NrdB) but result from an unidentified PTM that causes a shift to a lower apparent size on SDS-PAGE.

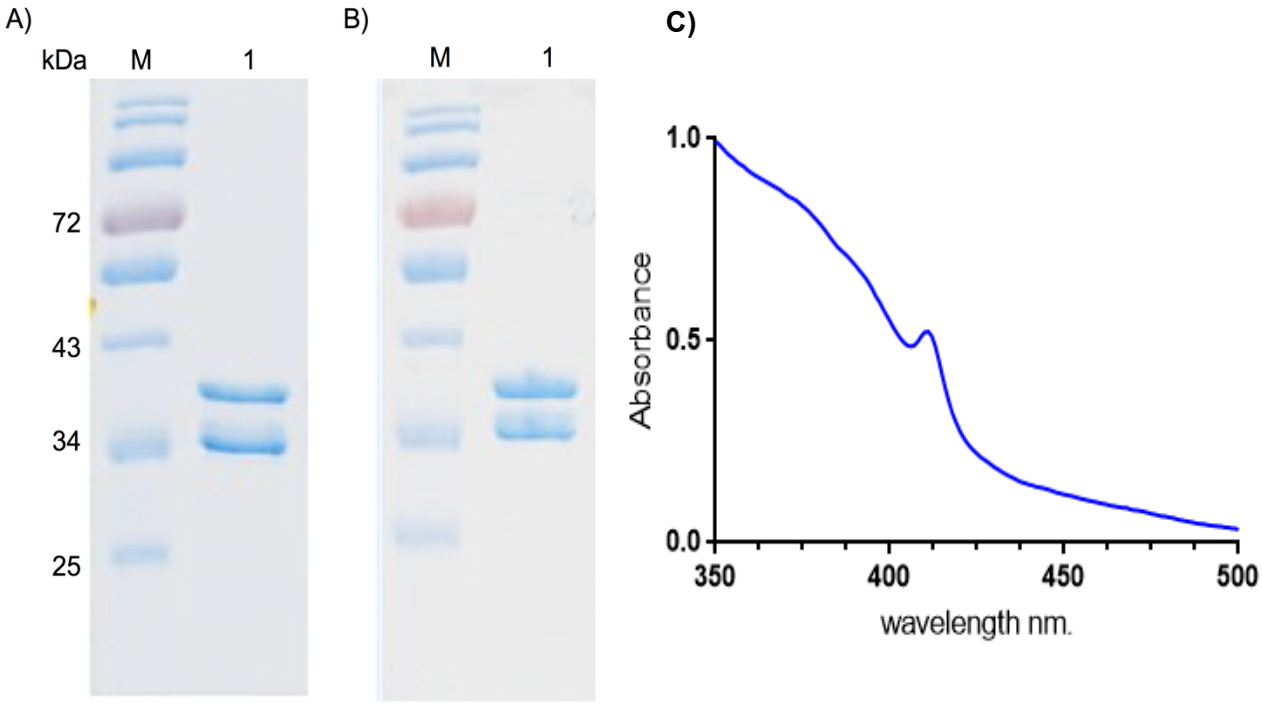

Figure 4.12: 12 % SDS-PAGE gel shows NrdB protein purified by His-column. **(A)** Lane 1: C-terminally his-tagged NrdB protein. **(B)** Lane 1: N-terminally his-tagged NrdB protein. **(C)** UV-VIS absorption spectrum of purifed *C. jejuni* NrdB (C-terminal His) with tyrosyl radical signal at 411 nm.

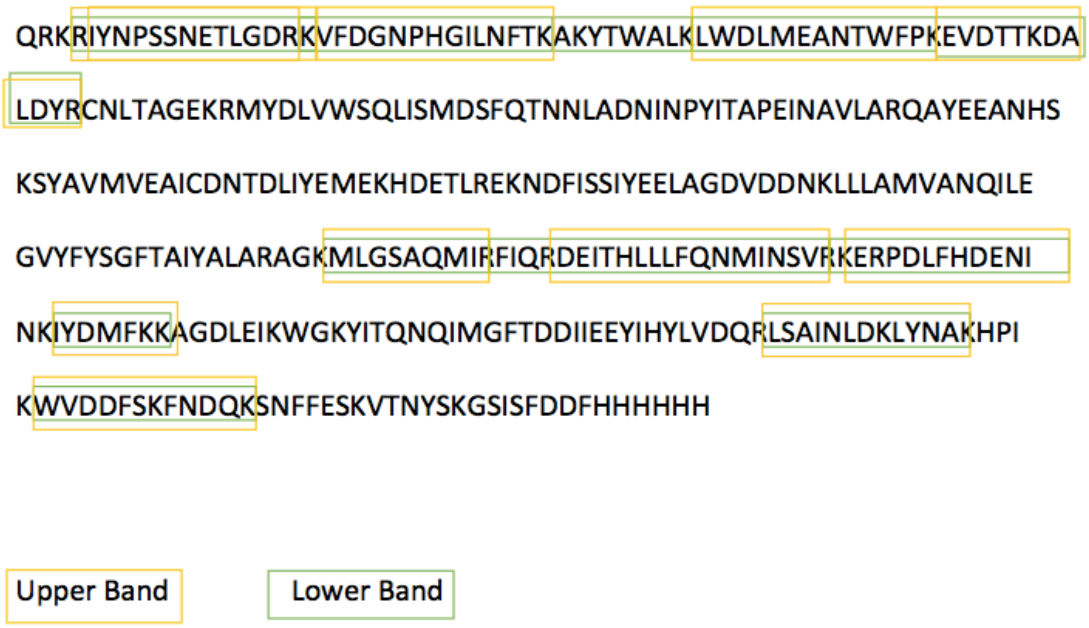

Figure 4.13: MS analysis of NrdB protein bands. Both bands seen on SDS-PAGE were digested by trypsin and the peptides identified by MS in the upper band are indicated in the yellow box and lower band in green box. Both bands contain the same peptides.

4.2.7 Characterisation of NrdB, the RNR beta subunit of *C. jejuni*

The peak at 411 nm in the absorption spectrum of purified NrdB (Figure.4.12C) is diagnostic of a stable tyrosine radical. The RNR tyrosyl radical is formed within the cells; however, it can be lost after proteins are purified. In this respect, *C. jejuni* NrdB is more like *E. coli* NrdB, *M. tuberculosis* NrdF or *S. typhimurium* NrdF in that they keep the tyrosyl radicals upon purification, but unlike mouse NrdB and *B. anthracis* NrdF that are purified as radical free apoproteins. The metal content of independently purified batches of the protein was determined by ICP-MS after growth in either unsupplemented, iron- or manganese supplemented media (Figure 4.14 A). In each case, the molar ratio of Fe/protein (1.0, 1.4 and 0.85 respectively) was significantly higher than the Mn/protein ratio (0.14, 0.05 and 0.25 respectively). Overall, the data confirm that the *C. jejuni* RNR is indeed an Fe enzyme; although the expected ratio of Fe/monomer is 2, a suboptimal stoichiometry is commonly found in heterologously expressed RNRs (Roca *et al*., 2008). Figure. 4.14 B shows a typical sharp feature at 411 nm

diagnostic of the presence of a stable tyrosyl radical as well as weaker charge transfer bands centred around 325 nm and 370 nm arising from the μ-oxo-bridged diferric centre. We found that treatment of the protein with 1 mM hydroxylamine (HA) for 30 minutes efficiently scavenged the Y radical, as evidenced by the disappearance of the 411 nm signal (Figure 4.14B). Although the optical spectrum of the HA treated protein also appeared to lack the 370 nm absorbance associated with the di-ferric centre, comparison of the EPR spectra of the as-purifed and HA-treated protein showed equivalent features at g = 4.3 attributed to residual magnetically isolated ferric iron, suggesting no loss of iron (Figure 4.14 C). Calculation of the difference spectrum of HA treated versus untreated protein (Figure 4.14 B) and applying a literature value for the extinction coefficient of 3.25 mM cm^{-1} for the radical (Peterson *et al*., 1980) resulted in an estimation of the radical yield in the purified protein of 0.7 per monomer, comparable with data for other enzymes (Roca *et al*., 2008). In contrast to hydroxylamine, treatment with the commonly used radical scavenger hydroxyurea (HU) did not result in quenching, even in the presence of the metal chelator EDTA (Figure 4.14 A). However, from Figure 4.14 B it can be seen that the growth of *C. jejuni* cells is sensitive to the radical scavenger hydroxyurea, indicating that hydroxyurea may scavenge other radicals that are essential for growth or it scavenges the radical from one of the intermediates that are formed during the tyrosyl radical (Y•) transfer (~35 Å or 3.5 nm) from the radical generator (NrdB) to the thiyl radical site in NrdA where it is needed to reduce NDPs.

4.2.8 Crystallization and structure determination of *C. jejuni* NrdB

The *C. jejuni* RNR clearly has some unusual properties compared to other Class Ia RNRs. Most importantly, the NrdB subunit utilizes flavodoxin for radical fomation, whereas other Class 1a RNRs which are thought to use ferredoxin as the reductant. Also, the tyrosyl radical within the *C. jejuni* NrdB protein is resistant to hydroxyurea, which readily scavenges the radical in other NrdB proteins. The primary sequence of *C. jejuni* NrdB indicates it should be a “typical”

Class Ia protein, but the 3D-structure may reveal the basis for its interesting properties. In order to explain the reasons behind these differences, I have therefore tried to obtain the crystal structure of *C. jejuni* NrdB.

The *C. jejuni* NrdB was overexpressed and purified, concentrated to at least 10 mg ml^{-1} (~100 µM NrdB) and kept in 50 mM Tris-HCl buffer pH 7.5 at 4 °C. Crystallization trials were carried out using 3 different screen buffers (PACT, JCSG, and Proplex) in different pH conditions (pH 6, pH 6.5, pH 7 and pH 7.5) and PEG3350 concentrations (14%, 16%, 18%, 20%, 22% and 24% w/v PEG) with a 100 mM Bis-Tris buffer. After two weeks incubation, small crystals could be seen in the screen buffer JCSG condition with 100 mM Bis-Tris pH 7.5; 22 % w/v PEG3350. Then, hanging drop experiments were set up in this same JCSG condition (100 mM Bis-Tris pH 7.5; 22 % w/v PEG3350). However, after 18 days incubation, no crystal formations were observed. There could be various reasons for this failure, but the most likely explanation is that the unidentified post-translational modification that causes purified NrdB to run as 2 bands on SDS-PAGE results in heterogeneity in the protein population that prevents large crystals from forming (Figure 4.12). In future work, it will be important to identify what this PTM is and to try to produce a pure unmodified protein preparation for crystallisation studies.

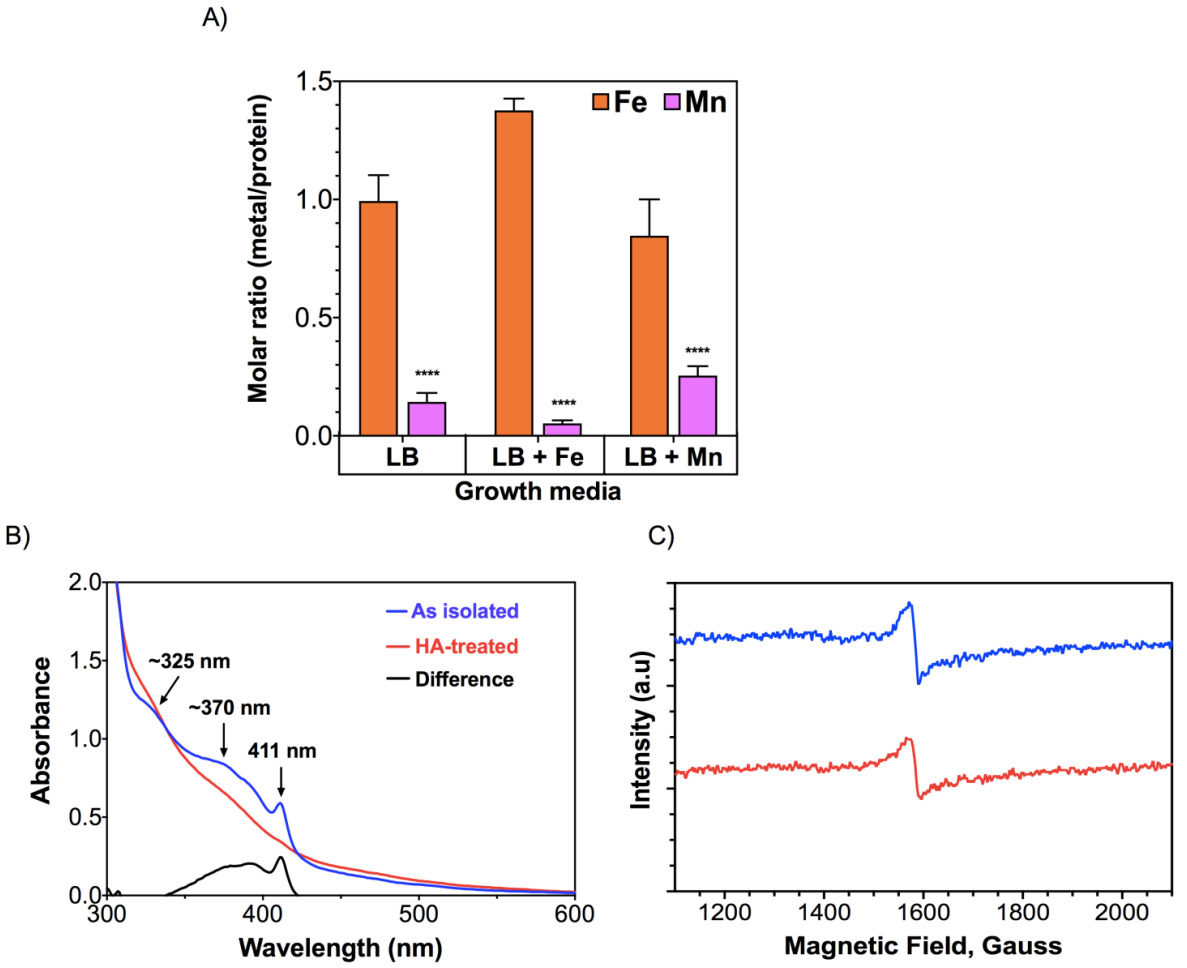

Figure 4.14: Characterisation of the NrdB subunit of *C. jejuni* RNR. His-tagged NrdB was purified from *E. coli* BL21 (pETNrdB) as described in Materials and Methods. **(A)** Iron (orange) and manganese (pink) content of NrdB, measured by ICP-MS. The data are the means and SD of 3 independent purifications from cells grown in LB alone, LB + Fe (50 μM ferrous ammonium sulphate) or LB + Mn (50 μM manganese chloride). The sulfur content of the samples was used to normalize the data to the protein content and is expressed as a molar ratio. In each case the Mn ratio is significantly lower than the Fe ratio (****, P <0.0001 by Students t-test). (**B**) Optical absorption spectroscopy of NrdB. The blue trace shows the spectrum of as-purifed NrdB (100 μM) with the tyrosine radical peak at 411 nm and charge transfer bands of the di-ferric centre at 325 nm and 370 nm. The red trace shows the spectrum after 30 minutes treatment with 1 mM hydroxylamine (HA), quenching the radical. The black trace is the difference spectrum, illustrating the Y-radical contribution. The EPR spectrum in (**C**) shows that HA treatment does not significantly alter the signal for residual magnetically isolated iron.

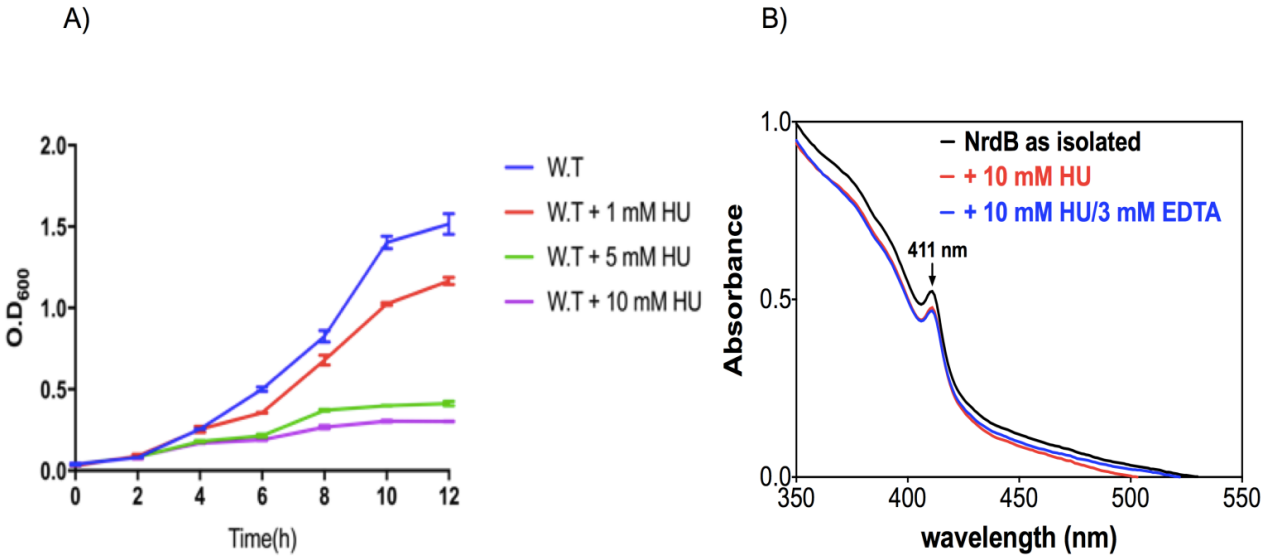

Figure 4.15: Hydroxyurea treatment of *C. jejuni* cells and NrdB protein. (A) growth curve to show that *C. jejuni* cells are sensitive to the radical scavenger hydroxyurea. **(B)** optical spectroscopy shows that a high concentration of hydroxyurea (HU), either with (blue trace) or without (red trace) EDTA does not appreciably quench the NrdB Y-radical.

4.2.9 Tyrosyl radical regeneration in NrdB can be catalyzed by FldA, FqrB and NADPH

The ability to produce a radical free NrdB preparation by hydroxylamine treatment followed by removal (Figure. 4.16) allowed us to investigate the requirements for radical formation in this protein. Incubation of HA-treated and dialysed NrdB with an equimolar concentration of the flavodoxin FldA (50 μM) plus a catalytic amount of FqrB (5 μM) and excess NADPH resulted in the build up of the characteristic Y radical absorbance at 411 nm (Figure 4.17A). A series of control incubations lacking any single component of this mixture resulted in no increase in absorbance at 411 nm (Figure 4.17B), showing that radical formation was dependent on reduced flavodoxin formed through the NADPH dependent reductase activity of FqrB. In order to further confirm that the Y radical had indeed been re-generated in the reconstituted system with characteristics similar to the native NrdB, we compared the EPR spectrum of a sample of as-purified NrdB with HA-treated NrdB and that obtained after reconstitution with NADPH, FqrB and FldA. The optical spectra of the samples used for EPR are shown in

Figure 4.18 A, which again confirm the presence of the 411 nm band after reconstitution, and the corresponding 10K EPR spectra are shown in Figure. 4.18 B. Essentially identical EPR spectra were recorded from both the as-purified protein and after reconstitution with NADPH, FqrB and FldA (Figure. 4.18B). The spectra also show that HA treatment effectively removed the radical from NrdB, with only very weak EPR signals remaining. The centre of the free radical EPR signals is at ~g=2.0052 and the lineshape is typical of that of Fe^2-Y radical containing Class 1a RNRs (Minnihan *et al.,* 2013).

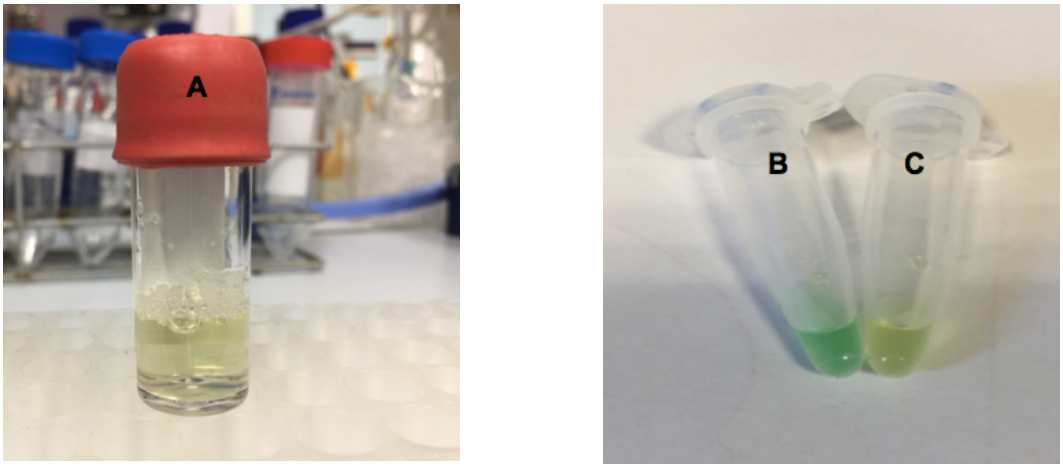

Figure 4.16: NrdB treatment with hydroxylamine and washing off was tested by formation of the green indooxine dye from hydroxylamine and 8-hydroxyquinoline. (A) as-purified NrdB. **(B)** HA-treated NrdB. **(C)** HA-treated and dialysed NrdB.

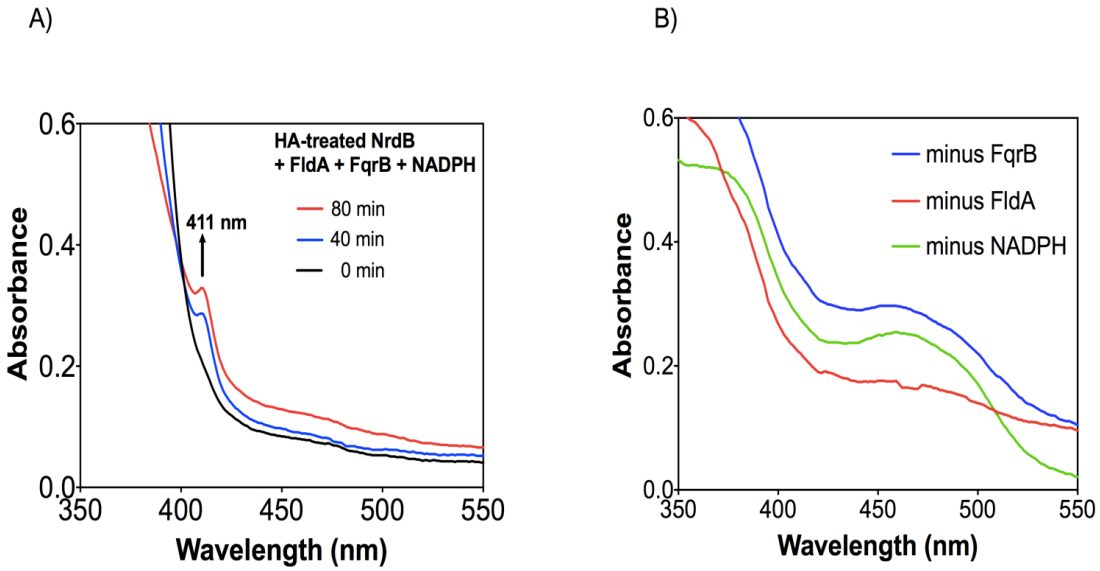

Figure 4.17: Reduced flavodoxin catalyses tyrosyl radical regeneration in NrdB. (A) a mixture of hydroxylamine-treated NrdB (50 μM final concentration), FldA (50 μM), FqrB (5 μM) and NADPH (1 mM) in 50 mM Tris-HCl buffer pH 7.5 was incubated at 37 °C and spectra recorded at the times shown. The build-up of the Y radical in NrdB is evident at 411 nm. **(B)** the spectra of a series of control incubations missing one of the components in **(A),** as indicated, was obtained after 80 minutes incubation at 37 °C.

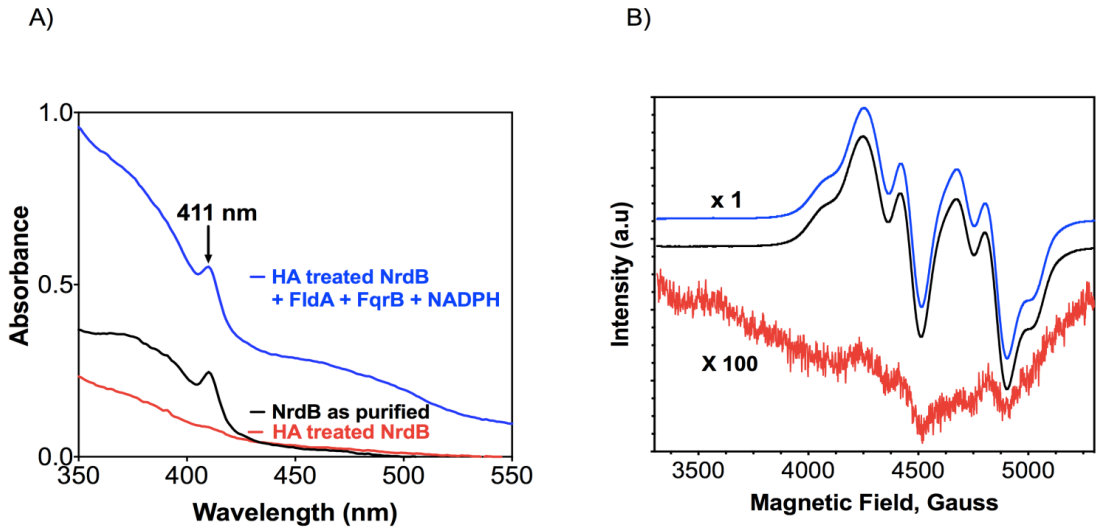

Figure 4.18: (A) The UV-visible spectrum of RNR *β*-subunit (NrdB) displayed a sharp band at 411 nm, indicative of the tyrosyl radical (Black line) (Minnihan *et al.,* 2013). After treating the protein with the radical scavenger hydroxylamine (1 mM 30 minutes), the tyrosyl radical quenched (Red line). The tyrosyl radical at 411 nm build up, after mixing of FqrB (5 μM), FldA (50 μM), NrdB (50 μM) and NADPH (1 mM) (blue line). **(B)** The EPR spectra of the *C. jejuni* NrdB RNR subunit as prepared (Blue line), or treated with hydroxylamine (NrdB+1 mM hydroxylamine) (Red line) and after the free radical has been reconstituted by flavodoxin (FldA) and flavodoxin reductase (Fqr) in the presence of 2 mM NADPH (Black line).

4.2.10 Is superoxide involved in FldA catalysed Y radical formation?

The di-ferrous centre in Class Ia RNRs is readily oxygen reactive and the electron input required for re-reduction has been proposed to be supplied by a small ferredoxin, YfaE (Wu *et al*., 2007), which is not present in *C. jejuni*. Given the *C. jejuni* RNR is a class Ia enzyme it seems most likely that the role of FldA identified above is as a simple electron donor to NrdB in place of YfaE. However, in class 1b RNRs that use oxygen unreactive Mn as cofactor, the NrdI flavodoxin generates superoxide which acts as the oxidant to form the Y radical (Berggren *et al*., 2014). The possible involvement of superoxide in the regeneration of the Y radical in the *C. jejuni* NrdB by reduced FldA was investigated in two ways. First, we added excess superoxide dismutase to a mixture of FqrB, FldA and HA-treated NrdB before adding NADPH to start the reaction. After prolonged incubation, Y radical formation was only slightly suppressed compared to

incubations lacking SOD (Figure 4.19A and 4.19B), but was still readily detectable. The caveat here is that superoxide could be channeled from flavodoxin to NrdB by close interaction, so may not be sensitive to SOD (Bergrren *et al*., 2014). Secondly, we incubated purifed HA-treated NrdB with the well-known xanthine oxidase /hypoxanthine superoxide generating system, as a way of generating superoxide independently of flavodoxin and FqrB. A time dependent formation of the Y radical could be observed, as evidenced by the absorbance increase at 411 nm (Figure. 4.19C). This suggests that at least *in vitro* superoxide can result in Y radical formation in *C. jejuni* NrdB.

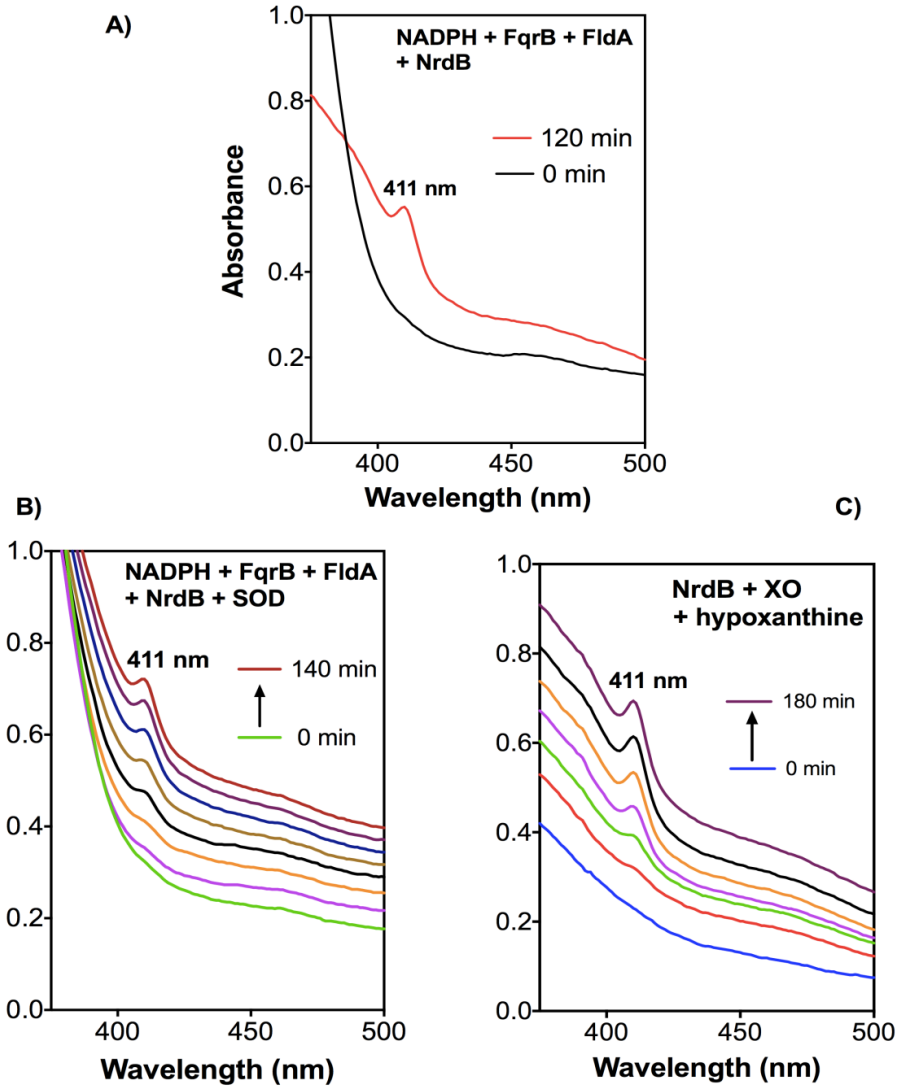

Figure 4.19: Superoxide can catalyse tyrosyl radical formation in NrdB *in vitro*. In **(A),** the complete reconstituted system of HA treated NrdB (50 μM), FldA (50 μM), FqrB (5 μM) and NADPH (1 μM) was incubated at 37 °C for up to 120 minutes to show formation of the tyrosyl radical at 411 nm. In **(B)** the same components were incubated with the addition of 20 units of SOD and the spectra recorded at 20 minutes intervals for the times shown. In **(C)**, HA-treated NrdB (50 μM) was incubated at 37 °C with 1 mM hypoxanthine and 0.5 units of xanthine oxidase for 3 hr and spectra recorded every 30 minutes as shown.

4.2.11 Comparisons of the FqrB mutant strain to other strains that are deleted in FldA reductase genes *por* and *oor*

In order to provide further *in vivo* support to our results, we attempted to isolate *C. jejuni* mutant strains deleted in the other FldA reductase genes *por* and *oor*. These mutant strains would be grown on media supplemented with deoxyribonucleosides and other substrates depending on the pathway that the protein contributes to. POR and OOR are normally found in anaerobic bacteria. These two proteins contain iron-sulphur (Fe-S) clusters that are very sensitive to ROS. Therefore, it is difficult to overproduce and purify them to repeat *in vitro* experiments that have been done with the FqrB protein. POR and OOR are responsible for oxidative decarboxylation of pyruvate and 2-oxoglutarate that leads to production of acetyl-CoA and Succinyl-CoA respectively.

We hypothesized that we might observe increased growth of these mutants after adding deoxyribonucleosides, similar to that of the *fqrB* mutant, because the flavodoxin pool might be under-reduced in these mutants, which would limit RNR activity.

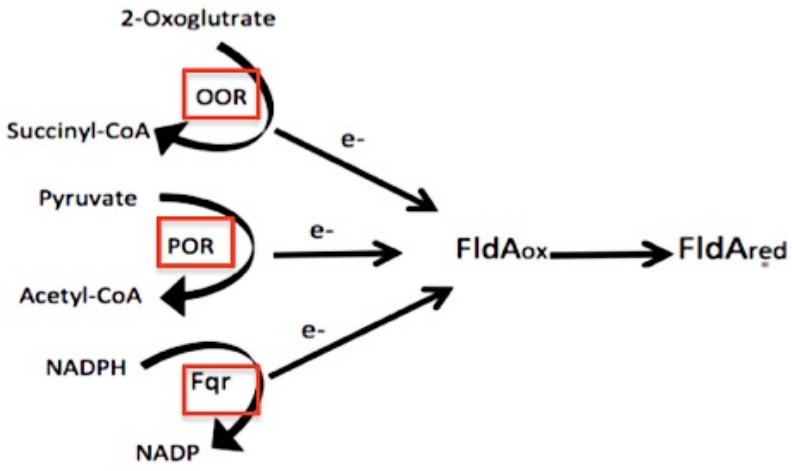

Figure 4.20. In addition to FqrB, flavodoxin is the electron acceptor for POR and OOR.

4.2.12 Constructing a mutagenesis plasmid for *por* and *oor* using ISA cloning

One-step synthesis of *C. jejuni* gene-knockout vectors with kanamycin resistance cassettes was achieved by using an adapted isothermal assembly (ISA) cloning method (Gibson *et al*., 2009) to produce pGEM*POR* (Figure. 4.21), pGEM*oorDABC* (Figure. 4.22) and pGEM*oorB* (Figure. 4.23). These plasmids were electroporated into *C. jejuni* NCTC 11168. As mentioned above, POR contributes to an essential pathway that is synthesising acetyl-CoA. However, acetate can be utilised to produce acetyl-CoA, using the enzyme acetyl-CoA synthetase (Wright *et al*., 2009). *C. jejuni* transformed with pGEMPOR were plated on media supplemented with acetate and sodium formate (alternative electron donor). Different concentrations of acetate and sodium formate were used, yet we could not isolate a *por* mutant strain, indicating the essentiality of POR. The same was found for the isolation of a mutant deleted for *oorDABC*. Supplementing the plate with sodium formate, could not help in isolating a *oorDABC* mutant strain. However, we successfully isolated a *C. jejuni* mutant strain deleted in the *oorB* gene. The mutant itself has a very severe growth defect because the TCA cycle has been interrupted and it can only be grown in complex media (MHS) in the presence of the additional electron donor formate plus succinate to aid succinyl-CoA formation, which is absent in this mutant. However, upon the addition of different concentrations of deoxyribonucleosides, the growth of this mutant did not show any significant improvement (Figure. 4.24).

A) B)

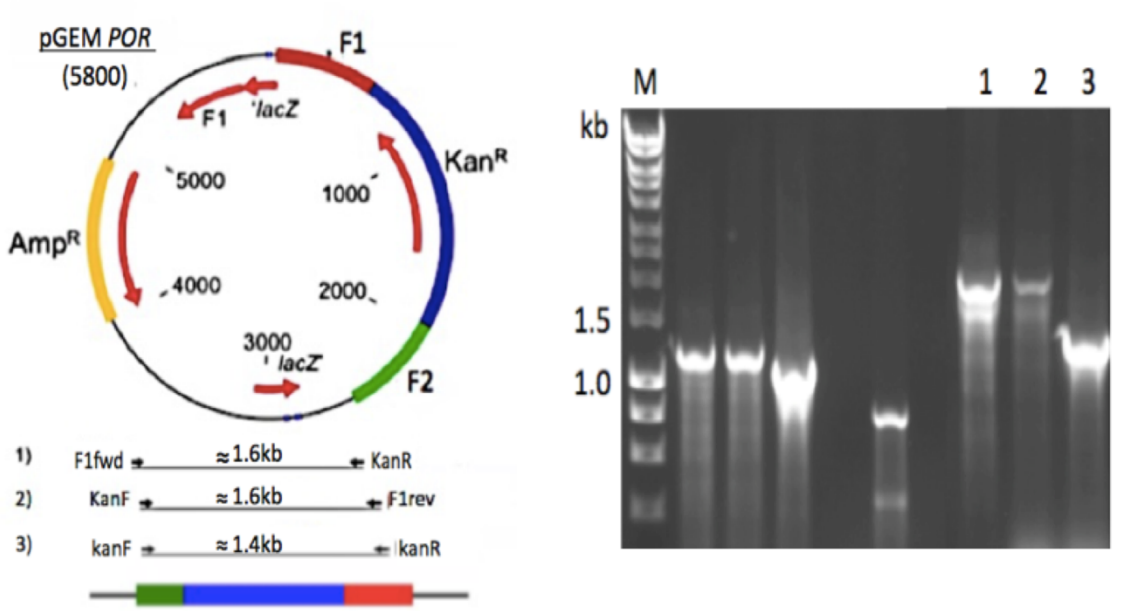

Figure 4.21: Generation of *por* mutagenesis plasmid by ISA using pGEM-3Zf plasmid digested at the HincII restriction site. (A) Plasmid map of pGEM*POR* shows the flanking regions of targeted gene. Red is Flank 1 (F1), 600 bp that is upstream of *por* gene. Green is Flank 2 (F2) that is downstream of *por* gene. Targeted gene is interrupted by kanamycin resistant cassette (blue). The other regions in the plasmid are AmpR region (gold), F1 origin of replication and the lacZ. **(B)** Different combination of KanR, F1 and F2 primers were used to confirm cloning. M is ladder. Lane 1, PCR product is 2.0 kb. Lane 2, PCR product is 2.0 kb. Lane3 PCR product is 1.4 kb.

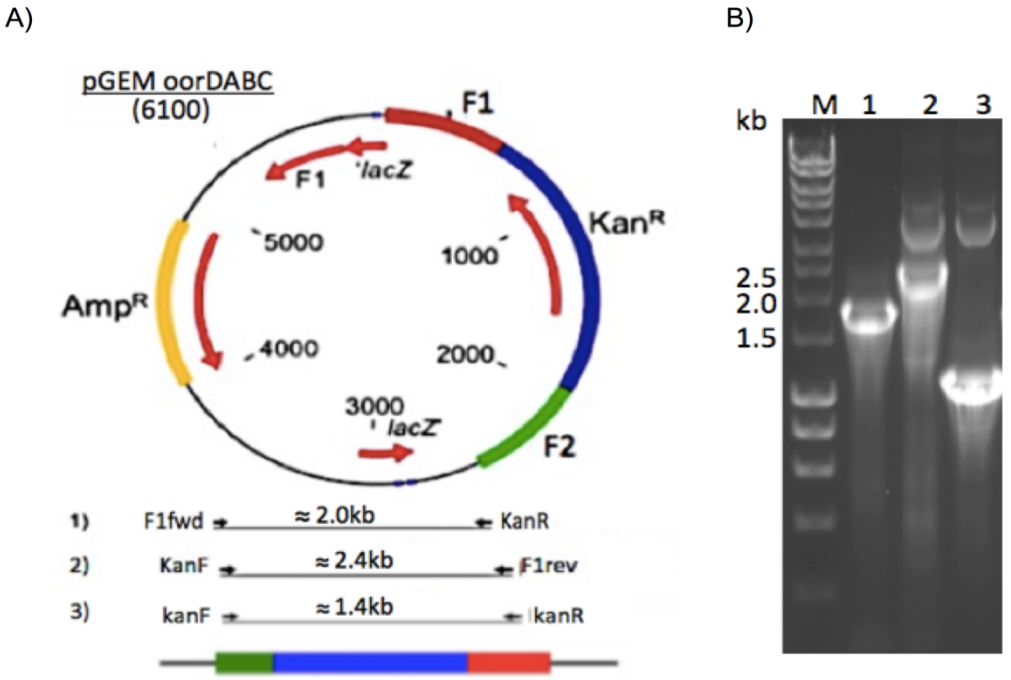

Figure 4.22. Generation of *oorDABC* mutagenesis plasmid by ISA using pGEM-3Zf plasmid digested at the HincII restriction site. (A) Plasmid map of pGEM *oorDABC* shows the flanking regions of targeted gene. Red is Flank 1 (F1), 900 bp that is upstream of *oorDABC* genes. Green is Flank 2 (F2) 600bp that is downstream of *oorDABC* genes. Targeted gene region is interrupted by kanamycin resistant cassette (blue). The other regions in the plasmid are AmpR region (gold), F1 origin of replication and the lacZ. **(B)** Different combination of KanR, F1 and F2 primers were used to confirm cloning. M is ladder. Lane 1, PCR product is 2.0 kb. Lane 2, PCR product is 2.4 kb. Lane3 PCR product is 1.4 kb.

A) B)

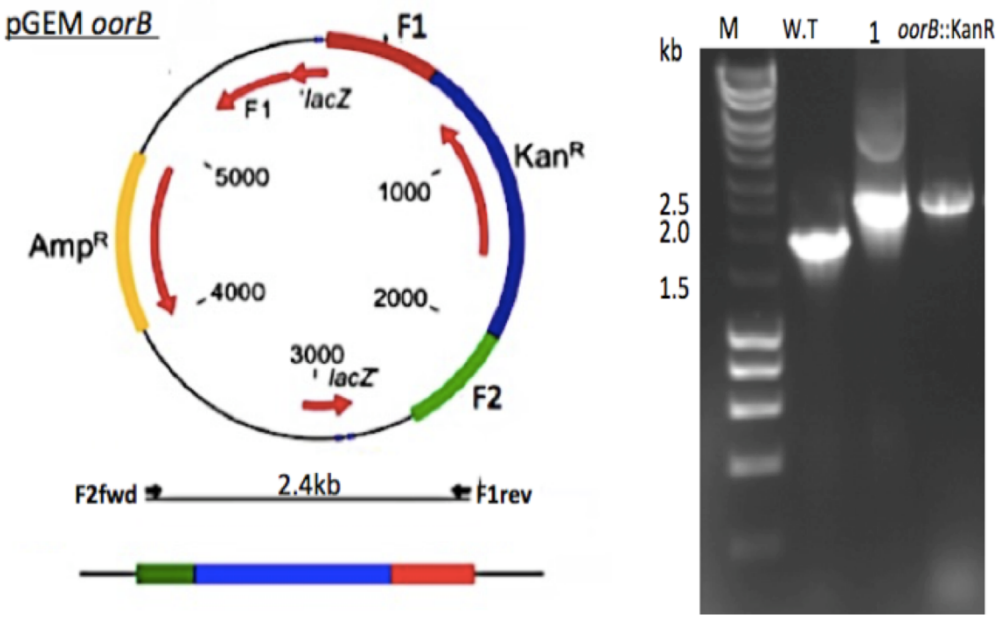

Figure 4.23. Generation of *oorB* mutagenesis plasmid by ISA using pGEM-3Zf plasmid digested at the HincII restriction site. **(A)** Plasmid map of pGEM*oorB* shows the flanking regions of the targeted gene. Red is Flank 1 (F1), 500 bp that is upstream of *oorA* gene. Green is Flank 2 (F2) 500bp that is downstream of *oorB* gene. Targeted gene is interrupted by kanamycin resistant cassette (blue). The other regions in the plasmid are AmpR region (gold), F1 origin of replication and the lacZ. **(B)** Confirmation of *oorB* gene deletion in *C. jejuni*. PCR amplification of *oorB* mutant in *C. jejuni*, the expected size is 2.4 kb. PCR amplification of wild-type genome with F2fwd and F1rev primers (Lane= W.T PCR product = 2.0 kb). The same primers used to amplify the pGEM *oorB* plasmid and *fqr*::KanR genome, the PCR product =2.4kb.

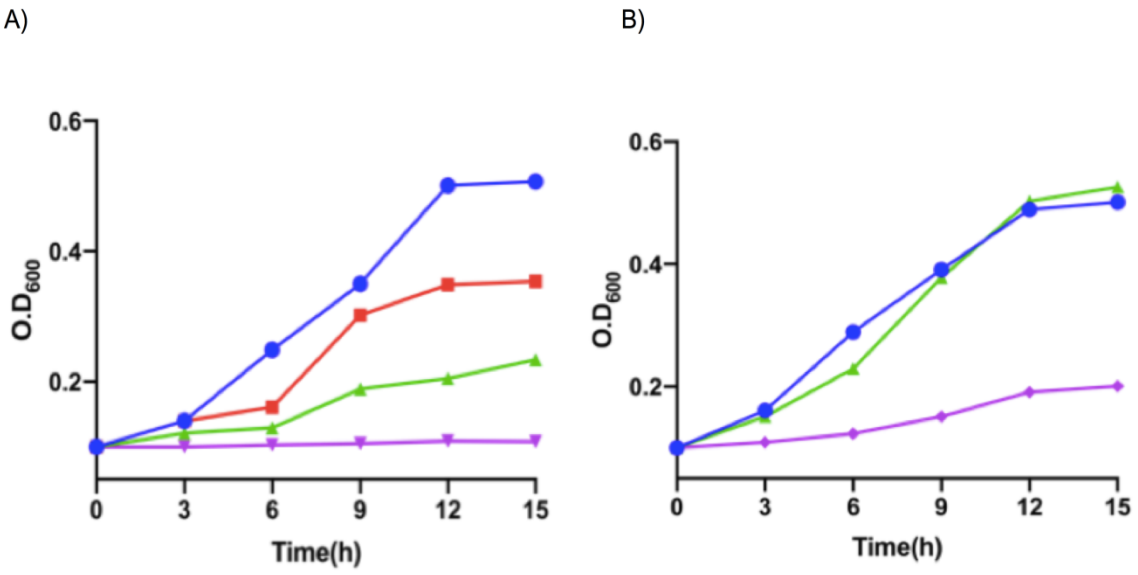

Figure 4.24. Growth curve of the *oorB* mutant. **(A)** Blue trace is mutant grown in MHS + 20 mM sodium formate + 5 mM sodium succinate. Red trace is *oorB* mutant grown in MHS + 10 mM sodium formate +5 mM sodium succinate. Green trace *oorB* mutant grown in MHS + 5 mM sodium formate + 5mM sodium succinate. Purple trace is *oorB* mutant grown in MHS. **(B)** Blue trace is *oorB* mutant grown in MHS + 20 mM sodium formate + 5 mM sodium succinate. Green trace is *oorB* mutant grown in MHS + 20 mM sodium formate + 5 mM sodium succinate + 100 μM dRNS. Purple trace is *oorB* mutant grown in MHS + 20 mM sodium formate + 5 mM sodium succinate + 1 mM dRNS. Adding of 100 μM dRNS made no significant difference in growth rate. There is growth inhibition after adding 1 mM dRNS.

4.3 Discussion

In addition to POR and OOR, we have identified the *cj0559* encoded FqrB as an additional FldA reductase and phenotypic analysis of a deletion mutant lacking FqrB has revealed a hitherto unknown link between FldA and deoxyribonucleotide reduction. FqrB from *C. jejuni* is an NADPH specific flavodoxin reductase that has a phylogenetic relationship to a group of similar enzymes from Gram positive bacteria, some of which are known to be redox partners for NrdI-like flavodoxins necessary for Y radical formation in class 1b RNRs. FqrB was initially identified in *H. pylori* as a quinone and flavodoxin reductase that was suggested to participate in the production of NADPH by operating in the reverse direction to that proposed here, i.e. coupling the reduction of $NADP^+$ to the oxidation of

reduced flavodoxin that had been generated by the action of POR (St Maurice *et al*., 2007). This seemed to confirm earlier data from Hughes *et al* (1998) who detected pyruvate, CoA and FldA dependent NADPH production in *H. pylori* cell-free extracts. The same reaction could also be demonstrated in *C. jejuni* crude extracts (St Maurice *et al*., 2007). However, the rates of NADPH production in these studies were very low (of the order of nmol min^{-1} mg $protein^{-1}$). From the results presented in Chapters 3 and 4, we can now explain this in view of the relatively high midpoint redox potential of FldA (-180 mV) compared to NADPH (-320 mV), such that it is thermodynamically unfavourable for FldA to reduce NADP. It is therefore unlikely that this mechanism would be relevant *in vivo*; other known enzymes in *C. jejuni* central metabolism operate to reduce NADP directly (e.g. isocitrate dehydrogenase). On the contrary, our data suggests that FqrB catalyses NADPH dependent reduction of FldA, in addition to POR and OOR, and this contributes to the maintenance of a reduced pool of FldA for the diverse metabolic reactions requiring this electron carrier (Figure 4.20).

The phenotype of an *fqrB* deletion mutant implicates FqrB in ribonucleotide reduction. The fact that this mutant was viable, although with a large growth defect, is presumably because POR and OOR are also still able to contribute to FldA reduction. Although POR is essential (Kendall *et al*., 2014) an *oorB* mutant has previously been reported (Weerakoon and Olson, 2007) and we were able to isolate an *oorB* mutant but not an *oorDABC* mutant. The stimulation of *fqrB* mutant growth by dRNS was significant although not large in magnitude, but this would be consistent with the additional functions that FldA has in electron transport to Complex I and isoprenoid biosynthesis as well as other possible cellular redox processes yet to be identified. It should also be noted that although a potential transport system and phopshoribosyl phosphotransferase for nucleotide salvage has been identified in *C. jejuni* (Yahara *et al*., 2017), *Epsilonproteobacteria* including *C. jejuni* are not thought to possess a deoxyribonucleoside kinase that would efficiently phosphorylate these precursors (Sandrini *et al*., 2006; Konrad *et al*., 2012), which could account for

the poor growth response observed. It is also possible that FqrB can reduce other as yet unidentified substrates that are important for optimum growth. We might have expected to observe dRNS stimulation of growth in the *oorB* mutant, but this was not the case. It is possible that *in vivo*, FqrB makes the largest contribution to keeping the FldA pool reduced and thus shows the most obvious dRNS stimulation in the mutant.

Biochemical evidence for a role of FqrB and FldA in RNR activation was obtained by an *in vitro* reconstitution approach with the relevant purified proteins. The tyrosyl radical in purified NrdB was remarkably resistant to quenching by hydroxyurea, despite growth being sensitive to this compound and causing filamentation in treated cells consistent with RNR inhibition (Sellars *et al*., 2002). Hydroxylamine proved an effective radical scavenger however and we were able to show, with appropriate controls, that radical re-formation could be promoted in the presence of NADPH, FqrB and FldA. Importantly, the EPR data show that the characteristics and environment of the radical formed *in vitro* is indistinguishable from that in the as-purifed NrdB protein. The *fqrB* mutant phenotype data taken together with the *in vitro* reconsitution experiments would therefore strongly support a physiological role for FqrB and FldA in NrdB Y radical formation, and thus ribonucleotide reduction, in *C. jejuni*.

In class 1a RNRs a small ferredoxin, exemplified by YfaE in *E. coli* (Wu *et al*., 2007) has been implicated in supplying electrons to reduce the di ferric centre in NrdB to allow oxygen to react with the di-ferrous state, necessary to form the Y radical. No homologue of YfaE exists in *C. jejuni* and indeed only 29 % of 181 NrdAB containing genomes were found to encode a *yfaE*-like gene linked to *nrdA* (Wu *et al*., 2007), implying that in most bacteria, other redox proteins satisfy this requirement. Our data suggests that *C. jejuni* use the flavodoxin FldA instead of a ferredoxin as the electron donor to NrdB. YfaE is a [2Fe-2S] ferredoxin that directly supplies electrons, one at a time, to reduce the NrdB diferric centre (Wu *et al*., 2007). FldA, with E_1 and E_2 separated by only 20 mV could act in a similar

manner. Neverthelss, *in vitro* generated superoxide also formed the radical in NrdB, as found with the NrdI flavodoxins interacting with the class Ib NrdF (Berggen *et al*., 2014). However, the physiological significance of this is difficult to judge, given that the NrdB/Class Ia type of Fe-containing RNR should be fully capable of generating the Tyr radical from the oxidation of ferrous to ferric iron at the di-iron centre mediated by molecular oxygen alone. It would clearly be informative to examine the relative reactivity of the *C. jejuni* NrdB di-iron centre with superoxide versus oxygen in more detail.

Chapter 5: Comparison of the NADPH-FqrB-FldA-RNR pathway in the related Epsilonproteobacterium *Arcobacter butzleri*

5.1 Introduction

The classification of *Arcobacter spp*. was suggested to describe microorganisms that used to be named as "aerotolerant campylobacters" (Vandamme *et al.,* 1991). Based on 16S rRNA sequence analysis and16S rRNA-DNA hybridization, *Arcobacter spp*. and *Campylobacter spp.* are closely related and many phenotypic features of *Arcobacter spp*. and *Campylobacter spp.* are similar. However, there are two key differences that separate them; *Arcobacter spp*. are aerotolerant and can grow at low temperatures (15-25 °C) (Vandamme *et al*., 1992a). After revealing these phylogenetic and phenotypic characteristics, it was proposed both genera should be contained within the family Campylobacteraceae (Vandamme and Deley, 1991). This family contains Gram-negative, non-spore forming, curved rods (sometimes straight or spiral) members. Average size of *Arcobacter spp.* is 1-3 μm by 0.2-0.9 μm with a polar single flagellum that enables darting or corkscrew motility (Mansfield and Forsythe, 2000). They grow in the temperature range of 15 to 37 °C (optimum growth at 30 °C) and microaerophilic conditions (10 % CO_2, 5 % O_2, 85 % N_2). *Arcobacters* have 27-30 % C+G content. They can be free living or associate with animals. They are morphologically similar to *Helicobacter* and *Campylobacter* with average similarity level (determined by 16S rRNA sequence) are approximately 85 % and 86 %, respectively (Wesley *et a*l, 1995). *Arcobacter butzleri, Arcobacter cryaerophilus, Arcobacter skirrowii* and *Arcobacter nitrofigilis* were the species included when genus *Arcobacter* was first proposed. Analyzing 16S rRNA data showed that these species displayed good interspecies similarity levels with no less than 93.8 %, establishing a strong connection between them (Vandamme *et al.,* 1992b). The free living nitrogen-fixing, *A. nitrofigilis* displays the least similarity with other species of *Arcobacters*, while, the other three pathogens of humans and animals display 97 % similarity (McClung *et al.,* 1983).

At present, twenty-seven species (isolated from food, water, environment, animals and clinical human samples) have been named and included in the genus *Arcobacter* (Ramees *et al*. 2017; Gilbert *et al*. 2019). The presence of *Arcobacters* in such a vast variety of environments and hosts makes *Arcobacters'* genetic material a worthy target for analyzing and characterizing in order to shed light on genes responsible for their environmental adaptation and host association. The availability of multiple genome sequences enables us to identify genes that might be responsible for *Arcobacter's* ability to adapt to a much wider range and variety of hosts and environments compared to *Campylobacter*.

Aim of the chapter

In relation to this thesis, we are specifically interested to compare the NADPH-FqrB-Flavodoxin-RNR pathway we have characterized in *C. jejuni* with that occurring in the different species of *Arcobacter*. In order to determine the presence or absence of our interested genes, the genome sequences of *Arcobacter spp.* will be analyzed. Then, these proteins will be overexpressed and purified. The NrdB/FldA redox system will be tested in *Arcobacter butzleri*, the type species and best characterised member of the genus. Also, the Nuo complexes in *Arcobacter spp.* and *C. jejuni* will be studied to show the similarities and the differences between them. Finally, we will investigate aerotolerance in *Arcobacter spp.* in order to provide comparisons with the microaerophilc *C. jejuni.*

5.2 Results

Dr William Miller (United States Department of Agriculture, USA) supplied us with annotations of the genes in 27 species of *Arcobacter*. We recorded the presence or absence of genes/proteins of interest and tabulated these in table 5.1. All species have OOR and lack ODH for production of succinyl-CoA. However, for production of acetyl-CoA, there is much variation and different species use either POR or PDH or a combination of both. It can be seen that there is a complete correlation between the presence of POR and at least one flavodoxin. This may

indicate that *Arcobacter* POR is similar to *C. jejuni* in utilizing FldA as an electron carrier, although in many species additional flavodoxins are encoded in the genome. There are also some species that do not encode POR but do still have a flavodoxin. As we know from previous chapters in this thesis, FldA may have multiple functions. With regard to Complex I, two distinct types can be identified in different species of *Arcobacter* (analysed in more detail below). One type contains the NADH binding module NuoEF and the other lacks these proteins (designated here as Nuo2). All species encode the NuoEF-type, while some species lack Nuo2 – generally those that also lack POR. Reduced FldA or another flavodoxin (generated by POR and OOR) may be the electron donor for Nuo2. Species that contain a PDH, which generates NADH, presumably use the NuoEF-complex I to oxidize NADH. In *C. jejuni*, we demonstrated that FldA can also be an electron donor for NrdB, which is present in all species of *Arcobacter* examined here. Some *Arcobacter* strains have two [2Fe-2S] ferredoxin proteins none of which are homologous to YfaE (percentage sequence identity less than 13 %).

In this chapter, *A. butzleri* strain BU4018 will be studied in detail. It has no [2Fe-2S] ferredoxin or Nuo2 proteins and has two flavodoxin proteins. For pyruvate decarboxylation, *A. butzleri* (BU4018) utilizes oxygen stable pyruvate dehydrogenase (PDH) with no pyruvate oxidoreductase (POR). (purple row table 5.1).

Table 5.1: Comparions of key proteins encoded in 27 species and strains of *Arcobacter*.

	POR	OOR	FldA	Nuo2	PDH	ODH	NuoEF	FqrB	NrdAB	NrdDG
ANA	✓ 2	✓	✓ 2	✓	✓	x	✓	✓ 2	✓	✓
AQM	✓	✓	✓	✓	x	x	✓	✓	✓	✓
BIV	✓ 1	✓	✓ 3	✓	✓	x	✓	✓	✓	✓
BU4018	x	✓	✓ 2	x	✓	x	✓	✓	✓	✓
BU7h1h	x	✓	✓	x	✓	x	✓	✓	✓	✓
CIB	x	✓	x	✓	✓	x	✓	x	✓	✓
CLO	✓	✓	✓	✓	x	x	✓	✓	✓	✓
CRYA	x	✓	x	x	✓	x	✓	✓	✓	✓
CRYD	x	✓	x	x	✓	x	✓	✓	✓	✓
DEF	✓	✓	✓	✓	✓	x	✓	✓	✓	✓
EBR	✓ 2	✓	✓	✓	✓	x	✓	✓ 2	✓	✓
ELL	✓	✓	✓	✓	x	x	✓	✓	✓	✓
FAE	x	✓	✓	✓	✓	x	✓	x	✓	✓
HAL	✓ 1	✓	✓ 3	✓	✓	x	✓	✓	✓	✓
LAN	x	✓	✓	x	✓	x	✓	✓	✓	✓
LEK	✓	✓	✓ 3	✓	x	x	✓	✓	✓	✓
MAR	✓ 1	✓	✓ 3	✓	✓	x	✓	✓	✓	✓
MOL	✓ 1	✓	✓ 3	✓	✓	x	✓	✓	✓	✓
MYT	✓ 2	✓	✓ 3	✓	✓	x	✓	✓ 2	✓	✓
NIT	✓	✓	✓ 2	✓	✓	x	✓	✓	✓	✓
PAC	✓	✓	✓	✓	✓	x	✓	✓	✓	x
PORC	x	✓	✓	x	✓	x	✓	x	✓	✓
SKI	x	✓	✓	x	✓	x	✓	✓	✓	✓
SUIS	✓	✓	✓ 2	✓	✓	x	✓	x	✓	✓
THE	x	✓	✓	x	✓	x	✓	x	✓	✓
TRO	x	✓	x	x	✓	x	✓	x	✓	✓
VEN	✓	✓	✓	✓	✓	x	✓	✓	✓	✓

The data was compiled from the annotations of the genome sequences carried out by Dr William Miller (United States Department of Agriculture, USA; personal communication) using publicly available genomes. The abbreviations for the species names are as follows: ANA, *Arcobacter nitrofigilis* DSM7299; AQM, *A. aquimarinus* LMG 27923^T; BIV, *A. bivalviorum* LMG 26154^T; BU4018, *A. butzleri* RM4018; BU7h1h, *A. butzleri* 7h1h; CIB, *A. cibarius* RM15232; CLO, *A. cloacae* LMG 26153^T; CRYA, *A. cryaerophilus* ATCC 43158^T; CRYD, *A. cryaerophilus*

ATCC 49615; DEF*, A. defluvii* LMG 25694^T; EBR*, A. ebronensis* LMG 27922^T; ELL*, A. ellisii* LMG 26155^T; FAE*, A. faecis* LMG 28519^T; HAL*, A. halophilus* CCUG 53805^T; LAN*, A. lanthieri* LMG 28516^T; LEK*, A. lekithochrous* DSM 100870^T; MAR*, A. marinus* JCM 15502^T; MOL*, A. molluscorum* LMG 25693^T; MYT*, A. mytili* LMG 24559^T; NIT*, A. nitrofigilis* DSM7299; PAC*, A. pacificus* LMG 26638^T; PORC*, A. porcinus* LMG 24487^T; SKI*, A. skirrowii* LMG 6621^T, SUIS*, A. suis* LMG 26152^T; THE*, A. thereius* LMG 24486^T; TRO*, A. trophiarum* LMG 25534^T; VEN, *A. venerupis* LMG 26156^T. The abbreviations for the enzymes names are as follows: POR, pyruvate:flavodoxin oxidoreductase; PDH, pyruvate dehydrogenase; OOR, 2-oxoglutarate:acceptor oxidoreductase; ODH, 2-oxoglutarate dehydrogenase; NuoEF and Nuo2: Nuo complex; FldA, Flavodoxin; NrdDG, anaerobic ribonucleotide reductase; NrdAB, aerocbic ribonucleotide reductase. The purple row is *A. butzleri* strain BU4018 that will be studied in detail in this chapter.

5.2.1 The Nuo complex in *Arcobacter spp*.

The electron transport chain (ETC) for both prokaryotes and eukaryotes utilize Complex I as the first enzyme to catalyse the transfer of two electrons, leading to pump 4 protons across the membrane. Then, the proton motive force (PMF) and ATP synthase enzyme are used to form ATP. In prokaryotic cells the Nuo complex consists of 13-15 subunits each of which has iron-sulphur clusters facilitating the flow of electrons (Yagi *et al.* 1998). Two types of genetically distinct Complex I are found in *Arcobacter spp.* (Figure 5.1). One type contains NuoEF, which shuttles electrons from NADH, via FMN and iron-sulfur centres. The other type is designated here as Nuo2. It lacks NuoEF proteins and presumably uses flavodoxin as electron donor. Another difference between the NuoEF and Nuo2 types of Complex I is the location of Fe-S centres within the NouG subunit (Figure 5.2). In Nuo2, it is unclear how FldA might interact with the Nuo complex, but it does contain two unidentified genes in place of *nuoEF* that have greater than 30 % sequence similarity at the protein level to NuoX and NuoY in *C. jejuni* (Fig. 5.3).

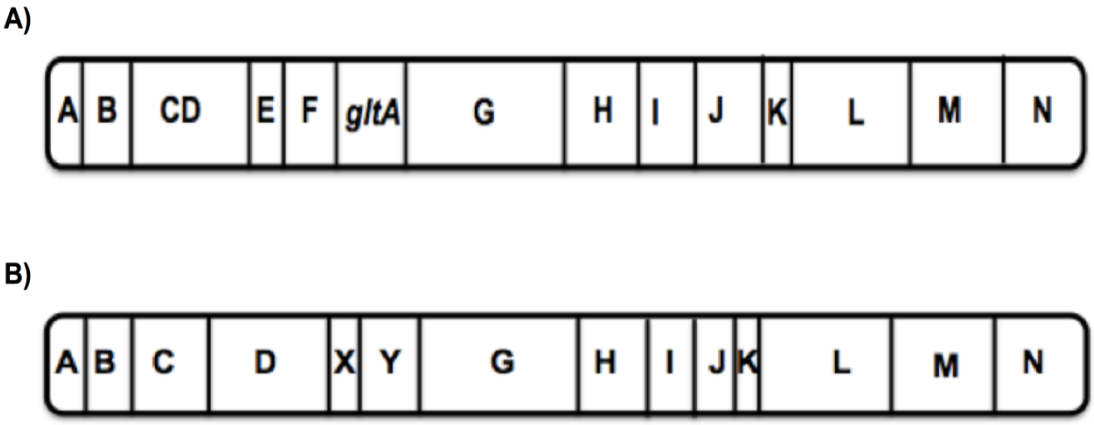

Figure 5.1: The organisation of *nuo* complex genes in *Arcobacter* genomes. There are two types of nuo complexes. **(A)** nuoEF complex and **(B)** nuo2 complex has *nuoX* and *nuoY* genes. The letters A–N represent the *nuo* genes. *gltA* gene is citrate synthase.

```
A. butzleri   MAEVVNITINGVQMQATKGSLLIDKLLDENIHIPHFCYHQALGKDGNCRMCMVEIEGQKR   60
A. cibarius   MAETVSITINGIQFQAKKGSLLIDKLIDENIHIPHFCYHQALGKDGNCRMCMVEIDGQKR   60
C.jejuni      ----MTVKINGIDCAFEEGEYILNIARRNDIFIPAICYLSGCSPTLACRMCMVEADGKK-   55
A. cibarius   MSEQIKLTINGKEFTAEPSETILNIARRNNIFIPAICYLNSCSATLACRLCLVEVDGKQ-   59
                 : . ::.       .  :::    . :.:* .**         **:*:*   *::

A. butzleri   PQIACDTPVKDGMVVRTKGQNIEKVRRDILELELINHPIDCPTCDQAGECKLQDYYMESG   120
A. cibarius   PQIACDTPIKDGMIVRTKGEKIEKVRKDILELELINHPIDCPTCDQAGECKLQDYYMESG   120
C.jejuni      -VYSCNTKAKEGMVVESDLQNLWDERNEIMQAYCINHPLECGVCDKSGECELQNFTHKSR   114
A. cibarius   -VYACNAKAKENIQIVTSNPSIEKERNAIMQVYCVNHPLQCGVCDKSGECELQNYTLYMQ   118
                 .*::  * .: : :   .:   *. :::   :***::* .**::*:*:**::

A. butzleri   FYDSRVNLEVKNHARKRIDLGSNVMLDQERCVLCTRCVRFCSTITKTNELGVISRADHSV   180
A. cibarius   FYASRVNLDAKNEARKRVDLGSNVMLDEERCVLCLRCVRFCKDITKTAELGVVSRTDHST   180
C.jejuni      VNVQKH--WIKDTHKPHKHWG-MINYDPALCIVCERCITVCKDKIGESALKTVPRGGDSV   171
A. cibarius   VTEQNY--SIKDTHKPKQHWG-VMNYDPALCIVCERCVTVCSDIIGSNSLSTTKRGGNEL   175
              .  .     :         *  :  *   *::* :*: .*        * .  *  .

A. butzleri   IGTFPGRPLNNPYAM----------------------NVVDLCPVGALTSKDFRFKQRV   217
A. cibarius   IGTFPGRPLNNPYAM----------------------NVVDLCPVGALTSKDFRFKQRV   217
C.jejuni      DNSFKESMGKDAYAIWTKFQKSLIGPANGDTLDCSFCGECTSVCPTGALIGSKFQYTSNI   231
A. cibarius   DKNLKESMPKDAYAMWNKLNKSLIAHD---SDSCISCGECIAVCPTGAMISNNFQYTSNA   232
                 : *::                    :    **.**: . .*:: ..

A. butzleri   WFLESFDAICNGCSKACNIHVDHRKEKYKDDVIYRFRPRVNKAINGWFMCDEGRLSYTKE   277
A. cibarius   WFLQSFEAICNGCSKGCNISIDHRKEKYKDDMIYRFRPRTNKAVNGWFICDYGRLSHHNE   277
C.jejuni      WELKRIPASN-PHSSDCELMYYDIKQSGISNQ-KEKIYRVSNDFAFASLNKAARFAFDTQ   289
A. cibarius   WELEKIPAAN-PFYSDCSFMYYEVKQTSIDDT-RKRVYRVTNEFHFQELCGAVRFCFDYE   290
              * :  . :        *     . *.           : .      :    *. .  :
```

Figure 5.2: Protein sequence alignments of NuoG in *C. jejuni* and *Arcobacter spp.* Fe-S cluster of NuoG proteins are highlighted in red, green, blue, purple and yellow. The Fe-S cluster segments are $CX_{10}CX_2CXnC$ Red, $HX_3CX_2CX_5C$ Green, $CX_2CX_2CX_{42\text{-}43}CP$ Blue, $CXnCX_2CX_2C$ Yellow, $CX_2CX_3C_{27}CD$ Purple. Both NuoG proteins contain 4 Fe-S clusters (NuoG from NuoEF has red, green, blue and purple Fe-S cluster) (NuoG from Nuo2 has red, green, blue and yellow Fe-S cluster).

A)

```
C.jejuni NuoX       MRRVDLRKSKELF-EDLAQ-IIKEAKQGEVLVVLFEIGDFSPVEKSFSFVKEQGCELLNS    58
Arcobacter NuoX     MKRFDLRHLKNDFYERMLELLDKQIAPQEVAIIMFEIGDFSNIQKSADVIYEAGYTLMNS    60
                    *:*.***: *: * * : : : *:    ** :::******* ::** ..: * *  *:**

C.jejuni NuoX       LKFNQVDWTIVIKKERV-------------  75
Arcobacter NuoX     IKFNEVDWTLVVKKVKPEPRPVAEESAKDE  90
                    :***:****:*:** :
```

B)

```
C.jejuni NuoY       ------------------------------MIYDNALCFLDMPSLKNKNLCEKIGVNSI     29
Arcobacter NuoY     MNKVEQILKSDFIISFATFLENEELKNSIEQAVKNNDAKFVYMHPIDNSNLK--------     52
                                                  : :*   *: *  :.*.**
C.jejuni NuoY       NISCLEDKNLKAKFYKCEIASLS-------FVLALLCKLSDEGQFCDLDEGYLSAESCFG     82
Arcobacter NuoY     --------SFYSQLIKYEVGSEEGIVALLLNSFSSNCDEKTKEFIEDLDLGYISAESSAG     104
                            .: ::: * *:.* .          ::  *. . :  : *** **:****. *
C.jejuni NuoY       EEEAGEVLAFLK--EVKYLIIDKNIHSYKDSENIKYFLNFLSV--KYGLKILDSDEE--E     136
Arcobacter NuoY     EEEFEEAFESSSNSKIKTLIIGDDILKHQRVENIIKIVALIKKYSDFNLVVLNEDLEQKI     164
                    ***  *.:   .  ::* ***..:* .::  ***  :: ::.   .:.* :*:.* *
C.jejuni NuoY       CDFKKAKLNTLKELDNYDGLVLFRANLQ-DKNLHCSKQFLQIAKCKDQSEVEILAKDFSF     195
Arcobacter NuoY     NSCINFDLEELEELKSFNGTLIYKLIGQDSKELIVSQTFANIAKVADNNEVFVIFKNEKI     224
                     .  : .*: *:**..::* ::::   * .*:*  *: * :***  *:.** :: *: .:
C.jejuni NuoY       KTKLCLDENLQGTIAFLNYENN-----GFDFTPIRIKEAK-   230
Arcobacter NuoY     KKILKVDENLHGTIAILKTKNSKDIFNGYSYKQVKIEKVEV   265
                    *. * :****:****:*: :*.     *:.:. ::*::.:
```

Figure 5.3: Protein sequence alignment of **(A)** *C. jejuni* NouX and *Arcobacter spp* NuoX (37.8 %). **(B)** *C. jejuni* NouY and *Arcobacter spp* NuoY (30.4 %). The percentage sequence identity is shown in brackets.

5.2.2 Studying the NrdB/FldA redox system in *Arcobacter butzleri*

Arcobacter butzleri is interesting because it encodes three separate FqrB-like flavoproteins (ABU_0004, ABU_1047 and ABU_1058) and two flavodoxins (ABU_1189 and ABU_1769). We wished to investigate which of these putative FqrBs donates electrons to flavodoxin and which flavodoxin might activate the NrdAB RNR, assuming a similar pathway to that we identified in *C. jejuni.* Unfortunately, attempts to overexpress the putative flavodoxin (ABU_1189) were not successful. Therefore, the role of the FldA homologue ABU_1769 as electron donor for NrdB was tested *in vitro* and *in vivo* and the ability of FldA to be reduced by each FqrB was tested. *In vitro* experiments started with overexpressing and purifying NrdB, FldA and the three FqrB-like proteins.

5.2.2.1 Overexpression and purification of FldA, NrdB and FAD-containing FqrB-like proteins

The *fldA, nrdB and fqrB* genes were cloned between the NdeI and XhoI sites of the pET21a vector, resulting in a 6-his tag attached in-frame to the C-terminus of the cognate protein. The primers used are shown in Chapter 2 Table 2.2. Then the pETFldA (ABU_1769; FldA15), pETNrdB (ABU_0021), pETFqrB89 (ABU_0004; FqrB89) pETFqrB18 (ABU_1047; FqrB18) and pETFqrB07 (ABU_1058; FqrB07) (Figure 5.4) plasmids were transformed into *E. coli* BL21 (DE3), grown in 1-5 L batches of LB media (plus carbenicillin 50 μg ml^{-1}) at 37 °C to an OD_{600} nm of 0.5, then protein production induced by 0.4 mM isopropyl-thiogalactoside (IPTG) for up to 5 hr. The predicted size of FqrB89 is 36 kDa, FldA is 18 kDa, NrdB is 40 kDa, FqrB07 is 20 kDa and FqrB18 is 22 kDa. The proteins were purified by nickel affinity chromatography. The purity of the proteins was verified by SDS-PAGE (Figure 5.6). FldA and the FqrBs are yellow-coloured proteins with absorption spectra typical of flavoproteins with maxima at ~375 nm and ~460 nm (Figure 5.6 A, B, C, D). The UV-VIS absorption spectrum of purifed NrdB shows the tyrosyl radical signal at 411 nm (Figure 5.6 E).

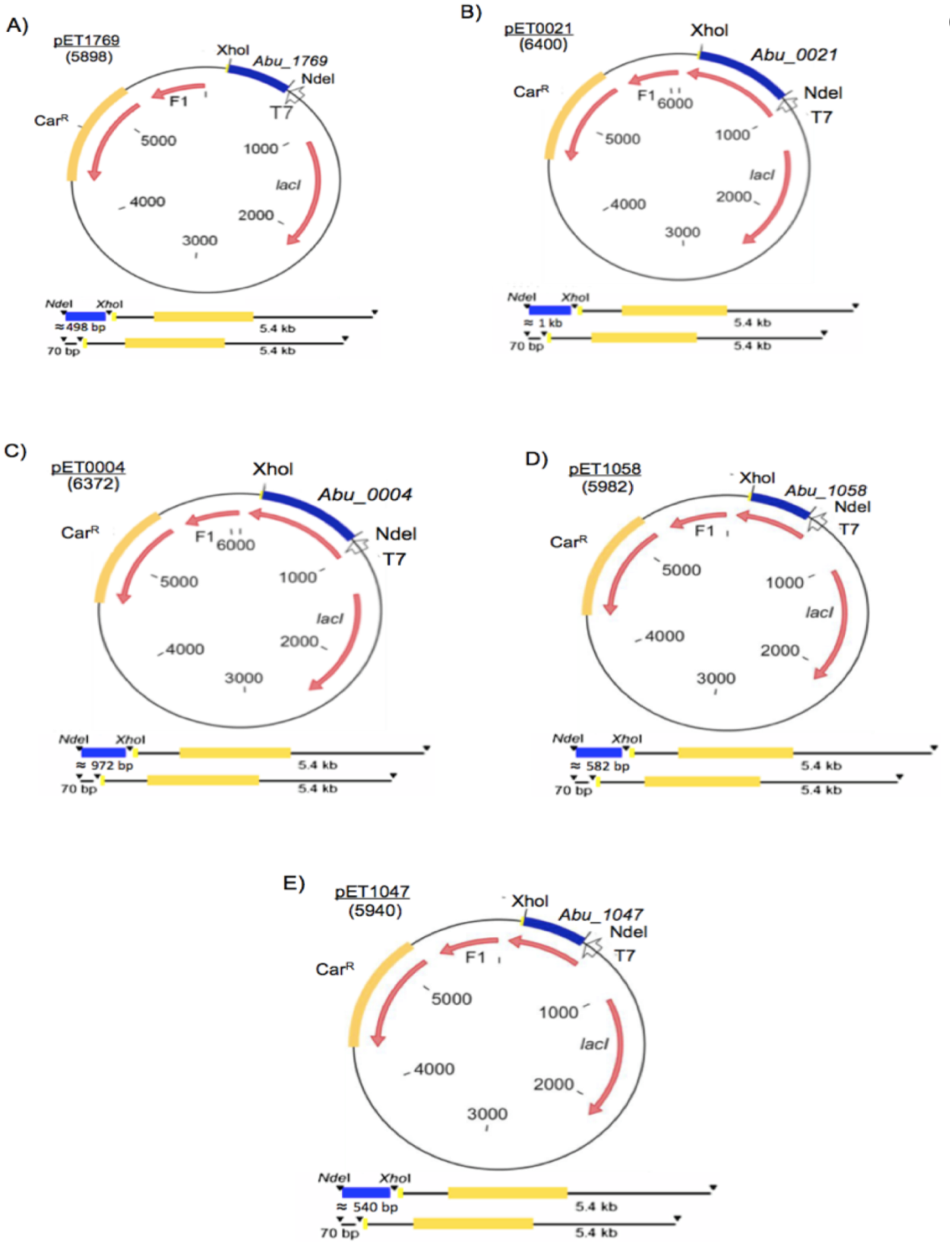

Figure 5.4. Generation of overexpression plasmids. Plasmids were made by inserting PCR amplified genes between the NdeI and XhoI restriction sites in pET21a. **(A)** pETFldA plasmid. **(B)** pETNrdB plasmid **(C)** pETFqrB89 plasmid **(D)** pETFqrB18 plasmid **(E)** pETFqrB07 plasmid**.**

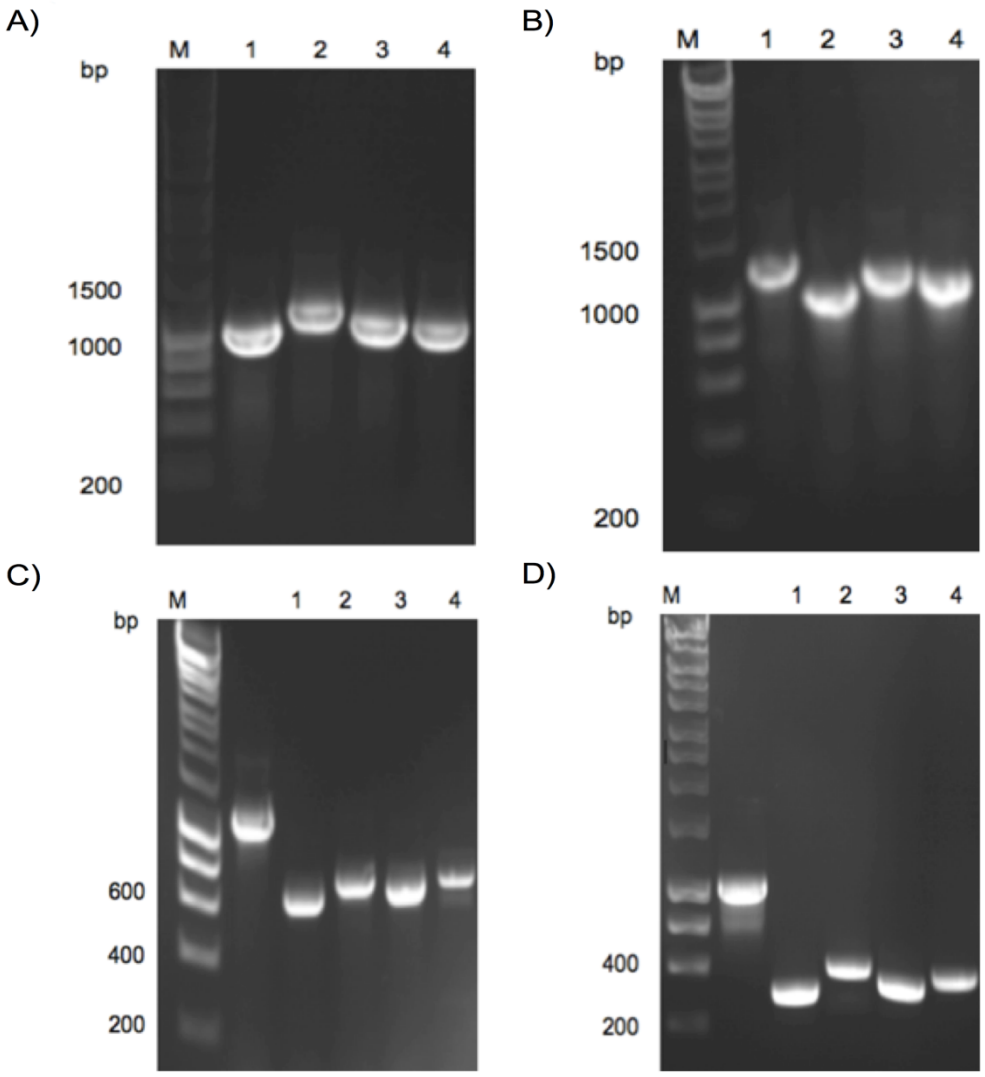

Figure 5.5: The cloning was confirmed by using PCR with different combination of T7 primers and gene primers and the plasmid as template. **(A)** pETNrdB plasmid. Lane1 T7F + T7R. Lane 2 NrdBF + T7R**.** Lane 3 T7F + NrdBR. Lane 4 FldAF + FldAR. **(B)** pETFqrB89 plasmid. Lane1 T7F + T7R. Lane 2 FqrB89F + T7R**.** Lane 3 T7F + FqrB89R. Lane 4 FqrB89F + FqrB89R. **(C)** pETFqrB18 plasmid. Lane1 T7F + T7R. Lane 2 FqrB18F + T7R**.** Lane 3 T7F + FqrB18R. Lane 4 FqrB18F + FqrB18R. **(D)** pETFqrB07 plasmid. Lane1 T7F + T7R. Lane 2 pETFqrB07F + T7R**.** Lane 3 T7F + pETFqrB07R. Lane 4 pETFqrB07F + pETFqrB07R.

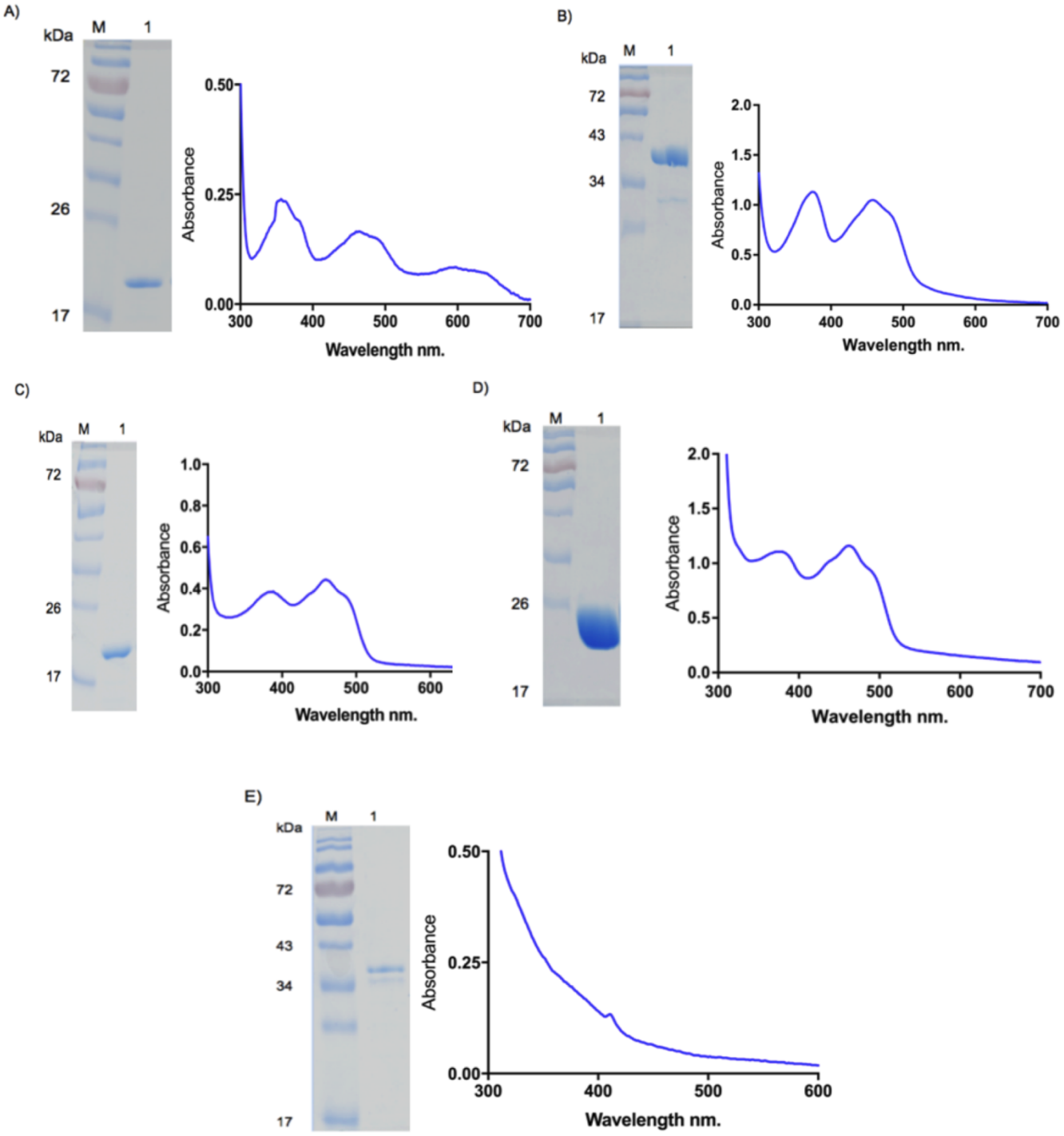

Figure 5.6. 12 % SDS-PAGE gel shows proteins purified by His-column. Panel **(A)** Lane 1: C-terminally his-tagged FldA. Panel **(B)** Lane 1: C-terminally his-tagged FqrB89. Panel **(C)** Lane 1: C-terminally his-tagged FqrB07. Panel **(D)** Lane 1: C-terminally his-tagged FqrB18. Panel **(E)** Lane 1: C-terminally his-tagged NrdB. UV-VIS absorption spectrum of purified flavoproteins show two peaks at ~375 nm and ~460 nm **(A, B, C** and **D). (E)** Purified NrdB shows tyrosyl radical signal at 411 nm. M = Protein Molecular Weight marker.

5.2.2.2 The redox properties of the Fqr proteins and FldA15 reduction

In order to first determine which is the best electron donor for each of the Fqr's, either NADH or NADPH was used with O_2 as substrate. From figures 5.7 and 5.9 it can be seen that both Fqr18 and Fqr07 have oxidase activity with both NADH and NADPH. With oxygen, the results indicated that Fqr89 preferentially uses NADPH rather than NADH as an electron donor (Figure 5.8). Then, FldA/Fqr oxidation/reduction studies were done to explore whether any of the three Fqr's would interact with and reduce FldA15. This was done by monitoring the reduction of the FldA15 flavin in the 460 nm region in absorption spectra where the flavodoxin was present in excess. From Figure 5.10 it can be seen that Fqr89 is the only Fqr that can reduce FldA15.

A)

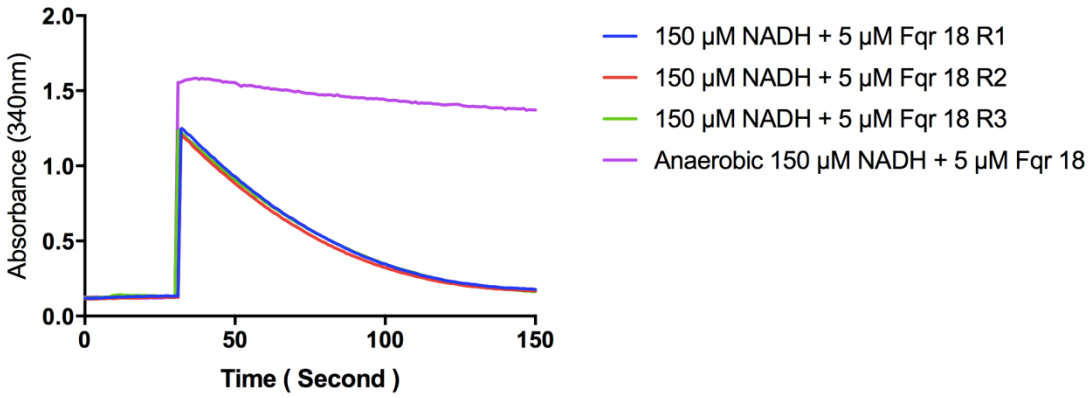

B)

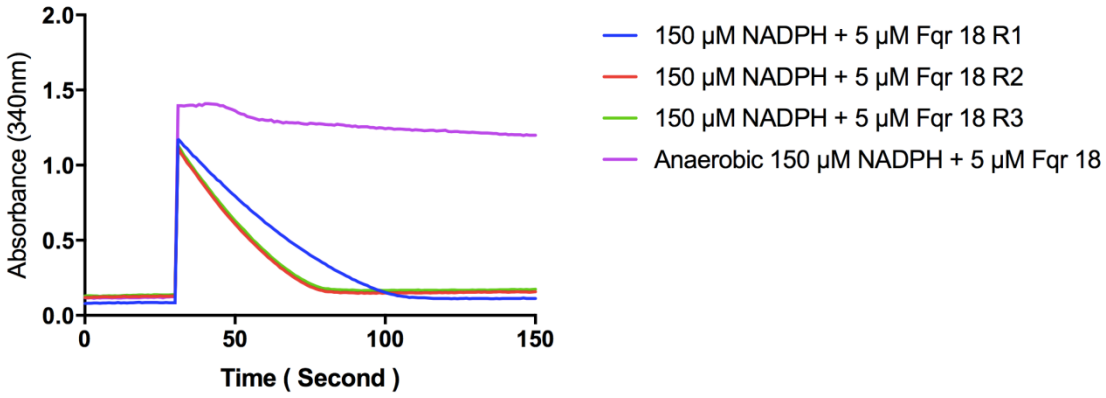

Figure 5.7. NAD(P)H oxidase activity of Fqr18. The absorbance of 5 µM Fqr18 in 50 mM Tris-HCl buffer pH 7.5 was recorded alone for 30 seconds. Then, 150 µM NADH/NADPH was added to start the reaction and recorded for 3 minutes. **(A)** Oxidation of NADH was followed aerobically at 340 nm in the presence of pure Fqr18. **(B)** Oxidation of NADPH was followed aerobically at 340 nm in the presence of pure Fqr18. The oxidation reaction was measured thrice for NADH and NADPH. As a control the same reactions were measured anaerobically.

A)

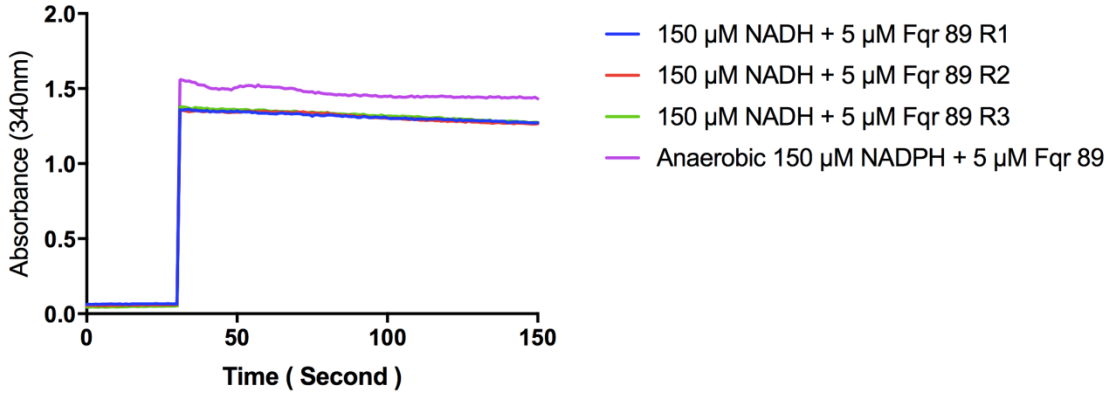

B)

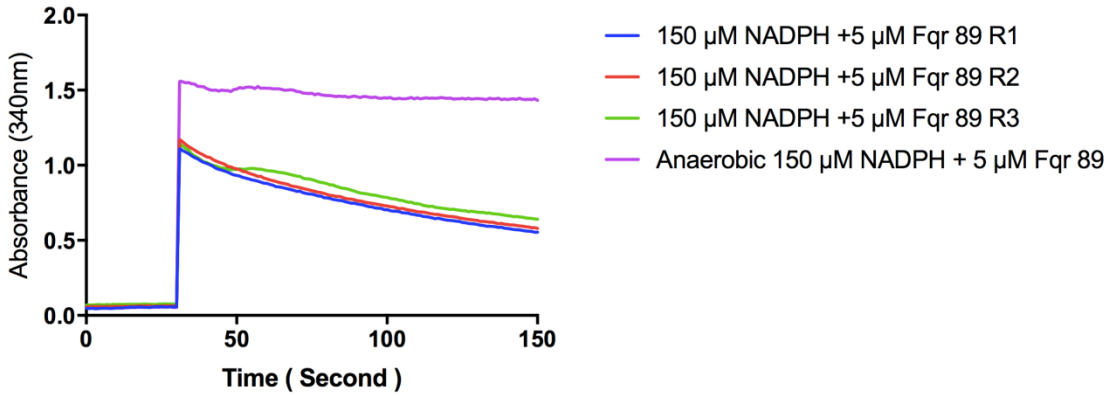

Figure 5.8. NAD(P)H oxidase activity of Fqr89. The absorbance of 5 µM Fqr89 in 50 mM Tris-HCl buffer pH 7.5 was recorded alone for 30 seconds. Then, 150 µM NADH/NADPH was added to start the reaction and recorded for 3 minutes. **(A)** Oxidation of NADH was followed aerobically at 340 nm in the presence of pure Fqr89. **(B)** Oxidation of NADPH was followed aerobically at 340 nm in the presence of pure Fqr89. The oxidation reaction was measured thrice for NADH and NADPH. As a control the same reactions were measured anaerobically.

A)

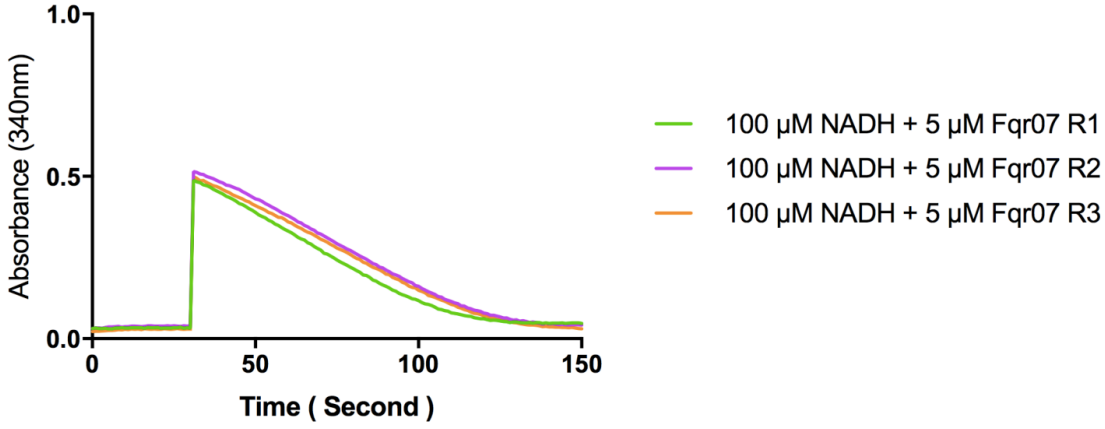

B)

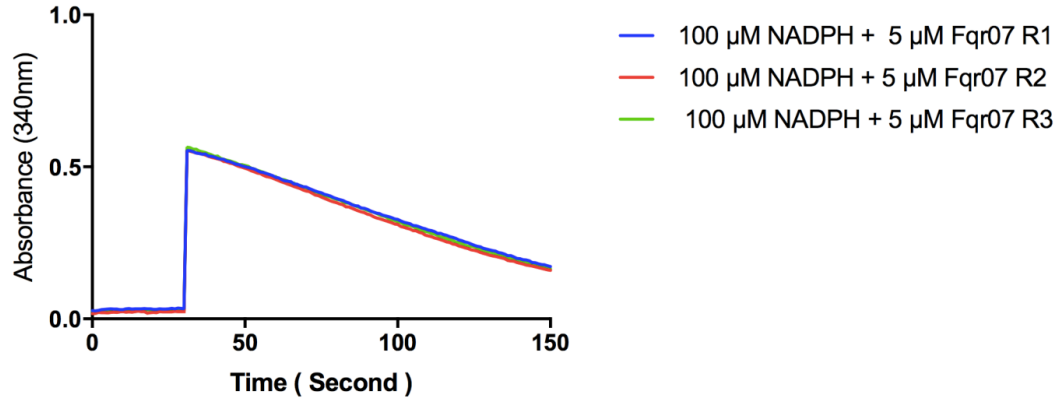

Figure 5.9. NAD(P)H oxidase activity of Fqr07. The absorbance of 5 µM Fqr07 in 50 mM Tris-HCl buffer pH 7.5 was recorded alone for 30 sesonds. Then, 100 µM NADH/NADPH was added to start the reaction and recorded for 3 minutes. **(A)** Oxidation of NADH was followed aerobically at 340 nm in the presence of pure Fqr07. **(B)** Oxidation of NADPH was followed aerobically at 340 nm in the presence of pure Fqr07. The oxidation reaction was measured thrice for NADH and NADPH.

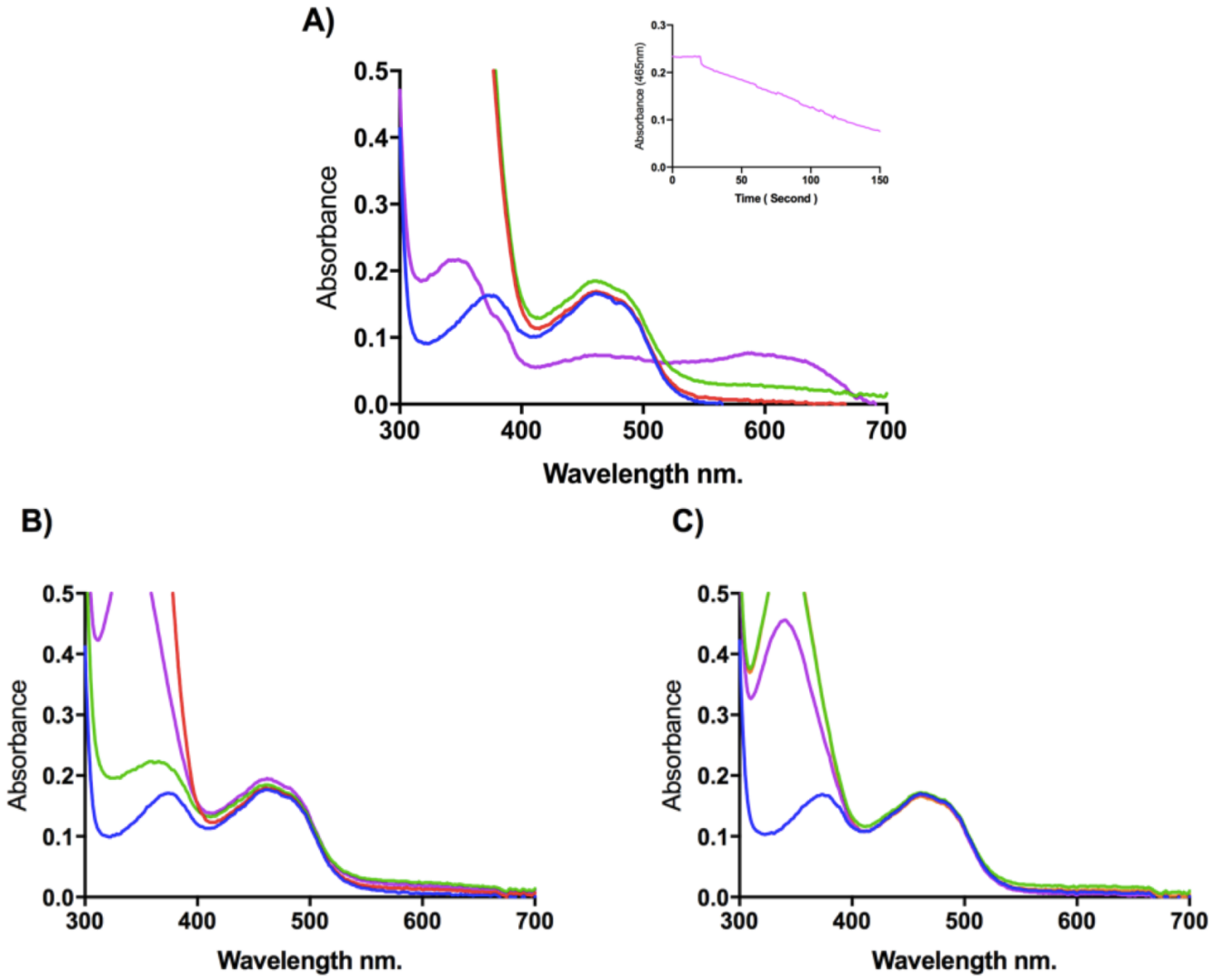

Figure 5.10. Fqr89 is an NADPH specific FldA15 reductase. (A) NADPH dependent reduction of FldA15 catalysed by Fqr89. The absorbance spectrum of FldA15 (50 μM) (blue trace), a mixture of FldA15 (50 μM) and Fqr89 (0.1 μM) in 50 mM Tris-HCl buffer pH 7.5 was recorded alone (red trace) or 5 minutes after the addition of NADPH (150 μM final concentration) (purple trace). Green trace is a mixture of FldA15 (50 μM), Fqr89 (0.1 μM) and NADH 150 μM. The *inset* shows a kinetic trace at 465 nm to show reduction of FldA FMN anaerobically. **(B)** and **(C)** same as **(A)** but with Fqr18 **(B)** and Fqr07 **(C).** It can be seen that Fqr89 is the only Fqr that can reduce FldA15.

These results could suggest a potential pathway that *A. butzleri* (BU4018) may use to reduce NrdB, this pathway will be investigated *in vivo* and *in vitro.*

NADPH ⟶ Fqr89 ⟶ FldA15 ⟶ NrdB

An *in vitro* assay was done by trying to regenerate the tyrosyl radical in NrdB after quenching it. Two radical scavengers were used, hydroxyurea (HU) and hydroxylamine (HA). Only hydroxylamine scavenges the tyrosyl radical (1 mM HA, 30 minutes) (Figure 5.11 A). Then, HA treated NrdB (40 μM) was mixed with FqrB89 (50 μM) and FldA15 (50 μM). The reaction was started by adding NADPH (150 μM) as a source of electrons and spectra were taken every 30 minutes. After 3 hr, there was no sign of a peak at 410 nm that would indicate the presence of the tyrosyl radical (Figure 5.11 B).

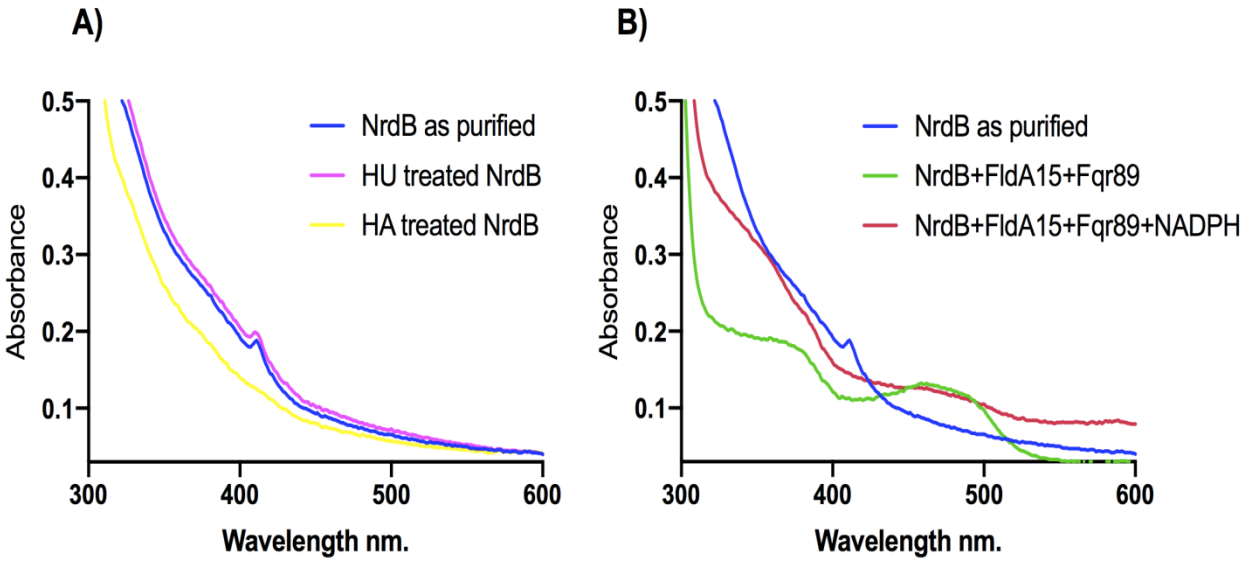

Figure 5.11: (A) Hydroxyurea (HU) and hydroxylamine (HA) treatment of NrdB protein. Either 10 mM of Hydroxyurea (purple trace) or 1 mM of hydroxylamine (yellow trace) were added to NrdB and incubated for 30 minutes. Optical spectroscopy shows that hydroxyurea (HU) does not appreciably quench the NrdB Y-radical compared to HA. **(B)** Blue trace is NrdB as purified, green trace is HA treated NrdB, FldA15, Fqr89 and red trace is a mixture of HA treated NrdB (40 μM), FldA 15 (50 μM), Fqr89 (5 μM) and NADPH (150 μM) in 50 mM Tris-Hcl buffer pH 7.5 was incubated at 37 °C and spectra recorded six times for 3 hr.

5.2.2.3 Constructing a mutagenesis plasmid for *fldA15* and *fqr89* using ISA cloning

Given the connection between FqrB89 and FldA15 and the fact that there are two flavodoxins and three putative FqrB-like proteins in *A. butzleri*, it would be desirable to obtain mutants in the corresponding genes to observe any growth defects that might be related for example, to lack of RNR activation. In order to use the appropriate antibiotic cassette that will be used as selective antibiotic, wild type *A. butzleri* (BU4018) was grown on two blood BHI agar plates plus kanamycin, vancomycin and amphotericin B for 48 hr at 30 °C and incubated in microaerobic and aerobic conditions. After 48 hr, these two plates were checked and there was no growth, suggesting *A. butzleri* is kanamycin sensitive. After selecting the appropriate antibiotic cassette, pJMK30 along with kanamycin cassette primers Kan_F and Kan_R were used to amplify the resistance gene. The other 2 PCR amplified fragments are two regions of ~ 500 bp flanking *fldA15 or fqr89* genes. The ISA reaction assembled these 3 PCR amplified fragments plus HincII digested pGEM3Zf(-) vector. The constructed mutagenesis plasmids (pGEM*fldA15 and* pGEM*fqr89)* were electroporated into *A. butzleri* (BU4018) competent cells. Transformed cells were transferred into 2 ml pre-warmed BHI broth and incubated at 30 °C under microaerobic and shaking conditions for 3 hr. Then, cells plated out on blood BHI agar plates plus kanamycin, vancomycin and amphotericin B, incubated overnight in microaerobic conditions at 30 °C. Correct mutants were identified by colony PCR with ISA and KAN primers.

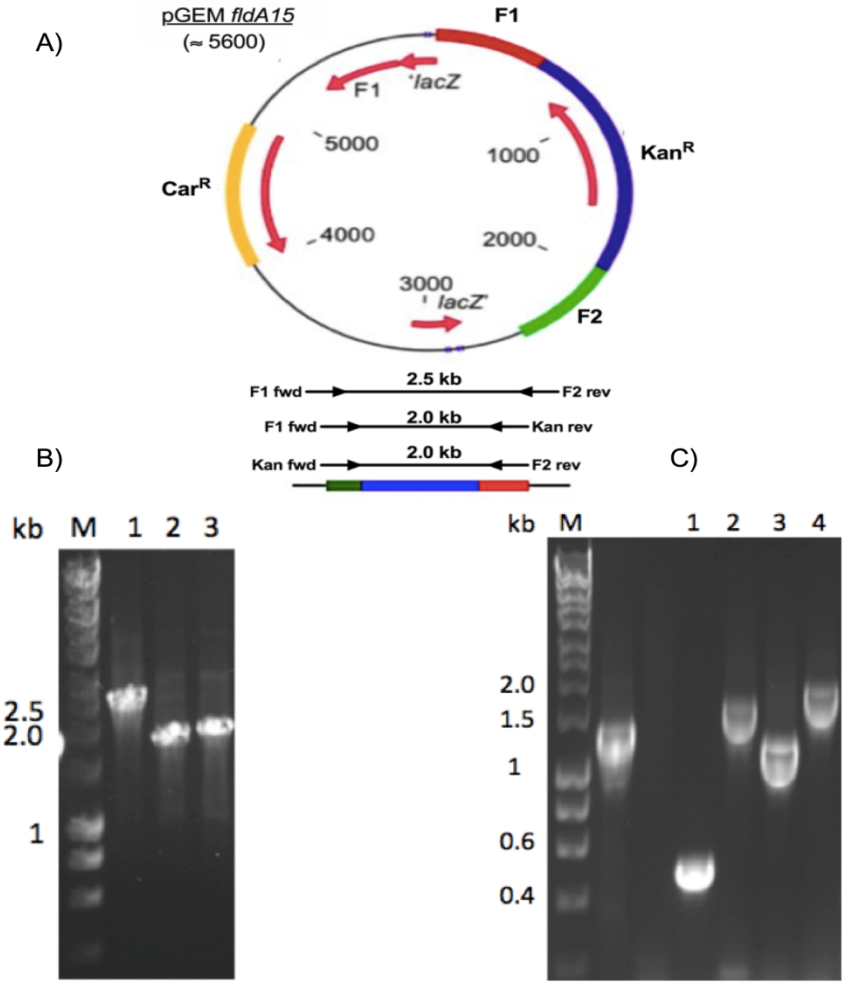

Figure 5.12: Generation of *fldA15* mutagenesis plasmid by ISA using pGEM-3Zf plasmid digested at the HincII restriction site. **(A)** Plasmid map of pGEM *fldA15* shows the flanking regions of the targeted gene. Red is Flank 1 (F1), 500 bp that is upstream of *fldA15* gene. Green is Flank 2 (F2) 500 bp that is downstream of *fldA15* gene. Targeted gene is interrupted by kanamycin cassette (blue). The other regions in the plasmid are Car^R region (gold), F1 origin of replication and the lacZ. **(B)** Confirmation of cloning using pGEM *fldA15 as* template with different combination of kanamycin cassette, Flanks (F1 and F2) primers. Lane1, using Flanks primers, the expected size is 2.5 kb. Lane2, using kanamycin cassette rev primer and Flank1 fwd, the expected size is 2.0 kb. Lane3**,** using kanamycin cassette fwd primer and Flank2 rev, the expected size is 2.0 kb. **(C)** Confirmation of *fldA15* gene deletion in *A. butzleri* (BU4018). Lane1, PCR amplification of wild-type genome using *fldA15* gene primers, the size of *fldA15 gene* is 0.5 kb. Lane2, Lane3 and Lane4, PCR amplification of *fldA15* mutant in *A. butzleri* (BU4018) using different primers, Lane2 (using *fldA15* gene primers, the expected size is 1.6 kb), Lane3 (using kanamycin cassette primers, the expected size is 1.4 kb. Lane4 (using *fldA15* gene fwd primer and kanamycin cassette rev primer). M is ladder.

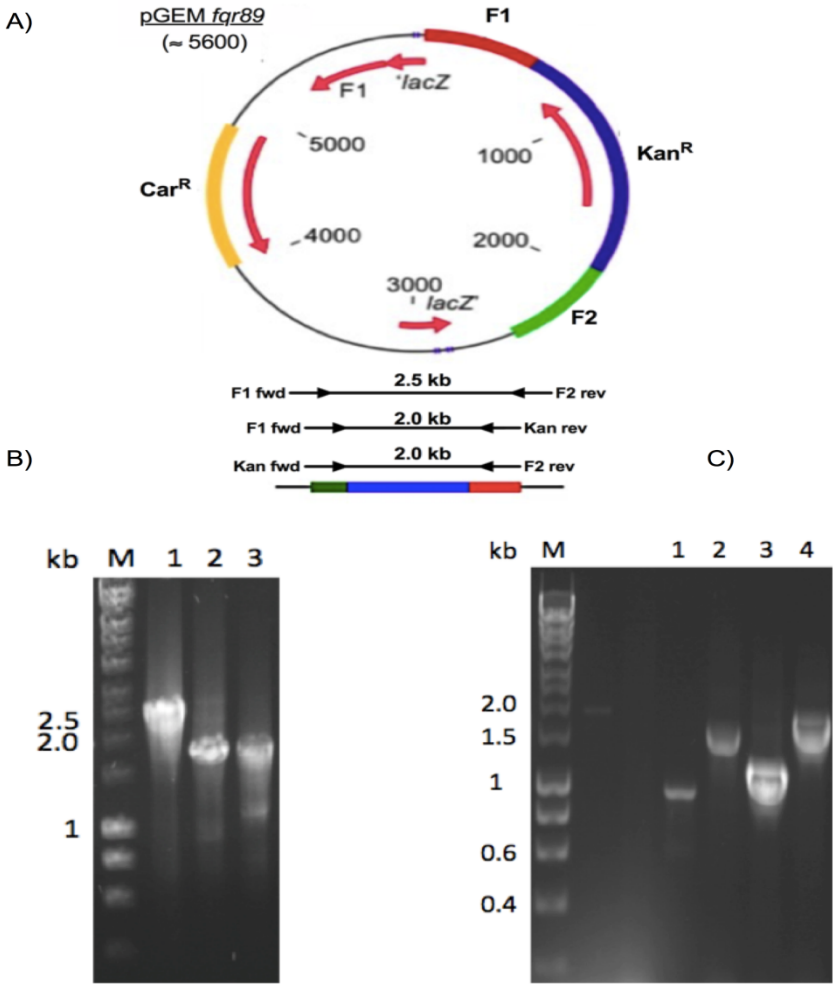

Figure 5.13. Generation of *fqr89* mutagenesis plasmid by ISA using pGEM-3Zf plasmid digested at the HincII restriction site. **(A)** Plasmid map of pGEM*fqr89* shows the flanking regions of the targeted gene. Red is Flank 1 (F1), 500 bp that is upstream of *fqr89* gene. Green is Flank 2 (F2) 500 bp that is downstream *fqr89* gene. Targeted gene is interrupted by kanamycin cassette (blue). The other regions in the plasmid are Car^R region (gold), F1 origin of replication and the lacZ. **(B)** Confirmation of cloning using pGEM *fqr89 as* template with different combination of kanamycin cassette, Flanks (F1 and F2) primers. Lane1, using Flanks primers, the expected size is 2.5 kb. Lane2, using kanamycin cassette rev primer and Flank1 fwd, the expected size is 2.0 kb. Lane3, using kanamycin cassette fwd primer and Flank2 rev, the expected size is 2.0 kb. **(C)** Confirmation of *fqr89* gene deletion in *A. butzleri* (BU4018). Lane1, PCR amplification of wild-type genome using *fqr89* gene primers, the size of *fqr89 gene* is 1.0 kb. Lane2, Lane3 and Lane4, PCR amplification of *fqr89* mutant in *A. butzleri* (BU4018) using different primers, Lane2 (using *fqr89* gene primers, the expected size is 2.0 kb), Lane3 (using kanamycin cassette primers, the expected size is 1.4 kb. Lane4 (using *fqr89* gene fwd primer and kanamycin cassette rev primer). M is ladder.

Studying the growth phenotype of the deleted *fldA15* or *fqr89* genes in the mutant *A. butzleri* (BU4018) strains created shows that there is no growth defect compared to wild type (Figure 5.14) in complex media, indicating these two proteins are not essential or there are other proteins playing the same role. This may explain why some *Arcobacter* strains (*A. cibarius*, *A. trophiarum*, *A. cryaerophilus* ATCC 43158^{T} and *A. cryaerophilus* ATCC 49615) have nether *fldA* nor *fqr* genes (Table 5.1).

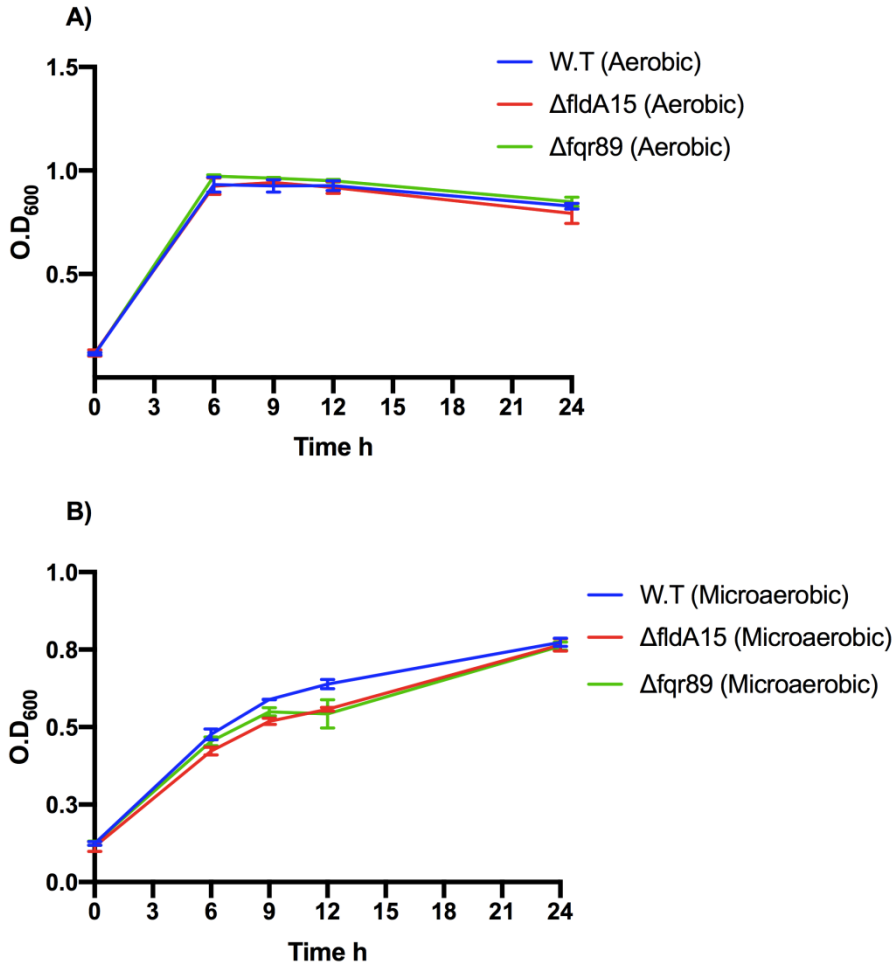

Figure 5.14: Aerobic growth **(A)** and Microaerobic growth **(B)** curve of the *A. butzleri* (BU4018), *fldA15* mutant and *fqr89* mutant. There is no growth defect in mutant strains.

5.2.2.4. Aerotolerance in *Arcobacter spp.*

Unlike *Campylobacter, Arcobacter* are aerotolerant. Although *Campylobacter* has enzymes to protect against oxidative stress such as superoxide dismutase, catalase and some other enzymes, it still cannot grow at high oxygen levels. *Campylobacter* relies on oxygen labile enzymes for its viability as discussed in the Introduction to this thesis. These enzymes contain iron sulphur clusters as cofactors that are inactivated and/or damaged by aerobic conditions with an insufficient repair rate. Some of these enzymes include Por, Oor, Acn, and SdaA. POR and OOR enzymes are responsible for the oxidative decarboxylation of pyruvate and 2-oxoglutrate to acetyl- CoA and succinyl-CoA, respectively. Both *Arcobacter* and *Campylobacter* have OOR. While 23 *Arcobacter* species contain an oxygen stable PDH enzyme, the other 4 in Table 5.1 have only POR. *C. jejuni* utilizes an anaerobic-type serine dehydratase (SdaA) which is an important enzyme for amino acid catabolism (Hofreuter *et al.,* 2012), while *Arcobacter* do not possess this protein. In regards of the other dehydratase enzymes aconitase (Acn) and fumarase (Fum), *Arcobater butzleri* encodes two aconitase (Acn) and fumarase (Fum) enzymes. The two *Arcobacter* aconitase enzymes are annotated as AcnB and AcnD. *Arcobacter butzleri* AcnB shares 66.6 % identity with *C. jejuni* AcnB (Figure 5.15) while AcnD shares 43.5 % identity with *E. coli* AcnA and only 10 % with *C. jejuni* AcnB (Figure 5.16). Whether these are differentially oxygen stable will need to be investigated. The *A. butzleri* FumC is predicted to be oxygen stable, sharing 55.8 % identity with *E. coli* FumC which does not contain an Fe-s cluster (Figure 5.17) (Miller *et al*., 2007).

We performed an aerobic growth curve of *A. cloacae* (Figure 5.18) which possesses only POR – unlike *A. butzleri* which possesses only PDH. Figure 5.18 shows that this species in fact grows very well aerobically. This might suggest that a simple dependence on POR (and OOR) is not the only reason that determines whether most Epsilonproteobacteria cannot grow aerobically. In many bacteria there are two Fe-S cluster biosynthesis systems known as Isc and Suf (Roche *et al*., 2013). The Isc system genes are constitutive while

the Suf system genes are induced under oxidative stress (Jang and Imlay, 2010). Analyzing *Arcobacter* and
C. jejuni genomes shows that *Arcobacter* have both Isc and Suf systems (IscS a nd IscU plus SufB, SufC, SufD, SufS, SufE and SufT) and another protein involved in Fe-S cluster biosynthesis (CsdA) while *C. jejuni* possesses genes of the Isc system but there is no evidence of a functional Suf system. Thus, more efficient FeS cluster repair and biosynthesis may be an important factor in the aerotolerance of *Arcobacter*.

```
ArcobacterAcnB      MSLLATYKAHTEERIEEGGLPPLALTAEQTAELVELLKANPVEETEYCLDLFKNRINPGV     60
C.jejuniAcnB        MSFMQEYNKLVEERA-ALGIPPLPLNANQTRELCKLLENENN---EELANLLENRVNPGV     56
                    **::  *:  .***    *:*** *.*:** ** :**: :     *   :*::**:****
ArcobacterAcnB      DDAAYVKAAFLNDIVQGNVTCSVISKADAIEILGTMMGGFNVTPLIEALKVEEVAELAAT    120
C.jejuniAcnB        DDAALVKCEFLDSILKGKISAPNIDKKRALRMLGTMLGGYNVKVLIDALKDENIAKDAAE    116
                    **** **. **:.*::*:::.  *.*  *:.:****:**:**. **:*** *::*: **
ArcobacterAcnB      QLKNTILVYDAFNDVKELMDSGNAKAKEIIESWANAEWFTNKPALEEEIKLTVYKIPGET    180
C.jejuniAcnB        VLKNIIFVHDNFHTIAELS-KNNPHAKEVLQSWANADWFNKKEKLPQVIKCIVFKVAGET    175
                     *** *:*:* *: : **  ..* :***:::*****:**.:*  * : **  *:*: ***
ArcobacterAcnB      NTDDLSPATVAFTRPDIPLHATAMLQSRMEKPLETMAKLKEKGNPLAYVGDVVGTGSSRK    240
C.jejuniAcnB        NTDDLSPAGDAFTRSDIPLHANAMLKVRQTGSLEKIKELKKSGREVVYVGDVVGTGSSRK    235
                    ********  **** ******.***: *    **.: :**:.*. :.**************
ArcobacterAcnB      SGINSVQWHMGRDIPGVPNKRTGGVVIGSIIAPIFFNTAEDSGCLPVVAPVDELETGDEI    300
C.jejuniAcnB        SAINSIQWHLGKEIEGVPNKHSGGIIMGSTIAPIFFNTAQDSGALPIICDVTNLEMGDEF    295
                    *.***:***:*::* *****::**:::** *********:***.**::. * :** ***:
ArcobacterAcnB      VLKPYAGVIEKNGKVVSEFKLSPNTLTDEMRAGGRIPLIIGKGLTAKAREALGLGASDMF    360
C.jejuniAcnB        EIHPYEGKIIKNGSTIAEFTLSPNTLLDEVRAGGRIPLIIGRGLCTKAREFLGMESENIF    355
                     ::** * * ***..::**.****** **:***********:** :**** **: :.::*
ArcobacterAcnB      IAPEQPEDNGKGYSQAQKMVGRACGIEGVKPGMYVEPIATTVGSQDTTGPMTRDEIKELA    420
C.jejuniAcnB        TKPEQPKSSSGGYTLAQKMLGRACGVEGVRPGMYIEPITLTVGSQDTTGPMTRDEIKELA    415
                      ****:... **: ****:*****:***:****:***: **********************
ArcobacterAcnB      ALSFGADMVMQSFCHTAAYPKPADINLRHTLPDFINSRGGVTLKPGDGVIHSWLNRLCLP    480
C.jejuniAcnB        SLGFNADFVMQSFCHTAAYPKVSDSNLHKTLPNFMTSRGGVSLKPGDGVIHSWLNRFVLP    475
                    :*.*.**:************** :* **::***:*:.*****:*************: **
ArcobacterAcnB      DTVGTGGDSHTRFPIGISFPAGSGLIAFAAVTGMMPLTMPESVLVKFKGEMQPGITLRDL    540
C.jejuniAcnB        DTVGTGGDSHTRFPIGISFPAGSGLVAFAAVTGSMPLNVPESVLVRFSGELQAGVTLRDL    535
                    *************************:******* ***.:******:*.**:* *:*****
ArcobacterAcnB      VNAIPYYAIKQGLLTVPKKNKKNIFAGKIIEIQGLPDLKVEQAFELSDASAERSAAACSV    600
C.jejuniAcnB        VNAIPYYAIKQGQLTVEKKNKKNIFAGKILEIEGLPNLKVEQAFELSDASAERSAAACSV    595
                    ************ *** ************:**:***:************************
ArcobacterAcnB      QLDKEPIIEYLSSNIALIEKMIEEGYEDKRTLQRRADKMKEWLANPELIQPDADAEYAAV    660
C.jejuniAcnB        DLSIESVSEYIKSNISLIEAMIEVGYENKATLARRAEKMREWLKNPTLLRADKDAKYAYI    655
                    :*. * : **:.***:*** *** ***:* ** ***:**:*** ** *:: * **:** :
ArcobacterAcnB      IEIDLNDVKEPILACPNDPDDVATLSEILADDSRPKNIDEVFVGSCMTNIGLFRALGEVL    720
C.jejuniAcnB        IDINLNNIKEPILACPNDPDDVATLSEILADDKRPKNIDEVFVGSCMTNIGHYRALGEIL    715
                    *:*:**::**********************.********************* :*****:*
ArcobacterAcnB      KGEGVAPAKLWVAPPTKMDEAQLTEEGYYSIFAAAGARIEIPGCSLCMGNQAQVNEGAVV    780
C.jejuniAcnB        KDKGILKTRLWVVPPTKMDKAQLINEGYYSIFGAAGARIEVPGCSLCMGNQARVNDGAVV    775
                    * .**.  .:*** ******.*** .******** ********.***********.**.*****
```

Figure 5.15: Protein sequence alignment of *C. jejuni* AcnB and *Arcobacter* AcnB. The percentage sequence identity is 66.6 %.

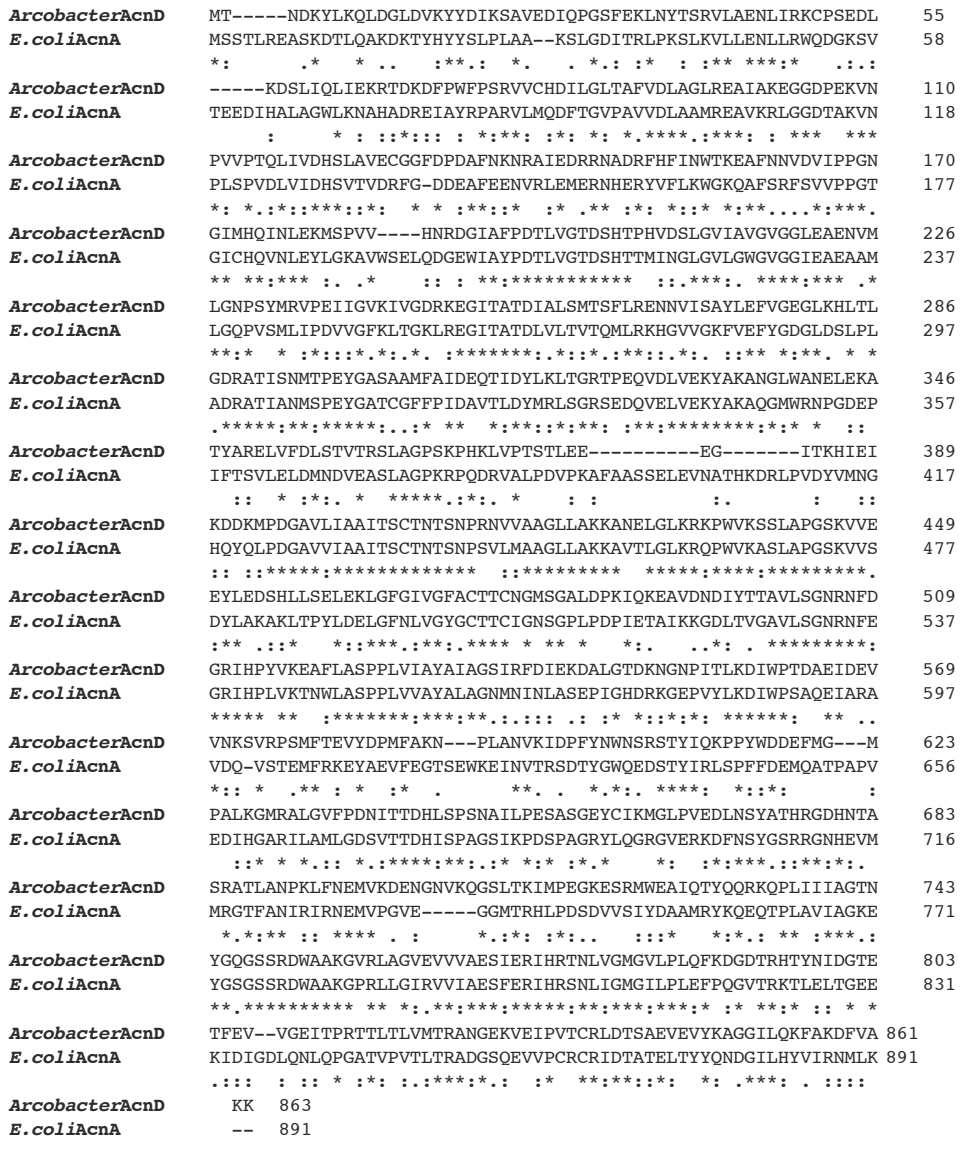

Figure 5.16: Protein sequence alignment of *E. coli* AcnA and *Arcobacter* AcnD. The percentage sequence identity is 43.4 %.

Figure 5.17: Protein sequence alignment of *E. coli* FumC and *Arcobacter* FumC. The percentage sequence identity is 55.8 %.

A)

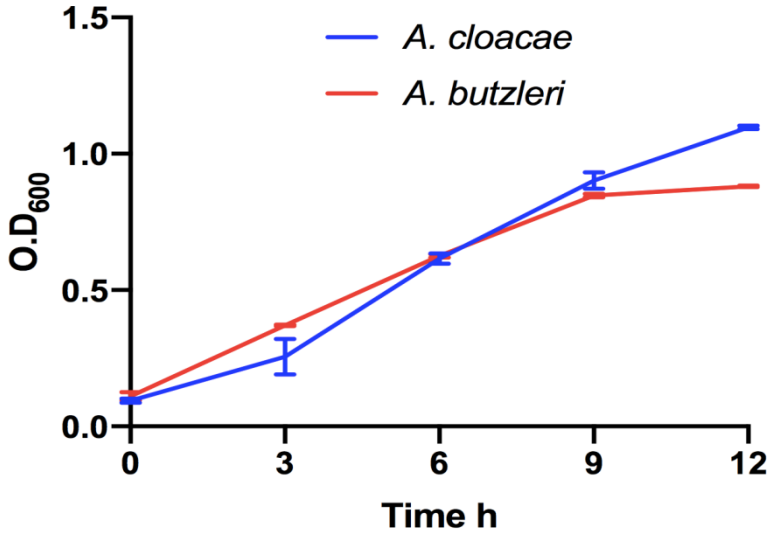

B)

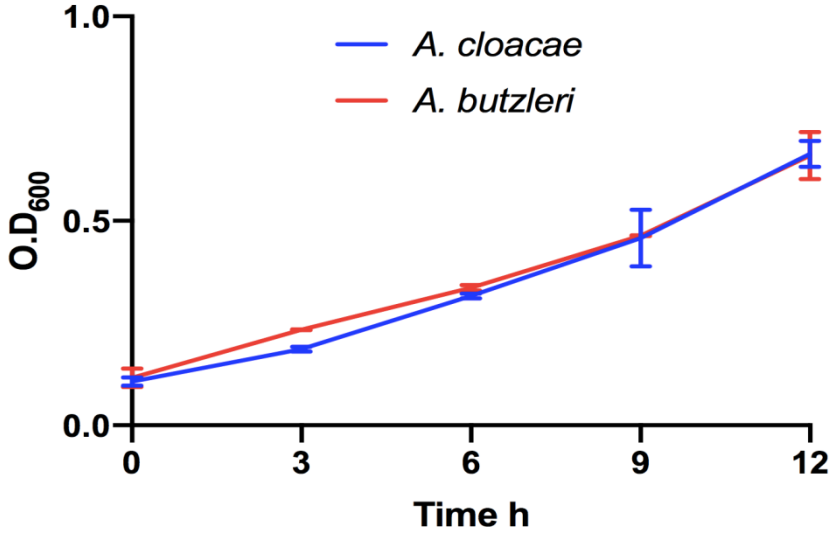

Figure 5.18. Comparison of aerobic **(A)** and microaerobic **(B)** growth curves of the *A. butzleri* (BU4018) red trace and *A. cloacae* blue trace.

5.3 Discussion:

Arcobacter spp and *Campylobacter spp*, are classified in the Campylobacteraceae family. However, from Table 5.1 it can be seen that *Arcobacter spp* possess some key genes relating to energy metabolism that *Campylobacter spp* do not have. For instance, some *Arcobacter spp* have an additional Nuo complex. In addition to a NuoEF containing complex it contains a "Nuo2" complex that is homologous to the *C. jejuni* Nuo complex. Similar to the *C. jejuni* Nuo complex, Nuo2 contains unknown function proteins in place of NuoE/F that are similar to NuoX and NuoY.

Given the presence of PDH (generating NADH) rather than POR (generating reduced flavodoxin) in *A. butzleri*, our hypothesis is that the NuoEF Complex I is necessary to oxidize NADH, while the Nuo2 Complex I is necessary to re-oxidise the reduced flavodoxin resulting from the activity of OOR. This needs to be tested experimentally; it would be very informative to make mutants in each of these Complex I systems (assuming they will be viable) and see how this affects growth and respiration rates with pyruvate and 2-oxoglutarate. The other main observation from Table 5.1 is the presence of more than one ribonucleotide reductase, flavodoxin and FqrB homologue in many of the *Arcobacters*.

In the annotations supplied by Dr William Miller, *A. butzleri* has two flavodoxin proteins, one annotated FqrB (Table 5.1) and two other putative FAD- containing FqrB-like proteins, they are described as putative flavodoxin-like fold domain-containing protein, NAD(P)H (quinone) dehydrogenase/reductase. Bioinformatic analysis of these two FAD containing proteins shows that they have only 9 % and 13 % identity with FqrB. Also, they were added to phylogenetic tree in chapter 4 Figure 4.1. Different groups FAD containing proteins were used to generate the phylogenetic tree such as reductases from Gram-positive, thioredoxin reductases (TrxR) and CoA disulphide reductases (Cdr). The annotated *A. butzleri* FqrB clusters with *C. jejuni* FqrB and reductases from Gram-positive bacteria while the

two other FAD containing proteins are distinct from all groups. Despite the differences, the proteins were tested as flavodoxin (FldA15) reductases and we showed that these two FAD- containing proteins have no ability to interact with flavodoxin (FldA15) and to reduce it. Presumably, they are involved in other cellular redox reactions e.g. relating to oxidative stress defenses.

In addition to a class I ribonucleotide reductase (aerobic NrdAB), *A. butzleri* (and most other species) has a Class III RNR (anaerobic NrdDG). The NrdD protein contains an oxygen-sensitive glycyl radical, which is activated by NrdG protein under anaerobic growth condition. *Campylobacter* contains only the NrdAB class that is reduced by the FldA/FqrB system (From chapter 3). *A. butzleri* has the same proteins that *C. jejuni* utilizes in the RNR activation pathway with significant identity (Figure 5.19). It is noteworthy that upon protein purification there appear to be some differences such as FldA15 was a more greenish colored protein perhaps due to stabilization of the semiquinone form (Figure 5.6 A) while *C. jejuni* FldA was purified as a yellow protein (consistent with the fully oxidized state of flavin). Another difference is that the tyrosyl radical concentration within *A. butzleri* NrdB (Figure 5.6), seemed lower (as based on peak height at 410 nm) no matter how much culture was grown (1, 3 or 5 L), compared to *C. jejuni* NrdB tyrosyl radical (grown in 1 L L.B). This may indicate that the *C. jejuni* NrdB is more stable once formed than that in the *A. butzleri* protein. The regeneration of the tyrosyl radical was done by mixing *A. butzleri* FldA, FqrB and NrdB but there was no evidence of tyrosyl radical re-formation (Figure 5.11). Given this negative result, it is possible that there is either a problem with the protein preparation of NrdB used (eg residual hydroxylamine remaining that would quench any radical formation) or else that reduced FldA is not able to activate the protein in the way that was seen with *C. jejuni*. It is unfortunate that we were unable to purify the alternative flavodoxin for comparison, as this could be an alternative candidate for the electron donor.

FldA and fqrB were successfully deleted in *A. butzleri* but with no growth defect,

indicating that *A. butzleri* may indeed use an unidentified protein as electron donor for NrdB, consistent with the possibility is that the *A. butzleri* putative flavodoxin protein that we could not purify may replace FldA15. According to Tobias *et al* (2011), flavodoxin is an essential protein as electron donor/acceptor of the non-mevalonate pathway of isoprenoid biosynthesis (for IspG and IspH) in Gram-negative bacteria. In *E. coli* Flavodoxin I is an essential protein for its role in the non-mevalonate (MEP) pathway. *A. butzleri* FldA15 is homologous to *E. coli* Flavodoxin I with 43.8 % identity while the other putative flavodoxin shares only 4 % identity. Clearly, more work is needed to identify the physiological function of both flavodoxins in *A. butzleri*. Intriguingly, genomic analysis of *Arobacter spp* shows that *A. cibarius*, *A. trophiarum*, *A. cryaerophilus* ATCC 43158^{T} and *A. cryaerophilus* ATCC 49615 have neither a flavodoxin similar to FldA of *C. jejuni* nor putative alternative flavodoxins.

A)

```
C.jejuniFqrB      --MKKIDLIVVGAGPTGIGCAVEAKLKNKE-VLILEKSNNICQTLMQFYKDGKRVDKAYK   57
A.butzleriFqrB    MNEKIYDIIVIGAGSAGIACIIEAKLKNIENILLIEKTSNHSETIRKFYKDGKRVDKDWK   60
                     *  *:**:*** :**.* :****** * :*::**:.* .:*: :********** :*

C.jejuniFqrB      GCEGTNHGHVPFEDGTKESTIETFQNALKEHNIEVEFGSEVESVKN--ENGVFLVSTAKG   115
A.butzleriFqrB    NQVIKLEGNIDFMDGTKESTLEYFEELLNKNEISPVYNTEVEKIIKNENTNLFEVHTLNK   120
                  .   . .*:: * *******:* *:: *::::*.  :.:***.: :  :..:* * * :

C.jejuniFqrB      VYECKNIIVAIGRMGKPNKPDYKLPMTLTKIINFNANSVLGNEKILVVGGGNSAAEYAVD   175
A.butzleriFqrB    IYQTKFAIICIGKMGKPNKPDYKIPTNIKKYINFNLDDCTTNEKILVIGGGNSAAEYAYF   180
                  :*: *  *:.**:**********:* .:.* **** :.   ******:**********

C.jejuniFqrB      LAN-SNQVSLCYRKKEFTRLNDINLKDIHEAGNSGKVELKLGIDINEVED-DNGKAKVNF   233
A.butzleriFqrB    LTNEKNNVTLAYRKPTFTRLNPINEKLLMQYQNDKKLTIKMNKEIKELEEAENLKVKVIY   240
                  *:* .*:*:*.***  ***** ** * : :  *. *: :*:. :*:*:*: :* *.** :

C.jejuniFqrB      TDGTSDIYDRIIYAIGGSTPLDFLQKCGINVDDKGVPLMDENKQSNVKGIFVAGDIATKN   293
A.butzleriFqrB    TDEEIEIFDRLIYAIGGTTPIDFLKACNVKIDENLNPICDGNFESSTKGIYLAGDIASKG   300
                  **   :*:**:******:**:***: *.:::*::  *: * * :*..***::*****:*.


C.jejuniFqrB        GASIVTGLNDAVKILSVL-----      311
A.butzleriFqrB      EGSISTALNHGYHIIKDISAKNV      323
                     .** *.**.. :*:. :
```

B)

```
C.jejuniFldA      MSVAVIYGSAMGNTEGAANTIASKLGISDVFNISDIDAAKMNSYDKLICGTSTWGSGDLQ   60
A.butzleriFldA    MATAIFFGSSTGNCEEIAKKISSKLGKIEVFDLSGTKIEKMNDYDKIILGSSTWGDGELN   60
                  *:.*:::**: ** *  *:.*:****  :**::*. .  ***.***:* *:****.*:*:

C.jejuniFldA      DDWDG--FDFSGLSLGGKTVAVFGMGDSESYSDTFCGGMGKLAQNLKDAGANLVGEVSTD   118
A.butzleriFldA    DDWEDAWSDFSKLDLSNKTIALFGLGDQESYSDEFASAMGIIYEHIKTTNAKIIGFTSTE   120
                  ***:.   *** *.*..**:*:**:**.***** *...** : :::* :.*:::* .**:

C.jejuniFldA      GYTFEASDAVVDGKFVGLALDNDNQEDQTESRIDAWVEQIKPYFA      163
A.butzleriFldA    GYYHDGSKAQIDDKFVGLVIDEDNQSDLTDERIESWVNNIKSEIL      165
                  ** .:.*.* :*.*****.:*:***.* *:.**::**::**  :
```

C)

```
C.jejuniNrdB      MQRKRIYNPSSNETLGDRKVFDGNPHGILNFTKAKYTWALKLWDLMEANTWFPKEVDTTK   60
A.butzleriNrdB    MERKTNYNPDSKESLNDRRVFGGNSDGMINFTRMKYQWALNLWDTMEANTWFPREVQMTG   60
                  *:**  ***.*:*:*.**:**.** .*::***: ** ***:*** ********:**: *
C.jejuniNrdB      DALDYRCNLTAGEKRMYDLVWSQLISMDSFQTNNLADNINPYITAPEINAVLARQAYEEA   120
A.butzleriNrdB    DAKDYKF-LTPAEKRMYDLVLSQLIFMDSLQTNNLMDNINPYITAPEINACLARQSYEEA   119
                  ** **:  ** .******** **** ***:***** ************** ****:****
C.jejuniNrdB      NHSKSYAVMVEAICDNTDLIYEMEKHDETLREKNDFISSIYEELAGDVDDNKLLLAMVAN   180
A.butzleriNrdB    NHSKSYAVMVESISDNTDLIYDMWKNDAKLREKNTYIAEVYKNLSGDIDDRKIVLALFAN   179
                  ***********:*.*******:* *:* .***** :*:.:*:::*:**:**.*:::**:.**
C.jejuniNrdB      QILEGVYFYSGFTAIYALARAGKMLGSAQMIRFIQRDEITHLLLFQNMINSVRKERPDLF   240
A.butzleriNrdB    QILEGLYFYAGFAAIYALGKSGKMLGSSQMIRFIQRDEVTHLLLFQNMINSVRKERPDLF   239
                  *****:***:**:*****.::******:**********:**********************
C.jejuniNrdB      HDENINKIYDMFKKAGDLEIKWGKYITQNQIMGFTDDIIEEYIHYLVDQRLSAINLDKLY    300
A.butzleriNrdB    TSELEETVRAMFRKAVDLEASWGAYITQGQILGFTDGIIRQ-------------------    280
                  .*  :.:  **:** *** .** ****.**:****.**.:
C.jejuniNrdB       NAKHPIKWVDDFSKFNDQKSNFFESKVTNYSKGSISFDDF     340
A.butzleriNrdB     ---------------------------------------     280
```

Figure 5.19: Protein sequence alignment of *C. jejuni* FqrB-FldA-NrdB pathway and *A. butzleri* FqrB89, FldA15 and NrdB proteins. In **(A)** *C. jejuni* FqrB and *A. butzleri* FqrB89. In **(B)** *C. jejuni* FldA and *A. butzleri* FldA15. In **(C)** *C. jejuni* NrdB and *A. butzleri* NrdB. The percentage sequence identity of *C. jejuni* FqrB-FldA-NrdB and *A. butzleri* FqrB89, FldA15 and NrdB are 43.5 %, 55 % and 69 %, respectively.

Chapter 6: General conclusion and future work

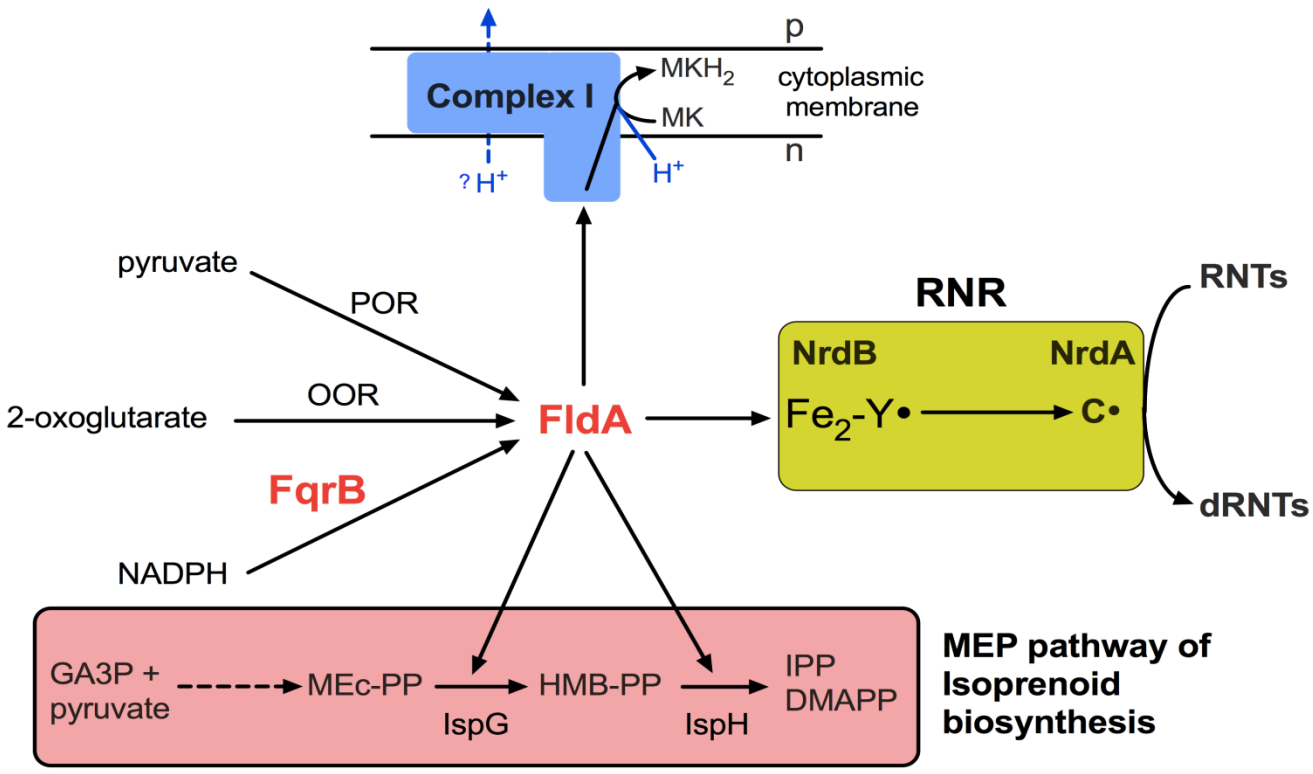

Figure 6.1: Multiple pathways for FldA reduction and its role in electron transport, isoprenoid biosynthesis and deoxyribonucleotide reduction. FldA can be reduced by electrons from at least three sources; from pyruvate oxidation via pyruvate:flavodoxin oxidoreductase (POR), from 2-oxoglutarate reduction via 2-oxoglutarate:flavodoxin oxidoreductase (OOR) or from NADPH oxidation via flavodoxin quinone reductase (FqrB). FldA is the only known electron donor for respiratory Complex I in *C. jejuni* but given the relatively small redox potential difference (~ 100 mV) between $FldA_{ox}$/$FldA_{red}$ couple and the menaquinone (MK)/menaquinol (MKH_2) couple it is unclear if Complex I is proton translocating. Our results suggest that FldA is an electron donor to the NrdB subunit of ribonucleotide reductase (RNR), to generate the tyrosine radical (Y·), possibly via a superoxide intermediate. This is then transferred to the NrdA subunit to generate a radical at the active site cysteine (C·), necessary for reduction of ribonucleotides (RNTs) to deoxyribonucleotides (dRNTs). FldA is also thought to be required as a source of electrons for two consecutive steps in the final section of the MEP isoprenoid biosynthesis pathway, catalysed by IspG which converts methylerythritol cyclic pyrophosphate (MEc-PP) into 4-hydroxy-3-methylbut-2-enyl pyrophosphate (HMB-PP) and IspH which converts HMB-PP into the products isopentyl pyrophosphate (IPP) and dimethylallyl pyrophosphate (DMAPP). MEc-PP is produced in several enzymatic steps from pyruvate and glyceraldehyde-3-phosphate (GA3P).

This thesis mainly concentrated on studying the role of flavodoxin in *C. jejuni*. Flavodoxin, an essential protein, seems to contribute to multiple pathways as electron donor/acceptor (Figure 6.1). Instead of pyruvate/2-oxoglutrate dehydrogenase that utilizes NAD (midpoint potential -320 mV) as electron carrier in aerobic bacteria, *C. jejuni* uses FldA that has a surprisingly high midpoint redox potential of the flavin (FMNox/FMNred) of around -180 mV. Like flavodoxin proteins from other bacteria, the W- and Y-loop regions involved in FMN binding in *C. jejuni* flavodoxin contain conserved anionic residues (Table 3.1). These conserved anionic residues are expected to cause a much lower redox potential. The three-dimensional structure of flavodoxin will be useful in future work to clarify the reason behind the high redox potential. *C. jejuni* possesses only two types of menaquinone; MK-6 with an estimated midpoint potential of -75 mV and also 8-methylmenaquinone, MMK with a redox potential estimated to be between -125 and -140 mV. Therefore, it seems that although FldA can reduce MK-6, the redox span is nowhere near enough to pump protons against a pmf of ~ 200 mV. Also, the function of Complex I here seems to be to allow fldA reoxidation and to contribute to the reduced quinone pool, but perhaps not in energy conservation. The way by which FldA interacts with Complex I is still unclear. In *C. jejuni,* Complex I does not contain NuoE/F that usually interacts with the electron donor, instead it has NuoX/Y. *nuoX/Y* are essential genes and these proteins have no known redox centers (prosthetic group). Two techniques have been used to investigate the interaction between FldA and Complex I, the *in vitro* technique using AKTA prime system with tagged and untagged proteins and an *in vivo* technique using the bacterial two hybrid system (chapter 3). Both methods showed that there is no interaction. It is possible that FldA donates the electrons directly to NuoG within which there are several iron-sulphur clusters. Therefore, purified NuoG needs to be confirmed to contain the whole set of Fe-S clusters in order to test the ability of NouG to oxidize FldA under anaerobic conditions.

This study provides *in vivo* and *in vitro* evidence that flavodoxin (FldA) contributes to the ribonucleotide reductase pathway. It is still elusive how FldA is

involved in this pathway at the molecular level. There are two possibilities; either flavodoxin reduces ferric Fe^{+3} to ferrous Fe^{+2} in RNR and then the ferrous iron interacts with O_2 (typical of class 1a RNRs) or FldA interacts with O_2 to produce superoxide that will interact with di-iron centre, similar to class 1b RNR that use manganese. In order to study the relative reactivity of the NrdB di-iron centre with superoxide versus oxygen, apoNrdB should be produced. Unsuccessful attempts to remove iron from NrdB by unfolding the protein were done using high concentration urea (5M) with dialysis or with the AKTA prime system. According to Huque *et al* (2000), producing apoNrdB could be achieved by using dialysis against 50 mM Tris-HCl, pH 7.5, 50 mM EDTA, 50 mM 8-hydroxyquinoline, 1 mM dithiothreitol (DTT) solution for 5 hr. *C. jejuni* NrdB is extremely stable against the radical scavenger hydroxyurea which is effective against the tyroyl radical of NrdB from other organisms. According to Gerez *et al* (1997), the stability of the radical in NrdB depends on the site of the radical. In *E. coli* NrdB, the hydrophobic pocket in which the tyrosyl radical is located enables it to be stable. Replacing the hydrophobic residues with hydrophilic ones leads to shortening of the half-life of the tyrosyl radical. Therefore, a crystal structure for *C. jejuni* NrdB will be needed to reveal the tyrosyl radical site topology.

Finally, analyzing *Arcobacter spp* genomes shows that unlike *Campylobacter*, *Arcobacters* possess multiple flavodoxins, FqrBs and two types of Complex I. Also, some *Arcobacter* species have no flavodoxin protein that is thought to be essential in many other Gram-negative bacteria for its role as electron acceptor/donor in the isoprenoid pathway (MEP pathway), meaning these species may use a ferrodoxin protein as in plants and cyanobacteria or utilize the mevalonate pathway as in Gram-positive bacteria (Parvaiz *et al*., 2018). This hypothesis needs more investigation.

References

Alagaratnam, S., G. Van Pouderoyen, T. Pijning, B. W. Dijkstra, D. Cavazzini, G. L. Rossi, W. M. Van Dongen, C. P. Van Mierlo, W. J. Van Berkel, and G. W. Canters, 2005, A crystallographic study of Cys69Ala flavodoxin II from *Azotobacter vinelandii*: structural determinants of redox potential: Protein science, v. 14, p. 2284-2295.

Altekruse, S. F., N. J. Stern, P. I. Fields, and D. L. Swerdlow, 1999, *Campylobacter jejuni*—an emerging foodborne pathogen: Emerging infectious diseases, v. 5, p. 28.

Al-Haideri, H., M. A. White, and D. J. Kelly, 2016, Major contribution of the type II beta carbonic anhydrase CanB (C j0237) to the capnophilic growth phenotype of *Campylobacter jejuni*: Environmental microbiology, v. 18, p. 721-735.

Anbar, A. D., and A. H. Knoll, 2002, Proterozoic ocean chemistry and evolution: a bioinorganic bridge?: Science, v. 297, p. 1137-1142.

Ando, N., E. J. Brignole, C. M. Zimanyi, M. A. Funk, K. Yokoyama, F. J. Asturias, J. Stubbe, and C. L. Drennan, 2011, Structural interconversions modulate activity of *Escherichia coli* ribonucleotide reductase: Proceedings of the National Academy of Sciences, v. 108, p. 21046-21051.

Atack, J. M., P. Harvey, M. A. Jones, and D. J. Kelly, 2008, The *Campylobacter jejuni* thiol peroxidases Tpx and Bcp both contribute to aerotolerance and peroxide-mediated stress resistance but have distinct substrate specificities: Journal of bacteriology, v. 190, p. 5279-5290.

Atack, J. M., and D. J. Kelly, 2009, Oxidative stress in *Campylobacter jejuni:* responses, resistance and regulation: Future microbiology, v. 4, p. 677-690.

Barker, P. D., H. A. O. Hill, G. S. Sanghera, R. R. Eady, and R. N. Thorneley, 1988, The direct electrochemistry of flavodoxin from *Azotobacter chroococcum* at a graphite electrode promoted by aminoglycosides, Portland Press Ltd.

Berggren, G., N. Duraffourg, M. Sahlin, and B.-M. Sjöberg, 2014, Semiquinone-induced maturation of *Bacillus anthracis* ribonucleotide reductase by a superoxide intermediate: Journal of Biological Chemistry, v. 289, p. 31940-31949.

Birben, E., U. M. Sahiner, C. Sackesen, S. Erzurum, and O. Kalayci, 2012, Oxidative stress and antioxidant defense: World Allergy Organization Journal, v. 5, p. 9-19.

Bolton, F., and D. Coates, 1983, A comparison of microaerobic systems for the culture of *Campylobacter jejuni* and *Campylobacter coli*: European journal of clinical microbiology, v. 2, p. 105-110.

Brown, N. C., R. Eliasson, P. Reichard, and L. Thelander, 1968, Nonheme iron as a cofactor in ribonucleotide reductase from *E. coli*: Biochemical and biophysical research communications, v. 30, p. 522-527.

Burns, B. P., S. L. Hazell, and G. L. Mendz, 1995, Acetyl-CoA carboxylase activity in *Helicobacter pylori* and the requirement of increased CO2 for growth: Microbiology, v. 141, p. 3113-3118.

Butzler, J.-P., P. Dekeyser, M. Detrain, and F. Dehaen, 1973, Related vibrio in stools: The Journal of pediatrics, v. 82, p. 493-495.

Cameron, A., and E. C. Gaynor, 2014, Hygromycin B and apramycin antibiotic resistance cassettes for use in *Campylobacter jejuni*: PLoS One, v. 9, p. e95084.

Carlone, G. M., and F. A. Anet, 1983, Detection of menaquinone-6 and a novel methyl-substituted menaquinone-6 in *Campylobacter jejuni* and *Campylobacter fetus* subsp. fetus: Microbiology, v. 129, p. 3385-3393.
Chabes, A., and L. Thelander, 2003, DNA building blocks at the foundation of better survival: Cell Cycle, v. 2, p. 171-172.

Cotruvo Jr, J. A., T. A. Stich, R. D. Britt, and J. Stubbe, 2013, Mechanism of assembly of the dimanganese-tyrosyl radical cofactor of class Ib ribonucleotide reductase: enzymatic generation of superoxide is required for tyrosine oxidation via a Mn (III) Mn (IV) intermediate: Journal of the American Chemical Society, v. 135, p. 4027-4039.

Cotruvo Jr, J. A., and J. Stubbe, 2011, Class I ribonucleotide reductases: metallocofactor assembly and repair *in vitro* and *in vivo*: Annual review of biochemistry, v. 80, p. 733-767.

de Boer, R. F., A. Ott, P. Güren, E. van Zanten, A. van Belkum, and A. M. Kooistra-Smid, 2013, Detection of *Campylobacter* species and *Arcobacter butzleri* in stool samples by use of real-time multiplex PCR: Journal of clinical microbiology, v. 51, p. 253-259.

Eklund, H., U. Uhlin, M. Färnegårdh, D. T. Logan, and P. Nordlund, 2001, Structure and function of the radical enzyme ribonucleotide reductase: Progress in biophysics and molecular biology, v. 77, p. 177-268.

Elvers, K. T., S. M. Turner, L. M. Wainwright, G. Marsden, J. Hinds, J. A. Cole, R. K. Poole, C. W. Penn, and S. F. Park, 2005, NssR, a member of the Crp-Fnr superfamily from *Campylobacter jejuni*, regulates a nitrosative stress-responsive regulon that includes both a single-domain and a truncated haemoglobin: Molecular microbiology, v. 57, p. 735-750.

Gaballa, A., G. L. Newton, H. Antelmann, D. Parsonage, H. Upton, M. Rawat, A. Claiborne, R. C. Fahey, and J. D. Helmann, 2010, Biosynthesis and functions of bacillithiol, a major low-molecular-weight thiol in *Bacilli*: Proceedings of the National Academy of Sciences, v. 107, p. 6482-6486.

Gao, B., H. Vorwerk, C. Huber, M. Lara-Tejero, J. Mohr, A. L. Goodman, W. Eisenreich, J. E. Galán, and D. Hofreuter, 2017, Metabolic and fitness determinants for *in vitro* growth and intestinal colonization of the bacterial pathogen *Campylobacter jejuni*: PLoS biology, v. 15, p. e2001390.

Gerez, C., E. Elleingand, B. Kauppi, H. Eklund, and M. Fontecave, 1997, Reactivity of the tyrosyl radical of *Escherichia coli* ribonucleotide reductase: Control by the protein: European journal of biochemistry, v. 249, p. 401-407.

Gibson, D. G., L. Young, R.-Y. Chuang, J. C. Venter, C. A. Hutchison, and H. O. Smith, 2009, Enzymatic assembly of DNA molecules up to several hundred kilobases: Nature methods, v. 6, p. 343-345.

Gilbert, M. J., B. Duim, A. L. Zomer, and J. A. Wagenaar, 2019, Living in cold blood: *Arcobacter*, *Campylobacter*, and *Helicobacter* in reptiles: Frontiers in microbiology, v. 10, p. 1086.

González-Hein, G., B. Huaracán, P. García, and G. Figureueroa, 2013, Prevalence of virulence genes in strains of *Campylobacter jejuni* isolated from human, bovine and broiler: Brazilian Journal of Microbiology, v. 44, p. 1223-1229.

Grant, K. A., and S. F. Park, 1995, Molecular characterization of katA from *Campylobacter jejuni* and generation of a catalase-deficient mutant of *Campylobacter coli* by interspecific allelic exchange: Microbiology, v. 141, p. 1369-1376.

Guccione, E., M. Del Rocio Leon-Kempis, B. M. Pearson, E. Hitchin, F. Mulholland, P. M. Van Diemen, M. P. Stevens, and D. J. Kelly, 2008, Amino acid-dependent growth of *Campylobacter jejuni*: key roles for aspartase (AspA) under microaerobic and oxygen-limited conditions and identification of AspB (Cj0762), essential for growth on glutamate: Molecular microbiology, v. 69, p. 77-93.

Guccione, E., A. Hitchcock, S. J. Hall, F. Mulholland, N. Shearer, A. H. Van Vliet, and D. J. Kelly, 2010, Reduction of fumarate, mesaconate and crotonate by Mfr, a novel oxygen-regulated periplasmic reductase in *Campylobacter jejuni*: Environmental microbiology, v. 12, p. 576-591.

Guest, J. R., S. J. Angier, and G. C. Russell, 1989, Structure, Expression, and Protein Engineering of the Pyruvate Dehydrogenase Complex of *Escherichia coli* a: Annals of the New York Academy of Sciences, v. 573, p. 76-99.

Hanahan, D., 1983, Studies on transformation of *Escherichia coli* with plasmids: Journal of molecular biology, v. 166, p. 557-580.

Heering, H., and W. Hagen, 1996, Complex electrochemistry of flavodoxin at carbon-based electrodes: results from a combination of direct electron transfer, flavin-mediated electron transfer and comproportionation: Journal of Electroanalytical Chemistry, v. 404, p. 249-260.

Ho, H. T., L. J. Lipman, and W. Gaastra, 2006, *Arcobacter*, what is known and unknown about a potential foodborne zoonotic agent!: Veterinary microbiology, v. 115, p. 1-13.

Hofer, A., M. Crona, D. T. Logan, and B.-M. Sjöberg, 2012, DNA building blocks: keeping control of manufacture: Critical reviews in biochemistry and molecular biology, v. 47, p. 50-63.

Hughes, N. J., C. L. Clayton, P. A. Chalk, and D. J. Kelly, 1998, *Helicobacter pylori* porCDAB and oorDABCGenes Encode Distinct Pyruvate: Flavodoxin and 2-Oxoglutarate: Acceptor Oxidoreductases Which Mediate Electron Transport to NADP: Journal of bacteriology, v. 180, p. 1119-1128.

Huque, Y., F. Fieschi, E. Torrents, I. Gibert, R. Eliasson, P. Reichard, M. Sahlin, and B.-M. Sjöberg, 2000, The active form of the R2F protein of class Ib ribonucleotide reductase from *Corynebacterium ammoniagenes* is a diferric protein: Journal of Biological Chemistry, v. 275, p. 25365-25371

Imlay, J. A., 2006, Iron-sulphur clusters and the problem with oxygen: Molecular microbiology, v. 59, p. 1073-1082.

Johansson, R., E. Torrents, D. Lundin, J. Sprenger, M. Sahlin, B. M. Sjöberg, and D. T. Logan, 2010, High-resolution crystal structures of the flavoprotein NrdI in oxidized and reduced states–an unusual flavodoxin: The FEBS journal, v. 277, p. 4265-4277.

Juhnke, H. D., H. Hiltscher, H. R. Nasiri, H. Schwalbe, and C. R. D. Lancaster, 2009, Production, characterization and determination of the real catalytic properties of the putative ‘succinate dehydrogenase’from *Wolinella succinogenes*: Molecular microbiology, v. 71, p. 1088-1101.

Karimova, G., J. Pidoux, A. Ullmann, and D. Ladant, 1998, A bacterial two-hybrid system based on a reconstituted signal transduction pathway: Proceedings of the National Academy of Sciences, v. 95, p. 5752-5756.

Kelly, D., 2001, The physiology and metabolism of *Campylobacter jejuni* and *Helicobacter pylori*: Journal of Applied Microbiology, v. 90, p. 16S-24S.

Kendall, J. J., A. M. Barrero-Tobon, D. R. Hendrixson, and D. J. Kelly, 2014, Hemerythrins in the microaerophilic bacterium *Campylobacter jejuni* help protect key iron–sulphur cluster enzymes from oxidative damage: Environmental microbiology, v. 16, p. 1105-1121.

Kerscher, L., and D. Oesterhelt, 1982, Pyruvate: ferredoxin oxidoreductase—new findings on an ancient enzyme: Trends in Biochemical Sciences, v. 7, p. 371-374.

Kim, J.-C., E. Oh, J. Kim, and B. Jeon, 2015, Regulation of oxidative stress resistance in *Campylobacter jejuni*, a microaerophilic foodborne pathogen: Frontiers in microbiology, v. 6, p. 751.

Kist, M., 1985, The historical background of Campylobacter infection: new aspects: Proceedings of the 3rd International Workshop on *Campylobacter* Infections, Ottawa, ed Pearson AD, Public Health Laboratory Service, London, p. 23-27.

Konrad, A., E. Yarunova, T. Tinta, J. Piškur, and D. A. Liberles, 2012, The global distribution and evolution of deoxyribonucleoside kinases in bacteria: Gene, v. 492, p. 117-120.

Larsson, A., M. Karlsson, M. Sahlin, and B. Sjöberg, 1988, Radical formation in the dimeric small subunit of ribonucleotide reductase requires only one tyrosine 122: Journal of Biological Chemistry, v. 263, p. 17780-17784.

Lau, S., P. Woo, J. Teng, K. Leung, and K. Yuen, 2002, Identification by 16S ribosomal RNA gene sequencing of *Arcobacter butzleri* bacteraemia in a patient with acute gangrenous appendicitis: Molecular Pathology, v. 55, p. 182.

Liu, Y. W., Denkmann, K., Kosciow, K., Dahl, C., and D. J. Kelly, 2013, Tetrathionate stimulated growth of *Campylobacter jejuni* identifies a new type of bi-functional tetrathionate reductase (TsdA) that is widely distributed in bacteria. Molecular Microbiology, v. 88, p.173-188.

Lofstad, M., I. Gudim, M. Hammerstad, Å. K. Røhr, and H.-P. Hersleth, 2016, Activation of the class Ib ribonucleotide reductase by a flavodoxin reductase in *Bacillus cereus*: Biochemistry, v. 55, p. 4998-5001.

Marchant, J., B. Wren, and J. Ketley, 2002, Exploiting genome sequence: predictions for mechanisms of *Campylobacter* chemotaxis: Trends in microbiology, v. 10, p. 155-159.

Maurice, M. S., N. Cremades, M. A. Croxen, G. Sisson, J. Sancho, and P. S. Hoffman, 2007, Flavodoxin: quinone reductase (FqrB): a redox partner of pyruvate: ferredoxin oxidoreductase that reversibly couples pyruvate oxidation to NADPH production in *Helicobacter pylori* and *Campylobacter jejuni*: Journal of Bacteriology, v. 189, p. 4764-4773.

Mayhew, S. G., and G. Tollin, 1992, General properties of flavodoxins: Chemistry and Biochemistry of Flavoenzymes, F. Muller, Ed.(CRC Press, Boca Raton, Ann Arbor, London, 1992), v. 3, p. 389-426.

McClung, C., D. Patriquin, and R. Davis, 1983, *Campylobacter nitroFigureilis sp*. nov., a nitrogen-fixing bacterium associated with roots of Spartina alterniflora Loisel: International Journal of Systematic and Evolutionary Microbiology, v. 33, p. 605-612.

McIver, L., C. Leadbeater, D. J. Campopiano, R. L. Baxter, S. N. Daff, S. K. Chapman, and A. W. Munro, 1998, Characterisation of flavodoxin $NADP^+$ oxidoreductase and flavodoxin; key components of electron transfer in *Escherichia coli*: European journal of biochemistry, v. 257, p. 577-585.

Mikheyeva, I. V., J. M. Thomas, S. L. Kolar, A. R. Corvaglia, N. Gaïa, S. Leo, P. Francois, G. Y. Liu, M. Rawat, and A. L. Cheung, 2019, YpdA, a putative bacillithiol disulfide reductase, contributes to cellular redox homeostasis and virulence in *Staphylococcus aureus:* Molecular Microbiology, v. 111, p. 1039-1056.

Minnihan, E. C., D. G. Nocera, and J. Stubbe, 2013, Reversible, long-range radical transfer in *E. coli* class Ia ribonucleotide reductase: Accounts of chemical research, v. 46, p. 2524-2535.

Muraoka, W. T., and Q. Zhang, 2011, Phenotypic and genotypic evidence for L-fucose utilization by *Campylobacter jejuni*: Journal of bacteriology, v. 193, p. 1065-1075.

Nordlund, P., and P. Reichard, 2006, Ribonucleotide reductases: Annu. Rev. Biochem., v. 75, p. 681-706.

Parkhill, J., B. Wren, K. Mungall, J. Ketley, C. Churcher, D. Basham, T. Chillingworth, R. Davies, T. Feltwell, and S. Holroyd, 2000, The genome sequence of the food-borne pathogen *Campylobacter jejuni* reveals hypervariable sequences: Nature, v. 403, p. 665-668.

Parvaiz, N., S. W. Abbasi, R. Uddin, and S. S. Azam, 2018, Targeting isoprenoid biosynthesis pathway in Staphylococcus lugdunensis: Comparative docking and simulation studies of conventional and allosteric sites: Journal of Molecular Liquids, v. 269, p. 426-440.

Pesci, E. C., D. L. Cottle, and C. L. Pickett, 1994, Genetic, enzymatic, and pathogenic studies of the iron superoxide dismutase of *Campylobacter jejuni*: Infection and immunity, v. 62, p. 2687-2694.

Pittman, M. S., K. T. Elvers, L. Lee, M. A. Jones, R. K. Poole, S. F. Park, and D. J. Kelly, 2007, Growth of *Campylobacter jejuni* on nitrate and nitrite: electron transport to NapA and NrfA via NrfH and distinct roles for NrfA and the globin Cgb in protection against nitrosative stress: Molecular microbiology, v. 63, p. 575-590.

Platts-Mills, J. A., and M. Kosek, 2014, Update on the burden of *Campylobacter* in developing countries: Current opinion in infectious diseases, v. 27, p. 444.

Puan, K.-J., H. Wang, T. Dairi, T. Kuzuyama, and C. T. Morita, 2005, fldA is an essential gene required in the 2-C-methyl-D-erythritol 4-phosphate pathway for isoprenoid biosynthesis: FEBS letters, v. 579, p. 3802-3806.

Rahman, H., R. M. King, L. K. Shewell, E. A. Semchenko, L. E. Hartley-Tassell, J. C. Wilson, C. J. Day, and V. Korolik, 2014, Characterisation of a multi-ligand binding chemoreceptor CcmL (Tlp3) of *Campylobacter jejuni*: PLoS Pathog, v. 10, p. e1003822.

Ramees, T. P., K. Dhama, K. Karthik, R. S. Rathore, A. Kumar, M. Saminathan, R. Tiwari, Y. S. Malik, and R. K. Singh, 2017, *Arcobacter*: an emerging food-borne zoonotic pathogen, its public health concerns and advances in diagnosis and control–a comprehensive review: Veterinary Quarterly, v. 37, p. 136-161.

Reichard, P., 1987, Regulation of deoxyribotide synthesis: Biochemistry, v. 26, p. 3245-3248.

Reichard, P., A. Baldesten, and L. Rutberg, 1961, Formation of deoxycytidine phosphates from cytidine phosphates in extracts from *Escherichia coli*: Journal of Biological Chemistry, v. 236, p. 1150-1157.

Reichard, P., and B. Estborn, 1951, Utilization of desoxyribosides in the synthesis of polynucleotides: Journal of Biological Chemistry, v. 188, p. 839-846.

Roca, I., E. Torrents, M. Sahlin, I. Gibert, and B.-M. Sjöberg, 2008, NrdI essentiality for class Ib ribonucleotide reduction in *Streptococcus pyogenes*: Journal of bacteriology, v. 190, p. 4849-4858.

Sancho, J., 2006, Flavodoxins: sequence, folding, binding, function and beyond: Cellular and Molecular Life Sciences CMLS, v. 63, p. 855-864.

Sandrini, M., A. R. Clausen, B. Munch-Petersen, and J. Piškur, 2006, Thymidine kinase diversity in bacteria: Nucleosides, Nucleotides and Nucleic Acids, v. 25, p. 1153-1158.

Schuller, J. M., J. A. Birrell, H. Tanaka, T. Konuma, H. Wulfhorst, N. Cox, S. K. Schuller, J. Thiemann, W. Lubitz, and P. Sétif, 2019, Structural adaptations of photosynthetic complex I enable ferredoxin-dependent electron transfer: Science, v. 363, p. 257-260.

Sebald, M., and M. Veron, 1963, Teneur en bases de lADN et classification des vibrions: Annales de l Institut Pasteur, p. 897-&.

Seagal, H. M., T. Spatzal, M. G. Hill, A. K. Udit, and D. C. Rees, 2017, Electrochemical and structural characterization of *Azotobacter vinelandii* flavodoxin II: Protein Science, v. 26, p. 1984-1993.

Sellars, M. J., S. J. Hall, and D. J. Kelly, 2002, Growth of *Campylobacter jejuni* supported by respiration of fumarate, nitrate, nitrite, trimethylamine-N-oxide, or dimethyl sulfoxide requires oxygen: Journal of Bacteriology, v. 184, p. 4187-4196.

Sengupta, R., and A. Holmgren, 2014, Thioredoxin and glutaredoxin-mediated redox regulation of ribonucleotide reductase: World journal of biological chemistry, v. 5, p. 68.

Skirrow, M. B., 2006, John McFadyean and the centenary of the first isolation of *Campylobacter* species: Clinical infectious diseases, v. 43, p. 1213-1217.

Smith, T., 1918, Spirilla associated with disease of the fetal membranes in cattle (infectious abortion): The Journal of experimental medicine, v. 28, p. 701-719.

Stahl, M., J. Butcher, and A. Stintzi, 2012, Nutrient acquisition and metabolism by *Campylobacter jejuni*: Frontiers in cellular and infection microbiology, v. 2, p. 5.

Stubbe, J., and J. A. Cotruvo Jr, 2011, Control of metallation and active cofactor assembly in the class Ia and Ib ribonucleotide reductases: diiron or dimanganese?: Current opinion in chemical biology, v. 15, p. 284-290.

Taylor, A.J. and D.J. Kelly, 2019, The function, biogenesis and regulation of the electron transport chains in *Campylobacter jejuni*: New insights into the bioenergetics of a major food-borne pathogen. Adv Microb Physiol v. 74, p. 239-329.

Thelander, L., and P. Reichard, 1979, Reduction of ribonucleotides: Annual review of biochemistry, v. 48, p. 133-158.

Torrents, E., 2014, Ribonucleotide reductases: essential enzymes for bacterial life: Frontiers in cellular and infection microbiology, v. 4, p. 52.

Torrents, E., M. Sahlin, D. Biglino, A. Gräslund, and B.-M. Sjöberg, 2005, Efficient growth inhibition of *Bacillus anthracis* by knocking out the ribonucleotide reductase tyrosyl radical: Proceedings of the National Academy of Sciences, v. 102, p. 17946-17951.

van der Stel, A. X., F. C. Boogerd, S. Huynh, C. T. Parker, L. van Dijk, J. P. van Putten, and M. M. Wösten, 2017, Generation of the membrane potential and its impact on the motility, ATP production and growth in Campylobacter jejuni: Molecular Microbiology, v. 105, p. 637-651.

Van Vliet, A. H., K. G. Wooldridge, and J. M. Ketley, 1998, Iron-responsive gene regulation in a *Campylobacter jejuni* fur mutant: Journal of Bacteriology, v. 180, p. 5291-5298.

Vandamme, P., E. Falsen, R. Rossau, B. Hoste, P. Segers, R. Tytgat, and J. De Ley, 1991, Revision of *Campylobacter*, *Helicobacter*, and *Wolinella* taxonomy: emendation of generic descriptions and proposal of Arcobacter gen. nov: International Journal of Systematic and Evolutionary Microbiology, v. 41, p. 88-103.

Vandamme, P., P. Pugina, G. Benzi, R. Van Etterijck, L. Vlaes, K. Kersters, J. Butzler, H. Lior, and S. Lauwers, 1992a, Outbreak of recurrent abdominal cramps associated with *Arcobacter butzleri* in an Italian school: Journal of Clinical Microbiology, v. 30, p. 2335-2337.

Vandamme, P., M. Vancanneyt, B. Pot, L. Mels, B. Hoste, D. Dewettinck, L. Vlaes, C. Van Den Borre, R. Higgins, and J. Hommez, 1992b, Polyphasic taxonomic study of the emended genus *Arcobacter* with *Arcobacter butzleri*

comb. nov. and *Arcobacter skirrowii* sp. nov., an aerotolerant bacterium isolated from veterinary specimens: International Journal of Systematic and Evolutionary Microbiology, v. 42, p. 344-356.

Vegge, C. S., L. Brøndsted, Y.-P. Li, D. D. Bang, and H. Ingmer, 2009, Energy taxis drives *Campylobacter jejuni* toward the most favorable conditions for growth: Applied and environmental microbiology, v. 75, p. 5308-5314.

Velayudhan, J., M. A. Jones, P. A. Barrow, and D. J. Kelly, 2004, L-serine catabolism via an oxygen-labile L-serine dehydratase is essential for colonization of the avian gut by *Campylobacter jejuni*: Infection and immunity, v. 72, p. 260-268.

Velayudhan, J., and D. J. Kelly, 2002, Analysis of gluconeogenic and anaplerotic enzymes in *Campylobacter jejuni:* an essential role for phosphoenolpyruvate carboxykinase: Microbiology, v. 148, p. 685-694.

Vinzent, Dumas, Picard, and Lemierre, 1947, * Septicemie Grave AU Cours DE LA Grossesse, Due A UN Vibrion-Avortement Consecutif: Semaine Des Hopitaux, p. 709-709.

Wagley, S., J. Newcombe, E. Laing, E. Yusuf, C. M. Sambles, D. J. Studholme, R. M. La Ragione, R. W. Titball, and O. L. Champion, 2014, Differences in carbon source utilisation distinguish *Campylobacter jejuni* from *Campylobacter coli*: BMC microbiology, v. 14, p. 262.

Weerakoon, D. R., N. J. Borden, C. M. Goodson, J. Grimes, and J. W. Olson, 2009, The role of respiratory donor enzymes in *Campylobacter jejuni* host colonization and physiology: Microbial pathogenesis, v. 47, p. 8-15.

Weerakoon, D. R., and J. W. Olson, 2008, The *Campylobacter jejuni* NADH: ubiquinone oxidoreductase (complex I) utilizes flavodoxin rather than NADH: Journal of bacteriology, v. 190, p. 915-925.

Wu, C.-H., W. Jiang, C. Krebs, and J. Stubbe, 2007, YfaE, a ferredoxin involved in diferric-tyrosyl radical maintenance in *Escherichia coli* ribonucleotide reductase: Biochemistry, v. 46, p. 11577-11588.

Yahara, K., G. Méric, A. J. Taylor, S. P. de Vries, S. Murray, B. Pascoe, L. Mageiros, A. Torralbo, A. Vidal, and A. Ridley, 2017, Genome-wide association of functional traits linked with *Campylobacter jejuni* survival from farm to fork: Environmental microbiology, v. 19, p. 361-380.

Zautner, A. E., R. Lugert, W. O. Masanta, M. Weig, U. Groß, and O. Bader, 2016, Subtyping of *Campylobacter jejuni ssp*. doylei isolates using Mass Spectrometry-based PhyloProteomics (MSPP): JoVE (Journal of Visualized Experiments), p. e54165.

Zilbauer, M., N. Dorrell, B. W. Wren, and M. Bajaj-Elliott, 2008, *Campylobacter jejuni*-mediated disease pathogenesis: an update: Transactions of the Royal Society of Tropical Medicine and Hygiene, v. 102, p. 123-129.